cGMP signalling regulates S-palmitoylation in sensory neurons

Inaugural-Dissertation
to obtain the academic degree
Doctor rerum naturalium (Dr. rer. nat.)

submitted to the Department of Biology, Chemistry and Pharmacy
of Freie Universität Berlin

by

Alexandre Dumoulin

from Geneva, Switzerland

Berlin, 2017

This thesis was prepared between September 2013 and April 2017 under the supervision of Prof. Dr. Fritz G. Rathjen at the Max Delbrück Center for Molecular Medicine, Department of Developmental Neurobiology.

1st Reviewer: **Prof. Dr. Fritz G. Rathjen**
2nd Reviewer: **Prof. Dr. Stephan Sigrist**

date of defence: 29.09.2017

ACKNOWLEDGMENTS

TABLE OF CONTENTS

2

LIST OF ABBREVIATIONS

488	Alexa Fluor® 488
647	Alexa Fluor® 647
µl	microliter
µM	micromolar
µm	micrometer
2BP	2-bromopalmitate
2D	two dimensions
3D	three dimensions
8-pCPT-cGMP	8-(4-chlorophenylthio) guanosine-3', 5'-cyclic monophosphate
A.U.	arbitrary unit
ab	antibody
AIS	axon initial segment
APS	ammonium persulfate
Asp	aspartic acid
Atl2	atlastin-2
bp	base pair
BSA	bovine serum albumin
CA	commissural axons
CAM	cell adhesion molecule
cDNA	complementary DNA
cf	cytosol fraction
cGKI	cGMP-dependent protein kinase 1
cGMP	cyclic guanosine monophosphate
CHAPS	3-[(3-cholamidopropyl)dimethylammonio]-1-propanesulfonate
chDRGs	chick DRGs
cKO	conditional knockout
CNP	c-type natriuretic peptide
CO_2	carbon dioxide
CoA	coenzyme A
CNTN-1	contactin-1
Ctrl	control
$CuCl_2$	copper(II) chloride
$CuSO_4$	copper sulfate
Cy3	cyanine dye 2
Cy5	cyanine dye 5
Cys	cysteine
D	donkey
DAPI	4',6-diamidino-2-phenylindole

DCC	deleted in colorectal cancer
ddH$_2$O	distilled deionized water
DF	dorsal funiculus
DiI	1,1'-dioctadecyl-3,3,3',3'-tetramethylindocarbocyanine perchlorate
DMEM	Dulbecco's modified Eagle's medium
DMSO	dimethyl sulfoxide
DREZ	dorsal root entry zone
DRG	dorsal root ganglion
DRGs	dorsal root ganglia
DSC	dorsal spinal cord
E	embryonic day
ECM	extracellular matrix
EDTA	ethylenediaminetetraacetic acid
ER	endoplasmic reticulum
EtOH	ethanol
F-actin	filamentous actin
FAK	focal adhesion kinase
FCS	fetal calf serum
fl	floxed
FN	fibronectin
G	goat
GAPDH	glyceraldehyde-3-phosphate dehydrogenase
GC	growth cone
GM130	golgin subfamily A member 2
Gp	guinea pig
HBSS	Hanks' Balanced Salt solution
HCl	hydrogen chloride
His	histidine
Hprt	hypoxanthine-guanine phosophoribosyltransferase
HRP	horseradish peroxidase
HS	horse serum
IB	immunoblot
ICC	immunocytochemistry
IHC	immunohistochemistry
Itga3, -6 or -7	integrin α3, α 6 or α 7
Itgb1 or -4	integrin β1 or β4
K$_2$CO$_3$	potassium carbonate
kDa	kilodalton
KMnO$_4$	Potassium permanganate
KO	knockout
L	liter
L1CAM	Neural cell adhesion molecule L1
LAMP-1	lysosomal-associated membrane protein 1

LB	lysis buffer
LC-MS	liquid chromatography–mass spectrometry
LN	laminin
LOF	loss of function
LR	lipid rafts
M	mouse
Map4	microtubule-associated protein 4
MAPs	microtubule-associated proteins
MCC	Mander´s colocalization coefficient
Mcoln1	mucolipin-1
mDRGs	mouse DRGs
mf	membrane fraction
min	minute
ml	milliliter
mM	millimolar
MW	molecular weight
NaOH	sodium hydroxide
NC	nitrocellulose
NCAM	neural cell adhesion molecule 1
Ndst1	N-deacetylase/N-sulfotransferase (heparan glucosaminyl) 1
NEM	n-ethylmaleimide
NeuN	neuronal Nuclei
NF-M	neurofilament-M
NGF	nerve growth factor
nm	nanometer
nM	nanomolar
Npr2	natriuretic peptide receptor 2
Nrp1	neuropilin-1
OD	optic density
P	postnatal day
PBS	phosphate buffer saline
PCR	polymerase chain reaction
PDI	protein disulfide isomerase
PDL	poly-D-lysine
PEG4	4 times polyethylene glycol
PFA	paraformaldehyde
Ph.I.	phosphatase inhibitors
PIs	protease inhibitors cocktail
PVVs	plasmalemmal precursor vesicles
PM	plasma membrane
PNF or pnf	post-nuclear fraction
PPT	protein palmitoyl thioesterase
PTM	post-translational modification

Rab5	Ras-related protein Rab-5
Rac1	Ras-related C3 botulinum toxin substrate 1
Rb	rabbit
RFP	red fluorescent protein
ROI	region of interest
rpm	rotations per minute
RT	room temperature
Rt	rat
RT-PCR	reverse transcription polymerase chain reaction
SC	spinal cord
SD	standard deviation
SDS	sodium dodecyl sulfate
SDS-PAGE	sodium dodecyl sulfate polyacrylamide gel electrophoresis
SEM	standard error of the mean
sema	semaphorin
SER	smooth endoplasmic reticulum
TAE	tris-acetate-EDTA
TAG-1	axonal glycoprotein TAG-1
TBS	Tris-buffered saline
TCA	trichloroacetic acid
TCEP	tris(2-carboxyethyl)phosphine
TEMED	N,N,N′,N′-Tetramethylethane-1,2-diamine
tg	transgene
TGN38	transgolgin 38
Tln2	talin-2
TN-C	tenascin-C
Tris	tris(hydroxymethyl)-aminomethan
trkA	tropomyosin related kinase A
u	unit
v/v	volume/volume
VASP	vasodilator-stimulated phosphoprotein
w/v	weight/volume
WB	Western blot
wnt	wintless
wnt1Cre	wintless-1-cre recombinase
WT	wild-type
YFP	yellow fluorescent protein

ABSTRACT

During the development of the vertebrate nervous system, neurons from the central and the peripheral nervous systems generate an axon which navigates through the tissues. In many cases it might innervate multiple target regions by forming branches and by this build a complex and well-ordered network. Impairment of the formation of the neuronal network often leads to neurological disorders like schizophrenia. Thus, understanding the molecular mechanisms behind the different axonal branching events is of critical importance.

In this work, I focused on a cGMP signalling cascade that regulates the dorsal root ganglion (DRG) and the cranial sensory ganglion (CSG) axon bifurcation, a specific form of axonal branching, in the mouse. This signalling cascade is composed of the ligand C-type natriuretic peptide (CNP), the natriuretic peptide receptor 2 (Npr2) and the cGMP-dependent kinase I subunit α (cGKIα). Each component was shown to be essential in the process of bifurcation of DRG and CSG axons entering the developing mouse spinal cord and hindbrain, respectively, using genetic approaches. However, downstream events triggered by cGKI that are involved in the sensory axon bifurcation are so far unknown. Moreover, direct biochemical and molecular approaches to find out cGKI substrate proteins resulted in a number of false-positive components that couldn´t be confirmed by genetic methods to be involved in sensory axon bifurcation *in vivo*.

Thus, the principal aim of this work was to reconsider other approaches to characterize events taking place downstream of cGKI in sensory neurons that could help understand mechanisms that are triggered *in vivo* when DRG axons bifurcate.

Using cell culture approaches, initially, I characterized the effects of CNP or a cGMP analogue on cultured embryonic DRG neurons and the F11 cell line. Importantly, one of the observed phenotypes was that the CNP-Npr2-cGKI signalling pathway triggered a growth cone remodelling leading to its enlargement. In addition to that, study on the localization of cGKI in cultured embryonic mouse DRG neurons using immunocytochemistry and click chemistry revealed its omnipresence close to intracellular membranes of the central domain of the growth cone. This region of the growth cone was found to be enriched in palmitoylated proteins suggesting a regulation of protein trafficking via S-palmitoylation by cGKI that would lead to a remodelling of the growth cone. Furthermore, cell culture approaches demonstrated

the essential role of S-palmitoylation in the Npr2-mediated DRG growth cone remodelling downstream of cGKI pinpointing its possible regulation by this signalling pathway. Moreover, a biochemical approach revealed that cGMP signalling regulates S-palmitoylation in DRG-like F11 cells supporting this idea. Altogether, this study shed the light on an interplay between cGKI-mediated phosphorylation and the regulation of S-palmitoylation and its central role in Npr2-mediated cGMP signalling *in vitro* and possibly *in vivo*.

In parallel to this, the focal adhesion kinase (FAK)-mediated axon guidance was investigated. Its absence in mouse DRG neurons *in vivo* induced an overshooting of some of their axons entering the spinal cord. This study described FAK as playing a central role in the guidance of a proprioceptive and nociceptive subpopulation of DRG axons entering the developing mouse spinal cord in a cell-autonomous manner.

ZUSAMMENFASSUNG

Während der Entwicklung des Vertebraten Nervensystems erzeugen Neurone aus dem zentralen und peripheren Nervensystem ein Axon, das durch den Wachstumskegel navigiert und Zielregionen innerviert, indem es neue Äste bildet. Somit entsteht ein komplexes und gut geordnetes Netzwerk. Eine Beeinträchtigung der Bildung des neuronalen Netzes führt oft zu neurologischen Störungen wie zum Beispiel Schizophrenie. So ist das Verständnis der molekularen Mechanismen, die zu Bildung von Axonverzweigung führen, von großer Bedeutung.

In dieser Arbeit konzentrierte ich mich auf eine intrazelluläre cGMP-Signalkaskade, die die Bifurkation, eine spezifische Form der Verzweigung, von Axonen der Spinalganglien (DRG) und kranialen sensorischen Ganglien (CSG) reguliert. Diese Signalkaskade besteht aus dem Liganden CNP (natriuretisches Peptid Typ C), dem Rezeptor Npr2 (natriuretischen Peptidrezeptor 2) und der Kinase cGKIα (cGMP-abhängigen Kinase Iα). Für jede Komponente wurde unter Verwendung genetischer Ansätze gezeigt, dass die Signalkaskade bei der Bifurkation von DRG- und CSG-Axonen benötigt wird, wenn diese in das Rückenmark und das Hinterhirn einwachsen. Allerdings sind nachgeschaltete Ereignisse, die durch die cGKI ausgelöst werden und an der sensorischen axonalen Bifurkation beteiligt sind, bislang unbekannt. Darüber hinaus konnten bislang keine relevanten cGKI-Substratproteine, die an diesem Bifurkationsprozess beteiligt sind, durch direkte biochemische und molekulare Ansätze identifiziert werden.

Das Hauptziel dieser Arbeit war es also, andere Ansätze zu entwickeln, um Ereignisse zu charakterisieren, die stromabwärts von der cGKI in den sensorischen Neuronen stattfinden, damit DRG-Axone bifurkieren.

Mit Zellkulturansätzen charakterisierte ich zunächst die Wirkung von CNP oder einem cGMP Analogen auf kultivierte embryonale DRG-Neuronen und F11 Zellen. Interessanterweise war eines der beobachteten Phänomene die Vergrößerung des Wachstumskegels ausgelöst durch die CNP-Npr2-cGKI-Signalkaskade. Darüber hinaus zeigten Lokalisierungsstudien von der cGKI in den kultivierten embryonalen Maus-DRG-Neuronen mittels Immunzytochemie und der „click chemistry" eine Lokalisierung der cGKI an den intrazellulären Membranen und am stärksten in der zentralen Domäne (ZD) des Wachstumskegels. Die ZD zeigte eine Omnipräsenz von

palmitoylierten Proteinen. Somit könnte die cGKI über S-Palmitoylierung den intrazellulären Transport von Proteinen zur Wachstumskegel-Plasmamembran modulieren. Interessanterweise zeigten Zellkulturansätze eine zentrale Rolle der S-Palmitoylierung in der Npr2-vermittelten Umgestaltung des DRG-Wachstumskegels. Außerdem zeigte ein biochemischer Ansatz, dass die cGMP-vermittelte Signaltransduktion die S-Palmitoylierung in F11 Zellen reguliert. Zusammengefasst habe ich in dieser Studie ein Zusammenspiel zwischen der cGKI-vermittelten Phosphorylierung und der Regulation der S-Palmitoylierung und ihre Funktion bei der Npr2-vermittelten cGMP-Signalkaskade *in vitro* und möglicherweise *in vivo* untersucht.

Zusätzlich habe ich die fokale Adhäsionskinase (FAK)-vermittelte axonalen Lenkung untersucht. Die Abwesenheit von FAK in Maus-DRG-Neuronen induzierte ein Überschießen von einigen Axonen, die in das Rückenmark einwachsen. In dieser Studie beschreibe ich die FAK als einen zentralen Faktor bei der Lenkung einer Subpopulation von propriozeptiven und nozizeptiven DRG-Axonen, die in das sich entwickelnde Maus-Rückenmark in einer Zell-autonomen Weise einwachsen.

1. INTRODUCTION

The adult human central nervous system (CNS) and the peripheral nervous system (PNS) are together composed of billions of neurons connected with each other in a precise pattern allowing complex information to be transmitted between different regions of the brain and the rest of the body for example (Kandel et al. 2014). Each neuron is involved in a precise task based on its localization, type and connections (Kandel et al. 2014). As already characterized by Santiago Ramón y Cajal more than 100 years ago like in the sparrow optic tectum, neurons can be classified in different types based on their morphology and localization (Figure 1A) (Ramón y Cajal 1905). Generally, neurons are composed of short branched dendrites close to their soma (shown in black, Figure 1B) and a long central axon with a complex branching pattern (shown in green, Figure 1B) (Schmidt & Rathjen 2010; Helmstaedter et al. 2009). During the propagation of an action potential, synaptic inputs are generally coming from the dendrites and outputs transmitted to the next neuron at the axon terminals (Spruston 2008). The correct connectivity between neurons in the CNS like in the brain or the spinal cord (SC) and the PNS has to be established so that neuronal circuits can work correctly (Bullmore & Sporns 2009; Lai et al. 2016). For instance, disturbances in the brain network are often linked to neurological disorders such as Alzheimer´s disease, schizophrenia or dementia (Stam 2014; Engle 2010). Investigating how the neuronal network is established during the development is therefore crucial to understand the essential mechanisms that might be affected in such neurological disorders.

In this first part, it will be discussed how axons projecting from their neuronal soma can navigate and form new branches to increase the complexity of the neuronal circuits. Secondly, A Npr2-mediated cGMP signalling involved in a precise type of axonal branching called bifurcation will be described as well as the neuronal growth cone (GC) structure where guidance and some branching decisions take place. Finally, the post-translational modification (PTM) S-palmitoylation and its involvement in neurodevelopment will be introduced.
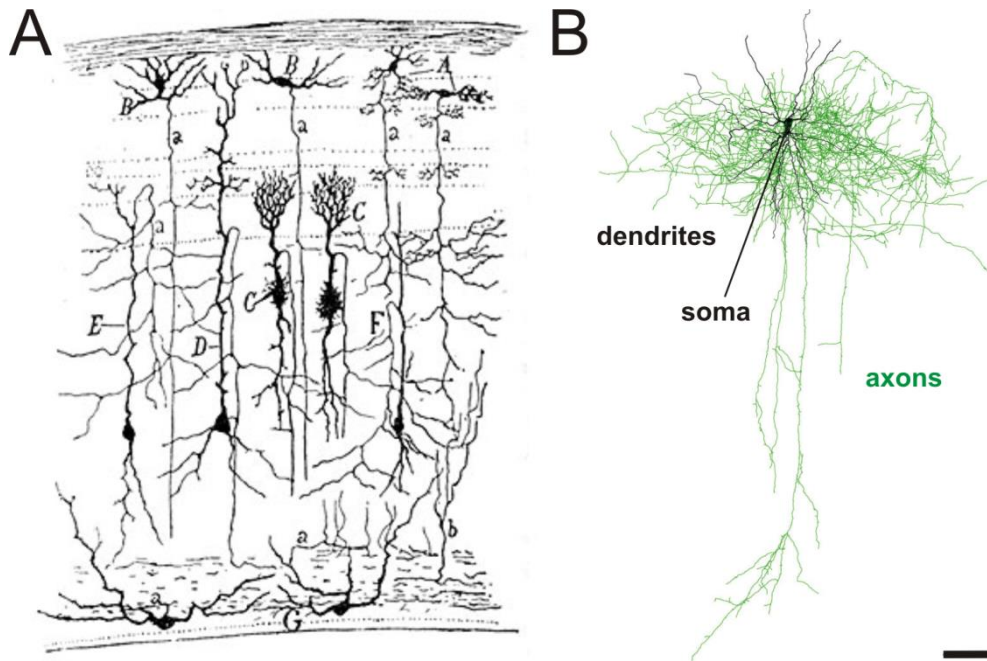
Figure 1 : Neurons and their shape. **(A)** Optic tectum of a sparrow drawn by Santiago Ramón y Cajal in 1905 showing the high variety of neurons that could be determined based on their morphology and localization. **(B)** Model of a layer 2/3 interneuron from rat barrel cortex as it appeared *in vivo* showing the complexity of the axonal branching pattern (in green) (Helmstaedter et al. 2009). Dendrites are shown in black. (A) and (B) were adapted from (Ramón y Cajal 1905) and (Schmidt & Rathjen 2010), respectively. Scale bar: 100 µm.

1.1 AXON GUIDANCE

During the development of the nervous system, neurites are sprouting from the neurons cell body and start elongating. One neurite will elongate much longer and become an axon and neurons will therefore get a polarized morphology (Polleux & Snider 2010; van Beuningen & Hoogenraad 2016).

At the tip of axons the GC is leading the trajectory sensing and responding to extracellular chemorepulsive and chemoattractive cues (Figure 2A) (Kolodkin & Tessier-Lavigne 2011; Vitriol & Zheng 2012). This was described as the fundamental principle of axon guidance (Tessier-Lavigne & Goodman 1996). Repelling and attracting cues will guide axons in their journey and force them to reach their specific target regions or neurons so that a very precise neuronal circuitry can be established (Kolodkin & Tessier-Lavigne 2011).

The developing mouse spinal cord (SC) is a useful model to study axon guidance due to its relative simple structure compared to the brain (Figure 2B). On one hand, starting around embryonic day 10 (E10) in the mouse, dorsal root ganglion (DRG) axons are entering the spinal cord at the dorsal root entry zone (DREZ) (Schmidt &

Rathjen 2010). They encounter there several repelling guidance cues, which are expressed within the dorsal spinal cord (DSC) like Semaphorin 3A (Sema3A), Slits and Netrin-1 (red dots, Figure 2B), that prevent them entering prematurely the DSC and confine them within the dorso-lateral part of the SC (Figure 2B) (Masuda et al. 2009; Gu et al. 2003; Ma & Tessier-Lavigne 2007). On the other hand, GCs of commissural axons (CA) originally localized in the dorsal side of the developing SC are responding for example to the guidance cue Netrin-1 which is expressed in the floor plate (FP) and the ventricular zone (Figure 2B) (Serafini et al. 1996; Lai Wing Sun et al. 2011). Thus, they are attracted to the FP and by other mechanisms cross the midline of the SC and then were also described to turn anteriorly responding to an anterior-posterior gradient of the attracting cue wnt4 (Figure 2B) (Avilés et al. 2013; Zou 2012). Very often, guidance of a subpopulation of neurons was shown to be regulated by attracting and repulsive cues at the same time and the localization as well as temporal expression regulation of these cues allows the fine tuning of the axonal projection pattern (Kolodkin & Tessier-Lavigne 2011; Chédotal & Richards 2010).
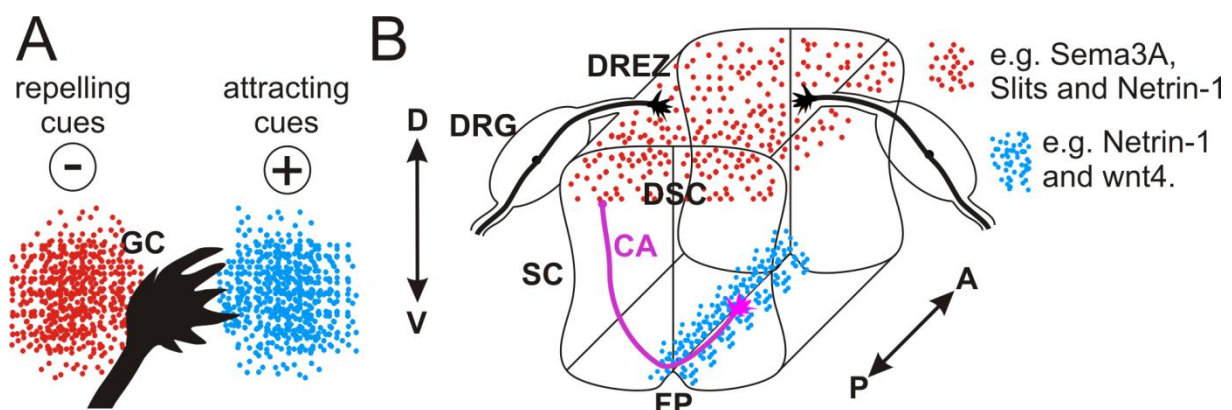
Figure 2 : Principle of axon guidance: the spinal cord model. **(A)** During the development of the nervous system, growth cones (GCs) localized at the tip of axons are sensing the environment and responding to attracting (in blue) and repelling guidance cues (in red) leading to correct axonal projections and therefore precise neuronal connectivity in the CNS and PNS (Vitriol & Zheng 2012; Kolodkin & Tessier-Lavigne 2011). **(B)** The developing spinal cord is a useful system to study axon guidance. On one hand, DRG axons (in black) are entering the cord at the DREZ and are repelled, for example, by semaphorin 3A (sema3A), Slits or Netrin-1 (in red) what hinders them to prematurely enter the dorsal horn of the SC (Masuda et al. 2009; Gu et al. 2003; Ma & Tessier-Lavigne 2007); on the other hand, commissural axons (CA, in magenta) are attracted and guided ventrally toward the floorplate by Netrin-1 (in blue) and after crossing the midline they respond to a gradient of wnt4 making them to turn anteriorly in direction of the brain stem (Vitriol & Zheng 2012; Kolodkin & Tessier-Lavigne 2011). (A) was adapted from (Vitriol & Zheng 2012). (B) was adapted from (Masuda & Shiga 2005; Masuda et al. 2009; Avilés et al. 2013; Lai Wing Sun et al. 2011). GC, growth cone; D, dorsal; V, ventral; DREZ, dorsal root entry zone; DRG. Dorsal root ganglion, SC, spinal cord; DSC, dorsal spinal cord; CA, commissural axons, FP, floor plate; A, anterior; P, posterior.

1.2 AXONAL BRANCHING

In the adult nervous system, it was already pretty clear in the studies of Santiago Ramón y Cajal that one neuron appeared to connect more than one target neuron or region (Figure 1A) (Ramón y Cajal 1905). In order to increase the complexity of the connectivity between neurons, axons during or in the end of their trip through different tissues create multiple branches (Kalil & Dent 2014; Schmidt & Rathjen 2010). Thus, instead of only going from a point A (the soma) to a point B (target neuron or region), axons are capable of reaching several targets on their projection pathway by axonal branching processes having in the end numerous branches that can continue navigating independently from each other and reach a multitude of different targets (Kalil & Dent 2014; Schmidt & Rathjen 2010; Gallo 2011).
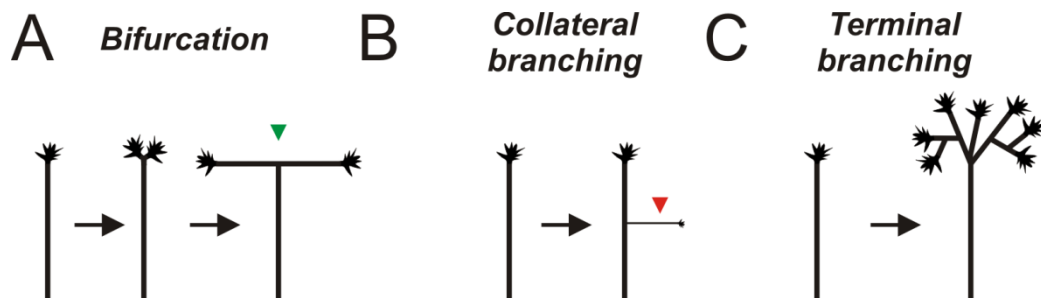
Figure 3 : Different modes of axonal branching. Branching of developing axons can be classified in 3 different types: bifurcation, collateral branching and terminal branching. **(A)** The bifurcation consists in a GC splitting and the creation of two daughter branches (green arrowhead). **(B)** The collateral branching resides in the sprouting of a new branch from the central axon shaft (red arrowhead). **(C)** The terminal branching takes place at axon terminals where a complex branching pattern is created before synapse formation (Kalil & Dent 2014; Schmidt & Rathjen 2010). Adapted from (Schmidt & Rathjen 2010).

There are 3 different modes of axonal branching. There is the bifurcation which consists in a GC splitting and the creation of two daughter branches resulting in a T or Y-shape branching pattern (green arrowhead, Figure 4A) (Schmidt & Rathjen 2010). There is also the collateral branching (also termed interstitial branching) which resides in the sprouting of a new branch from the central axon shaft (red arrowhead, Figure 4B) (Schmidt & Rathjen 2010). Finally, there is the terminal branching or arborisation happening at axon terminals where a complex branching pattern is created before forming synapses (Figure 4C) (Schmidt & Rathjen 2010). So far, it is thought that the three different types of axonal branching use distinct mechanisms (Schmidt & Rathjen 2010; Gallo 2011; Gibson & Ma 2011).

The developing mouse SC is also a very useful system to study axonal branching. Especially, DRG projections to the SC are of particular interest because they undergo

all three different kinds of axonal branching in a temporally regulated manner (Schmidt & Rathjen 2010; Masuda et al. 2009; Gibson & Ma 2011). Starting around embryonic day E10 in the mouse, GCs are entering the cord at the DREZ and first bifurcate. Their daughter branches are growing posteriorly and anteriorly in the dorso-lateral part of the SC (green arrowhead, Figure 4A) (Schmidt & Rathjen 2010). After a "waiting period" of about two days, collateral branches are sprouting from the central axon shafts and grow in deeper layers of the SC where they later arborize and form synapses (red arrowhead, Figure 4A) (O'Leary & Terashima 1988; Schmidt & Rathjen 2010; Masuda et al. 2009).
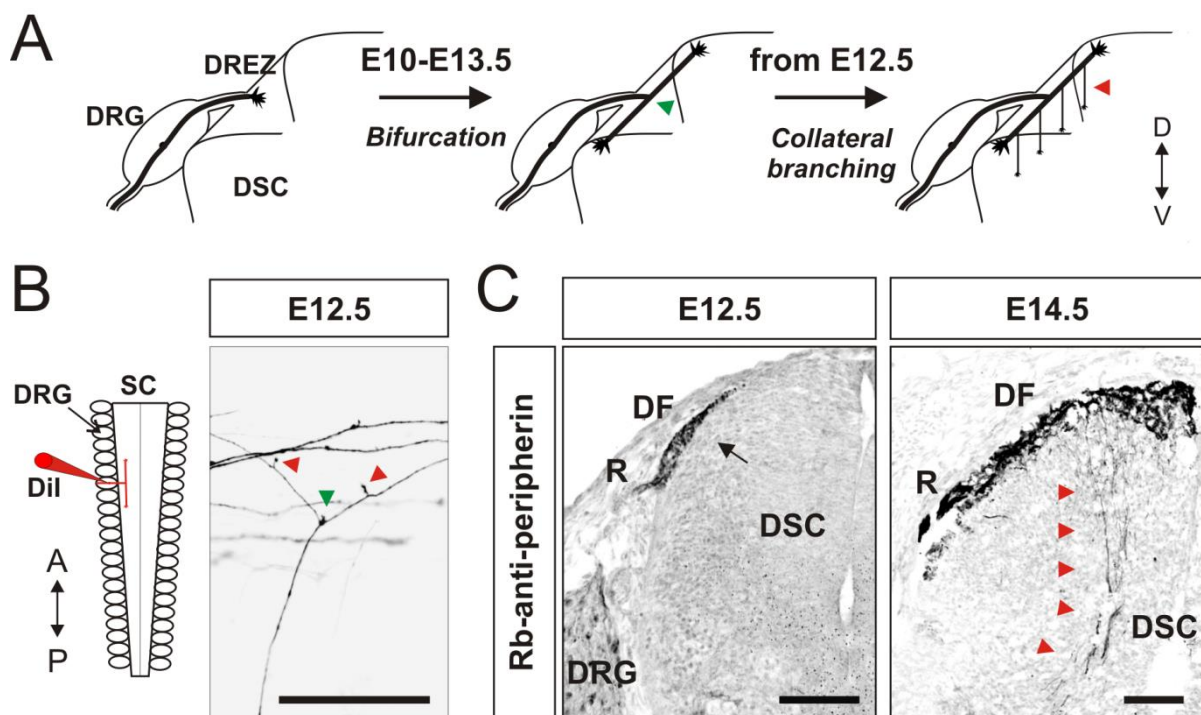
Figure 4: Different modes of axonal branching: the DRG system. **(A)** The branching of developing DRG axons within the mouse SC is temporally regulated. Starting embryonic stage ~E10, axons reaching the DREZ bifurcate (green arrowhead) and their daughter branches grow in two opposite directions within the dorso-lateral part of the spinal cord in the anterior-posterior axis forming the dorsal funiculus. After a "waiting period" of about 2 days, they start forming collateral branches which invade the superficial and deeper layers of the spinal cord (red arrowheads) where they will lately reach their termination zone and branch (terminal branching) before forming synapses (Schmidt & Rathjen 2010; Masuda et al. 2009; Gibson & Ma 2011; O'Leary & Terashima 1988). **(B)** DRG axon bifurcation (green arrowhead) and collateral branching (red arrowheads) at the DREZ can be visualized using the lipophilic dye tracing method by which DiI crystals are implanted in DRGs of E11.5-E14.5 mouse embryos (Schmidt & Rathjen 2011). **(C)** Bundles of axon collaterals can be also visualized on transverse SC sections immunostained for peripherin at embryonic stage E14.5 (red arrowheads) whereas they can hardly be visualized at E12.5 demonstrating the temporal regulation of the collateral branching (black arrow) (Schmidt & Rathjen 2010; Masuda et al. 2009; Gibson & Ma 2011; O'Leary & Terashima 1988). DRG: dorsal root ganglion; DREZ: dorsal root entry zone; DSC: dorsal spinal cord; R: root; DF: dorsal funiculus; D: dorsal; V: ventral; A: anterior; P: posterior. Scale bars: 100 µm. (A) was adapted from (Perrin et al. 2001) and (Schmidt & Rathjen 2010).

In complement of being a relative simple system to investigate, DRG axons can be visualized by very accessible methods. DRG labelling by crystal injection of the

fluorescent carbocyanine dye DiI, for example, allows visualizing single axon morphology at the DREZ of the developing mouse SC (Honig & Hume 1989; Schmidt & Rathjen 2011). Bifurcated axons can be therefore visualized as well as the collateral branches sprouting out from the daughter branches shaft (green and red arrowheads, Figure 4B) (Honig & Hume 1989; Schmidt & Rathjen 2011). Bundles of axon collaterals growing into deeper layers of the SC can be also visualized on transverse SC sections immunostained for peripherin at embryonic stage E14.5 (red arrowheads, Figure 4C) whereas they can hardly be visualized at E12.5 (black arrow, Figure 4C) demonstrating the temporal regulation of the collateral branching shown in Figure 4A (Schmidt & Rathjen 2010; Masuda et al. 2009; Gibson & Ma 2011; O'Leary & Terashima 1988).

1.3 A NPR2-MEDIATED cGMP SIGNALLING CASCADE REGULATES AXONAL BIFURCATION OF SENSORY NEURONS

Cyclic guanosine monophosphate (cGMP) is a cyclic nucleotide converted by particulate (membrane) or soluble guanylyl cyclase from guanosine triphosphate (GTP) (Kuhn 2016). It is a second messenger that has been described to be involved in multiple signalling events regulating, for instance, the vasodilatation of vascular smooth muscle cells, bone growth or ion transport in the intestine (Kuhn 2016).

cGMP level in parallel to the cyclic adenosine monophosphate (cAMP) level has been shown to be implicated in axon guidance regulating calcium levels at the GC in response to extracellular repelling guidance cues like semaphorins (Semaphorin-Plexin signalling) *in vitro* and *in vivo* (Tojima et al. 2011; Bashaw & Klein 2010).

A natriuretic peptide receptor 2 (Npr2)-mediated cGMP signalling cascade was shown to regulate the bifurcation of DRG axons in the developing mouse SC (Schmidt & Rathjen 2010). This signalling pathway was found to contain so far three protein components: a ligand, a receptor and a kinase (Schmidt & Rathjen 2010). The ligand is the C-type natriuretic peptide (CNP) which is expressed in the DSC when DRG axons are entering the cord starting around embryonic day E10 (blue dots, Figure 5A and B) (Schmidt et al. 2009). CNP binds and activates Npr2, a particulate guanylyl cyclase, which is expressed the DRG axons entering the DREZ what leads to the production of cGMP from GTP (Figure 5A and B) (Schmidt & Rathjen 2010; Schmidt et al. 2009; Kuhn 2016). The second messenger cGMP in

turn activates the cGMP-dependent protein kinase Iα (cGKIα, also termed PKG1α), a serine/threonine protein kinase (Figure 5A) (Schmidt & Rathjen 2010; Hannes Schmidt et al. 2002). Only the α-form and not the β-form of cGKI is expressed in embryonic DRGs (Schmidt et al. 2002). When either the ligand CNP, the Npr2 or the cGKI is knocked out, instead of bifurcating at the DREZ of the SC (black arrow, Figure 5B), sensory axons are turning either anteriorly or posteriorly (red arrowhead, Figure 5C) (Schmidt et al. 2009; Schmidt et al. 2007; Schmidt et al. 2002).
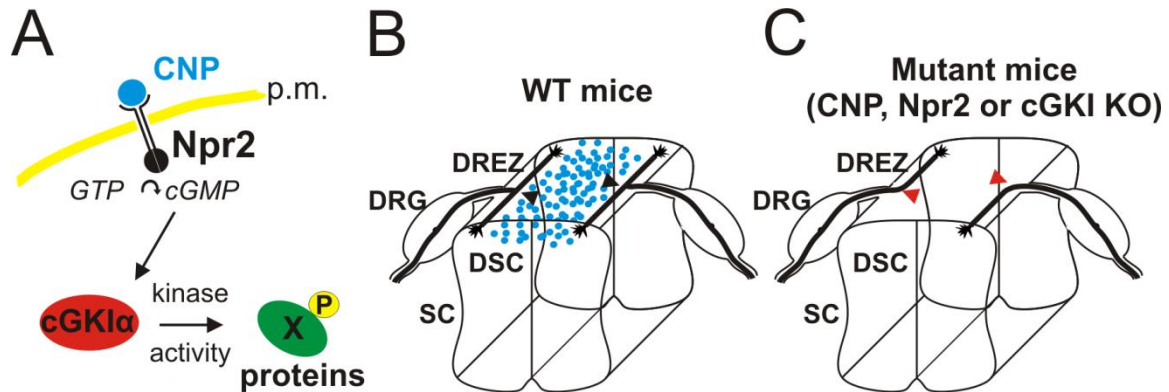
Figure 5: Npr2-mediated cGMP signalling regulates axonal bifurcation of sensory neurons at the DREZ. **(A)** The Npr2-mediated signalling cascade is composed of a C-type natriuretic peptide (CNP) that binds and activates the natriuretic peptide receptor 2 (Npr2), a guanylyl cyclase receptor which produces cGMP from GTP. Then, cGMP activates the cGMP-dependent kinase Iα (cGKIα) a serine-threonine kinase that phosphorylates downstream target proteins. **(B)** Axons entering the DREZ of the SC in mice expressing all components of the cGMP signalling cascade bifurcate normally (black arrowheads). At this point, the ligand CNP (in blue) is expressed by cells localized in the DSC. **(C)** However, if only one of the three components is missing, sensory axons are not able to bifurcate anymore and form instead turns (red arrowheads) (Schmidt & Rathjen 2010). DRG: dorsal root ganglion; DREZ: dorsal root entry zone; DSC: dorsal spinal cord; SC: spinal cord.

Furthermore, this signalling cascade also regulates the axonal bifurcation of cranial sensory ganglion (CSG) axons entering the developing mouse hindbrain in the same way as DRG axons are and deletion of the same components leads to a branching error resulting in a turning phenotype as well (Ter-Avetisyan et al. 2014). Interestingly, the Npr2-mediated signalling pathway is not implicated in collateral branching of neither DRG axons nor CSG axons suggesting a specificity of this cascade in this type of branching (Schmidt et al. 2007; Schmidt et al. 2009; Ter-Avetisyan et al. 2014).

So far, phosphoprotein substrates downstream of cGKIα that are involved in the bifurcation of DRG axons are still unknown (Schmidt & Rathjen 2010; Ter-Avetisyan et al. 2012).

1.4 THE NEURONAL GROWTH CONE

The neuronal growth cone (GC) is localized at the tip of axons or dendrites during the development and remodelling of the nervous system and, as introduced above, it plays a crucial role in responding to guidance and branching cues (Schmidt & Rathjen 2010; Vitriol & Zheng 2012). Thus, the GC is one very important neuronal compartment to study as mechanisms of axon guidance and branching, for example, are triggered at its surface and intracellularly transduced (Conde & Cáceres 2009; Lowery & Vactor 2009; Vitriol & Zheng 2012). Although their large similarities, axonal and dendritic GCs won´t be introduced as a whole. Here the GC will be uniquely referred to the axonal GC.
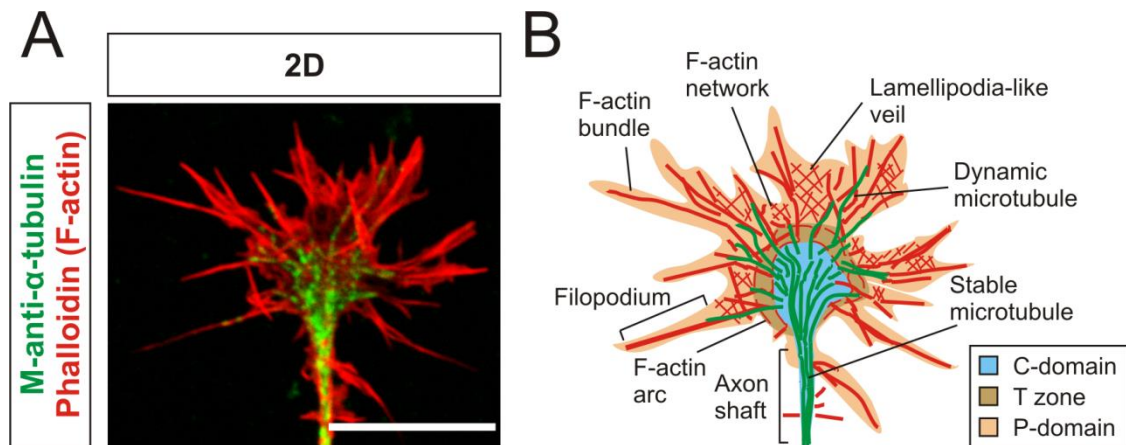
Figure 6: Structure of the neuronal GC in culture. **(A)** Typically, GCs that are growing on a 2D substrate contain an extended and polarized structure as shown here in an E7 chDRG GC cultured on PDL/laminin double-coated substrate. They contain a central (C) domain rich in microtubules (immunostained for α-tubulin in green) and a peripheral (P) domain containing filopodia and lamellipodia rich in F-actin (stained with phalloidin in red). **(B)** Cartoon model of the picture shown in (A). Basically, the neuronal GC contains 3 domains: the C-domain in cyan rich in stable microtubules (shown in green), the P-domain in sand-colour rich in F-actin forming bundles (filopodia) or a network (lamellipodia) and the transition zone (T zone, in pale brown) containing arcs of F-actin (Neukirchen & Bradke 2011; Lowery & Vactor 2009). (B) was adapted from (Lowery & Vactor 2009). Scale bar: 15 µm.

The GC has a highly polarized structure like illustrated in a GC from an embryonic chick DRG (chDRG) explant cultured on a 2D substrate which was fixed and stained for α-tubulin (green) and phalloidin (in red, revealing the filamentous(F)-actin, Figure 6A) (Zou 2012). It contains a central domain (C-domain) rich in microtubule and a peripheral domain (P-domain) rich in F-actin (Figure 6A and B) (Lowery & Vactor 2009). The P-domain contains highly dynamic filopodium and lamellipodium protrusions which are involved in sensing the close environment where the GC is navigating (Figure 6B) (Lowery & Vactor 2009; Dent et al. 2011). In-between both the

21

C- and P-domains, the transition zone (T zone) contains F-actin arcs and dynamic microtubules invading the P-domain (Figure 6B) (Lowery & Vactor 2009; Dent et al. 2011). In contrast, stable microtubules are mostly localized in the axon shaft and at a lesser extend in the C-domain (Figure 6B) (Lowery & Vactor 2009; Dent et al. 2011; Conde & Cáceres 2009).
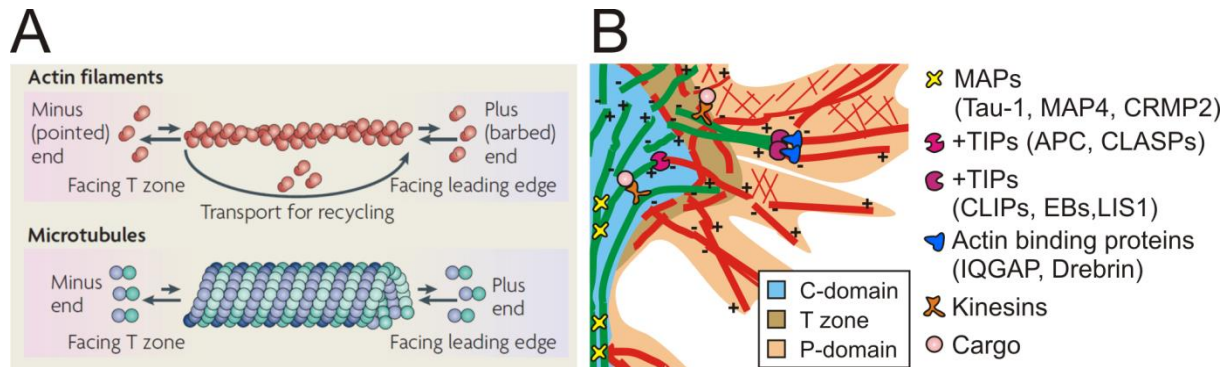
Figure 7 : Dynamicity of microtubule and actin cytoskeletons at the GC. **(A)** Actin filaments are polarized polymers containing a plus (barbed) end, where ATP-bound actin monomers are added, and a minus (pointed) end, where ADP-bound actin monomers are dissociated (Dent et al. 2011). The plus end is usually facing the leading edge whereas the minus end the T zone of the GC (Lowery & Vactor 2009). Microtubules are also polarized linear structures composed of heterodimers of α and β tubulin subunits. GTP-tubulin dimers are added to the plus end facing the leading edge and GDP-tubulin dimers dissociate form the minus end facing the T zone of the GC after GTP hydrolysis (Lowery & Vactor 2009). **(B)** Proteins that associate with the microtubule cytoskeleton (microtubule-associated proteins, MAPs) can stabilize it or regulate its interaction with the actin cytoskeleton. MAPs interact with microtubule lattices at the C-domain to stabilize it and create bundles (e.g. Tau-1) but also at the tip of the microtubules (+TIPs) allowing direct interaction with actin filaments (e.g. APC) or via actin binding proteins (e.g. CLIPs) (Neukirchen & Bradke 2011; Dent et al. 2011). Transport of cargos (e.g. vesicles) along microtubules occurs with the help of motor proteins kinesins (Dent et al. 2011; Neukirchen & Bradke 2011). (A) was adapted from (Lowery & Vactor 2009) and (B) from (Neukirchen & Bradke 2011).

The control of shape and motility of the GC closely depends on the dynamic of both actin and microtubule cytoskeletons (Lowery & Vactor 2009; Vitriol & Zheng 2012; Dent et al. 2011). The versatility of filopodia and lamellipodia protrusions is given by the actin cytoskeleton regulation (Dent et al. 2011). Actin filaments are polarized polymers containing a plus (barbed) end, where ATP-bound actin monomers are added, and a minus (pointed) end, where ADP-bound actin monomers are dissociated (Figure 7A and B) (Dent et al. 2011). The plus end is usually facing the leading edge whereas the minus end the T zone of the GC (Figure 7A and B) (Lowery & Vactor 2009). Microtubules are also polarized linear structures composed of heterodimers of α and β tubulin subunits. GTP-tubulin dimers are added to the plus end facing the leading edge and GDP-tubulin dimers dissociate form the minus end facing the T zone of the GC after GTP hydrolysis (Figure 7A and B) (Lowery & Vactor 2009).

Proteins that associate with the microtubule cytoskeleton (microtubule-associated proteins, MAPs) regulate its interaction with the actin cytoskeleton. MAPs interact with microtubule lattices at the C-domain to stabilize it and create bundles (e.g. Tau-1) but also at the tip of the microtubules (+TIPs) allowing direct interaction with actin filaments (e.g. the Adenomatous polyposis coli protein, APC) or via actin binding proteins (e.g. CAP-Gly domain-containing linker proteins CLIPs and Drebrin, Figure 7B) (Lowery & Vactor 2009; Neukirchen & Bradke 2011).

The C-domain of the GC is rich in organelles like mitochondria or exocytotic vesicles that are transported (cargos) from the cell body along microtubules with the help of motor proteins kinesins (Figure 7B) (Dent et al. 2011; Neukirchen & Bradke 2011; Vitriol & Zheng 2012). This microtubule-based transport of organelles like plasmalemmal precursor vesicles (PPVs) to the C-domain is required to allow the plasma membrane expansion needed in the GC remodelling and axonal outgrowth (Vitriol & Zheng 2012; Pfenninger 2009).

1.5 PROTEIN S-PALMITOYLATION

Many proteins that play a major role in the neuronal GC are S-palmitoylated like the growth-associated protein 43 (Gap43) (Pate Skene & Virag 1989), the cytoskeleton protein Rac1 (Ras-related C3 botulinum toxin substrate 1) (Navarro-Lérida et al. 2012), or the IgSF cell adhesion molecules NCAM (Neural cell adhesion molecule 1) and L1CAM (Neural cell adhesion molecule L1) (Fukata & Fukata 2010). Moreover, a diminution of S-palmitoylation in cultured adult rat DRG neurons by S-nitrosylation competition or by tunycamicin-mediated inhibition was reported to induce GC collapse and a decrease in GC-mediated neurite extension, respectively (Hess et al. 1993; Patterson & Skene 1994). Accordingly, studying the dynamic regulation of S-palmitoylation in the developing nervous system is of particular interest.

S-palmitoylation is a post-translational modification (PTM) of proteins that takes place at the thiol residue of cysteines (Chamberlain & Shipston 2015). This is a lipid modification (fatty acylation) of proteins which results in a 16-carbon saturated fatty acid palmitate linked to cysteines (Cys) by a thioester bound (red arrow, Figure 8A) (Linder & Deschenes 2007). The chemistry of the linkage (thioester bound) is fundamental as it makes it reversible (Chamberlain & Shipston 2015; Dietrich & Ungermann 2004). For instance, other fatty acylations like N-palmitoylation or N-

myristoylation which takes place at the N-terminal cysteines and glycines, respectively, are irreversible (Figure 8A) (Linder & Deschenes 2007; Chamberlain & Shipston 2015). Other kinds of fatty acids can be S-linked to cysteines (at a much lesser extend compared to palmitate) and therefore the term S-palmitoylation will be used to describe S-acylation in general (Chamberlain & Shipston 2015; Linder & Deschenes 2007; Hess et al. 1993).

S-palmitoylation is catalysed by S-acyltransferases (also termed palmitoyl-transferases or Zdhhc enzymes) (Linder & Deschenes 2007; Chamberlain & Shipston 2015; Fukata & Fukata 2010; Dietrich & Ungermann 2004). Zdhhc enzymes are transmembrane proteins composed of 4 to 6 transmembrane domains and containing a zinc finger domain with a conserved DHHC (Aspartate-Histidine-Histidine-Cysteine) catalytic motif in a loop localized on the cytosolic face (Figure 8B) (Chamberlain & Shipston 2015). In mammalian genomes like human and mouse, 23 different Zdhhc enzymes are predicted (Fukata & Fukata 2010). Interestingly, one precise Zdhhc enzyme can palmitoylate several proteins and one protein might be S-palmitoylated by one or more Zdhhc enzymes giving to the S-palmitoylation code its complexity (Chamberlain & Shipston 2015). So far, studies on Zdhhc-mediated protein palmitoylation strongly suggested a two-step mechanism (Fukata et al. 2004; Jennings & Linder 2012; Lemonidis et al. 2014; Mitchell et al. 2014). Firstly, the palmitate from palmitoyl-coenzyme A (CoA) is transferred onto the Zdhhc enzyme (auto-palmitoylation step of the enzyme) and secondly, the palmitate is subsequently transferred onto the target protein at its cysteine residue (shown in yellow, Figure 8C) (Fukata et al. 2004; Jennings & Linder 2012; Lemonidis et al. 2014; Chamberlain & Shipston 2015; Dietrich & Ungermann 2004; Mitchell et al. 2014). The thioester bound confers to this PTM its reversibility as already mentioned above and this linkage can be hydrolysed by palmitoyl protein thioesterases (PPTs, Figure 8C) (Fukata & Fukata 2010; Chamberlain & Shipston 2015). Hence, S-palmitoylated proteins can cycle within minutes between the acylated and the non-acylated state similarly to phosphoproteins between the phosphorylated and the non-phosphorylated state (Chamberlain & Shipston 2015).
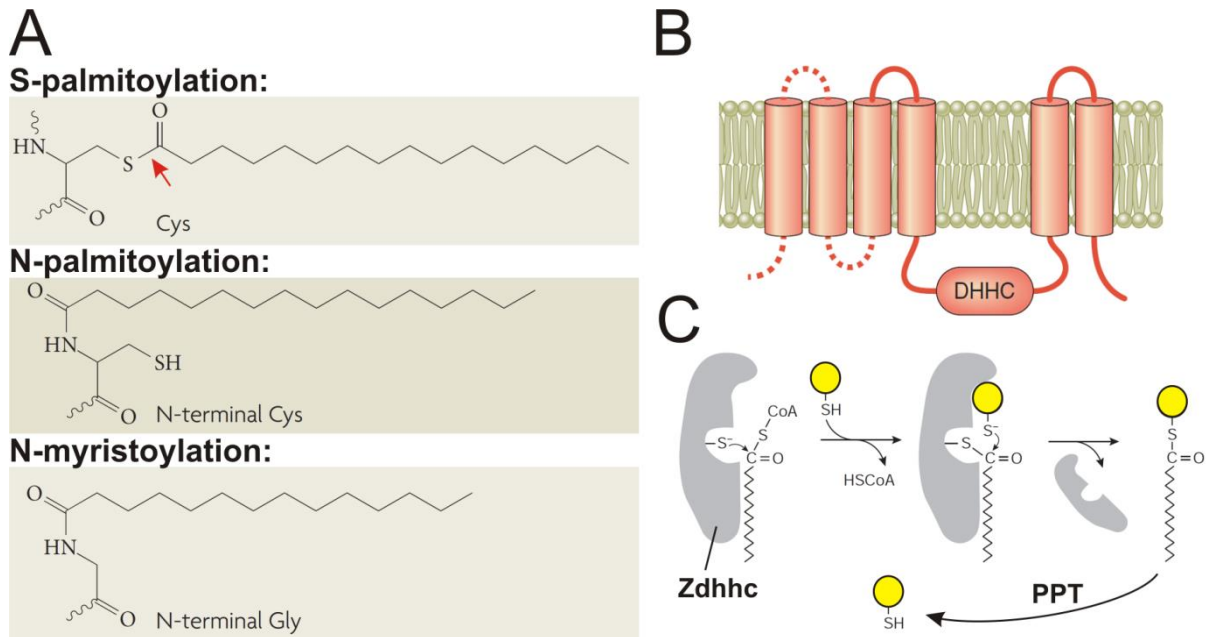
Figure 8 : The chemistry and mechanism of protein S-palmitoylation. **(A)** S-palmitoylation is a PTM resulting in an addition of a 16-carbon fatty acid onto a cysteine residue of a protein. It differs from other lipid modifications as it takes place at the thiol group of a cysteine (Cys) residue forming a thioester bound between the cysteine and the palmitate (red arrow) (Chamberlain & Shipston 2015; Linder & Deschenes 2007). **(B)** Palmitoyltransferases (Zdhhc) are transmembrane proteins composed of 4 to 6 transmembrane domains and containing a DHHC (Aspartate-Histidine-Histidine-Cysteine) catalytic motif in a loop localized on the cytosolic face (Chamberlain & Shipston 2015). **(C)** Zdhhc enzymes are thought to catalyse the transfer of palmitate onto cysteines in a 2-step mechanism. Firstly, palmitate from palmitoyl-CoA is transferred onto the cysteine of the DHHC domain (autoacylation of the enzyme). Secondly, the palmitate is transferred onto the cysteine of the substrate protein (in yellow) at its cysteine thiol residue (Chamberlain & Shipston 2015; Dietrich & Ungermann 2004). The thioester bond confers to this PTM its reversibility as it can be hydrolysed by palmitoyl protein thioesterases (PPTs) (Fukata & Fukata 2010; Chamberlain & Shipston 2015). (A) was adapted from (Linder & Deschenes 2007), (B) from (Chamberlain & Shipston 2015) and (C) from (Dietrich & Ungermann 2004).

S-palmitoylation is known to regulate for example the protein assembly, degradation or activation/inhibition and more interestingly in a neurodevelopmental context, it regulates the trafficking of integral (transmembrane) and peripheral membrane proteins (Chamberlain & Shipston 2015; Linder & Deschenes 2007; Fukata & Fukata 2010). The addition of one or several palmitates increases the lipophilicity of the protein leading to its association to membranes for example (soluble peripheral membrane proteins). Although the lack of data *in vivo* and of endogenously expressed Zdhhc enzymes *in vitro*, Zdhhc enzymes localization appeared to be heterogeneous within cells (Ohno et al. 2006; Chamberlain & Shipston 2015). For example, it means that some enzymes might be strictly localized at the Golgi complex whereas others in other subcellular compartments like in vesicles or at the plasma membrane conferring a spatial dependence in the substrate-enzyme relationship (Ohno et al. 2006; Chamberlain & Shipston 2015). Thus, an enzyme localized at the Golgi can S-palmitoylate a peripheral membrane protein (shown in

yellow, Figure 9), therefore increasing its lipophilicity, what leads to its shuttling to the plasma membrane by vesicle transport or diffusion (Figure 9) (Fukata & Fukata 2010). S-palmitoylation can also be involved in the translocation of peripheral membrane and transmembrane proteins to lipid rafts, cholesterol-rich microdomains (in green, Figure 9) (Lingwood & Simons 2010; Fukata & Fukata 2010). As already introduced before, PPTs can depalmitoylate proteins at the plasma membrane for example leading to a cycling of the peripheral membrane or transmembrane protein back to the cytosol/original subcellular compartment (Figure 9) (Fukata & Fukata 2010; Chamberlain & Shipston 2015).
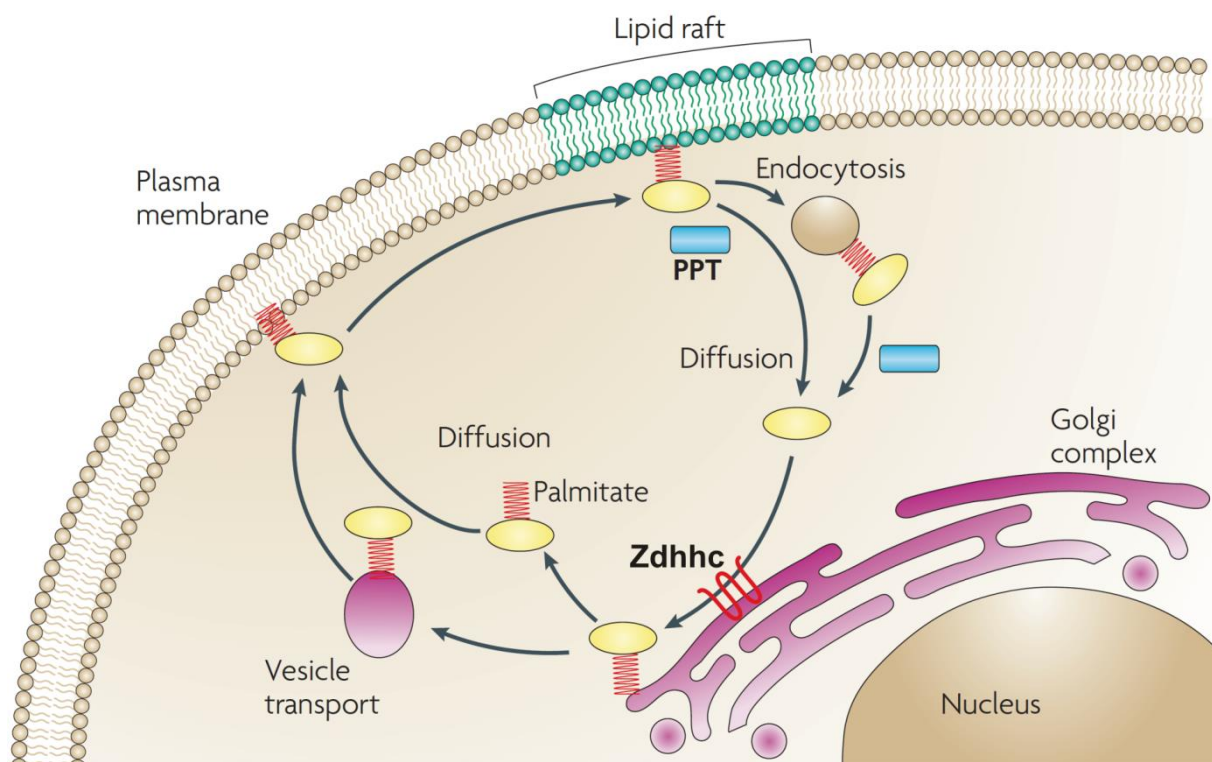
Figure 9 : S-palmitoylation regulates the trafficking of integral and peripheral membrane proteins. One of the well-characterized effects of protein S-palmitoylation is the regulation of membrane and peripheral membrane proteins trafficking. Here is depicted an example of the S-palmitoylation-dependent trafficking of a peripheral membrane protein (in yellow) which is palmitoylated at the Golgi complex by a Zdhhc enzyme and is subsequently shuttled to the plasma membrane (PM) by vesicle transport or diffusion (Fukata & Fukata 2010). Note that Zdhhc-mediated palmitoylation can happened at various intracellular membrane structures and at the PM as well (Chamberlain & Shipston 2015). S-palmitoylation can also mediate the partitioning of membrane proteins in microdomains at the PM (e.g. lipid rafts) (Fukata & Fukata 2010; Chamberlain & Shipston 2015). PPTs can depalmitoylate proteins at the PM for example leading to a cycling of the peripheral membrane proteins back to the cytosol/original subcellular compartment (Fukata & Fukata 2010; Chamberlain & Shipston 2015). Adapted from (Fukata & Fukata 2010).

Although specific examples in precise biological systems, how Zdhhc enzymes activity or substrate specificity is globally regulated is still poorly understood (Brigidi et al. 2015; Lievens et al. 2016). A few studies recently revealed an interplay between tyrosine phosphorylation and the activity and subcellular localization of

specific Zdhhc enzymes suggesting that they can be regulated and are not necessarily constitutively active toward all substrates (Brigidi et al. 2015; Lievens et al. 2016). Of course, much more cross-talks have been described downstream of Zdhhc enzymes between S-palmitoylation and phosphorylation as well as ubiquitination, for instance (Charych et al. 2010; Tian et al. 2008; Abrami et al. 2006; Blanc et al. 2015).

Since the late 2000s, much progress in the field of S-palmitoylation has been made thanks to new biochemical approaches that allowed the purification of S-palmitoylated and palmitoylated proteins together with the improvement in mass spectrometry methods to detect and quantify palmitoylomes (Roth et al. 2006; Martin & Cravatt 2009).

S-palmitoylation appeared to play a crucial role in the nervous system development, function and maintenance (Fukata & Fukata 2010; Chamberlain & Shipston 2015). During the last 20 years much effort was put in studying the role of S-palmitoylation at synapses. Bioinformatics revealed that 41% of synaptic genes encoded a palmitoylated protein according to a compilation of published MS-based palmitoylation screenings (Sanders et al. 2015). For instance, proteins which play a central role in synaptic plasticity like the postsynaptic density protein 95 (PSD-95) were reported to be dynamically S-palmitoylated in regard to synaptic activity (Fukata & Fukata 2010; Chamberlain & Shipston 2015; Fukata et al. 2004). Moreover, cell adhesion proteins like NCAM, ion channels like NMDA (N-methyl-d-aspartate) receptor subunits NR2A and NR2B, SNARE proteins like SNAP-25 (synaptosomal-associated protein 25) or kinases like the tyrosine-protein kinase FYN are all S-palmitoylated proteins revealing a really wide range of proteins that undergo this PTM at the pre- and postsynaptic compartments (Fukata & Fukata 2010; Chamberlain & Shipston 2015).

Whereas S-palmitoylation clearly plays a central role at the synapse, much less is known about its importance in axon guidance and branching. Knowing the number of cell adhesion proteins that were characterized to be S-palmitoylated like NCAM, L1CAM or the receptor for the guidance cue Netrin-1 DCC, this lack of knowledge appears to be mostly due to a lack of studies *in vitro* and *in vivo* (Fukata & Fukata 2010; Chamberlain & Shipston 2015; Hérincs et al. 2005). So far, few studies have reported the importance of S-palmitoylation in axonal branching. For example, S-palmitoylation of the c-jun N-terminal kinase 3 (JNK3) have been reported to be

crucial in the Wnt7a-mediated axonal branching of rat cortical neurons in culture (Yang et al. 2012). More recently, the lab of Joseph Gogos reported that the palmitoyl-transferase Zdhhc8-mediated S-palmitoylation played a role in both collateral and terminal branching of mouse callosal axons of layers 2/3 pyramidal neurons *in vitro* and *in vivo* (Mukai et al. 2015a). This work didn´t only reveal for the first time that S-palmitoylation was involved in axonal branching *in vivo* but also that it appeared to regulate two different axonal branching types suggesting that S-palmitoylation might be essential at some point for the axonal branching in general (Mukai et al. 2015a).

Many neurological diseases have been reported to have a link with a disturbance in the S-palmitoylation of proteins (Fukata et al. 2004; Chamberlain & Shipston 2015; Greaves & Chamberlain 2011). For instance, studies on schizophrenia mouse models and schizophrenic patients have shown a link between S-palmitoylation regulation and the development of the disease (Mukai et al. 2004; Mukai et al. 2015a; Karayiorgou & Gogos 2004; Charych et al. 2010; Pinner et al. 2015). Moreover, S-palmitoylation has been shown to be associated to X-linked intellectual disability, Alzheimer´s and Huntington´s diseases, for example, emphasizing the importance to investigate more in detail the regulative mechanisms of S-palmitoylation in developing and adult nervous system (Fukata & Fukata 2010; Greaves & Chamberlain 2011; Chamberlain & Shipston 2015; Cho & Park 2016).

1.6 THE AIMS OF THIS STUDY

Mouse DRG axons entering the developing spinal cord at the DREZ bifurcate in a CNP-Npr2-cGKI-mediated manner. So far, which signalling events are triggered downstream of cGKI when sensory axons bifurcate are still unknown. Furthermore, direct biochemical and molecular approaches to discover cGKI substrate proteins resulted in a number of false-positive components that couldn´t be confirmed by genetic methods to be essential in DRG axon bifurcation *in vivo*.

Therefore, the main aim of this study was to use a combination of new approaches, namely cell culture-based, which could give new indications on signalling events taking place downstream of cGKI in embryonic DRG neurons when they bifurcate.

From this, a further aim was to investigate the possible link between the Npr2-mediated cGMP signalling cascade and the S-palmitoylation in DRG neurons using cell culture, immunocytochemical and biochemical approaches.

In parallel to this, the role of the focal adhesion kinase (FAK) in the guidance of DRG and commissural axons was investigated using genetic methods complemented by axonal tracing and immunohistochemistry.

2. MATERIALS

2.1 CHEMICALS AND MATERIALS

Name	Company
2-bromopalmitate	Sigma
Acetic acid	Merck
Acrylamide	BioRad
Agarose NEO Ultra-Quality	Carl Roth
Aprotinin	Carl Roth
B27 supplement	Gibco
BA85 Nitrocellulose membrane	Schleicher & Schuell
Bromophenol blue	Sigma
Biotin-PEG4-alkyne	Sigma
CHAPS	Merck
Chloroform	Merck
CNP	Sigma
Collagen (rat tail)	Corning
Collagen (rat tail) for coating	Sigma
$CuSO_4$	Sigma
DiI	Sigma
DMEM	Gibco
DMEM 10X	Sigma
DMSO	Merck
dNTPs Mix (10 mM each)	Takara
dNTPs Mix (2.5mM each)	Invitrogen
EDTA	Merck
Ethanol	Merck
Ethidium bromide	Biochemica
F11 cell line	CLS cell lines service
F12 medium (F12 Nut mix, 1X GlutaMAX™)	Gibco
Fertilized SPF eggs	VALO
Fetal calf serum (FCS)	Gibco
Formaldehyde	Merck
Glycerol	Merck
Glycine	Merck
Goat serum (inactivated)	Gibco
HAT 50X	Gibco
HBSS	Gibco
HCl	Merck
HPDP-biotin	Pierce

HS	Gibco
human β-NGF	Alomone labs
Hydroxylamine (HA)	Sigma
Isofluran	Baxter
Isopropanol	Meck
Laminin	Sigma
Leupeptin hemisulfate salt	Sigma
Magnesium chloride	Merck
Manganese chloride	Merck
Methanol	Merck
NaOH	Merck
NEM	Thermoscientific
Palmitic acid, azide	Invitrogen
PBS	Biochrom
PC12 cell line	CLS cell lines service
Palmitic acid, azide	Invitrogen
Penicillin-Streptomycin (10000 U/ml)	Gibco
Pepstatin A	Sigma
PFA	Merck
Poly-D-lysine (PDL)	Sigma
Ponceau S	Sigma
Potassium acetate	Sigma
Potassium carbonate	Sigma
Potassium carbonate	Sigma
Potassium permanganate	Sigma
Proteinase K	Genaxxon
Silver nitrate	Sigma
Sodium chloride	Merck
Streptavidin agarose resin (high capacity)	Thermo Scientific
Sucrose	Merck
TCEP	Sigma
TEMED	GE Healthcare
Tris-Cl and Tris-base	Merck
Triton-X100	Merck
Trypan Blue	BioRad
Trypsin	Invitrogen
Tween-20	Sigma
Ultrafree-MC DV Centrifugal Filter	Millipore
β-mercaptoethanol	Sigma

2.2 BUFFERS

Name	Composition
0.8 M Hydroxylamine solution (+HA buffer)	0.8 M HA, 1 mM HPDP-Biotin (62.5 mM), 0.2% (v/v) Triton X-100, 20 u/µl aprotinin, 5 mM leupeptin, 5 mM pepstatin A, 1mM PMSF, pH 7-7.4. Solution of 0.8 M HA (+HA buffer) was first prepared as follow: 2.78 g HA (MW=69.49 g/mol) were diluted in ddH$_2$O, pH was adjusted with NaOH 5M and solution adjusted to 50 ml and kept on ice. For -HA control buffer, the same was prepared but instead +HA buffer Tris-Cl 50 mM, pH 7,4 was used.
1M NEM solution	0.125 g of NEM (MW= 125.15 g/mol) was solubilized in 1 mL EtOH.
4% PFA solution in PBS 1X	4% (w/v) PFA was solubilized in water at 60°C and the solution was cleared by adding some drops of 5M NaOH and pH was adjusted to 7.4. The solution was then filtrated, aliquoted and stored at -20°C.
4SB solution	4% SDS, 50 mM Tris, 5 mM EDTA, pH 7.4.
Agarose gel	1.7-3% (w/v) of agarose was solubilized in TAE 1X buffer by boiling in the microwave and short before pouring it in the gel tray, ethidium bromide (1:1000) was given.
Blotting buffer	192 mM glycine, 25 mM Tris and 20% methanol or iso-propanol (v/v) in ddH$_2$O.
Biotin-PEG4-alkyne solution	Biotin-PEG4-alkyne was dissolved in DMSO at a concentration of 5 mM at RT by sonication and aliquoted at -20°C up to 6 months.
DRG medium FCS	DMEM supplemented with 10% (v/v) FCS and Penicillin-Streptomycin (100 U/ml).
DRG medium without FCS	DMEM supplemented with Penicillin-Streptomycin (100 U/ml).
F11 cell medium	F12 medium supplemented with 10% (v/v) FCS and 1x HAT and 100 U/µL Penicillin/Streptomycin
HPDP-Biotin (62.5 mM stock solution)	HPDP-Biotin was diluted in DMSO and stored at -20°C at a concentration of 62.5 mM.
IB blocking buffer	3% (w/v) BSA, 0.5% Tween-20 in 1X TBS.
IB washing buffer	0.5% Tween-20 in 1X TBS.
ICC-blocking buffer	1:1000 goat serum in PBS 1X.
IHC-blocking buffer	1:1000 goat serum in IHC-washing buffer.
IHC-washing buffer	0.1% Triton X-100 in PBS 1X.
Laemmli sample buffer (5x)	5% (v/v) β-mercaptoethanol, 1% (v/v) SDS, 12.5% (v/v) glycerol, 50mM Tris–HCl pH 6.8, 0.01% (w/v) bromophenol blue.
LB	150 mM NaCl, 50 mM Tris, 5 mM EDTA, pH 7.4.
LB-NEM	10 mM NEM from a 1 M NEM solution, 20 u/µl aprotinin, 5 mM leupeptin, 5 mM pepstatin A , 1mM PMSF in LB.

Low HPDP-Biotin Solution	0.2 mM HPDP-biotin, 20 u/µl aprotinin, 5 mM leupeptin, 5 mM pepstatin A , 1mM PMSF, 0.2% Triton X-100 in LB
Lysis buffer (CHAPS)	1% CHAPS (v/v) in TBS 1X containing protease inhibitors cocktail (20 u/µl aprotinin, 5 mM leupeptin, 5 mM pepstatin A) and 100 mM PMSF.
Lysis buffer (lipid rafts)	20 u/µl aprotinin, 5 mM leupeptin, 5 mM pepstatin A, 1 mM PMSF, 1 mM $CaCl_2$ and 1 mM $MgCl_2$ in TBS 1X.
Lysis buffer (sucrose)	0.34 M sucrose in ddH_2O with a protease inhibitors cocktail (20 u/µl aprotinin, 5 mM leupeptin, 5 mM pepstatin A) and 100 mM PMSF.
Palmitic acid, azide	Palmitic acid, azide was dissolved in DMSO at a concentration of 100 mM at RT by sonication and stored at -20°C.
PBS/EDTA	Sterile 5 mM EDTA in 1X PBS.
PC12 cell medium	DMEM supplemented with 5% (v/v) HS, 10 % (v/v) FCS and 100 U/µL Penicillin/Streptomycin
Ponceau S staining solution	0.1% (w/v) Ponceau S in 5% (v/v) acetic acid.
Running buffer for SDS-PAGE	192 mM glycine, 25 mM Tris-Cl and 0.1% (w/v) SDS.
Solution W	10% (v/v) ethanol and 5% (v/v) acetic acid in ddH_2O.
TAE 1X	4.85 g Tris Base, 1.142 ml glacial acetic acid and 20 ml 0.5 M EDTA (pH 8.0) in 1 L ddH_2O.
TBS 1X	150 mM NaCl and 50 mM Tris-Cl, pH 7.4.
Trypsination buffer	1 mg/mL Trypsin in HBSS.

2.3 ANTIBODIES

Name	Company	Dilution
D-anti-G-488	Jackson Immunoresearch	1:400 (IHC and ICC)
D-anti-GP-HRP	Dianova	1:25000 (WB)
D-anti-Rb-Cy3	Invitrogen	1:400 (IHC and ICC)
DAPI	Dianova	1:1000 (IHC and ICC)
G-anti-Zdhhc8 (Eb07652)	Everest Biotech	1:500 (ICC and WB)
G-anti-M-488	Jackson Immunoresearch	1:400 (IHC and ICC)
G-anti-M-647	Dianova	1:400 (IHC and ICC)
G-anti-M-HRP	Dianova	1:25000 (WB)
G-anti-Rb-Cy3	Jackson Immunoresearch	1:400 (IHC and ICC)

G-anti-Rb-HRP	Dianova	1:25000 (WB)
Gp-anti-Npr2	Homemade (AG Rathjen)	1:5000 (WB)
M-anti-clathrin (Heavy Chain)	BD Transduction Laboratories	1:1000 (WB)
M-anti-FAK	Prof. Louis Reichardt	1:1000 (WB)
M-anti-flotillin-1	Transduction Laboratories	1:1000 (WB)
M-anti-GAPDH	Novus Biologicals	1:2000 (WB)
M-anti-GM130 (clone 35/GM130)	BD biosciences	1:250 (IHC, ICC and WB)
M-anti-NeuN	Millipore	1:500 (ICC)
M-anti-NF-M (clone 2H3)	Developmental Studies Hybridoma Bank	1:192 (IHC and ICC)
M-anti-PDI (clone 1D3)	Enzo	1:500 (ICC and WB)
M-anti-Rab11	BD biosciences	1:100 (ICC)
M-anti-Rab5 (clone D11)	Santa Cruz	1:500 (ICC and WB)
M-anti-TAG-1 (clone 4D4)	(Dodd et al., 1988)	1:125 (IHC)
M-anti-TGN38	BD biosciences	1:800 (ICC)
M-anti-α-tubulin (clone B-5-1-2)	Sigma	1:1000 (ICC and WB)
M-anti-α-tubulin (clone DM1A)	Calbiochem	1:1000 (ICC and WB)
M-anti-γ-adaptin	BD biosciences	1:250 (ICC)
Phalloidin-488	Thermo Scientific	1:100 (ICC)
Rb-anti-cGKI (clone 107)	Homemade (AG Rathjen)	1:1200 (IHC, ICC and WB)
Rb-anti-chNCAM	Homemade (AG Rathjen)	1:4800 (ICC)
Rb-anti-Gap43	Chemicon	1:1000 (WB)
Rb-anti-G-HRP	Dianova	1:25000 (WB)
Rb-anti-integrin-β1	Abcam	1:1000 (WB)
Rb-anti-L1CAM	Homemade (AG Rathjen)	1:3000 (ICC)

Rb-anti-M-Cy3	Jackson Immunoresearch	1:400 (IHC and ICC)
Rb-anti-Peripherin	Millipore	1:3000 (IHC)
Rb-anti-pFAK (Y397)	Santa Cruz	1:500 (WB)
Rb-anti-RFP	Antikörper-online	1:2500 (IHC)
Rb-anti-trkA	Millipore	1:2000 (IHC)
Rb-anti-VASP (clone 9A2)	Cell Signalling	1:1000 (WB)
Rb-anti-Zdhhc5	Sigma	1 :1000 (WB)
Rt-anti-LAMP-1 (clone 1D4B)	Santa Cruz	1:250 (ICC and WB)
Streptavidin-Cy5	Thermo Scientific	1:600 (ICC)
Streptavidin-HRP	Thermo Scientific	1:25000 (WB)

2.4 MOUSE LINES AND EMBRYOS

- C57BL/6 (bred at MDC)
- cGKI KO (received from Prof. Dr. R. Feil, Tübingen; (Wegener et al. 2002))
- L1CAM KO (received from Prof. Dr. A. Furley, Sheffield; (Cohen et al. 1998))
- Talin2 KO (obtained from EMMA; (Debrand et al. 2012))
- Thy1YFP-H (received from Prof. R. Martini, Würzburg; (Feng et al. 2000))
- Itgb1-flox (received from Prof. Dr. C. Birchmeier-Kohler, MDC Berlin; (Graus-Porta et al. 2001))
- wnt1Cre (received from Prof. Dr. C. Birchmeier-Kohler, MDC Berlin; Jackson lab; (Danielian et al. 1998))
- FAK-flox (received from Prof. Dr. B. Rico, Alicante/London; (Beggs et al. 2003))
- Npr2-CreER^{T2} (generated in Prof. Dr. F. G. Rathen´s lab; (Ter-Avetisyan et al. 2014))
- R26RtdT (received from AG T. Misgeld, München; (Madisen et al. 2010))
- Zdhhc5 KO (obtained from EMMA)
- Cofilin-flox (received from Prof. Dr. F. Bradke, Bonn; (Flynn et al. 2012))
- Rac1-flox (received from Prof. Dr. C. Birchmeier-Kohler, MDC Berlin; (Chrostek et al. 2006))

- Spastin KO (obtained from KOMP)
- Ndst1 KO (Grobe et al. 2005) and Zdhhc13 loss of function (LOF) (Saleem et al. 2010) PFA-fixed E12.5 embryos were received from Prof. Dr. Lena Kjellén (Uppsala) and Prof. Dr. Y. T. Chen (Taiwan), respectively.

2.5 SPECIAL EQUIPMENT

Name	Company
BioPhotometer	Eppendorf
Cell culture hood	Thermo Scientific
Cell culture incubator	Binder
Centrifuge 5424 R	Eppendorf
Centrifuge 5804	Eppendorf
Centrifuge Megafuge 10R	Thermo Scientific
Centrifuge Sorvall RCM159 GX	Thermo Scientific
Centrifuge Sorvall WX Ultra 80	Thermo Scientific
Chemi Doc	BioRad
Chicken egg incubator	EHRET
Confocal microscope LSM710	Zeiss
Cryostat CM1950	Leica
Gel Doc XR+	BioRad
Mastercycler Gradient	Eppendorf
Microscope Axiovert135	Zeiss
pH meter	Mettler Toledo
S100AT4-626 rotor	Thermo Scientific
SDS-PAGE cell Protean II	BioRad
Sorvall HS-4 swinging bucket rotor	Thermo Scientific
Sorvall M150 centrifuge	Thermo Scientific
Sorvall RC6+ centrifuge	Thermo Scientific
Sorvall TH-641	Dupont
Stereomicroscope Stemi 305	Zeiss
TC20™ automated cell counter	BioRad
Thermocycler C	Eppendorf
Thermocycler Supercycler	Kyratec
Western blot cell Protean II	BioRad

3. METHODS

3.1 CULTURE OF CELL LINES

3.1.1 F11 cells

F11 cells were cultivated in DMEM/F-12 medium supplemented with GlutaMAX™ (Gibco), 10% (v/v) FCS (Gibco), 1% (v/v) HAT media supplement (Invitrogen) and 100 U/µL Penicillin/Streptomycin (Gibco) at 37°C with 95% air and 5 % CO_2. The starvation medium was identical but without FCS.

3.1.2 PC12 cells

PC12 cells were cultivated in DMEM medium (Gibco) supplemented with 5% (v/v) HS (Gibco), 10% (v/v) FCS (Gibco) and 100 u/µL Penicillin/Streptomycin (Gibco) at 37°C with 95% air and 5% CO_2.

3.2 IMMUNOHISTOCHEMISTRY

Immunohistochemistry was performed on 15-µm thick cryosections of developing mouse embryo spinal cords that were fixed at 4°C for 4h in 4% PFA in 1X PBS, 45 min in 15% sucrose in 1X PBS and overnight in 30% sucrose in 1X PBS, embedded and frozen in O.C.T. compound (Tissue-Tek). Tissues were sectioned with the help of a cryostat (Leica) and disposed on gelatin-coated glass microscope slides (Thermo Scientific). A border was created with a special pen on each slide that was immunostained. Firstly, sections were blocked one hour at RT in blocking buffer containing 1X PBS, 0.1 Triton X-100, 1% heat-inactivated goat serum or 1% BSA if a primary antibody raised in goat was used. Next, blocking buffer was sucked off using vacuum and the primary antibody diluted in blocking buffer was added on top of the sections. Slides were incubated overnight at 4°C. The next day, slides were washed 3 times 10 min in washing buffer containing 1X PBS and 0.1% Triton X-100 at RT. Then, an appropriate secondary antibody coupled to a fluorophore diluted in blocking buffer was added on top of the sections. Slides were incubated 2 hours at RT with

diluted secondary antibody and were then washed 3 times 10 min in washing buffer and the procedure was repeated for another primary antibody without repeating the initial blocking step. In the end of the sequence, a DAPI counterstaining could be performed to stain nuclei 15 min, RT at a concentration of 1 µg/ml in blocking buffer (Dianova). Finally, sections were washed 3 times 10 min in washing buffer, 2 times 5 minutes in 1X PBS and briefly dipped into ddH_2O before being embedded in Immu-Mount (Thermo Scientific) and covered with a 50 mm cover slip (Thermo Scientific). Note that all incubations were performed in a humid chamber protected from light and that all solutions containing blocking buffer were centrifuged 5 min at 13´000 rpm and 4° C prior to any incubation in order to clear solutions from possible precipitate that could have led to unspecific staining.

3.3 COATING OF CELL CULTURE DISHES

Cell culture plates (Nunc), Lumox® dishes (Sarstedt) or 12-well chamber, removable glass slides (Ibidi) were coated 6h at 37°C with sterile 0.1 mg/ml poly-D-lysine solution (PDL, Sigma), washed 3 times with sterile ddH_2O and dried 30 min at RT before further laminin double coating.

Coating with laminin (from mouse, Gibco), collagen IV (from rat tail, Sigma), fibronectin (Sigma), TN-C (from chick, home-purified) and contactin-1 (from chick, home-purified) was performed overnight at 4°C in sterile PBS at a concentration of 10 µg/ml. Poly-D-lysine coating for cell adhesion assay was also done overnight at 4°C at a concentration of 0.1 mg/ml. After the coating was performed, cell culture plates, Lumox® dishes and 12-well glass slides were washed 3 times with sterile PBS and incubated at 37°C in HBSS (Gibco) containing 5 mg/ml BSA (biomol) for the adhesion assay or with medium used in the experiment until cells were plated. For the adhesion assay, wells were washed once with the experimental medium before plating cells.

3.4 CELL ADHESION ASSAY

3.4.1 Culture of embryonic mouse DRG dissociated cells

DRGs from E13.5 mouse embryos were collected and dissociated by trypsination as described below (section 3.5.1). 12-well glass slides from IBIDI were coated overnight with either 10 µg/ml of laminin-1 or 0.1 mg/ml poly-D-lysine in sterile 1X PBS at 4°C as described above (section 3.3). 20´000 cells were plated per well in 200 µl of DMEM medium (Gibco) containing 100 U/µL Penicillin/Streptomycin (Gibco), 500 nM CNP (Sigma) or its equivalent in ddH_2O, 1X B27 (Gibco) supplement and 10 ng/ml human β-NGF (Alomone labs) and incubated overnight at 37°C with 95% air and 5% CO_2. The next day cells were fixed in 4% PFA in 1X PBS at 37°C for 15 min and washed three times with 1X PBS prior to ICC.

3.4.2 Culture of F11 cells

F11 cells were starved overnight in a serum-free medium in order to lower possible stimulation effect coming from the FCS like cGMP, cAMP and other factors that could interfere with the cGMP stimulation. They were therefore incubated at 37°C with 95% air and 5% CO_2 in F-12 medium (with 1X GlutaMAX™) supplemented with 1% (v/v) HAT media supplement (Invitrogen) and 100 U/µL Penicillin/Streptomycin (Gibco). Cells were harvested in pre-warmed sterile PBS 1X containing 1 mM EDTA 15 min at 37°C, collected in 15 or 50-ml Falcon tubes and centrifuged 5 min, 1000 rpm at RT to separate them from the PBS/EDTA solution. Supernatant was discarded and the cell pellet washed with pre-warmed sterile PBS and again centrifuged 5 min, 1000 rpm at RT. The supernatant was discarded and 1 or 2 ml of starvation medium was added to the pellet. Cell concentration was assessed using Trypan Blue dye (BioRad) and the TC20™ automated cell counter (BioRad). Note that the cell living count was always more than 95%. F11 cells were plated in starvation medium at a concentration of 7000 cells per well (lumox® dishes, Sarstedt with 8-well Lab-tek chamber slides) or 20´000 cells per well (24-well cell culture plate, Cell Star). Cell culture plates were coated with either 10 µg/ml laminin-1, 10 µg/ml collagen IV, 10 µg/ml fibronectin, 0.1 mg/ml poly-D-lysine, 10 µg/ml TN-C or 10 µg/ml contactin-1. The cGMP analogue 8-pCPT-cGMP (Biomol) was added to a final concentration of 1 mM as well as its

equivalent in buffer (ddH$_2$O) in the control. Cells were incubated overnight at 37°C with 95% air and 5 % CO$_2$, then fixed 15 min with 0.25% glutaraldehyde in PBS at 37°C and washed 3 times with PBS 1X at RT.

3.4.3 Quantification of the cell adhesion

For embryonic DRG dissociated cells, cells were first stained by ICC for NeuN (Neuronal Nuclei) and L1CAM so that neuronal cells could be specifically visualized and all nuclei were counterstained by DAPI staining. Images were taken with a confocal microscope and a 20x objective. For each image, NeuN-L1CAM double-positive somas were counted and for each image this number was normalized by the average number of double-positive cells in the control of the replicate. The cell counting was performed with Zen 2011 Microscope software (Zeiss) and the statistical analysis with the Microsoft Excel 2010 program (Microsoft). The cell adhesion was assessed from 3 independent replicates.

For F11 cells, phase contrast images were taken with a light microscope using a 10x objective (Zeiss Axiovert 135). The cell counting was performed with Zen 2011 Microscope software (Zeiss) and the statistical analysis with the Microsoft Excel 2010 program (Microsoft). Note that values were normalized to the average value of control for each independent experiment. The cell adhesion was assessed at least from 3 independent replicates. P-values were calculated using an unpaired two-tailed Student´s t-test.

3.5 PRIMARY CELL CULTURE OF DRG NEURONS

3.5.1 2D culture of a single cell monolayer on a coated substrate

Mouse DRGs were collected from embryonic stage E12.5 C57BL/6 embryos and kept on ice in a 1.5-ml screw cap tube. They were then trypsinated 20-30 min at 37°C in HBSS (Gibco) containing trypsin. Trypsin-containing medium was carefully sucked off and fresh 1-ml pre-warmed DMEM/10%FCS/100 U/µL Penicillin/Streptomycin medium added (DMEM/FCS/P/S). Tissues were transferred into a 15-ml Falcon tube and 1-ml of DMEM/FCS/P/S medium was added with DNase I (10 ku/ml end

concentration, Sigma). Cells were dissociated with a fire polished Paster pipette (10 times up and down pipetting). They were then pelleted by centrifugation (5 min at 1000 rpm, RT) and the supernatant discarded. 2 ml of medium without FCS were added and cells were again dissociated and pelleted as above. Finally, they were re-suspended in 1 ml DMEM/P/S or DMEM/FCS /P/S and counted with the help of the Trypan Blue dye method (Biorad). Dissociated cells were plated at 10´000 cells per well (6-well Lumox® dishes from Sarstedt or 12-well glass slides from IBIDI) in corresponding medium of interest and incubated overnight at 37°C with 95% air and 5 % CO_2.

3.5.2 3D culture of single cells in a collagen gel matrix

200 µl of a collagen mix constituted of 1 mg/ml collagen (Collagen I, Rat Tail; Corning), 1X DMEM (from 10x DMEM, Sigma), 0.5X F12 medium (from 1X F12 medium, Gibco) and 0.8% $NaHCO_3$ (from a 7.5% (w/v) stock solution in ddH_2O) were given per well (8-well plastic slides, IBIDI). Note that a master mix without the $NaHCO_3$ had to be prepared before and kept on ice and when DRGs were ready to be added at a concentration of $2 \cdot 10^5$ cells/ml, 7.5% $NaHCO_3$ solution was added to the mix to trigger the polymerization of the collagen gel. Slides were incubated 45 minutes to one hour at 37°C with 95% air and 5% CO_2 until the gel was fully polymerized. After that, 200 µl of medium were added to each well on top of the gel and explants were incubated overnight at 37°C with 95% air and 5 % CO_2.

3.6 DRG EXPLANT CULTURE

DRGs were prepared from stage E12.5 mouse embryos (C57Bl/6N) or E7 chick embryos corresponding to Hamburger and Hamilton stage 30 (V. Hamburger 1951) (fertilized SPF eggs, VALO) in ice-cold sterile PBS under a sterile preparation hood with the help of a binocular microscope (Zeiss). DRGs were cleaned from their remaining roots with a small scissor and kept in PBS on ice until plating.

3.6.1 2D culture of explants on a coated substrate

For DRG explants culture on PDL/laminin double-coated 12-well glass slides (IBIDI) the procedure was adapted from (Wang & Marquardt 2012). Basically, 200 µl of medium were added in each well. With the help of fine forceps (Dumont) DRGs were positioned in the middle of the well at the medium surface (one DRG per well). Slides were incubated 20 min at room temperature allowing explants to sink down to the bottom of the wells and attach to the substrate. Slides were incubated at 37°C with 95% air and 5 % CO_2 overnight or longer.

3.6.2 3D culture of explants in a collagen gel matrix

200 µl collagen mix constituted of 1 mg/ml collagen (Collagen I, Rat Tail; Corning), 1X DMEM (from 10x DMEM, Sigma), 0.5X F12 medium (from 1X F12 medium, Gibco) and 0.8% $NaHCO_3$ (from a 7.5% (w/v) stock solution in ddH_2O) were given per well (8-well plastic slides, IBIDI). Note that a master mix without the $NaHCO_3$ had to be prepared before and kept on ice and when DRGs were ready to be plated, 7.5% $NaHCO_3$ solution was added to the mix to trigger the polymerization of the collagen gel. DRGs were immediately positioned in the middle of the collagen gel and forced to go down to the bottom with the help of fine forceps (one DRG per well). Slides were incubated 45 minutes to one hour at 37°C with 95% air and 5 % CO_2 until the gel was fully polymerized. After that, 200 µl of medium were added to each well on top of the gel and explants were incubated overnight at 37°C with 95% air and 5 % CO_2.

3.7 NEURITE OUTGROWTH ASSAY WITH F11 CELLS

3.7.1 Culture of F11 cells

F11 cells were starved overnight, plated at 3500 cells per well on poly-D-lysine-laminin double-coated Lumox® dishes (Sarstedt) with an 8-well silicon grid (Lab-tek) and fixed as described for the cell adhesion assay.

3.7.2 Quantification of neurite length

Contrast pictures were taken with a light microscope using a 10x objective (Zeiss Axiovert 135). Measure of the neurites length was done with the help of Simple neurite tracer plugin in ImageJ software (Longair et al. 2011). Neurites were traced from the axon initial segment (AIS) until the tips and from the shaft until the tips of secondary, tertiary and quaternary branches. This allowed to calculate two values of interest: the average neurite length and the maximum neurite length. The average neurite length is the average neurite length calculated from the AIS to the tips of the central neurite and also to the second/third/fourth order branches of one process whereas the maximum neurite length is the longest measured neurite length emanating from one process (starting from one AIS). Note that values were normalized to the average value of control for each independent experiment. Statistical analyses were performed with the Microsoft Excel 2010 software (Microsoft). P-values were calculated using unpaired two-tailed Student´s t-tests.

3.8 NEURITE OUTGROWTH ASSAY WITH DRG EXPLANTS

3.8.1 Culture of DRG explants in a collagen gel matrix

E7 chick DRG explants were cultured as described above for DRG single cells in a collagen gel in DMEM medium (Gibco) containing 100 U/µL Penicillin/Streptomycin (Gibco), 500 nM CNP (Sigma) or its equivalent in ddH$_2$O, 1X B27 (Gibco) supplement and either 10 ng/ml or 5 ng/ml human β-NGF (Alomone labs). In experiments where S-palmitoylation was blocked, 2BP was present at a concentration of 100 µM (from a freshly prepared 100 mM stock solution diluted in ethanol). Note that in experiments containing 2-BP, same amount of ethanol was added to the controls. Explants were incubated overnight at 37°C with 95% air and 5 % CO$_2$. The next day, media were sucked off and explants were fixed in 4% PFA in 1X PBS 2 hours at room temperature. PFA solution was then discarded. Gels were washed 3 times with 1X PBS and stored at 4°C until further ICC was performed.

3.8.2 Quantification of the axonal length

Explants were stained by ICC for NCAM and images were taken with the help of a confocal microscope and a 10x objective. Maximum projections pictures were used to quantify the axonal outgrowth per explants by averaging the axonal halo length in all 4 cardinal directions from the border of the explant to the tip of the halo front with the tracing bar in Corel Draw X3 software (Corel Corporation). Note that values were normalized to the average value of control for each independent experiment. Statistical analyses were performed with the Microsoft Excel 2010 software (Microsoft). P-values were calculated using unpaired two-tailed Student´s t-tests.

3.9 NEURITE OUTGROWTH ASSAY WITH DRG SINGLE CELLS

3.9.1 Culture of DRG single cells in a collagen gel matrix

E7 chDRG primary cells were cultured in collagen gel as described above overnight in DMEM (Gibco) serum free medium containing 1X B27 (Gibco), 10 ng/ml human β-NGF (Alomone labs) and either 500 nM CNP (from a 456 µM stock solution in ddH$_2$O, Sigma) or its equivalent in ddH$_2$O (control). Gels were then fixed with PFA and washed with PBS as described above for DRG explants.

3.9.2 Quantification of the axonal length

Single cells were stained by ICC for NCAM and pictures were taken with the help of a confocal microscope and a 10x objective. Maximum projection pictures were used to measure the axonal outgrowth at a single cell level using Simple neurite tracer plugin in ImageJ software as described above for the F11 cells (Longair et al. 2011). Note that values were normalized to the average value of control for each independent experiment. Statistical analyses were performed with the Microsoft Excel 2010 software (Microsoft). P-values were calculated using unpaired two-tailed Student´s t-tests.

3.10 GROWTH CONE MORPHOLOGY ASSAY

3.10.1 Culture of DRG explants on a coated substrate

E7 chDRG or E12.5 mDRG explants were cultured as described above on PDL/laminin double-coated 12-well glass slides (IBIDI). However, they were cultured overnight in 200 µl DMEM (Gibco) serum free medium containing 1X B27 (Gibco) and 10 ng/ml human β-NGF (Alomone labs). The next day, 50 µl pre-warmed DMEM containing 1X B27 and 2500 nM CNP (from a 456 µM stock solution in ddH$_2$O, Sigma) or its equivalent in sterile ddH$_2$O were added for an end concentration of 500 nM CNP and 8 ng/ml human β-NGF. In experiments where S-palmitoylation was blocked, 2BP was present in these 50 µl at a concentration of 100 µM (from a freshly prepared 100 mM stock solution diluted in ethanol) so that the end concentration was of 20 µM. Note that in experiments containing 2-BP, same amount of ethanol was added to the controls. Explants were then incubated 1 hour at 37°C with 95% air and 5 % CO$_2$. After the stimulation, 50 µl of medium were pipetted off from each well and 200 µl of pre-warmed 2% PFA, 15% sucrose in 1X PBS were gently added one sidewall of the wells. This allowed to fix the explants minimizing the morphological stress that could have led to the detachment of GCs (Wang & Marquardt 2012). Slides were incubated 45 min at RT allowing the fixative to slowly sink down to the bottom of the wells. The 200 µl of the upper phase containing the medium was then sucked off with a micropipette and 200 µl of fresh fixative solution were slowly added along the sidewall of the wells. Slides were incubated 3 hours at RT to complete the fixation. Explants were then washed 3 times 10 min with 1X PBS at RT and stored at 4°C until further ICC was performed.

3.10.2 Quantification of the GC area and filopodia length

Explants were stained by ICC for α-tubulin and phalloidin (F-actin) revealing the morphology of GCs. Images were taken with a confocal microscope and 100x oil objective. Merged double stained pictures were used and the tracing tool in Zen software blue edition (Zeiss) allowed the tracing of the GCs area. The beginning of the GC was identified by an enlargement of the axon shaft. As the general GC area varied from one independent experiment to another, GC areas were normalized by

the average GC area of the control for each independent experiment. The number of filopodia per GC was assessed using Zen software blue edition (Zeiss) and filopodia length using the Simple neurite tracer plugin in ImageJ software as described above for the F11 cells (Longair et al. 2011). Note that values were normalized to the average value of control for each independent experiment. Statistical analyses were performed with the Microsoft Excel 2010 software (Microsoft). P-values were calculated using paired and unpaired two-tailed Student´s t-tests.

3.11 IMMUNOCYTOCHEMISTRY

3.11.1 2D culture of a single cell monolayer or explants on a coated substrate

F11 cells and DRG primary cells were fixed 15 min at 37°C with pre-warmed 4% PFA in 1X PBS and washed 3 times 5 minutes in 1X PBS at RT. They were then incubated 4 min in 1X PBS, 0.1% Triton X-100 at RT so that the membranes could be permeabilized. Cells were washed 3 times 5 min with 1X PBS to get rid of the Triton-X100 and blocked 10 min in blocking buffer consisting in 1X PBS supplemented with 1% heat-inactivated goat serum or 1% BSA if a primary antibody was raised in goat. After that, the blocking buffer was discarded and the diluted primary antibody in blocking buffer was added. Cells were incubated 1h at RT and washed 3 times 5 min in 1X PBS. Diluted secondary antibody in blocking buffer was added and slides were once again incubated 1h at RT. They were then washed 3 times 10 min in 1X PBS and the procedure was repeated for another primary antibody without performing the initial blocking step. In the end of the sequence, a DAPI counterstaining (Dianova) could be performed to stain nuclei 15 min, RT at a concentration of 1 µg/ml in blocking buffer. Finally, cells were washed 3 times 5 min in 1X PBS, embedded in Immu-Mount (Thermo Scientific) and covered with a 50 mm cover slip (Thermo Scientific).

Note that all incubations were performed in a humid chamber protected from light and that all solutions containing blocking buffer were centrifuged 5 min at 13´000 rpm and 4° C prior to any incubation in order to clear solutions from possible precipitate that could have led to unspecific staining.

DRG explants were fixed and washed as described below for the GC morphology assay. The staining procedure and embedding was performed as for primary cells but

with some changes. The incubation time for primary antibodies was extended to overnight at 4°C. Moreover, the incubation time for secondary antibodies was extended to 2h at RT and all washing steps were performed 10 min at RT.

3.11.2 3D culture of single cells or explants in a collagen gel matrix

DRG single cells or explants were fixed 2h at RT in pre-warmed 4% PFA in 1X PBS and washed 3 times 10 min in 1X PBS. They were then blocked 1h at RT in blocking buffer containing 1% heat-inactivated goat serum, 2% BSA and 0.1% Triton X-100 in 1X PBS. Gels were incubated in primary antibody diluted in blocking buffer overnight at 4°C. The next day, gels were washed 5 times 1h with 1X PBS containing 0.1% Triton X-100 and were incubated overnight at 4°C in a secondary antibody diluted in blocking buffer. Finally, gels were washed 5 times 1h with 1X PBS containing 0.1% Triton X-100 and 3 times 5 min with 1X PBS. They were stored in 1X PBS at 4°C protected from light until microscopy was conducted.

3.12 COLOCALIZATION STUDY

Measure of the colocalization by the Mander´s approach (Mander´s colocalization coefficient, MCC) (Manders et al. 1993) to investigate the percentage of cGKI-positive pixels colocalizing to specific intracellular membranes markers (tM1) or vice-versa (tM2) after threshold calculation using the Costes regression (Costes et al. 2004) was assessed by selecting a region of interest (ROI, growth cone or whole cell) and with the help of the coloc 2 plugin from the image processing package Fiji running in Image J software.

3.13 CLICK CHEMISTRY

Visualization of the palmitoylome using bioorthogonal labelling and click chemistry was adapted from the previous work of the Rami Hannoush´s lab (Gao & Hannoush 2014b; Gao & Hannoush 2014a). This method takes advantage of the specific reaction between the azide and alkyne groups that allows by a copper-catalysed "click reaction" (Huisgen 1,3-dipolar cycloaddition reaction), using a click-conjugated

biotin, the labelling of palmitoylated proteins (Figure 10) (Gao & Hannoush 2014b; Gao & Hannoush 2014a). Embryonic DRG primary cells or F11 cells were first plated on poly-D-lysine-laminin double-coated plates and incubated overnight at 37°C with 95% air and 5 % CO_2. After that, the medium was changed with a fresh one containing 100 µM palmitic acid, azide (from a 100 mM stock solution, Invitrogen) or its equivalent in DMSO and cells were incubated again overnight under same conditions. This allowed the palmitate analogue to be incorporated onto palmitoylated proteins (Figure 10a-c). The next day, cells were washed 3 times with pre-warmed 1X PBS and then fixed 15 min at 37°C with pre-warmed 4% PFA in 1X PBS. They were then washed 3 times 5 min in 1X PBS at RT and stored at 4°C until click chemistry was performed (maximum one week).

Cells were permeabilized 4 min in 1X PBS, 0.1% Triton X-100 at RT and washed 6 times 5 min with 1X PBS at RT to get rid of the detergent. In each well, 100 µl of a mix containing 0.1 mM Biotin-PEG4-alkyne (from a 5 mM stock solution in DMSO, Sigma), 1 mM TCEP (from a 50 mM stock solution in ddH_2O, Sigma) and 1 mM $CuSO_4$ (from a 50 mM stock solution in ddH_2O, Sigma) in 1X PBS were added and cells were incubated 1h in the dark at RT (click reaction, Figure 10d). Note that the $CuSO_4$ and TCEP stock solutions had to be freshly prepared just before performing the experiment and the compounds had to be added in a alkyne-TCEP-$CuSO_4$ sequence to the PBS. Finally, cells were washed 6 times 5 min with 1X PBS at RT and stored at 4°C until immunocytochemistry was performed. Palmitoylated proteins could be visualized by strepatavidin-Cy5 (Figure 10e). The concentration of palmitic acid, azide was titrated in cultured F11 cells and 100 µM was chosen as a working concentration (Figure 11). Moreover, a control without palmitic acid, azide showed a low unspecific staining confirming the specificity of the click chemistry to the palmitate analogue (Figure 11).
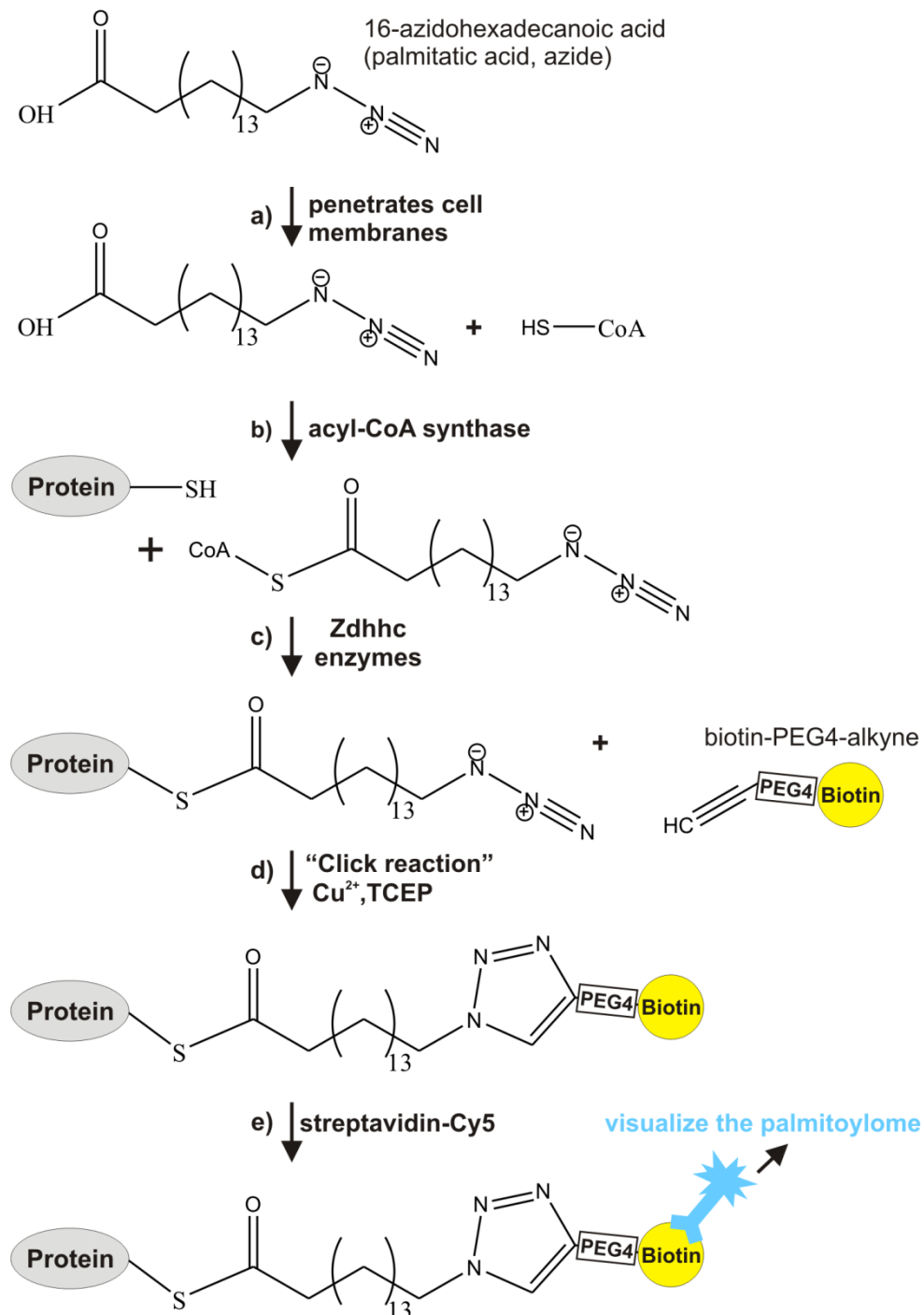
Figure 10 : Biorthogonal labelling of palmitoylated proteins: visualizing the palmitoylome in cultured F11 cells or DRG primary cells. **(a)** Cells were incubated with a standard medium supplemented with a palmitate analogue containing an azide (palmitic acid, azide). This compound penetrated cell membranes. **(b)** Inside the cell the acyl-coa synthase could couple the palmitate analogue to the coenzyme A (CoA). **(c)** The palmitate azide could therefore be transferred onto proteins by Zdhhc enzymes. **(d)** Cells were washed, fixed and incubated with biotin-PEG4-alkyne and the click reaction (cycloaddition) was catalysed by copper and TCEP in order to label palmitate analogues with biotin. **(e)** Hence, palmitoylated proteins could be detected with the help of streptavidin coupled to a fluorophore (Cy5, shown in cyan). Adapted from (Tom & Martin 2013; Gao & Hannoush 2014b; Gao & Hannoush 2014a).
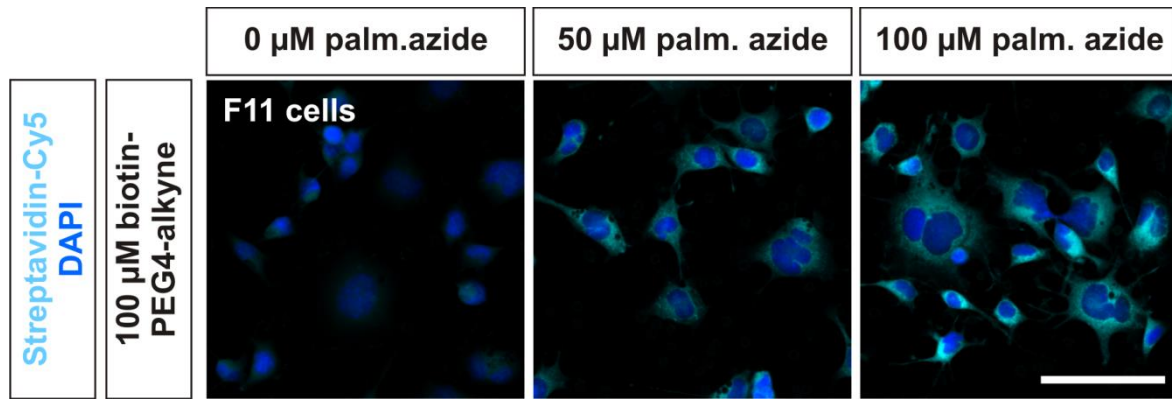
Figure 11 : Biorthogonal labelling of palmitoylated proteins: titration of palmitic acid, azide. F11 cells were incubated overnight in medium containing different concentrations of palmitic acid azide (palm. azide), washed, fixed and click chemistry reaction was used to label palmitoylated proteins with biotin (using biotin-PEG4-alkyne). Finally, biotinylated proteins were visualized with streptavidin coupled to the Cy5 fluorophore and nuclei were counterstained with DAPI. Cells treated with 0 μM palmitic acid, azide (palm. azide) showed almost no staining for streptavidin-Cy5 whereas 100 μM appeared to be the best concentration as reported by others for palmitic acid, alkyne (Gao & Hannoush 2014a; Gao & Hannoush 2014b). Scale bar: 100 μm.

3.14 cGMP AND CNP STIMULATION OF CELLS AND LYSATES

F11 cells were incubated overnight at 37°C with 95% air and 5 % CO_2 in starvation medium consisting of F11 cell medium (see above) without FCS. Cells were harvested with PBS/EDTA at 37°C, 13 minutes, washed once with pre-warmed 1X PBS and lysed in starvation medium using a 1-ml glass homogenizer. Lysates were split into two tubes. 50 mM of 8-pCPT-cGMP (Biolog) were added to one of the tube to a final concentration of 1 mM and equivalent amount of ddH_2O to the other (control). Samples were stimulated at 37°C, 10 min on a Thermomixer set at 600 rpm (Eppendorf). Then, samples were put on ice 10 min to stop the stimulation.

Freshly prepared E12.5-E13.5 mouse DRGs were collected in 2 different 1.5-ml screwed cap tubes and stimulated at 37°C, 10 min on a Thermomixer set at 600 rpm (Eppendorf) in 1X PBS containing either 1 μM CNP (Sigma) or its equivalent in ddH_2O (control).

The effect of the cGMP analogue (F11 cells) and CNP (DRG neurons) stimulation was confirmed by Western blotting of either cytosolic (F11 cells) or post-nuclear fractions (mouse DRGs) separated on a SDS-PAGE at 170 volts, 75 min. This allowed with the help of an antibody raised against VASP (a known target of cGKI (Lohmann & Walter 2005; Dhayade et al. 2016)) to verify the shift in the band of the

phosphorylated protein which migrate more slowly due to its charge compared to its non-phosphorylated form.

3.15 SUBCELLULAR FRACTIONATION

Cells or DRGs were lysed in a non-detergent lysis buffer typically containing 0.34 M sucrose in ddH_2O with a protease inhibitors cocktail (20 u/μl aprotinin, 5 mM leupeptin, 5 mM pepstatin A) and 100 mM PMSF or starvation medium (F11 cells). First, lysates were centrifuged 10 min at 2000 rpm, 4 °C to pellet the nuclei and remaining intact cells. Supernatants were the so-called post-nuclear fractions (PNFs) and were ultracentrifuged 15 min at 100´000 g, 4°C (Sorvall RC M150 GX in S100AT4-626 rotor). At this point the crude membrane protein fractions were pelleted by ultracentrifugation separating them from the supernatant containing the cytosolic protein fraction. The crude membrane pellets could be washed once again with the lysis buffer and ultracentrifuged like above to get rid of the maximum of cytosolic protein that were still in the first crude membrane pellet. The obtained crude membrane pellets were either further processed according to the acyl-biotin exchange chemistry protocol (see below) or solubilized if needed in 1% CHAPS in TBS 1X containing protease inhibitors and again ultra-centrifuged like above to pellet insolubilized material and debris. Supernatants were kept for further investigations. If needed, protein concentration of samples was assessed measuring the optical density at 280 nm (OD^{280}) with a photometer (Eppendorf).

3.16 ACYL-BIOTIN EXCHANGE CHEMISTRY

The acyl-biotin exchange (ABE) chemistry protocol was adapted from (Wan et al. 2007). This allowed to purify S-palmitoylated proteins using their specific hydroxylamine-sensitive cleavage of their thioester bond (Figure 12) (Wan et al. 2007; Roth et al. 2006). Cell lysates from either F11 cells crude membrane fractions, cytosolic fractions and PNFs (from 6 big culture flasks which contained at least 80% confluent cells) or mouse stage E13.5 DRG PNFs (from about 500 DRGs per condition) were used.

DRGs PNFs were first chloroform-methanol precipitated (see below) once in order to obtain a protein pellet.

Starting this point, F11 cells membrane fractions and DRGs PNFs were processed in the same way. Note that for DRG PNFs the volumes were scaled down because of the low amount of proteins and in order to fit within 1.5-mL screw-cap centrifuge tubes.

Pellets were dissolved in 600 µl 4% SDS buffer (4SB) 10 min at 37°C and 1.4 ml of ice-cold lysis buffer (LB) containing 10 mM N-ethylmaleimide (NEM, Thermo Scientific) and a protease inhibitors cocktail (20 u/µl aprotinin, 5 mM leupeptin, 5 mM pepstatin A) and 1mM PMSF was added. Triton X-100 (from a 20% stock solution in ddH$_2$O) was added to 1.7 % and tubes were incubated with end-over-end rotation for 1 hour at 4°C. This step allowed detergents to solubilize and denaturate proteins and give the NEM access to the free thiol groups of cysteines (Figure 12A). Insolubilized proteins and debris were pelleted at 2000 rpm, 10 min, and 4°C. Supernatants were transferred in 15-ml glass centrifuge tubes (Dupont Instruments) and a chloroform-methanol precipitation was performed to obtain a protein pellet. Pellets were solubilized in 600 µl 4SB containing 10 mM NEM 10 min at 37°C. 1800 µl of LB containing 1mM NEM, PIs (20 u/µl aprotinin, 5 mM leupeptin, 5 mM pepstatin A), 1mM PMSF and 0.2% Triton X-100 were added and samples were split into two 1,5-ml tubes and incubated overnight at 4°C with end-over-end rotation. This step allowed the NEM to maximally block the free cysteines (Figure 12A). The next day, samples were chloroform-methanol precipitated 3-times to get rid of the NEM. After the third precipitation, pellets were dissolved 10 min in a minimum of 250 µl 4SB at 37°C and were pooled for each treatment condition. Then, 240 µl were distributed into two 1.5-ml tubes and 960 µl +HA buffer or –HA buffer (control) were added and tubes were incubated at RT for 1 hour with end-over-end rotation. This step allowed on one hand to specifically cleave the S-palmitate from cysteines using hydroxylamine (HA, Sigma) and on the other hand the HPDP-biotin (Pierce) contained in the buffer could label newly free cysteines that were created (Figure 12B and C). The –HA buffer-treated samples were used as control as they were not incubated with hydroxylamine but still with HPDP-biotin which could serve to assess the unspecific labelling of the biotin moiety. Samples were chloroform-methanol precipitated once as before and pellets were dissolved 10 min in 250 µl 4SB at 37°C. 240 µl were then distributed into 1.5-ml tubes and 960 µl of low biotin buffer were

added. Tubes were incubated 1 hour at RT with end-over-end rotation. This step permitted to achieve the complete labelling of free cysteines with the HPDP-biotin moiety (Figure 12C). Samples were finally chloroform-methanol precipitated 3 times to get rid of the HPDP-biotin and after the third time pellets were dissolved in 2% SDS buffer (2SB) containing 20 u/µl aprotinin, 5 mM leupeptin, 5 mM pepstatin A and 1mM PMSF and were stored at -20°C until further experiments were performed.
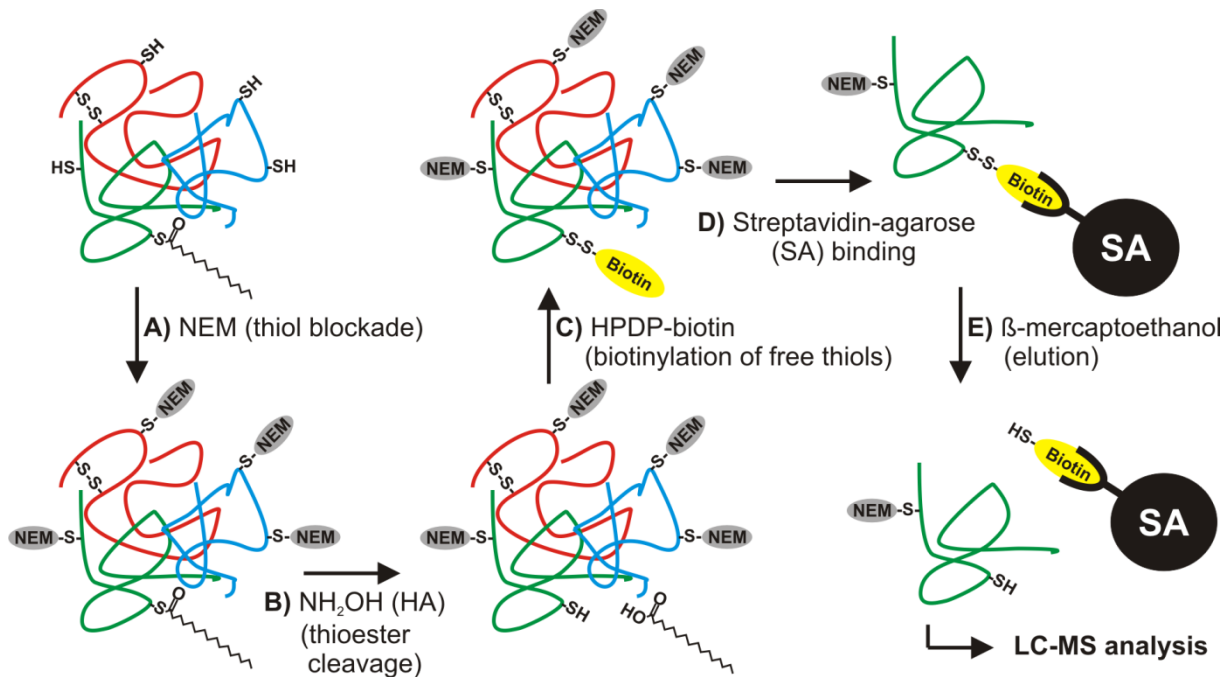
Figure 12 : Acyl-biotin exchange (ABE)-based approach to purify S-palmitoylated proteins. (A) Firstly, free cysteine thiols were blocked with N-ethylmaleimide (NEM, step A). Secondly, thioester bonds between cysteines and palmitates were specifically cleaved with hydroxylamine (NH_2OH or HA, step B). Thirdly, newly free thiols were specifically labelled with HPDP-biotin (step C). Finally, labelled proteins were pulled down with streptavidin-agarose (SA) beads and eluted with β-mercaptoethanol (step D and E). Adapted from (Wan et al. 2007)

3.17 CHLOROFORM-METHANOL PRECIPITATION

Chloroform-methanol precipitation was performed under the hood as described before and performed either in 15-ml glass centrifuge tubes (Dupont Instruments) or in 1.5-ml screw-cap centrifuge tubes (Wan et al. 2007). 4 volumes methanol were added to the samples and vortexed. Then, the same was done with 1.5 volumes chloroform. Finally, 3 volumes of ddH_20 were added to the mix and everything was vortexed a last time before being centrifuged at RT, 20 min, 6000 g in a Sorvall HS-4 swinging bucket rotor to separate phases. The solution separated into two phases (aqueous and organic phase) with proteins precipitated at the interphase. The upper

aqueous phase was discarded using a Pasteur pipette, taking care not to remove proteins at the interphase. 3 volumes methanol were added, tubes were inverted once to mix phases without much destroying the protein cluster and they were centrifuged 10 min like before. The supernatant could be discarded and the protein pellets was air-dried for maximum 5 min before further experiments.

3.18 AFFINITY PURIFICATION OF BIOTINYLATED PROTEINS

After the ABE chemistry was performed, the SDS concentration from samples was diluted to 0.1% with LB containing 0.2% Triton X-100, 20 u/μl aprotinin, 5 mM leupeptin, 5 mM pepstatin A and 1mM PMSF. Samples were then aliquoted in 1.5-ml tube (1 ml per tube) and incubated 30 min at RT with end-over-end rotation to dissolve insolubilized material. Samples were then centrifuged at 13´000 rpm for 5 min at RT (microcentrifuge) to pellet insolubilized material. Supernatants were transferred in a new 1.5-ml tube containing 15 μl pre-equilibrated high capacity streptavidin agarose resin (Thermo Scientific). Tubes were then incubated 90 min at RT with end-over-end rotation allowing the biotinylated proteins to bind streptavidin coupled to the agarose beads (Figure 12D). Afterwards, tubes were centrifuged at 13´000 rpm for 1 min (microcentrifuge), supernatants were discarded and beads pellets were washed 4 times with LB supplemented with 1% SDS, 0.2% Triton X-100 with a 10´000 centrifugation in-between each step (1 min at RT). This allowed to get rid of proteins which were not biotinylated. To reduce disulfide bridges from the HPDP-biotin and therefore to release proteins which were bound to the agarose beads, they were incubated 10 min in 15 μl β-mercaptoethanol-containing 1X sample buffer at 37°C (Figure 12E). Finally, samples were transferred and pooled into a filter spin columns (Ultrafree-MC DV Centrifugal Filter, Millipore) and centrifuged at 10´000 rpm for 5 min to separate the samples from the beads (Figure 12E). At this point samples were stored at -80°C until further experiments.

3.19 SDS-PAGE

Sodium dodecyl sulfate polyacrylamide gel electrophoresis (SDS-PAGE) was used to separate proteins by molecular weight (Laemmli 1970). The SDS contained in the gel

permitted to keep the proteins denatured. Denaturation of proteins is very important to keep the polypeptide chains unfolded. For that purpose, samples were boiled for 5 min in 1X sample buffer before loading (Laemmli 1970). β-mercaptoethanol contained in the sample buffer reduced disulfide bonds what allowed the denaturation of proteins. As an anionic detergent, SDS could bind proteins and give a net negative charge to proteins. Hence, proteins were separated based on their molecular weight. The size of the pores in the polyacrylamide gel allowed this separation: smaller proteins ran faster and further through the gel than bigger ones depending on the acrylamide concentration used.

The upper part of the gel was constituted of a stacking gel containing the wells in which samples were loaded. This gel contained a low concentration of acrylamide what allowed to stack proteins before entering the separating gel. Note that APS (GE Healthcare) and TEMED (GE Healthcare) were used to activate the polymerization of acrylamide (see table below). The separating gel contained a higher concentration of acrylamide. The higher the acrylamide concentration was, the better the separation of lower molecular weight proteins was because pores in the gel were smaller and only small proteins could run easily through the gel (Table 1). Gels were prepared in gel cassettes (BioRad). First, the separating gel solution was loaded up to 6-7 cm and isopropanol was then loaded to keep the upper gel front straight. Isopropanol stayed in the upper part because of its lower density. After the gel polymerized at RT (~20 min), isopropanol was removed and the stacking gel solution was loaded up to the top and a comb with ten 20-µl wells was inserted. After polymerization (~20-30 min) gels were stored at 4°C in a moistened box.

Solutions	Stacking gel	10 % separating gel	12 % separating gel
ddH$_2$O	3.7 ml	2.8 ml	2.1 ml
1 M Tris, pH 8.8	-	3.75 ml	3.75 ml
1 M Tris pH 6.8	0.65 ml	-	-
30% acrylamide	0.65 ml	3.3 ml	4 ml
10% SDS	50 µl	100 µl	100 µl
10% APS	25 µl	50 µl	50 µl
TEMED	10 µl	10 µl	10 µl

Electrophoreses were run in a 1-D vertical electrophoresis "Mini Protean Tetra Cell" (BioRad) in 1X running buffer (192 mM glycine; 25 mM Tris) containing 0.1% (w/v) SDS at 150 Volts for 60 minutes. Note that SDS-PAGE molecular weight standards

(BioRad) were used: a low standards mix and a high standards mix to assess the molecular weight of proteins (for silver staining, adapted standards were used). Note that for the "VASP test" gels were run at 170 Volts for 75 min in order to create a shift between the non-phosphorylated and the phosphorylated VASP bands.

3.20 SILVER STAINING OF SDS-PAGE

Silver staining was performed after that the purification of biotinylated proteins was achieved. Few microliters of each sample were run on SDS-PAGE and then silver stained. The purpose of this staining was to check whether the purification worked because one sample was used as control (without hydroxylamine treatment, -HA; see ABE chemistry) and also to see hypothetical differences in the palmitoylome of non-stimulated samples versus CNP or cGMP analogue-stimulated samples.

Silver staining after SDS-PAGE is a very sensitive colorimetric method used to detect protein bands in the low nanogram range. Silver ions bind amino acids as cysteines, glutamines and asparagines and then are reduced in metallic silver what permits to see bands of proteins in a polyacrylamide gel (Chevallet et al. 2006).

First, gel was transferred after SDS-PAGE in a glass container and proteins were fixed for 20 min (or overnight) in 6% TCA (Trichloroacetic acid), 1% $CuCl_2$ and 50 % methanol. The acid made proteins insoluble in the gel so they couldn't diffuse anywhere else in the gel during the subsequent steps. Then, the gel was washed 10 min in solution W (10% (v/v) ethanol, 5% (v/v) acetic acid) to wash all kinds of compounds that could hinder the silver staining (like detergents or ions). Next, the gel was incubated 10 min in 0.01% (w/v) $KMnO_4$ in ddH_2O, washed twice for 5 min in solution W and incubated 10 min in 10% (v/v) ethanol (sensitization step). The gel was then washed for 10 min in ddH_2O to eliminate sensitizing compounds. After this step, the silver impregnation was performed by incubating the gel for 10 min in 0.2% (w/v) $AgNO_3$. The gel was washed for 20 sec with ddH_2O to remove excess of silver ions and incubated 1 min in 10% (w/v) K_2CO_3. The gel was developed for 3-10 min in 2% (w/v) K_2CO_3, 0.01% formaldehyde in ddH_2O. Formaldehyde reduced the bound silver ions in metallic silver and bands of proteins appeared in the gel. Finally, it was washed for 10 min in solution W and transferred in ddH_2O.

Gel was first scanned (in case that the gel would have been damaged) and then put in-between two cellophane sheets and was dried by vacuum-drying for ~45 min. Finally, the gel was scanned again.

3.21 WESTERN BLOTTING

Western blot is a widely used method to transfer proteins that were previously separated via SDS-PAGE on a nitrocellulose (NC) membrane what allows then to identify selected proteins by immunoblotting with specific antibodies.

Here, the Mini Trans-Blot Electrophoretic Transfer Cell (BioRad) was used. The gel containing the separated proteins from the SDS-PAGE was typically mounted with a NC membrane on one side and "sandwiched" in-between 2 filter papers (Whatman) and 2 fiber pads. The layout was pressed in a gel holder cassette and introduced in a buffer tank inside an electrode module. The tank was filled with ice-cold blotting buffer (192 mM glycine, 25 mM Tris and 20% (v/v) methanol or isopropanol in ddH$_2$O). A cooling unit and a magnetic stirrer were also used to keep the blotting buffer cold and homogeneous. Proteins were transferred from the gel to the NC membrane for 60 min at 100 Volts, 4°C.

After that, the NC membrane was stained 5 min in Ponceau S solution (5% (v/v) acetic acid and 0.1% (w/v) Ponceau S in ddH$_2$O). Then, the membrane was washed with ddH$_2$0 and scanned. Ponceau S staining served to ensure that the transfer occurred and also to check whether the amount of proteins of each sample was more or less equally loaded. Molecular Markers were marked with a pencil. The membrane was blocked 1 hour in blocking buffer (3% BSA in 1X TBS supplemented with 0.5% (v/v) Tween-20). This step was essential to avoid non-specific binding of antibodies to the membrane. The NC membrane was incubated overnight with the primary antibody diluted in blocking buffer at 4°C on a rocking plate. The next day, the membrane was washed 5 times 5 min in washing buffer and incubated 3 hours in the secondary antibody diluted in blocking buffer at RT. Afterwards, the membrane was washed 5 times 5 min in washing buffer and one time 10 min in 1X PBS. All secondary antibodies were coupled to HRP (Horse Radish Peroxidase). Thus, an enhanced chemiluminescent assay was used for the detection of proteins bands tagged with the first and secondary antibodies (Pierce ECL Western Blotting Substrate, Pierce). After at least 5 minutes incubation in the ECL substrate in the

dark, the membrane was developed in a ChemiDoc XRS system (BioRad) coupled to a BioRad CCD-Kamerasystem and using Quantity One 4.6.5 software.

3.22 DiI TRACING

DiI tracing of DRG axons was mostly performed as described before (Schmidt & Rathjen 2011). Spinal cords with attached DRGs were dissected from stage E12.5-E13.5 mouse embryos in cold 1X PBS with the help of small forceps and a microscopic scissor (Fine Science Tools) under a microscope. Tissues were then fixed 4 hours in 1X PBS containing 4% PFA at 4°C and afterwards transferred into ice-cold 1X PBS. They were stored at 4°C until DiI tracing was performed. The day of injection, spinal cords were opened ventrally in order to have an inverted open-book preparation and disposed on a glass slide with the dorsal side up. A micropipette puller (Sutter) was used to create a glass needles with an extra thin tip with the following settings: 1. HEAT=620, VEL= 200, TIME=125; 2. HEAT=620, VEL= 210, TIME=125; 3. HEAT=620, VEL= 200, TIME=100). Under a microscope, approximatively 1 mm of the needle tip was broken using forceps. 0.8 µl of a DiI solution of 5 % (w/v) in ethanol (Sigma) was pipetted with a micropipette and pipetted out at the tip. The liquid could flow down the micropipette tip and ethanol evaporated resulting in the formation of crystals of DiI on its surface. Crystals were collected by gently scratching the surface with the needle tip. At this point, crystals were injected in every 2 DRGs by penetrating the tip of the needle within the DRGs. Note that two crystal-coated glass needles were used per spinal cord. Spinal cords were put back into 1X PBS and incubated overnight at RT in the dark so that the dye could diffuse along the plasma membrane. The next day, spinal cords were mounted with the dorsal side down on glass cover slips (Thermo Scientific) in 1X PBS and covered with a smaller cover slip. They were either immediately used for confocal microscopy or stored at 4°C for maximum 3-4 hours until microscopy was performed (Zeiss LSM710 confocal microscope).

DiI tracing of commissural axons was basically conducted in the same way with some modifications. Firstly, DRGs were cut off from the spinal cords. Spinal cords were opened on the dorsal side (open-book preparation) and the dye was injected laterally in the spinal cord within the first third of the dorsal side once every 2 segments

(Wilson & Stoeckli 2012). Moreover, tissues were incubated 2 days at RT instead of one and mounted with the ventral part down.

3.23 THY1-YFP-H^{tg} MOUSE SPINAL CORD PREPARATION

The Thy1-YFP-H mouse line express the fluorescent protein YFP under the Thy1 promotor inducing a sparse labelling of DRG axons in post-natal mice (Feng et al. 2000). Spinal cords together with the surrounding bone structure were dissected from P13-P21 Thy1-YFP-H heterozygous (Thy1-YFP-H[tg]) mice. The dorsal part of the bone structure was cut and removed. Dorsal roots were sectioned and spinal cords extracted from the remaining bone structure. Spinal cords were fixed 2-3h at 4°C in 1X PBS containing 4% PFA and flattened overnight at 4°C in 1X PBS in-between two microscopy slides (Thermo Scientific). The next day, spinal cords with the dorsal side down were investigated under a confocal microscope (Zeiss LSM710).

3.24 LIPID RAFTS ISOLATION

Lipid rafts isolation was performed using a detergent-free sucrose density centrifugation as described before (Persaud-Sawin et al. 2009; Ostrom & Liu 2007). Shortly, PC12 cells were harvested with PBS/EDTA, washed once with PBS and homogenized with a 1-ml glass-homogenizer in 500 µl detergent-free lysis buffer (20 u/µl aprotinin, 5 mM leupeptin, 5 mM pepstatin A, 1 mM PMSF, 1 mM $CaCl_2$ and 1 mM $MgCl_2$ in TBS 1X). Lysates were centrifuged 10 min, 2000 rpm at 4°C to pellet the insolubilized fraction and homogenization was repeated at least 3 times on the pellets until it reached a collected-volume of 2 ml of supernatant. 2-ml lysates were mixed with 2 ml 90% sucrose in TBS 1X and loaded at the bottom of a 12-ml ultracentrifuge tube (Sorvall). This was overlaid with 4 ml of 35% sucrose in TBS 1X and finally, 2 ml of 5% sucrose in TBS 1X were gently added on top of it. Tubes were centrifuged between 17-19 hours at 260´000 g (max velocity) in a swinging-bucket rotor (Sorvall TH-641, Dupont) and fractions were collected from the top to the bottom and immediately mixed with 5x sample buffer and boiled 5 min before being stored at -20°C.

3.25 MASS SPECTROMETRY

Mass spectrometry (MS) manipulations and raw data analysis were performed by the MS platform facility of the MDC Berlin (Alina Dagane and Dr. G. Dittmar). Samples were "in-gel digested" to get rid of the detergent and high throughput label-free LC-MS was used to analyse both stimulated and non-stimulated samples (Figure 12) (Egelhofer et al. 2013). Detected proteins which were increased or decreased upon cGMP analogue stimulation in all 3 stimulated samples from an independent experimental triplicate were selected and known false-positive proteins were discarded (Wan et al. 2007). Moreover, 2-hit candidates which were increased upon stimulation were also considered as potential interesting targets as the "in-gel digestion" and further purification might have led to the loss of peptides.

3.26 GENOTYPING OF MOUSE LINES

Either ear clips (adult mice) or a piece of paw (embryos) was incubated in PCR tail lysis buffer (homemade) containing proteinase K (1:100, Genaxxon) at 55°C overnight in order to degrade proteins, solubilize tissues and digest DNA. The next day, proteinase K was deactivated by incubating samples 45 min at 85°C. Genotyping of different mouse lines was performed using PCR reactions (Saiki et al. 1988). PCR products were separated by agarose gel electrophoresis in agarose gels containing ethidium bromide (1:10000, Biochemica) and developed using Gel Doc XR+ (BioRad). Note that the genotyping of cofilin-flox, L1CAM, Hprt and spastin mice was performed by Mechtild Henning.

3.26.1 PCR primers

Mouse Strain	Primer Name	Primer Sequence (5´-3´)	Product
cGKI	cGKI_RF_125	GTCAAGTGACCACTATG	284 bp (WT) 250 bp (KO)
	cGKI_RF_53	CCTGGCTGTGATTTCACTCC	
	cGKI_RF_118	AAATTATAACTTGTCAAATTCTTG	
L1CAM	L1F3	GGTGCAAGGGTGACATTCACGT	420 bp (WT) 260 bp (KO)
	L1B3	TGCTCTCCACCTCATCCAGTTCAG	
	NeoF1	TGGAGAGGCTATTCGGCTATGAC	
	NeoB5	AGCAAGGTGAGATGACAGGAGATC	
Tln2 (talin-2)	379	GGAGATGTTTAAAATGTGACTAGGC	150 bp (WT)
	380	TTGTCGAGTCATTAGGGAGAGA	
	381	TCTGGGCCACAGAATACAAGATG	292 bp (KO)
	382	ATAAAGCCATCTGCAACACAGCAA	
Thy1YFP-H	IL_oIMR0043	GTAGGTGGAAATTGTAGCATCATCC	324 bp (WT) 173 bp (mutant allele)
	IL_oIMR0042	CTACGCCACAGAATTGAAAGATCT	
	GFP_oIMR2416	TCCTTGAAGAAGATGGTGCG	
	GFP_oIMR0872	AAGTTCATCTGCACCACC	
Zdhhc5 KO	DHHC5_FOR	TGACAGTGGAGAAACCCAAA	152 bp (WT) 304 bp (KO)
	DHHC5_REV_WT	TGAAGCAACTTAAAAGTTTTTGGAC	
	DHHC5_REV_KO	TGGGACCACCTCATCAGAAG	
Itgb1-flox	Itgb1_for	GTGAAGTAGGTGAAAGGTAAC	320 bp (WT) 400 bp (flox)
	Itgb1_rev	GGGTTGCCCTTCCCTCTAG	
wnt1Cre	wnt1-Cre_215	TAAGAGGCCTATAAGAAGCGG	550 bp (mutant allele)
	Brn1-Rv	AGCCCGGACCGACGATGAA	
FAK-flox	FAK_flox_for	GAATGCTACAGGAACCAAATA	290 bp (WT) 400 bp (flox)
	FAK_flox_rev	GAGAATCCAGCTTTGGCTGTT	
Npr2-CreERT2	Cre-WT_right	CTCAGATTCCTCCCTTCTCG	456 bp (WT) 356 bp (mutant allele)
	Cre-rec_right	GGCATAGCTCAGGTTGTGTT	
	Cre-WT/Rec_left	TTGGACATGGTGGAATTCAT	
R26RtdT	oIMR9020	AAGGGAGCTGCAGTGGAGTA	297 bp (WT)
	oIMR9021	CCGAAAATCTGTGGGAAGTC	
	oIMR9103	GGCATTAAAGCAGCGTATCC	196 bp (mutant allele)
	oIMR9105	CTGTTCCTGTACGGCATGG	
Rac1-flox	Rac1-flox_for	GTCTTGAGTTACATCTCTGG	236 bp (WT) 318 bp (flox)
	Rac1-flox_rev	CTGACGCCAACAACTATGC	

3.26.2 PCR reaction mixes

cGKI KO		L1CAM KO	
16.8 µl	ddH$_2$O	13.3 µl	ddH$_2$O
2.5 µl	10x buffer (Inv.)	2 µl	10x buffer (Inv.)
1.5 µl	50 mM MgCl$_2$ (Inv.)	0.8 µl	50 mM MgCl$_2$ (Inv.)
0.5 µl	dNTPs (10 mM each)	0.4 µl	dNTPs (10 mM each)
0.3 µl	Primer cGKI_RF_125 (10 µM)	0.4 µl	Primer L1F3 (10 µM)
0.25 µl	Primer cGKI_RF_53 (20 µM)	0.4 µl	Primer L1B3 (10 µM)
0.4 µl	Primer cGKI_RF_118 (25 µM)	0.4 µl	Primer NeoF1 (10 µM)
2.5 µl	DNA template	0.4 µl	Primer NeoB5 (10 µM)
0.25 µl	Taq-polymerase (NEB)	1 µl	DNA template
		0.3 µl	Taq-polymerase (Inv.)

talin-2 WT		talin-2 KO	
16.6 µl	ddH$_2$O	16.6 µl	ddH$_2$O
2.5 µl	10x buffer (Inv.)	2.5 µl	10x buffer (Inv.)
0.75 µl	50 mM MgCl$_2$ (Inv.)	0.75 µl	50 mM MgCl$_2$ (Inv.)
2 µl	dNTPs (2.5 mM each)	2 µl	dNTPs (2.5 mM each)
0.2 µl	Primer 379 (100 µM)	0.2 µl	Primer 381 (100 µM)
0.2 µl	Primer 380 (100 µM)	0.2 µl	Primer 382 (100 µM)
2.5 µl	DNA template	2.5 µl	DNA template
0.25 µl	Taq-polymerase (Inv.)	0.25 µl	Taq-polymerase (Inv.)

Thy1YFP-H		Itgb1-flox	
13.3 µl	ddH$_2$O	19 µl	ddH$_2$O
2.5 µl	10x buffer (Inv.)	3 µl	10x buffer (Inv.)
1.5 µl	50 mM MgCl$_2$ (Inv.)	1.8 µl	50 mM MgCl$_2$ (Inv.)
0.25 µl	dNTPs (10 mM each)	3 µl	dNTPs (2.5 mM each)
1.25 µl	Primer IL_oIMR0043 (10 µM)	1 µl	Primer Itgb1_for (10 µM)
1.25 µl	Primer IL_oIMR0042 (10 µM)	1 µl	Primer Itgb1_rev (10 µM)
2.5 µl	Primer GFP_oIMR2416 (10 µM)	1 µl	DNA template
2.5 µl	Primer GFP_oIMR0872 (10 µM)	0.3 µl	Taq-polymerase (Inv.)
2.5 µl	DNA template		
0.25 µl	Taq-polymerase (NEB)		

wnt1Cre		FAK-flox	
18.65 µl	ddH$_2$O	16.6 µl	ddH$_2$O
2.5 µl	10x buffer (Inv.)	2.5 µl	10x buffer (Inv.)
1 µl	50 mM MgCl$_2$ (Inv.)	0.75 µl	50 mM MgCl$_2$ (Inv.)
0.5 µl	dNTPs (10 mM each)	2 µl	dNTPs (2.5 mM each)
0.1 µl	Primer wnt1-Cre_215 (100 µM)	0.2 µl	Primer P2 (100 µM)
0.1 µl	Primer Brn1-Rv (100 µM)	0.2 µl	Primer P3 (100 µM)
0.9 µl	DMSO	2.5 µl	DNA template
1 µl	DNA template	0.25 µl	Taq-polymerase (Inv.)
0.25 µl	Taq-polymerase (Inv.)		

Npr2-CreERT2		R26RtdT WT	
17.3 µl	ddH$_2$O	15.95 µl	ddH$_2$O
2.5 µl	10x buffer (Inv.)	2.5 µl	10x buffer (Inv.)
0.75 µl	50 mM MgCl$_2$ (Inv.)	2 µl	50 mM MgCl$_2$ (Inv.)
0.5 µl	dNTPs (10 mM each)	0.5 µl	dNTPs (10 mM each)
0.4 µl	Primer Cre-WT_right (50 µM)	0.4 µl	Primer oIMR9020 (50 µM)
0.4 µl	Primer Cre-rec_right (50 µM)	0.4 µl	Primer oIMR9021 (50 µM)
0.4 µl	Primer Cre-WT/Rec_left (50 µM)	3 µl	DNA template
2.5 µl	DNA template	0.25 µl	Taq-polymerase (Inv.)
0.25 µl	Taq-polymerase (NEB)		

Zdhhc5 KO		Rac1-flox	
17.39 µl	ddH$_2$O	17.6 µl	ddH$_2$O
2.5 µl	10x buffer (Inv.)	2.5 µl	10x buffer (Inv.)
3 µl	25 mM MgCl$_2$ (Takara)	1.5 µl	25 mM MgCl$_2$ (Takara)
0.5 µl	dNTPs (10 mM each)	0.25 µl	dNTPs (10 mM each)
0.12 µl	Primer DHHC5_FOR (100 µM)	0.2 µl	Primer DHHC5_FOR (100 µM)
0.12 µl	Primer DHHC5_REV_WT (100 µM)	0.2 µl	Primer DHHC5_REV_WT (100 µM)
0.12 µl	Primer DHHC5_REV_KO (100 µM)	2.5 µl	DNA template
1.5 µl	DNA template	0.25 µl	Taq-polymerase (Inv.)
0.25 µl	Taq-polymerase (Inv.)		

3.26.3 PCR programs

cGKI KO		L1CAM KO		talin-2 WT/KO	
5´	94°C	5´	94°C	2´	94°C
35x		30x		35x	
10´´	94°C	30´´	94°C	15´´	94°C
45´´	55°C	30´´	60°C	30´´	55°C
30´´	72°C	60´´	72°C	60´´	72°C
5´	72°C	10´	72°C	10´	72°C
forever	4°C	forever	4°C	forever	4°C

Thy1YFP-H		Itgb1-flox		wnt1Cre	
3´	94°C	2´	95°C	4´	94°C
35x		3x		40x	
30´´	94°C	2´	95°C	30´´	95°C
30´´	60°C	30´´	65°C	30´´	55°C
60´´	72°C	45´´	72°C	60´´	72°C
5´	72°C	3x		7´	72°C
forever	4°C	30´´	95°C	forever	4°C
		30´´	60°C		
		45´´	72°C		
		35x			
		30´´	95°C		
		30´´	55°C		
		45´´	72°C		
		10´	72°C		
		forever	4°C		

FAK-flox/Rac1-flox		Npr2-CreERT2		R26RtdT	
2´	94°C	3´	94°C	2´	94°C
35x		35x		10x	
15´´	94°C	30´´	94°C	20´´	94°C
30´´	55°C	30´´	57°C	15´´	65°C
60´´	72°C	30´´	72°C	25´´	68°C
10´	72°C	10´	72°C	28x	
forever	4°C	forever	4°C	15´´	94°C
				15´´	50°C
				25´´	72°C
				2´	72°C
				forever	4°C

Zdhhc5 KO	
3´	94°C
35x	
30´´	95°C
30´´	60°C
30´´	72°C
10´	72°C
forever	4°C

3.26.4 Examples of PCR
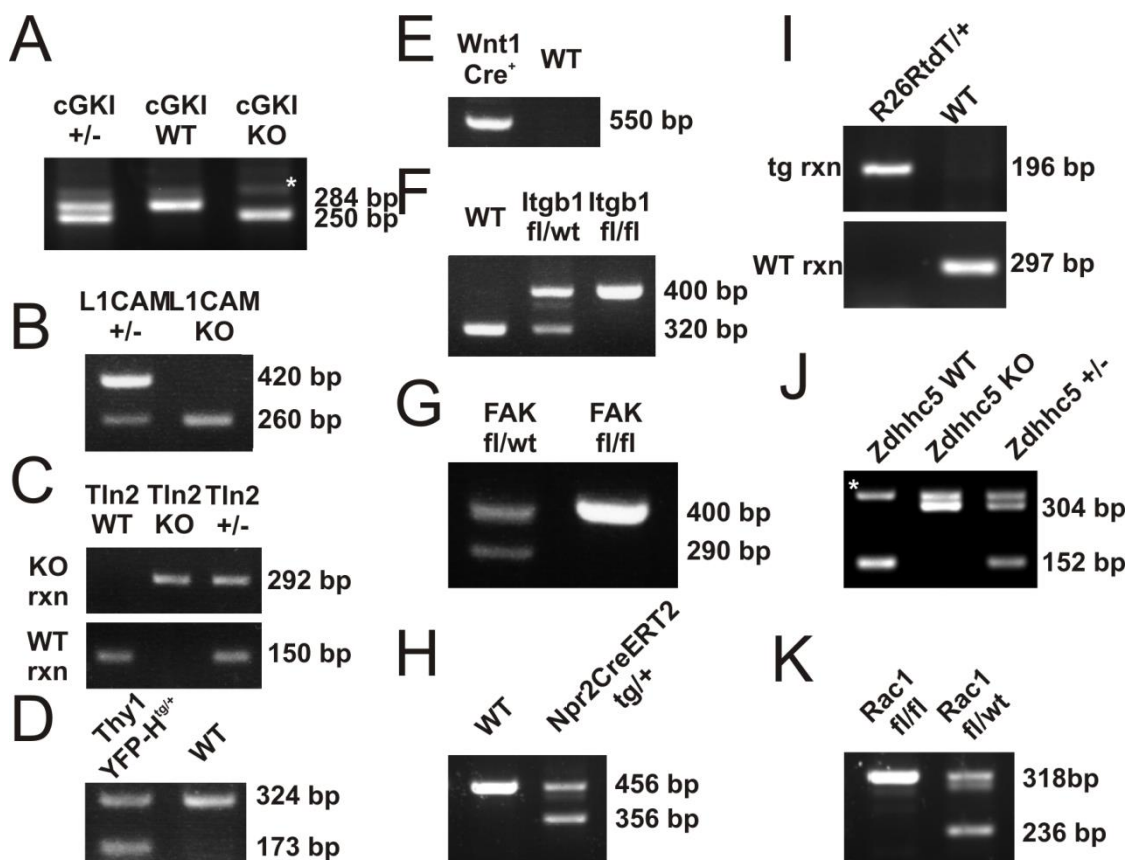
Figure 13 : Examples of genotyping of the various mouse lines used in this study. PCR products were separated by agarose gel electrophoresis containing ethidium bromide. **(A)** cGKI KO. **(B)** L1CAM KO. **(C)** Talin-2 (Tln2) KO. **(D)** Thy1YFP-H tg. **(E)** Wnt1cre tg. **(F)** Integrin-β1 (Itgb1)-flox. **(G)** FAK-flox. **(H)** Npr2CreERT2 tg. **(I)** R26RtdT tg. **(J)** Zdhhc5 KO. **(K)** Rac1-flox. WT, wild type; KO, knockout; +/-, heterozygous; rxn, reaction; bp, base pair; tg, transgene; fl, flox; *, unspecific bands.

3.27 RT-PCR

DRGs were collected from at least 8 stage E12.5 C57BL/6 embryos and RNA was purified with RNeasy kit (Qiagen) and reverse-transcribed the same day into cDNA

by reverse transcription using the SuperScript™ II Reverse Transcriptase kit (Thermo Scientific). Same was performed with E17 whole mouse embryos and used as a control cDNA library (Hannes Schmidt). PCRs were designed using Primer3Plus (Bioinformatics group), Edit Sequ (DNASTAR) and MapDraw (DNASTAR) softwares. Primers as well as PCR products are listed below.

Note that PCRs for itga3, itga6, itga7 and itgb1 were adapted from (Sutherland et al. 1993), PCRs for kindlin-1, 2 and 3 from (Ussar et al. 2006) and PCRs for talin-1 and 2 from (Senetar et al. 2007). The PCR reaction mix was always the same as shown below.

3.27.1 PCR primers

Primer Name	Primer Sequence (5´-3´)	Product
Arhgef2 forward	CTTAAAGGCTGGCTTCGTTG	197 bp
Arhgef2 reverse	AGTCCAAGGGTAAGGCTGGT	
Atl2 forward	GCTTGATGAAGAGGCTTTGG	187 bp
Atl2 reverse	GCCAGTCAAGGGTTCATTGT	
Atp2c1 forward	TCAGATGTGGCAAAGCAAAG	191 bp
Atp2c1 reverse	TAACCAGCCAACCAACATGA	
Dad1 forward	GCAGTTCGGCTACTGTCTCC	186 bp
Dad1 reverse	GTGCTGGCAAAGAGGAAGTC	
DHHC1 forward	TTGAAGACCTGCACTGCAAC	233 bp
DHHC1 reverse	GGGGTTGACAAAGAACTCCA	
DHHC13 forward	AGCTGGTTCTAGCCTGGACA	186 bp
DHHC13 reverse	AGCCCACAGGGTGATCATAG	
DHHC20 forward	AGCCAGGGCTACACAGAGAA	179 bp
DHHC20 reverse	CCACATCCTAGACAGCAGCA	
DHHC23 x9 forward	AGGTTTACGGCACTGAATGG	154 bp
DHHC23 x9 reverse	CATACTGGGGAGTGCATGTG	
DHHC3 forward	CAGTAGATGGCACTGCAGGA	173 bp
DHHC3 reverse	TGTCTTGAGGCCTTTTTGCT	
DHHC5 forward	ACTCCTTCAGACAGCCCTGA	176 bp
DHHC5 reverse	TAACGGACTGGTGAGGGTTC	
DHHC8 forward	TTGTCGGCTACATTCTGCTG	161 bp
DHHC8 reverse	GGATCTCCAGGCTACATCCA	
Gfpt1 forward	ATCCCTTGGTGCCAGTGTAG	250 bp
Gfpt1 reverse	TGCTGACCTGCATTTCTGAC	
Itga3 forward	ATTGACTCAGAGCTGGTGGAGGAG	304 bp
Itga3 reverse	TACTTGGGCATAATCCGGTAGTAG	

Itga6 forward	GAGGAATATTCCAAACTGAACTAC	400 bp
Itga6 reverse	GGAATGCTGTCATCGTACCTAGAG	
Itga7 forward	CCAGGACCTGGCCATCCGTG	402 bp
Itga7 reverse	CTATCCTTGCGCAGAATGAC	
Itgb1 forward	GTGACCCATTGCAAGGAGAAGGA	238 bp
Itgb1 reverse	GTCATGAATTATCATTAAAAGTTTCCA	
Itgb4 forward	TTCCAAACCTGAACCTCCC	150 bp
Itgb4 reverse	CTGGACAGCACCTACCCCT	
Kindlin-1 forward	CTACACCTTCTTTGACTTG	289 bp
Kindlin-1 reverse	AGGGATGTCAGTTATGTC	
Kindlin-2 forward	GTACCGAAGTAGACTGCAAGG	327 bp
Kindlin-2 reverse	CATACGGCATATCAAGGTAGGC	
Kindlin-3 forward	AGCTGTCTCTGCTGCGTGCTC	310 bp
Kindlin-3 reverse	ATACCTTGCTGCATGAGGCAC	
Map4 forward	ACCGTTTCAAAAGCCACATC	215 bp
Map4 reverse	CCAGTGGGAGTGGTGTTTCT	
Mcoln1 forward	AAACACCCCAGTGTCTCCAG	211 bp
Mcoln1 reverse	ACCAGCCATTGACAAACTCC	
Ndst1 forward	TGCCAGTGTGTTTTCTCTCG	161 bp
Ndst1 reverse	ATGGCTGTTAGTGGGACAGG	
Rps16 forward	TGAAGCCTCCAAGAAGGAGA	170 bp
Rps16 reverse	ACAAAGGTAAACCCCGATCC	
Slc25a13 forward	TGCTCTTAGCCGGTGCTATT	186 bp
Slc25a13 reverse	GAGCAGCAACTCCTTTCCAC	
Talin-1 forward	CCGACTGGCCTCACAAGCCAAGCCT	820 bp
Talin-1 reverse	GGCAGGTGGCTCTGGGGAACAGAAG	
Talin-2 forward	GCACCTGGCTCTCCAGGGCCAGATG	820 bp
Talin-2 reverse	TTCAGGTATGTCTTTTGACTGGAAC	
Tars forward	CCATGAACTTAGCCCTGGAA	216 bp
Tars reverse	GCAAACTGCTCCTTCTCCAC	

3.27.2 PCR reaction mix

All PCRs	
17.26 µl	ddH$_2$O
2.5 µl	10x buffer (Inv.)
3.0 µl	25 mM MgCl$_2$ (Takara)
0.5 µl	dNTPs (2,5 mM each)
0.12 µl	Primer forward (100 µM)
0.12 µl	Primer reverse (100 µM)
1 µl	cDNA (200 ng/µl)
0.5 µl	Taq-Polymerase (Inv.)

3.27.3 PCR programs

Itga3, a6, a7 and b1	
4´	94°C
5x	
60´´	94°C
60´´	65°C
60´´	72°C
35x	
60´´	94°C
60´´	60°C
2´	72°C
15´	72°C
forever	4°C

talin-1 and 2	
3´	94°C
35x	
30´´	95°C
30´´	60°C
45´´	72°C
10´	72°C
forever	4°C

all other PCRs	
3´	94°C
35x	
30´´	95°C
30´´	60°C
30´´	72°C
10´	72°C
forever	4°C

3.28 TAMOXIFEN

Tamoxifen was administrated orally to pregnant mice 11 days after positive-vaginal plug check was reported (E11.5). 0.1 mg per gram body weight was given to the mice from a solution of 20 mg/ml tamoxifen solubilized in corn oil with the help of a 1-ml syringe with a feeding needle at its tip (Fine Science Tools).

3.29 MOLECULAR STRUCTURES

Molecular structures were drawn using Chemdraw Ultra 8.0 software (CambridgeSoft).

4. RESULTS CHAPTER ONE – cGMP SIGNALLING REGULATES S-PALMITOYLATION IN SENSORY NEURONS

4.1 EFFECTS OF CNP AND cGMP ON SENSORY NEURONS

Biochemical or molecular biological approaches hitherto failed to identify a cGKIα target protein needed in the DRG axon bifurcation that could be verified *in vivo* by genetic methods. Hence, the approach to investigate events taking place downstream of cGKI in sensory neurons had to be reconsidered. Furthermore, reproducing CNP-Npr2-cGKIα-mediated axon bifurcation of DRG neurons *in vitro* is so far impossible avoiding facilitated screenings of downstream target proteins (Schmidt et al. 2009).

In order to investigate more in details what mechanisms might lead to the axonal bifurcation *in vivo*, more effort had to be invested in understanding the biological effects induced by the Npr2-mediated cGMP signalling cascade itself. In other words, it was crucial to investigate the impact of the activation of this signalling cascade on DRG axons and GCs in culture.

Thus, the aim of this first part was to identify downstream events of the CNP-Npr2-cGKIα signalling cascade in sensory neurons by characterizing the biological effects resulting from the activation of this signalling cascade in culture systems.

4.1.1 CNP STIMULATION INCREASED THE CELL ADHESION OF EMBRYONIC MOUSE DRG SINGLE CELLS TO LAMININ

DRG axon bifurcation at the DREZ of the spinal cord most likely results from a GC splitting (Figure 3A) (Schmidt & Rathjen 2010). Thus, the Npr2-mediated cGMP signalling should induce, at a certain level, changes at the plasma membrane of the DRG GCs allowing them to split. Interestingly, the use of an adhesion assay pinpointed that the E13.5 mouse DRG dissociated cell adhesion on the extracellular matrix (ECM) protein laminin was increased upon CNP stimulation as revealed by double ICC-staining for the neuronal marker NeuN (Neuronal Nuclei, in green) and L1CAM (in red, Figure 14A). The overnight stimulation of the dissociated cells with 500 nM CNP induced an increase of about 77% ± 12% (mean ± SEM, $p<0.0001$) in

the cell adhesion on laminin (LN) substrate whereas it didn´t have any effect on the control substrate poly-D-lysine (PDL, p=0.14, Figure 14B). This suggested that Npr2-mediated signalling in cultured embryonic mouse DRG neurons might trigger changes at the cell surface namely the plasma membrane resulting to the increase in cell adhesion on the ECM protein laminin.
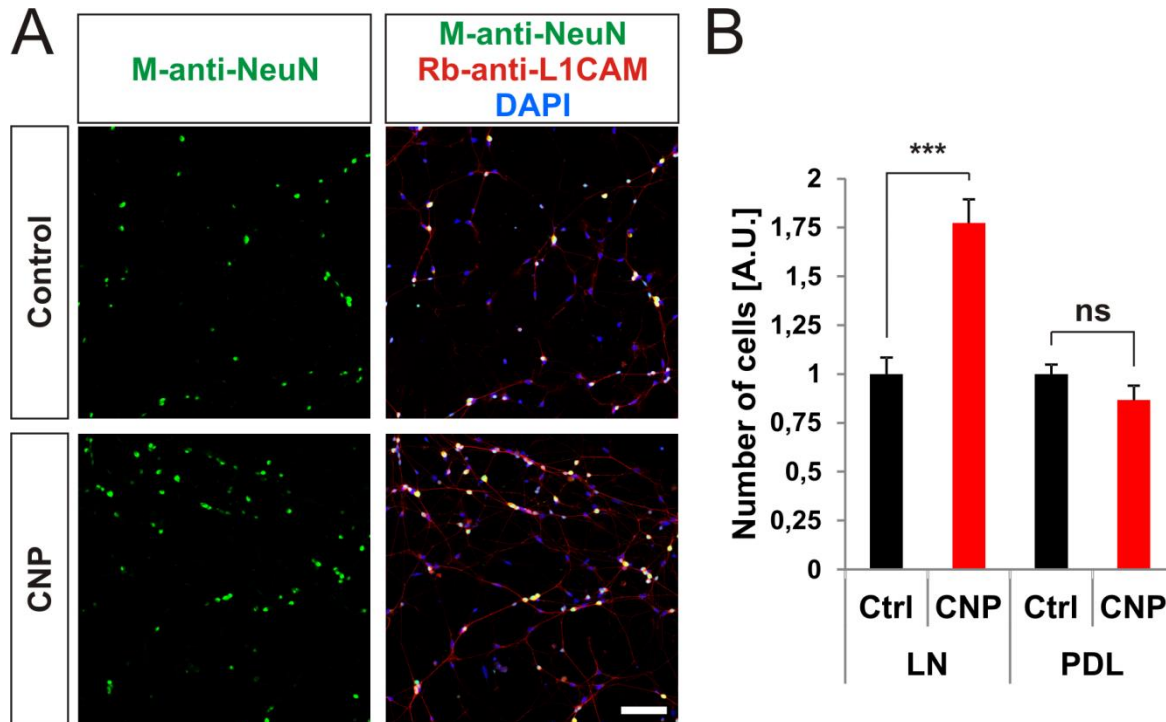

Figure 14 : CNP stimulation increased the cell adhesion of embryonic mouse DRG single cells to laminin-coated substrate. **(A)** E13.5 dissociated mouse DRG neurons were plated on a laminin coated substrate in presence or absence of 500 nM CNP and incubated overnight at 37°C. Then, they were fixed and stained by ICC for the neuronal marker NeuN (green) revealing DRG somas and counter stained for L1CAM (red). Upon CNP stimulation more neuN-L1CAM double-positive cells were attached on the substrate. Note that DAPI staining was used to reveal nuclei of neuronal and non-neuronal cells. **(B)** Quantification of the normalized number of DRG cells attached on laminin indicated a CNP-dependent increase in the adhesion of about 77% ± 12% (mean ± SEM). Note that on the control substrate ploy-D-lysine no change in cell adhesion was observed. n=3. p<0.0001 (***) or p>0.05 (ns), unpaired two-tailed t-test. Error bars represent SEM. Scale bar: 100 µm. LN, laminin-1; PDL, poly-D-lysine.

4.1.2 cGMP STIMULATION INCREASED THE CELL ADHESION OF F11 CELLS

In complement to the preliminary results shown above, the effect of a cGMP analogue on cell adhesion was investigated by the same assay using the F11 cell line and a larger panel of different substrates. The F11 cell line is derived from the fusion of E14 rat embryonic DRG neurons and the mouse N18TG-2 neuroblastoma cell line (Fan et al. 1992). They might have therefore a proteome similar to embryonic DRGs. F11 cells don´t express Npr2 at the protein level but do express cGKIα what

makes them a useful cell line to study cGKI-dependent downstream events (Stonkute 2010).
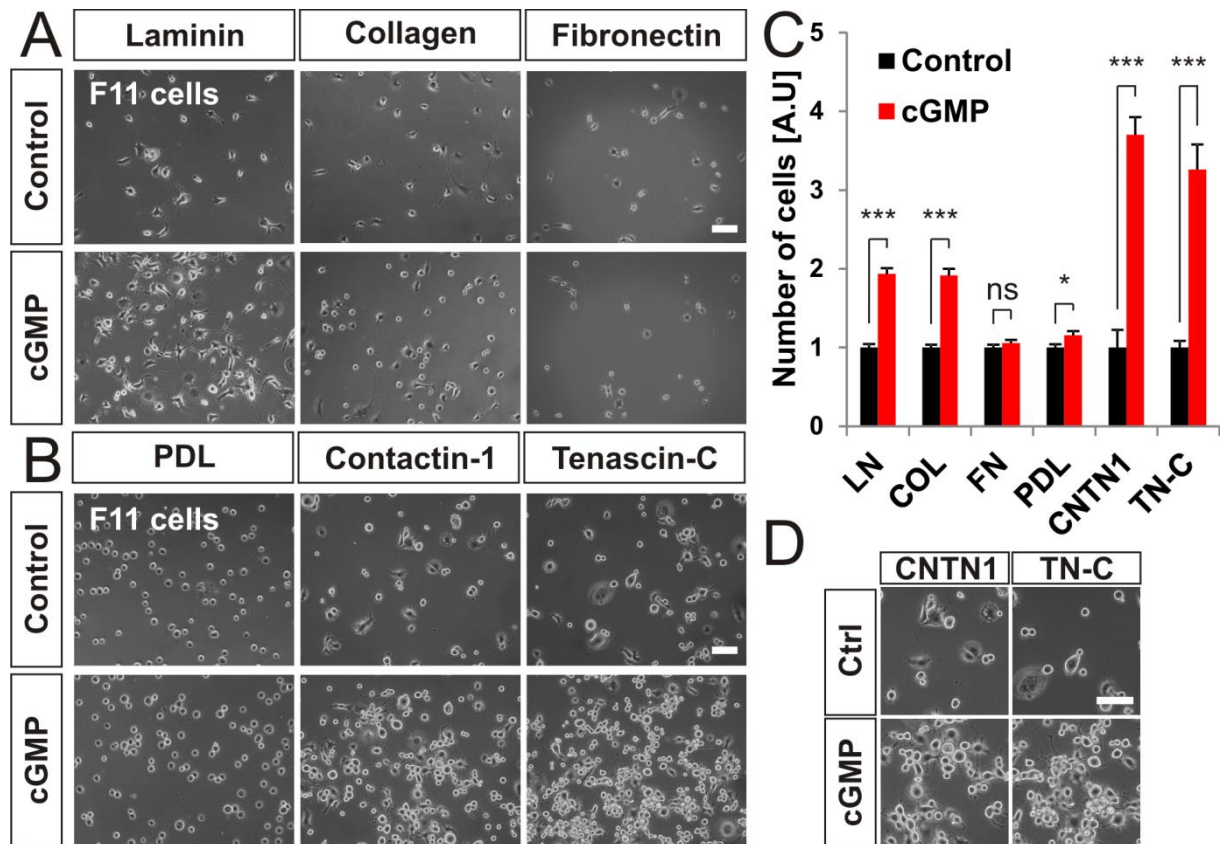
Figure 15 : cGMP stimulation increased the cell adhesion of F11 cells. **(A)** and **(C)** Overnight cGMP stimulation (1 mM 8-pCPT-cGMP) increased the adhesion of F11 cells cultured on ECM proteins laminin and collagen of about 94% ± 7% and 91% ± 9% (mean ± SEM) whereas no effect was seen on fibronectin. **(B)** and **(C)** Moreover, cGMP appeared to increase dramatically the cell adhesion on contactin-1 and tenascin-C proteins (+270% ± 22% and +226% ± 31%, mean ± SEM) while only a minor effect could be quantified on PDL substrate (+16% ± 5%,mean ± SEM). **(D)** Higher magnification pictures from **(B)** showing the cGMP-dependent increase in cell aggregation on contactin-1 and tenascin-C substrates. n≥3. p<0.0001 (***), p<0.05 (*) or p>0.05 (ns), unpaired two-tailed t-test. Error bars represent SEM. Scale bars: 100 μm. LN, laminin-1; COL, collagen; FN, fibronectin; CNTN1, contactin-1; TN-C, tenascin-C; PDL, poly-D-lysine; Ctrl, control.

By incubating F11 cells overnight in 1 mM 8-pCPT-cGMP, a cGMP analogue that can cross membranes, several effects could be observed. Firstly, cells plated on ECM proteins laminin and collagen and stimulated with the cGMP analogue showed an increase in their adhesion compared to the control of about 94% ± 7% and 91% ± 9%, respectively (Figure 15A and C, mean ± SEM, p<0.0001). However, cell adhesion was unchanged on the ECM protein fibronectin, suggesting a specificity of this biological effect to a subset of ECM proteins (Figure 15A and C, p=0.3). As a control substrate, PDL was used and only a minor increase of about 16% ± 5% was quantified (Figure 15B and C, mean ± SEM, p=0.02). Interestingly, cGMP stimulation strongly increased the cell adhesion on the IgSF cell adhesion protein contactin-1

(CNTN1, also termed F11, (Rathjen et al. 1987)) of up to 270% ± 22% (Figure 15B and C, mean ± SEM, p<0.0001). Moreover, the cGMP-mediated increase in cell adhesion also took place on the ECM protein tenascin-C (TN-C) at a pronounced level (Figure 15B and C, +226% ± 31%, mean ± SEM, p<0.0001). Note that on both CNTN1 and TN-C substrates F11 cells seemed to aggregate in the presence of cGMP compared to control suggesting an increase in adhesion between cells as well (Figure 15B and D).

Together with the increase in cell adhesion of embryonic mouse DRG single cells on laminin (Figure 14), these results confirmed that cGMP signalling also had an increasing effect on specific ECM proteins and on an IgSF cell adhesion protein supporting the idea of a regulation of the adhesion capacity at the cell surface when cGMP signalling is triggered.

4.1.3 cGMP STIMULATION INCREASED THE NEURITE OUTGROWTH OF F11 CELLS

In addition to the cGMP-dependent increase in cell adhesion, cGMP also appeared to enhance the neurite outgrowth of F11 cells cultured overnight on PDL/laminin double-coated substrate (Figure 16A). PDL double-coating was used to ensure a similar number of cells attached on the substrate in both conditions. Quantification showed that the presence of 1 mM cGMP analogue increased the average and maximum neurite lengths of about 51% ± 4% and 65% ± 4%, respectively (Figure 16B, mean ± SEM, p<0.0001).

Taken together, these results using the F11 cell system showed that cGMP signalling increased the cell adhesion on specific ECM proteins and on the IgSF cell adhesion protein contactin-1. Moreover, cGMP signalling seemed to be also important in the regulation of neurite outgrowth as it increased the F11 cell neurite branch length. Hence, activation of cGKIα might be involved in these effects.
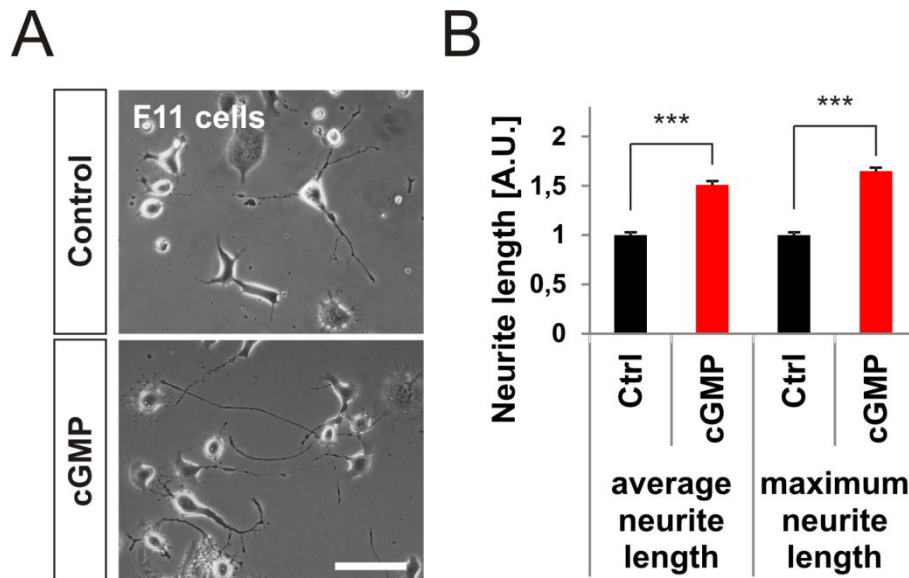
Figure 16 : cGMP stimulation the increased neurite outgrowth of F11 cells. **(A)** and **(B)** Overnight cGMP-analogue stimulation increased the average (+51% ± 4%, mean ± SEM) and maximum lengths (+65% ± 4%, mean ± SEM) of neurites from F11 cells cultured on PDL-laminin substrate. n=3. p<0.0001 (***), unpaired two-tailed t-test. Error bars represent SEM. Scale bar: 100 μm.

4.1.4 NPR2-MEDIATED cGMP SIGNALLING REGULATED AXONAL OUTGROWTH OF CULTURED EMBRYONIC CHICK DRG NEURONS

Having shown above that cGMP signalling seemed to play a role in the cell adhesion of embryonic mouse DRGs and F11 cells as well as in the neurite outgrowth of F11 cells, it was of great interest to assess possible biological changes induced by this signalling pathway in cultured DRGs at the axonal level. To this aim, embryonic stage E7 chick DRGs (chDRGs) were used and cultured in 3D and 2D culture systems. CNP stimulation was basically used to trigger the cGMP signalling via Npr2 avoiding by the same occasion side effects that could be generated by directly applying a high concentration of cGMP to the cultured neurons.

Firstly, E7 chDRGs explants were cultured overnight in a collagen gel in the presence or absence of 500 nM CNP. Explants were fixed and stained for NCAM by ICC so that the halo of axons growing in all directions could be visualized. CNP stimulation appeared to increase the axonal outgrowth of DRG explants compared to control (Figure 17A). Quantification of the axonal outgrowth was evaluated by measuring the relative halo length per DRG by averaging the sum of the halo length in the 4 cardinal directions (Figure 17B). This measurement approach showed that CNP stimulation increased the axonal outgrowth up to 40% ± 6% compared to control (mean ± SEM, p<0.0001).

Additionally, the same experiment was conducted with E7 chDRG single cells cultured in collagen gel. In presence of CNP, axons appeared to be longer with in some cases very long neurites (white arrowhead, Figure 17D). Quantification of the average and maximum neurite lengths revealed an increase of about 39% ± 3 % and 47% ± 3%, respectively (Figure 17E, mean ± SEM, p<0.0001). In short, it confirmed at a similar extend the Npr2-mediated increase in axonal outgrowth seen in the DRG explants culture system.
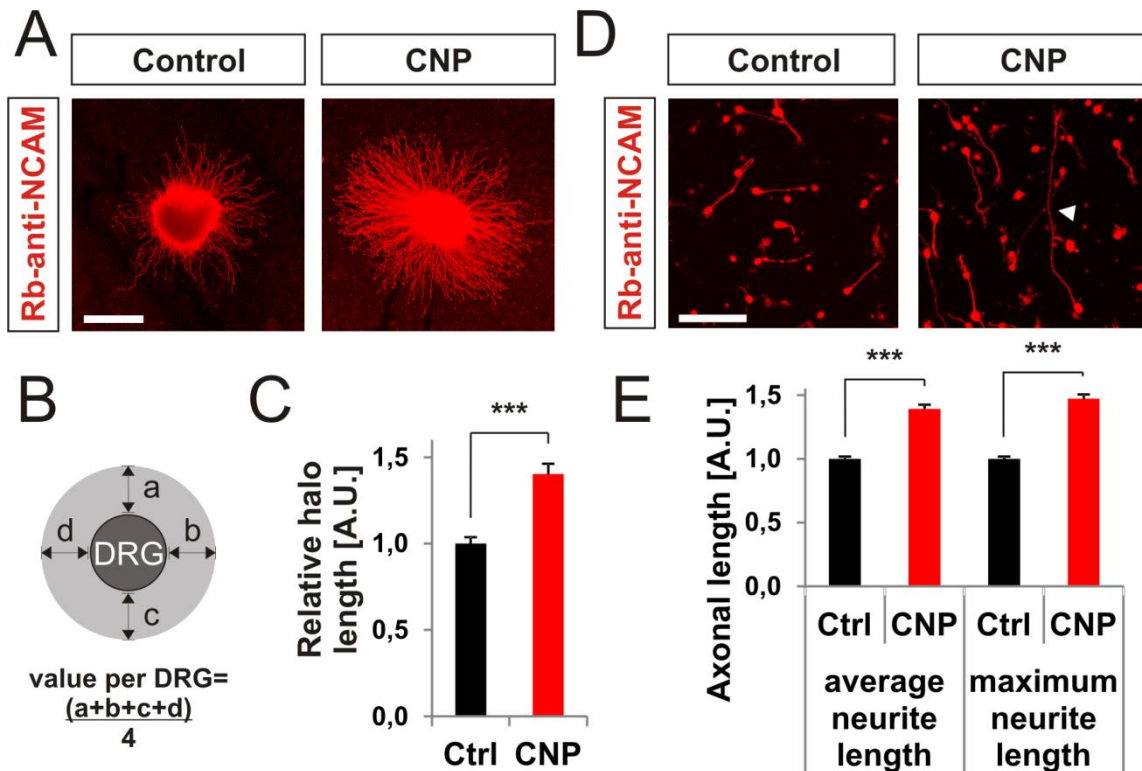

Figure 17 : CNP stimulation enhanced axonal outgrowth of cultured embryonic chDRG explants and single cells. **(A)** Overnight stimulation with 500 nM CNP increased the axonal outgrowth of E7 chick DRG explants cultured in collagen gel compared to control. Explants were fixed and stained for NCAM. **(B)** The relative halo length per DRG was calculated by averaging the sum of the halo length in the 4 cardinal directions. **(C)** The presence of CNP induced an increase of 40% ± 6% (mean ± SEM) in the relative halo length of explants. n=3 and 12 DRGs per condition were assessed. **(D)** A similar increase in axonal outgrowth was also seen in E7 chick DRG single cells cultured in collagen gel and stimulated overnight with 500 nM CNP. Very long axons could be observed in the CNP-stimulated samples (white arrowhead). **(E)** CNP provoked an increase of 39% ± 3 % and 47% ± 3% (mean ± SEM) in the average and maximum neurite lengths, respectively**.** n=4. p<0.0001 (***), unpaired two-tailed t-test. Error bars represent SEM. Scale bars: **(A)** 500 μm; **(D)** 100 μm.

4.1.5 NPR2-MEDIATED cGMP SIGNALLING INDUCED A GROWTH CONE REMODELLING OF CULTURED EMBRYONIC CHICK DRG EXPLANTS

Axonal bifurcation is an axonal branching type most likely happening at the GC (Figure 3A) (Schmidt & Rathjen 2010). To have more hints on what might happen

when the Npr2-mediated cGMP signalling cascade is triggered in DRG axons reaching the DREZ, another approach had to be designed. When DRG axons are at the point of bifurcating, GCs are far away from their somas located in the DRGs (Figure 4A). Hence, to reproduce in a more similar way the *in vivo* situation, E7 chDRG explants were firstly cultured overnight before CNP stimulation so they could already grow long axons. Secondly, they were cultured in a 2D culture system on PDL-laminin double-coated substrate allowing easier study of the GC morphology. Thirdly, 500 nM CNP was added to the cultured DRGs only for 1h, so that the time scale was more adapted to study dynamic changes induced by the Npr2-mediated cGMP signalling cascade.

Stimulated and control explants were fixed and stained by ICC for α-tubulin (in green) and F-actin was visualized by phalloidin counterstaining (in red, Figure 18A). This allowed to investigate the GC structure, namely the C-domain rich in tubulin and the P-domain rich in F-actin, when the Npr2-mediated cascade was activated (Figure 18A). GCs challenged with CNP appeared to be larger with in general a bigger C-domain and shorter filopodia (yellow and blue arrowhead, Figure 18A) than the control ones (white arrowheads, Figure 18A) whereas the GC area population was still heterogeneous in both cases. Some of the CNP-stimulated GCs even appeared to be steered and in the process of splitting (blue arrowheads, Figure 18A). In each independent experiment the area of each GC was normalized by the average GC area of the control so that the average GC area of the control was always of one A.U. (arbitrary unit) after normalization. Quantification of the average GC area indicated that the CNP-treated GCs were about 52 % ± 6% larger than the control ones (Figure 18B, mean ± SEM, $p<0.0001$). GCs were separated in three area categories: the small ones (≤1 A.U.), the medium ones (1 A.U.< x < 1.5 A.U.) and the large ones (≥ 1.5 A.U.). By doing this, it clearly appeared that the number of small GCs was drastically reduced (19% ± 3%, mean ± SEM) compared to control (60% ± 2%, mean ± SEM, $p<0.05$) and the number of large GCs was greatly increased (46% ± 1.5%, mean ± SEM) compared to control (12% ± 1%, mean ± SEM, $p<0.05$) when CNP was present (Figure 18C).

On the other hand, the average and maximum filopodia branch lengths at the GC were reduced upon CNP stimulation of about 30% ± 1% and 38% ± 1%, respectively (Figure 18D, mean ± SEM, p<0.0001). However, the number of filopodia per GC was unchanged by the CNP stimulation (Figure 18E).
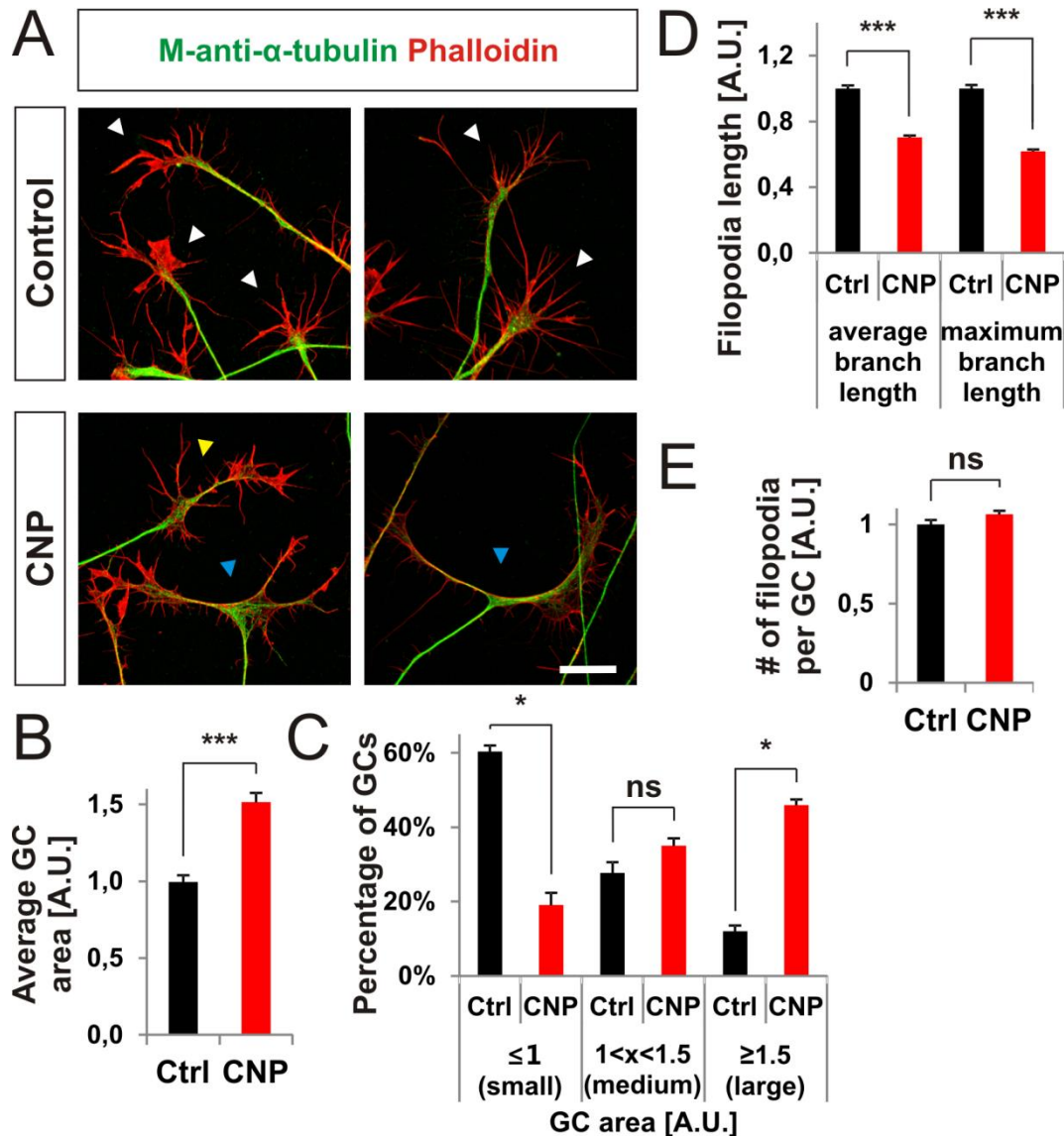

Figure 18 : CNP induced a GC-remodelling in cultured embryonic chick DRG explants. **(A)** 1-hour CNP stimulation seemed to increase the GC area of E7 chick DRGs cultured on a PDL-laminin substrate. DRG neurons were fixed and α-tubulin and F-actin (with phalloidin) were visualized. Control GC appeared with an extended P-domain containing long filopodia (white arrowheads) whereas CNP-stimulated GCs had a bigger C-domain, shorter filopodia (yellow and blue arrowheads) and in some cases they even appeared to be in the process of splitting (blue arrowheads). **(B)** The average area of CNP-stimulated GCs appeared to be increased up to 52 % ± 6% (mean ± SEM) compared to control. **(C)** The number of small GCs was drastically reduced (19% ± 3%, mean ± SEM) compared to control (60% ± 2%, mean ± SEM) and the number of large GCs was greatly increased (46% ± 2%, mean ± SEM) compared to control (12% ± 1%, mean ± SEM). **(D)** The average branch length and maximum branch length of filopodia at GCs were reduced upon CNP stimulation of about 30% ± 1% and 38% ± 1% (mean ± SEM), respectively. **(E)** The number of filopodia per GC was unchanged by the CNP application. n=3, 170 GCs (control) and 177 GCs (CNP) were assessed. p<0.0001 (***), p<0.05 (*) or p>0.05 (ns), unpaired (B, D and E) and paired (C) two-tailed t-test. Error bars represent SEM. Scale bar: 20 µm.

Taken together, these results strongly suggested a Npr2-mediated GC remodelling taking place within one hour after the CNP was added to the cultured DRG explants.

4.1.6 NPR2-MEDIATED cGMP SIGNALLING INDUCED A GROWTH CONE REMODELLING OF CULTURED EMBRYONIC MOUSE DRG EXPLANTS

Npr2-mediated GC remodelling observed in cultured embryonic chDRG explants was also investigated in cultured E12.5 C57BL/6N mDRG explants. Like above, explants were first cultured overnight on PDL/laminin double-coated substrate and then stimulated 1h with 500 nM CNP or its equivalent in buffer. They were then fixed and stained for α-tubulin (green) and phalloidin (red) to visualized GCs morphology (Figure 19A). GCs stimulated with CNP (blue arrowheads) appeared larger than control ones (white arrowheads, Figure 19A). Quantification of the average GC area revealed that CNP stimulation induced a 86% ± 8% (mean ± SEM) increase compared to control (Figure 19B, $p<0.0001$). More precisely, CNP stimulation drastically reduced the number of small GCs (19% ± 3%, mean ± SEM) compared to control (59% ± 1%, mean ± SEM, $p<0.05$) and greatly increased the number of large GCs (52% ± 1%, mean ± SEM) compared to control (13% ± 1%, mean ± SEM, $p<0.001$, Figure 19C). Note that filopodia length was not investigated as it didn´t seem to be strongly changed by the CNP presence.

Taken together, these results indicated that embryonic mDRG GCs behave similarly to the chDRG GCs in presence of CNP. They seemed to come also across a remodelling leading to an increase in their area indicating that this process is conserved between both species.
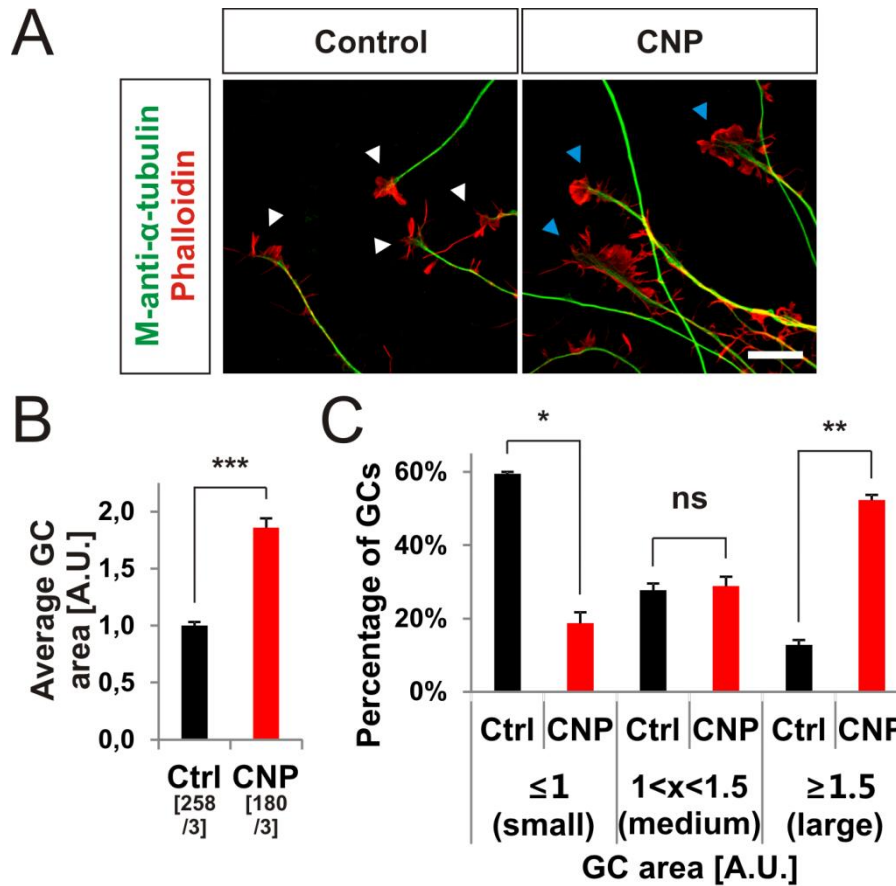
Figure 19 : CNP induced a GC-remodelling in cultured embryonic mouse DRG explants. **(A)** 1-hour CNP stimulation seemed to increase the GC area of E12.5 mouse DRGs cultured on a PDL-laminin substrate. DRG neurons were fixed and α-tubulin and F-actin (with phalloidin) were visualized by ICC. Control GC appeared small (white arrowheads) whereas CNP-stimulated GCs were larger (blue arrowheads). **(B)** The average area of CNP-stimulated GCs appeared to be increased up to 86 % ± 8% (mean ± SEM) compared to control. Between brackets are shown the number of GCs assessed versus the number of replicates. **(C)** The number of small GCs was drastically reduced (19% ± 3%, mean ± SEM) compared to control (59% ± 1%, mean ± SEM) and the number of large GCs was greatly increased (52% ± 1%, mean ± SEM) compared to control (13% ± 1%, mean ± SEM). $p < 0.0001$ (***), $p < 0.001$ (**), $p < 0.05$ (*) or $p > 0.05$ (ns), unpaired (B) and paired (C) two-tailed t-test. Error bars represent SEM. Scale bar: 20 µm.

4.1.7 NPR2-MEDIATED GROWTH CONE REMODELLING NEEDED cGKI TO TAKE PLACE

CNP stimulation was shown above to induce a remodelling of GCs in cultured mouse and chick embryonic DRG explants. This meant that so far the CNP-Npr2-cGMP signalling should play a role in this process. However, whether cGKIα also was part of this GC remodelling had to be elucidated.

To this aim, DRG explants from E12.5 mouse cGKI mutant embryos were used. cGKI WT and cGKI KO DRG explants were firstly cultured overnight on PDL-laminin

double-coated substrate. They were then stimulated 1h with 500 nM CNP, fixed and stained as previously described above.
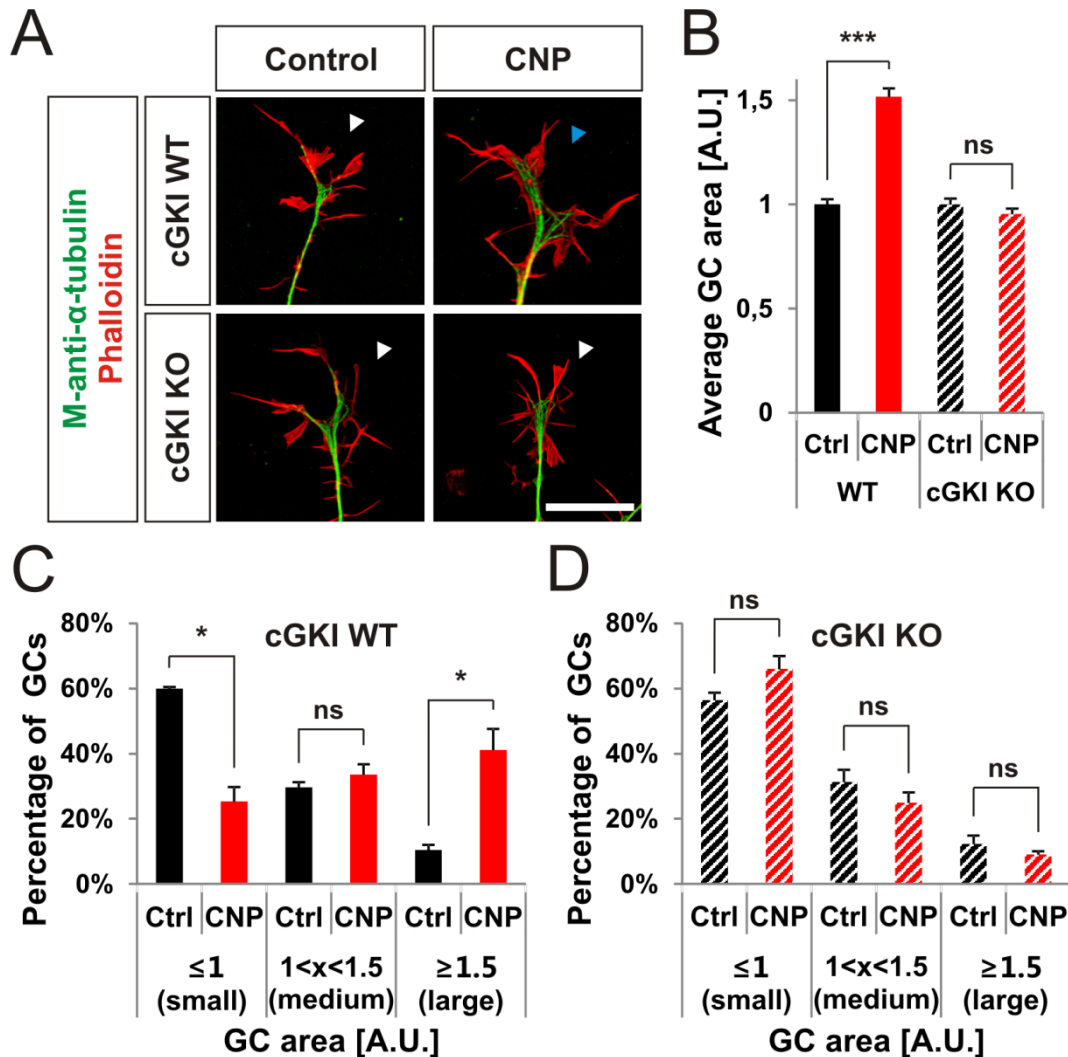

Figure 20 : Npr2-mediated GC remodelling needed cGKI to take place. . **(A)** 1-hour CNP stimulation seemed to increase the GC area of E12.5 cGKI WT mouse DRGs cultured on a PDL-laminin substrate but not in absence of cGKI. DRG neurons were fixed and α-tubulin and F-actin (with phalloidin) were visualized by ICC. Control GC appeared small (white arrowheads) whereas CNP-stimulated GCs were larger (blue arrowheads). When cGKI was absent (cGKI KO) the increase in the GC area was not observed anymore in presence of CNP (white arrowheads). **(B)** The average area of CNP-stimulated GCs appeared to be increased up to 52 % ± 4% (mean ± SEM) compared to control in cGKI WT DRGs. However, in absence of cGKI this effect could not be measured anymore and the average GC area was similar to control. **(C)** In cGKI WT DRGs, the number of small GCs was drastically reduced (25% ± 4%, mean ± SEM) compared to control (60% ± 6%, mean ± SEM) and the number of large GCs was greatly increased (41% ± 7%, mean ± SEM) compared to control (10% ± 2%, mean ± SEM). **(D)** When cGKI was absent (cGKI KO), no significant difference could be quantified in the percentage of small, medium or large GCs upon CNP stimulation. n=4 per genotype, 480 GCs (cGKI WT control), 319 GCs (cGKI WT CNP), 250 GCs (cGKI KO control) and 349 GCs (cGKI KO CNP) were assessed. $p < 0.0001$ (***), $p < 0.001$ (**), $p < 0.05$ (*) or $p > 0.05$ (ns), unpaired (B) and paired (C and D) two-tailed t-test. Error bars represent SEM. Scale bar: 20 µm.

The area of WT GCs appeared as expected to be enlarged in presence of CNP compared to control (blue arrowhead, Figure 20A). However, when cGKI was knocked out, GCs didn´t appeared to be influenced by the presence of CNP

compared to control (white arrowheads, Figure 20A). Quantification of the average GC area showed that CNP-treated WT GCs were about 52 % ± 4% (mean ± SEM) larger compared to control (Figure 20B, p<0.0001). However, in the absence of cGKI the average GC area of CNP-treated DRG explants was similar to the control (Figure 20B, p>0.05). In cGKI WT DRGs, the number of small GCs was drastically reduced (25% ± 4%, mean ± SEM) compared to control (60% ± 6%, mean ± SEM, p=0.003, Figure 20C) and the number of large GCs was greatly increased (41% ± 7%, mean ± SEM) compared to control (10% ± 2%, mean ± SEM, p<0.05, Figure 20C). When cGKI was absent (cGKI KO), no significant difference could be quantified in the percentage of small, medium or large GCs upon CNP stimulation (Figure 20D, p>0.05). The majority of GCs was small in both conditions (56% ± 2% in control and 66% ± 4% in CNP-treated GCs, mean ± SEM) whereas a minority was large (12% ± 3% in control and 9% ± 1% in CNP-treated GCs, mean ± SEM, Figure 20D).

Taken together, this analysis of cGKI mutated DRG GCs in presence of CNP indicated that the GC remodelling taking place by CNP stimulation needed cGKIα. In sum, it demonstrated that the CNP-Npr2-cGKIα signalling pathway, which is essential for DRG axon bifurcation *in vivo*, was crucial for the CNP-mediated increase in area of DRG GCs *in vitro*.

4.1.8 DRG GROWTH CONES AT THE DREZ APPEARED TO BE ENLARGED AND TO SPLIT

Based on the *in vitro* results showing a CNP-Npr2-cGKI-mediated embryonic DRG GC remodelling, the morphology of DRG GCs entering the SC at the DREZ, where they encounter CNP, was investigated. Single DRG axons were labelled by a lipophilic dye (DiI) in a preparation of fixed E12.5 mouse embryos (Schmidt & Rathjen 2011). GCs within the bifurcation zone and the elongation zone (>100 μm away from the bifurcation point) were visualized using confocal microscopy (Figure 21A). Interestingly, GC in the bifurcation zone which hadn´t still bifurcated (pre-bifurcating axons) appeared enlarged (red and orange arrowheads, Figure 21B) whereas GC in the elongation zone (from already bifurcated axons) appeared thin and elongated (green arrowheads, Figure 21B). Moreover, some of the GCs that were within the bifurcation zone even appeared to be in the process of splitting (orange arrowheads, Figure 21B). Quantification of the average GC area within the

elongation zone versus bifurcation zone indicated that GCs from pre-bifurcating axons were about twice bigger (+100% ± 17%, mean ± SEM, p<0.0001) than the ones within the elongation zone (Figure 21C).

In sum, these results pointed out that the GC remodelling observed in culture might also take place before the DRG axons bifurcate at the DREZ *in vivo*. Moreover, it also strengthened the hypothesis of a GC splitting taking place in bifurcating axons.
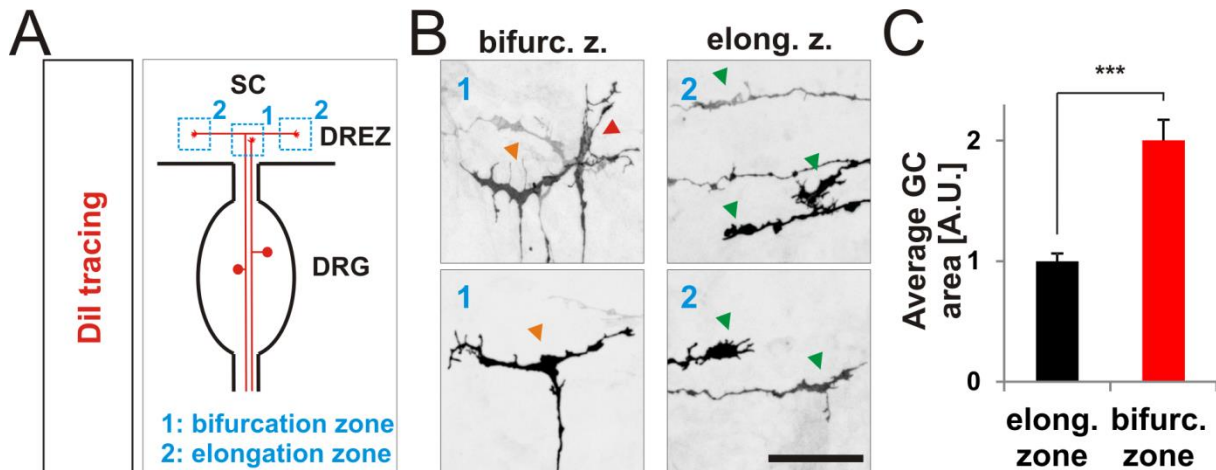

Figure 21 : Study of WT DRG GCs at the DREZ. **(A)** Single DRG axons were labelled with the help of a fluorescent lipophilic dye (DiI) and GCs were visualized at the DREZ. GCs at the bifurcation zone were compared to the ones located at a minimum of 100 µm away from the bifurcation point (elongation zone). **(B)** GCs within the bifurcation zone appeared bigger (red and orange arrowheads) than the ones in the elongation zone (green arrowheads). Moreover, some of them localized in the bifurcation zone seemed to be in the process of splitting (orange arrowheads). **(C)** Quantification of the average GC area showed that GCs within the bifurcation zone were about twice bigger (+100% ± 17%, mean ± SEM) that the ones within the elongation zone. 22 GCs in the bifurcation zone and 34 GCs in the elongation zone from 3 littermate WT embryos were assessed. p<0.0001 (***), unpaired two-tailed t-test. Error bars represent SEM. Scale bar: 50 µm.

4.2 STUDY OF AXONAL BRANCHING IN MICE LACKING INTEGRIN SIGNALLING COMPONENTS *IN VIVO*

Cell culture experiments using F11 cells and embryonic DRGs showed a cGMP or CNP-dependent increase in the cell adhesion, axonal outgrowth and GC remodelling. Importantly, these effects were observed on different ECM protein substrates (laminin, collagen, TN-C) or in collagen gel. These ECM proteins like laminins and collagens were shown to be expressed in the basement membrane surrounding the developing mouse spinal cord (Wright et al. 2012; Thorsteinsdóttir et al. 1995). DRG axons entering the SC at the DREZ have to consequently cross this membrane rich in ECM proteins and bifurcate.

Based on the greater cell adhesion increase of F11 cells on TN-C and contactin-1 when cGMP signalling was stimulated (Figure 15), it was first hypothesized that IgSF cell adhesion molecules might play a role in this effect. Contactin-1 was shown to interact with TN-C and also with contactin-2 (Zacharias et al. 1999; Pollerberg et al. 2013). Therefore, it was a very interesting candidate protein. However, as already published in 2001 it didn´t seem to play a role in DRG axon bifurcation in the developing chick embryo (Perrin et al. 2001). Interestingly, L1CAM, another IgSF cell adhesion molecule, was described to interact with contactin-1 and 2 (Olive et al. 1995; Rader et al. 1996). Moreover, its Drosophila homolog neuroglian was reported to play a role in the bifurcation of mushroom body axons (Goossens et al. 2011). Thus, L1CAM was considered as a potential important IgSF cell adhesion molecule in the Npr2-mediated axonal bifurcation. However, single axons from E12.5 L1CAM KO mouse embryos labelled with a fluorescent lipophilic dye appeared to bifurcate (orange arrowhead, Figure 22) like in control littermate embryos (green arrowhead, Figure 22) suggesting that it didn´t play a role in this process *in vivo*.
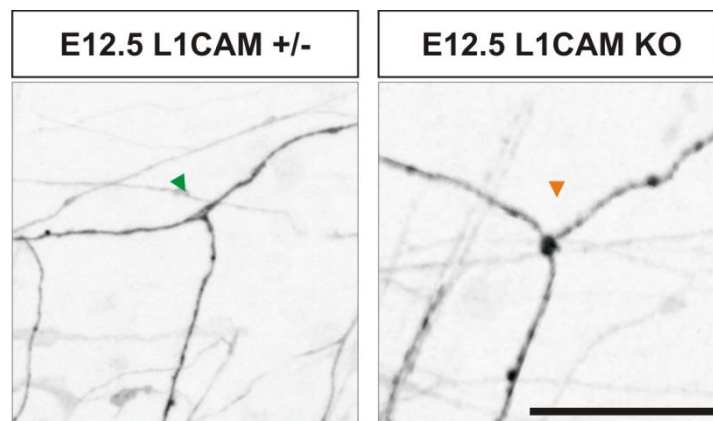
Figure 22 : The IgSF cell adhesion molecule L1CAM is not needed in the DRG axon bifurcation at the DREZ. DiI labelling of single DRG axons in E12.5 L1CAM KO embryos revealed that the absence of L1CAM didn´t alter the bifurcation at the DREZ of the SC. Sensory axons bifurcated normally (orange arrowhead) as they did in a control heterozygous embryo littermate for example (green arrowhead). Scale bar: 50 µm.

One other well-studied family of proteins which are receptors for ECM proteins is the integrin family. Integrins are transmembrane cell adhesion proteins constituted of an alpha and a beta subunit. They can form 24 different αβ heterodimers which recognize a wide variety of different ligands (Figure 23A and B). Integrins can be involved in cell-to-cell adhesion but can also bind components of the extracellular matrix (ECM) and their specific peptides (e.g. laminins, collagens and fibronectins) (Barczyk et al. 2010). There are two different ways by which integrins in a bent inactive conformation are activated and adopt therefore an extended active

conformation (Figure 23A) (Shattil et al. 2010). They can be activated by ligand binding at their extracellular domains what induces the conformational change and allows proteins, which keep integrins activated and link them to the actin cytoskeleton, to bind the intracellular domain of the β subunit (outside-in signalling) (Calderwood et al. 2013). Moreover, integrins can be directly activated by binding of activating proteins like kindlins and talins to their β subunit intracellular domains what induces the conformational change and permits the binding of ligands (inside-out signalling, Figure 23A) (Calderwood et al. 2013; Shattil et al. 2010).

ECM proteins and their integrins receptors were shown to be involved in several kinds of axon guidance mechanisms in vitro and in vivo (e.g. netrin repulsion of retinal ganglion cells neurons) and in axonal branching (e.g. branching of hippocampal neurons) (Myers et al. 2011; Rico et al. 2004). Furthermore, previous studies pointed out the role of cGKI in integrin-dependent cell adhesion and aggregation by integrin activation in platelets (Li et al. 2003; Z. Li et al. 2006).

Thus, it was conceivable that Npr2-mediated cGMP signalling might affect the inside-out signalling of integrins in DRG axons. It was speculated that integrin signalling might play a role in the CNP-Npr2-cGKI-mediated axonal bifurcation *in vivo*.

4.2.1 EXPRESSION OF INTEGRIN SIGNALLING COMPONENTS IN EMBRYONIC DRGS

As introduced above, talins and kindlins are important adaptor proteins involved in the inside-out activation of integrins (Calderwood et al. 2013). RT-PCR study of talins and kindlins expression showed that only talin-2 and kindlin-2 were expressed at the mRNA level in E12.5 mouse DRGs (Figure 23C). Moreover, same study but of the integrin subunits forming laminin receptors (see Figure 23B) showed that they were all expressed at the mRNA level (Figure 23D). Spliced variant integrin α3B (itgba3B) and α6B (itga6B) were both expressed as well as the integrin α7 (itga7), beta subunits 1 and 4 (itgb1 and itgb4, Figure 23D). These results corroborated to previous published data where Integrin β1 and α6 proteins were found to be strongly expressed in DRGs of E12.5 mouse embryos (Schwander et al. 2004; Thorsteinsdóttir et al. 1995).

Focal adhesion kinase (FAK) is a non-receptor tyrosine kinase member of the focal adhesion complex and known to interact with talins and many other proteins

downstream of talins and kindlins (Mitra et al. 2005). FAK is ubiquitously expressed and Western blot of E12.5 DRGs and F11 cells lysates confirmed its expression (black arrow, Figure 23C) (Mitra et al. 2005).
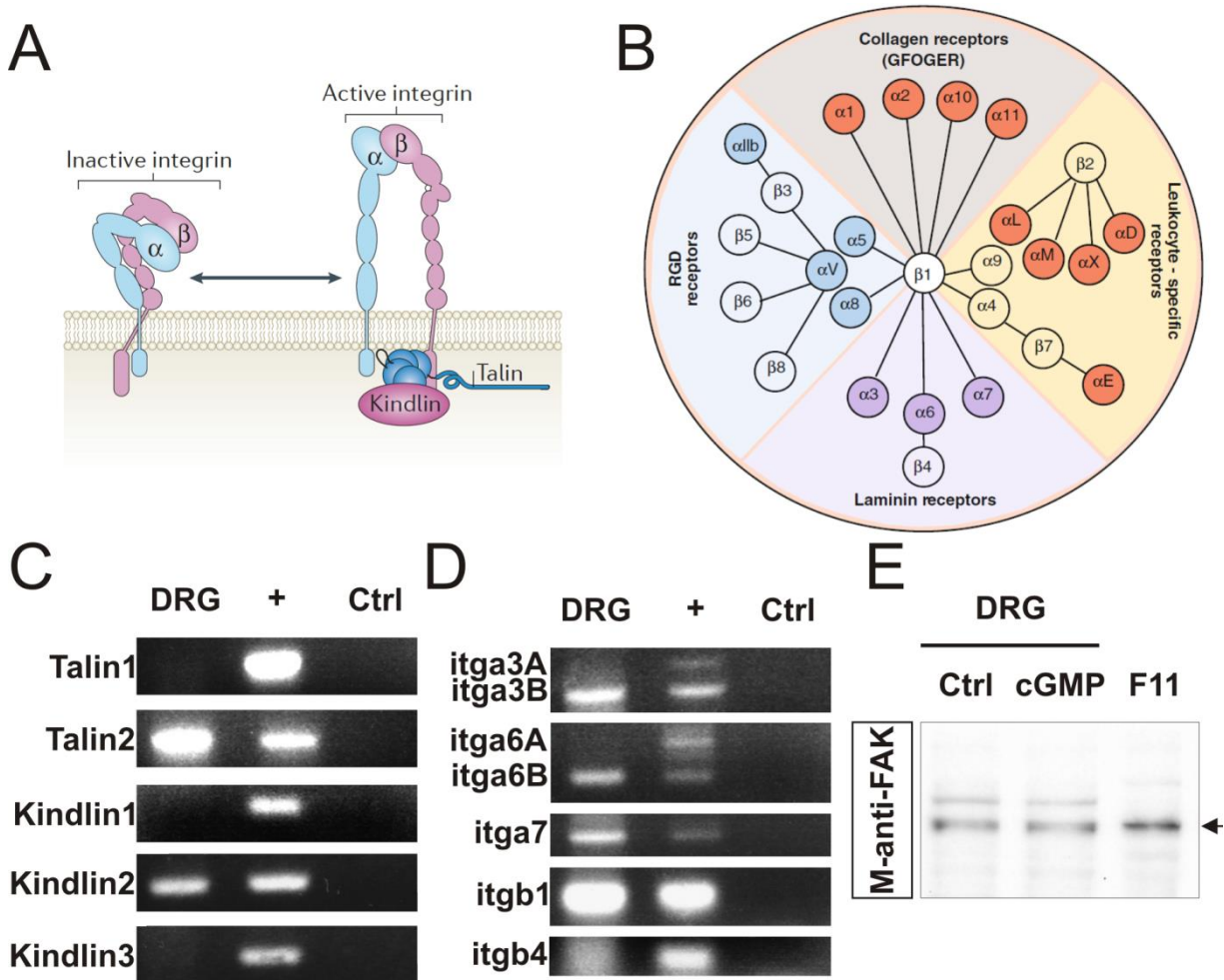

Figure 23 : Integrin signalling components expression in mouse embryonic DRGs. **(A)** Integrin receptors are composed of an α and β-subunits which are together in a bent low-affinity conformation when inactive. By binding at the β subunit C-terminal domain, talins trigger a conformational change what leads to the activation of the receptor (Calderwood et al. 2013). Kindlins might "potentiate talin-mediated activation" and also might play a role in modulating the integrins clustering (Calderwood et al. 2013; Ye et al. 2014). **(B)** Different combinations of α and β-subunits give receptors their affinity to specific ECM proteins. Note that the β1-subunit can form heterodimers with plenty of different α-subunits forming receptors for different ECM proteins making it a crucial subunit (Barczyk et al. 2010). **(C)** RT-PCR analysis of integrin adaptors kindlins and talins in E12.5 mouse DRGs and in E17 whole mouse embryo (positive control, +). **(D)** RT-PCR analysis of integrin subunits forming laminin receptors in E12.5 DRGs and in E17 whole mouse embryo (positive control, +). Note that the third row was loaded with the water control (ctrl). **(E)** Protein expression of FAK in E12.5 DRGs and F11 cells revealed by immunoblotting. A band at around 120 kDa was detected (black arrow). **(A)** and **(B)** were adapted from Ref. (Calderwood et al. 2013) and Ref. (Barczyk et al. 2010), respectively.

4.2.2 MICE LACKING THE ADAPTOR PROTEIN TALIN-2 APPEARED TO HAVE A NORMAL DRG AXON BRANCHING PATTERN

Talins and kindlins are thought to work in concert in order to activate integrins. However, talins have been accepted as the most important adaptor proteins involved in this process (Calderwood et al. 2013; Ye et al. 2014). Therefore, mice carrying a complete deletion of the talin2 coding sequence were examined (Debrand et al. 2012).
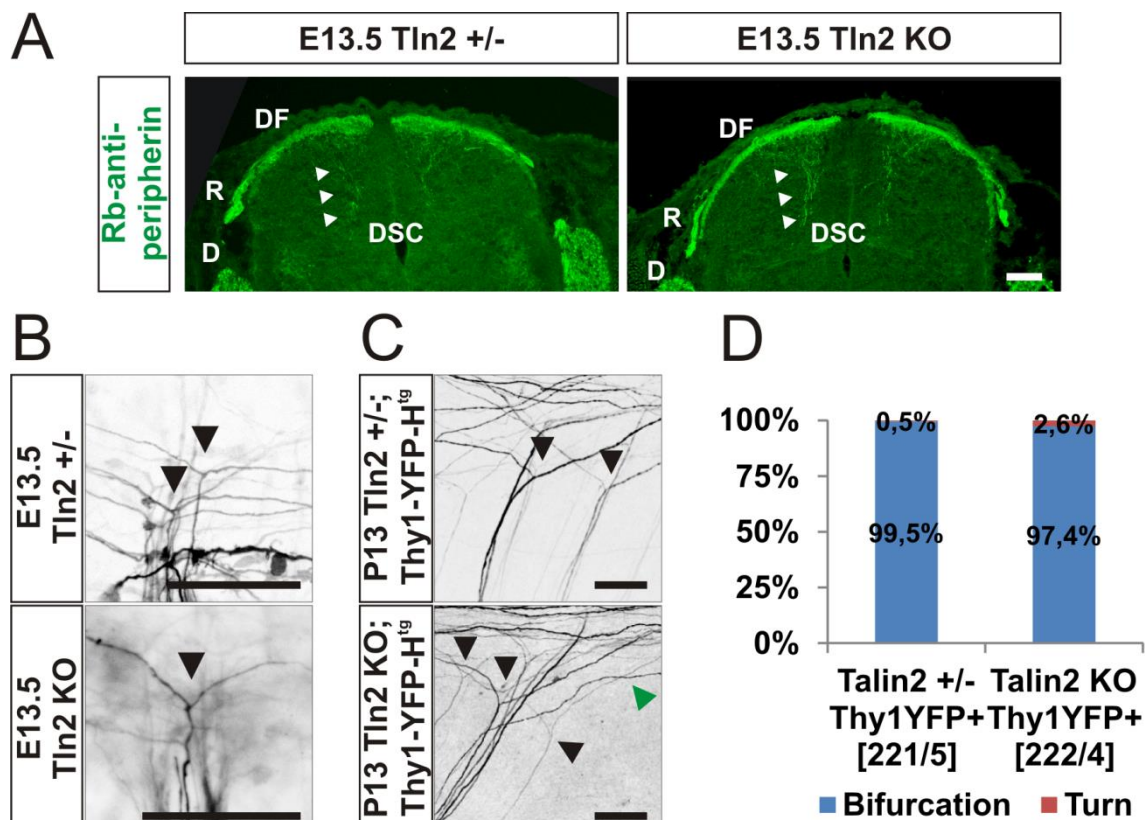

Figure 24 : DRG axon branching in talin-2 (Tln2) KO appeared to be normal. **(A)** Tln2$^{+/-}$ and Tln2 KO E13.5 transverse spinal cord sections were stained for peripherin to visualize DRG axonal projections into the spinal cord. Dorsal funiculi and bundles of collateral branches (white arrowheads) in absence of Tln2 looked similar to the heterozygous control. **(B)** Tln2 KO sensory axons labelled with DiI appeared to still bifurcate at the DREZ like in Tln2$^{+/-}$ control embryos (black arrowheads). **(C)** To get a statistically relevant study of bifurcation/turn of Tln2 mutant sensory axons, P13 Tln2 mutants expressing the Thy1YFP-H transgene reporter were analysed. Most axons were still bifurcating at the DREZ (black arrowheads) whereas some of them were found to turn (green arrowhead). **(D)** Quantification showed that absence of Tln2 didn´t have a major impact on axonal bifurcation compared to control. In brackets are written the number of axons versus the number of mice that were assessed. D, DRG; R, dorsal root; DF, dorsal funiculus; DSC, dorsal spinal cord. Scale bars: **(B)** 50 μm; **(A)** and **(C)** 100 μm.

First of all, transverse sections of E13.5 SCs from embryos lacking talin-2 (Tln2) and stained by IHC for peripherin (green) showed no obvious sensory projections defects (Figure 24A). Dorsal funiculi appeared to form normally and collateral axon bundles

invaded the deeper layers of the spinal cord (white arrowheads, Figure 24A) indicating that collateral branching was normal compared to control.

Then, branching of DRG axons at the DREZ was investigated using the DiI tracing method (Schmidt & Rathjen 2011). Talin-2 knockout (KO) DRG axons normally bifurcated at the DREZ like in the control (black arrowheads, Figure 24B). Axon bifurcation of talin-2 mutants was also investigated at P13 using the Thy1-YFP-H reporter mouse line crossed with the Tln2 KO line. Thy1-YFP-H mouse line expresses the fluorescent protein YFP under the Thy1 promotor inducing a sparse labelling of DRG axons in post-natal mice (Feng et al. 2000; Schmidt et al. 2007). Whereas the majority of the talin-2 KO axons was bifurcating (black arrowheads, Figure 24C) some of them were also making turns at the DREZ (green arrowheads, Figure 24C). Quantification showed that in talin-2 KO mice 2.6% of the axons were turning instead of bifurcating which was more than in the control mice (0.5%, Figure 24D). However, this was still a minor difference.

Altogether, these results demonstrated that talin-2 didn´t play a major role in DRG axon branching especially in the axon bifurcation at the DREZ.

4.2.3 INTEGRIN BETA 1 SUBUNIT WAS NOT INVOLVED IN AXONAL BIFURCATION *IN VIVO*

A central integrin subunit is the integrin β1 (itgb1) because it can make heterodimers with a wide panel of integrin α subunits and therefore form receptors for many kinds of ECM ligands (Figure 23B) (Barczyk et al. 2010). Hence, according to the earlier speculation, this was a critical subunit to study.

In order to create a conditional KO (cKO) where itgb1 was deleted in embryonic DGRs we crossed the floxed itgb1 allele mouse line with another line expressing a cre recombinase under the wnt1 promotor (wnt1Cre) (Graus-Porta et al. 2001; Kam et al. 2014). Firstly, itgb1 protein expression was assessed in E12.5 cKO DRGs by immunoblotting and no itgb1 expression could be detected in cKO compared to control embryos (Figure 25A). Note that clathrin immunoblot served as a loading control. Secondly, transverse sections of E13.5 itgb1 cKO (itgb1$^{fl/fl}$; wnt1Cre$^+$) SCs stained by IHC for peripherin (green) showed no obvious sensory projections defects (Figure 25B). Dorsal funiculi appeared to form normally and collateral axon bundles invaded the deeper layers of the spinal cord (white arrowheads, Figure 25B)

indicating that collateral branching happened normally as in control embryos. Finally, DiI tracing of itgb1 mutated DRG axons, showed that they were bifurcating at the DREZ of the SC as in control embryos (green arrowheads, Figure 25C). Moreover, collateral branches sprouting out from the daughter axon branches could be seen in cKO as well as in control embryos with no obvious differences (black arrowheads, Figure 25C).

Taken together, these results demonstrated that sensory projections in the spinal cord were totally normal in absence of itgb1 protein. DRG axons lacking itgb1 bifurcated at the DREZ and formed collateral branches.
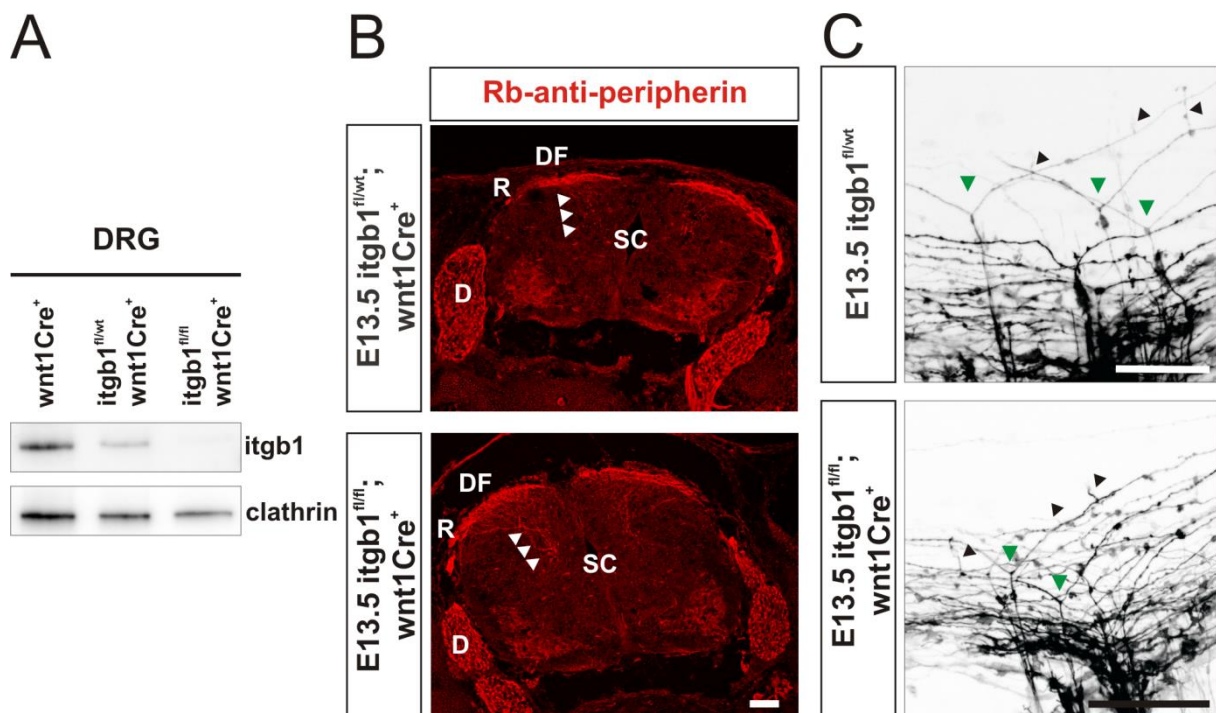
Figure 25 : Integrin-β1 (Itgb1) conditional KO DRG axons bifurcated normally at the DREZ of the SC. **(A)** Study of the Itgb1 protein level in Itgb1 cKO E12.5 DRGs by immunoblotting. Itgb1 expression appeared to be gone in Itgb1 cKO compared to the different controls. Clathrin was used as loading control. **(B)** Dorsal funiculi and collateral branch formation (white arrowheads) appeared to be normal in the absence of Itgb1 as shown here in peripherin-stained E13.5 transverse spinal cords. **(C)** Same was observed at the single axon level: DiI-labelled axons appeared to bifurcate (green arrowheads) and to form collaterals (black arrowheads) like in control. D, DRG; R, dorsal root; DF, dorsal funiculus; SC, spinal cord. Scale bars: **(B)** 100 μm; **(C)** 50 μm.

4.2.4 LOSS OF FOCAL ADHESION KINASE (FAK) DIDN NOT IMPACT THE DRG AXON BIFURCATION BUT APPEARED TO PLAY A ROLE IN AXON GUIDANCE

Finally, the focal adhesion kinase (FAK) was investigated. Interestingly, FAK was described to play a role in axonal branching of Purkinje cells and hippocampus neurons *in vitro* (Rico et al. 2004). When integrin signalling is activated, FAK gets in

turn also activated (Mitra et al. 2005). Usefully, its activation state can be assessed by examining its autophosphorylation at the tyrosine 397 (Y397) (Mitra et al. 2005). To this end, the F11 cell system was used. Cells were stimulated 10 min with 1 mM cGMP analogues 8-pCPT-cGMP and lysates were then studied by immunoblotting. Previous studies showed that activation of cGKI with cGMP led to the phosphorylation of vasodilator-stimulated phosphoprotein (VASP) (Valtcheva et al. 2009; Dhayade et al. 2016).
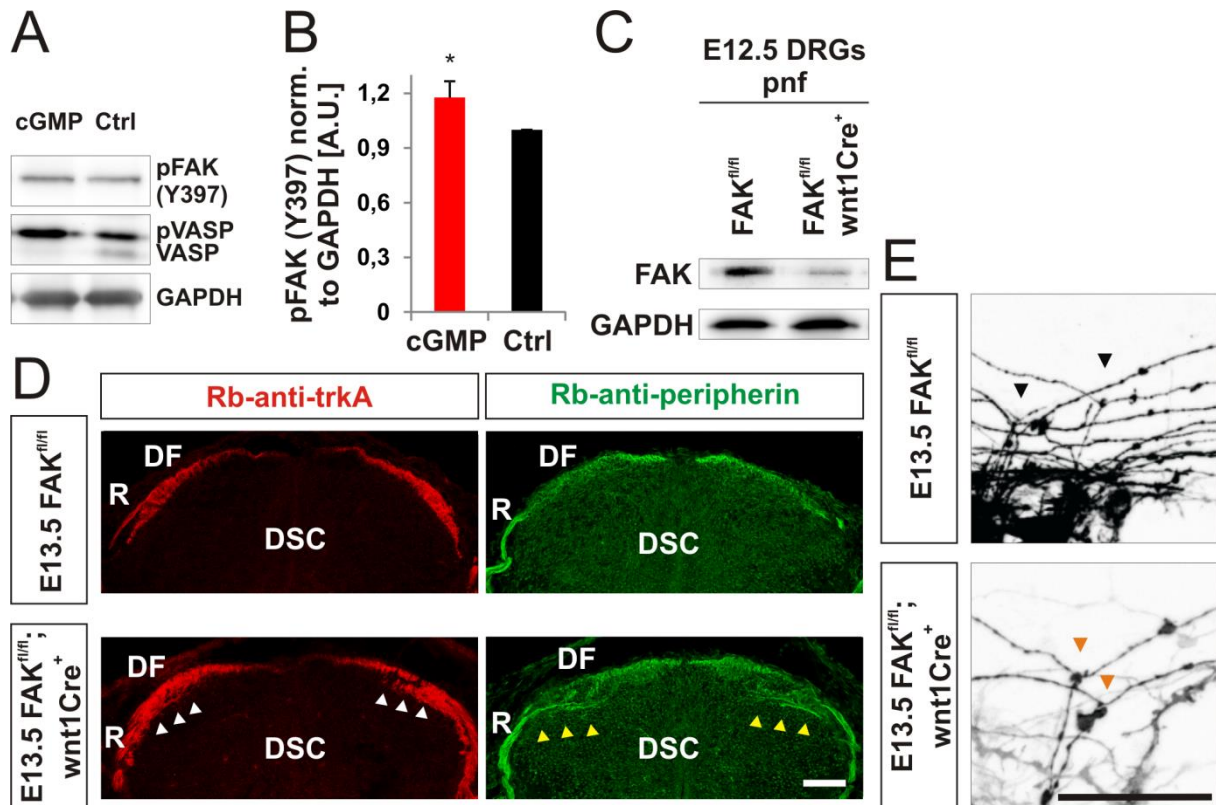

Figure 26 : Lack of FAK in DRG did not hampered axon bifurcation but seemed to disturbed axon guidance. **(A)** and **(B)** cGMP stimulation of F11 cell lysate significantly increased (+18% ± 9%, mean ± SD) the phosphorylation of FAK at its Y397 residue (pFAK). Note that VASP phosphorylation-shift was used as a cGMP-stimulation control and GAPDH as loading control. n=3. p<0.05 (*), paired two-tailed t-test. Intensity of pFAK was normalized to the GAPDH intensity. **(C)** Study of the FAK protein level in FAK cKO E12.5 DRGs by immunoblotting. FAK expression appeared to be drastically reduced but not completely gone in FAK cKO compared to control. GAPDH was used as loading control. **(D)** Dorsal funiculi of E13.5 FAK cKO embryos appeared to be disorganized at the level of the DREZ. TrkA-positive (nociceptive, white arrowheads) and peripherin-positive (nociceptive and proprioceptive, yellow arrowheads) axons were found to invade the dorsal horn at its most anterior part. **(E)** No lack of bifurcation was seen at the single axon level: DiI-labelled axons appeared to bifurcate (orange arrowhead) like in control embryos (black arrowheads). R, dorsal root; DF, dorsal funiculus; DSC, dorsal spinal cord. Error bars represent standard deviation. Scale bars: **(D)** 100 µm; **(E)** 50 µm.

Immunoblot of VASP showed that cGMP stimulation created a shift between the phosphorylated VASP band (pVASP) and the non–phosphorylated as previously reported (Figure 26A) (Valtcheva et al. 2009; Stonkute 2010; Dhayade et al. 2016). This was used as a control of the cGMP stimulation. Glyceraldehyde-3-phosphate

dehydrogenase (GAPDH) was used as a loading control. Interestingly, stimulation with cGMP induced a slight significant increase in the phosphorylation state of FAK of about 18% ± 9% (mean ± SD, Figure 26A and B, $p<0.05$). This suggested therefore a possible regulation of FAK activity by cGMP signaling in F11 cells.

After that, embryos lacking FAK in DRGs were generated by breeding the floxed FAK allele mouse line with the wnt1Cre line as explained above for itgb1 (Beggs et al. 2003). FAK protein level was assessed by immunoblot from E12.5 DRG lysates and showed that FAK deletion resulted to a drastic but not total decrease in its protein expression (Figure 26C). GAPDH was used as a loading control. The remaining signal in the cKO DRGs might have come from wnt1-negative cells present in or around DRGs. IHC study of E13.5 transverse SC sections showed that sensory projections in the spinal cord were partly disturbed. Tropomyosin related kinase A (TrkA)-positive nociceptive as well as peripherin-positive axons misguided and prematurely invaded the dorsal horn of the SC resulting in disorganized dorsal funiculi (white and yellow arrowheads, Figure 26D). Albeit the guidance defect caused by the lack of FAK, E13.5 DRG axons bifurcated normally at the DREZ like in control embryos as shown by DiI tracing (orange and black arrowheads, Figure 26E). Altogether, these results suggested that FAK was needed in the guidance of DRG axons entering the SC but not in the bifurcation process itself.

In sum, *in vivo* study of the sensory axon bifurcation at the DREZ of mutated talin-2, itgb1 and FAK embryos indicated that integrin signaling might not be needed in this type of axonal branching.

4.3 LOCALIZATION OF cGKI IN DRG NEURONS

Second messengers compartmentalization at the neuronal GC like cAMP and cGMP has been recently demonstrated to play a role in axon guidance and branching (Averaimo et al. 2016; Hayashi-Nishino et al. 2009). Hence, the localization of the Npr2-mediated cGMP signalling cascade components in developing DRG GCs was of interest to understand the mechanism triggering axon bifurcation at the DREZ. In parallel to cell culture assays using DRG neurons and F11 cells in presence of CNP or cGMP, respectively, the localization of cGKI in extending sensory GCs was analyzed. Characterization of its precise localization might help to shed light on its phosphorylation targets in the GC.

4.3.1 cGKI APPEARED AS A VESICLE-LIKE PATTERN IN THE GROWTH CONE OF CULTURED EMBRYONIC DRGs

By its kinase activity, cGKI might phosphorylate substrate proteins in discrete regions of the GC what would lead to its remodelling. It has been previously shown that cGKI is localized at the GC of embryonic DRGs (H Schmidt et al. 2002). However, due to a lack of a very specific antibody, its localization couldn´t be properly assessed within the GC. By a very specific polyclonal antibody raised against cGKI its localization in the DRG GC could be assessed.
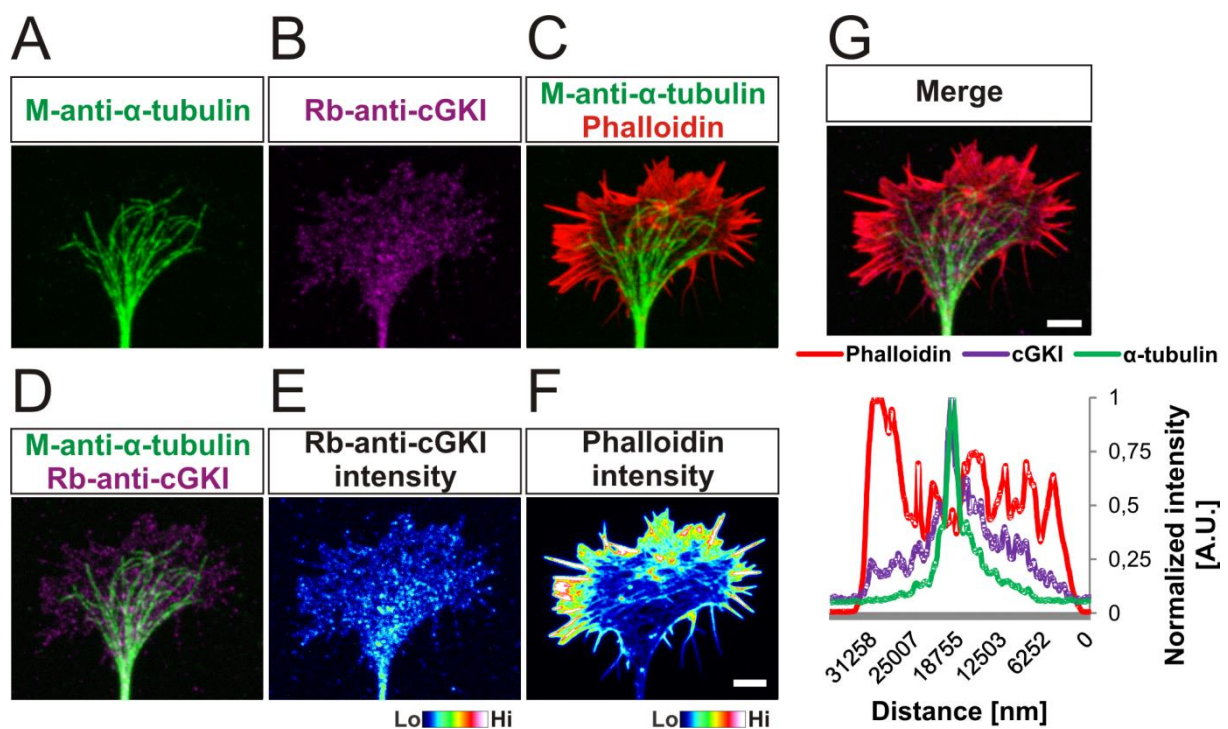
Figure 27 : Localization of cGKI in the embryonic DRG GC. **(A)-(F)** E12.5 mouse DRG explants were cultured on a PDL/laminin substrate, fixed and stained for α-tubulin, phalloidin (F-actin) and cGKI. cGKI appeared as a dot-like pattern in the GC and seemed to be omnipresent at the C-domain whereas it was less expressed at the P-domain rich in F-actin (see heat map pictures in **(E)** and **(F)**). **(G)** Study of normalized intensities in the GC clearly showed an overlap between cGKI and α-tubulin. Lo, low; Hi, high. Scale bars: 5 μm.

Hence, cultured E12.5 mouse DRGs on PDL/laminin double-coated substrate were fixed and stained using ICC for α-tubulin (in green, Figure 27A and C) and cGKI (in magenta, Figure 27B) and also counterstained with phalloidin to visualize F-actin filament (in red, Figure 27C). Remarkably, cGKI was detected as a dot-like or vesicle-like pattern at the GC (Figure 27B). Moreover, it also seemed to be more concentrated in the C-domain of the GC as visualized by its intensity pattern (Figure 27B and E). It even looked to be quite the opposite of the F-actin (phalloidin) intensity pattern (Figure 27E and F). Most likely, cGKI-positive structures with higher

intensities looked to overlap with the microtubule network (Figure 27D) and visualization of the normalized intensities of cGKI, α-tubulin and F-actin confirmed this overlap within the C-domain (Figure 27G). Interestingly, same observations were made in cultured E7 chick DRGs suggesting a conserved localization of cGKI at early embryonic stages between both species (data not shown).

Taken together, these results suggested that cGKI due to its discrete expression pattern might be present close to intracellular membrane structures in the GC. This also indicated that the kinase was localized mostly within the C-domain of mouse embryonic DRG GCs in culture.

4.3.2 cGKI LOCALIZED CLOSE TO INTRACELLULAR MEMBRANES IN THE GROWTH CONE OF CULTURED EMBRYONIC DRGs

To investigate the possible localization of cGKI close to intracellular structures in the GC, a colocalization study was conducted using several markers. Smooth endoplasmic reticulum structures were previously shown to be present in the neuronal GC migrating along microtubules (Dailey & Bridgman 1989; Ramirez & Couve 2011). Therefore, ER structures were visualized by ICC for the chaperone protein disulfide isomerase (PDI) (Zhang et al. 2003).

First of all qualitative colocalization was assessed, given as an example in Figure 28, between cGKI and PDI in E12.5 DRG explants cultured on PDL/laminin substrate, fixed and stained by ICC for cGKI (shown in magenta), PDI (shown in green) as well as phalloidin (shown in red which stained F-actin, Figure 28A). This nicely revealed the ER structures within the C-domain of the GC (white arrowhead, Figure 28A). Cross-visualization in the z-axis (dashed lines, Figure 28B) clearly showed colocalized structures between cGKI and PDI (black arrowheads) as well as not colocalized ones at an axon shaft growing on the GC (red arrowheads) (Figure 28B). In addition to that, quantification of the colocalization was conducted using the Mander´s approach by which the Mander´s colocalization coefficient (MCC) was calculated (Manders et al. 1993; Dunn et al. 2011). In short, MCC from cGKI-positive pixels colocalizing with marker-positive pixels (tM1) and vice-versa (tM2) could be measured. Both tM1 and tM2 values represent the proportion of pixels from one channel colocalizing with the other after threshold calculation with the Costes automatic thresholding method (Dunn et al. 2011; Costes et al. 2004). Note that tM1

represents always the MCC for cGKI and tM2 the MCC for the used marker and measures were performed within a region of interest (ROI) which was traced around the border lines of GCs.
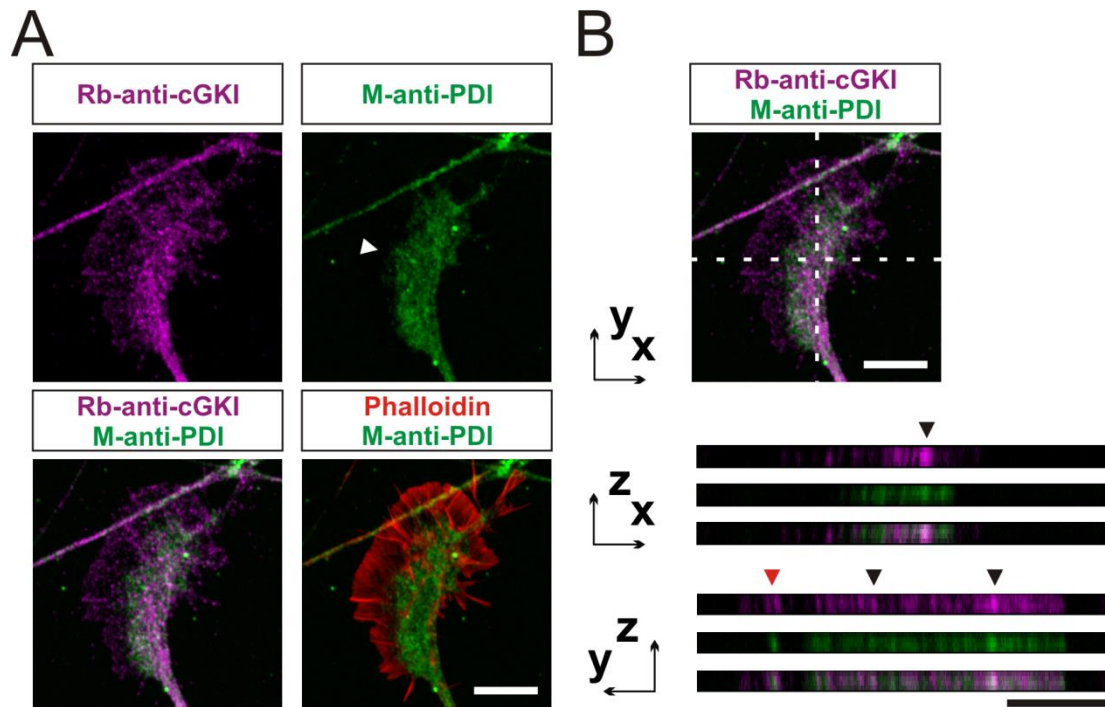

Figure 28 : Example of qualitative colocalization between cGKI and the ER marker PDI. **(A)** A Z-stack image was taken from E12.5 DRG explants cultured on PDL/laminin substrate, fixed and stained by ICC for cGKI (shown in magenta), PDI (shown in green) and phalloidin (shown in red, revealing F-actin). **(B)** Visualization in the z-axis (dashed lines) showing colocalized structures (black arrowheads) as well as not colocalized ones at an axon shaft growing on the GC (red arrowheads) between cGKI and PDI. Scale bars: 10 µm.

PDI-positive structures appeared to overlap with cGKI-positive ones (Figure 28). MCC calculation indicated a tM1 of 53% ± 3% and a tM2 of 66% ± 3% (mean ± SEM) indicating a robust colocalization between cGKI and the ER structures (Figure 30A). Additionally, an ICC for the small GTPase Ras-related protein Rab-5 (Rab5) was performed to reveal early endosomes in the GC (Bucci et al. 1992; Nguyen et al. 2016; Falk et al. 2014). The staining pattern of Rab5 (in green) in the GC looked more spread than PDI (Figure 29A). Moreover, it seemed to colocalize at a lesser extend with cGKI (in magenta, Figure 29A) and MCC quantification showed tM1 and tM2 values of about 43% ± 2% and 41% ± 3%, respectively (mean ± SEM, Figure 30A).

Then, lysosomes present at the DRG GCs were also assessed by ICC for lysosomal-associated membrane protein 1 (LAMP-1), a known lysosomal marker (Carlsson & Fukuda 1989; Tian et al. 2015). LAMP-1 staining pattern appeared as a vesicle-like pattern within the C-domain of the GC (in green and shown by a white arrowhead,

Figure 29B). LAMP-1 and cGKI (in magenta, Figure 29B) appeared to partly colocalize in the GC as tM1 value was about 22% ± 2% and tM2 42% ± 3% (mean ± SEM, Figure 30A).
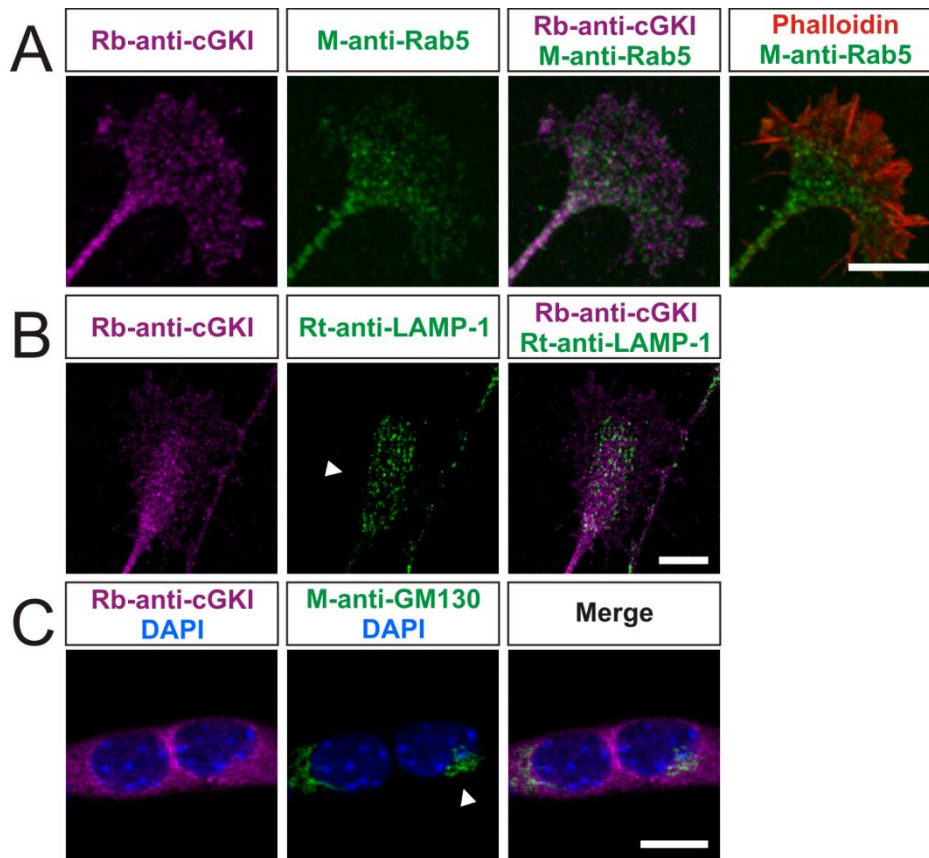
Figure 29 : Colocalization study of cGKI with intracellular membrane markers in the DRG GC and soma. **(A-C)** GCs from E12.5 DRG explants co-stained for cGKI and the following intracellular membrane markers were visualized: Rab5 (marker of early endosomes (Bucci et al. 1992)), LAMP-1 (marker of lysosomes (Carlsson & Fukuda 1989)) and GM130 (marker of cis-Golgi complex (Nakamura et al. 1995)). Scale bars: 10 µm.

Finally, colocalization of cGKI (in magenta) with the cis-Golgi marker 130 kDa cis-Golgi matrix protein (GM130, in green) at the soma of cultured DRG single cells (white arrowhead, Figure 29C) could also be quantified (tM1, 23% ± 1% and tM2, 66% ± 4%, Figure 29C and Figure 30A, mean ± SEM) (Nakamura et al. 1995). Note that the specificity of antibodies used in this study was assessed by immunoblotting of E12.5 DRG post-nuclear fraction (PNF). All showed expected band(s) at the correct size with low unspecific signal (Figure 30B).

Taken together, this colocalization study confirmed the presence of cGKI close to intracellular membrane structures at the embryonic DRG GC as suggested by its vesicle-like pattern. It also indicated that the kinase is not only confined close to one type of intracellular structure but several types in which it is compartmentalized.

Moreover, these results also indicated that it was enriched at the C-domain of the GC and less present at the P-domain (in filopodia and lamellipodia).
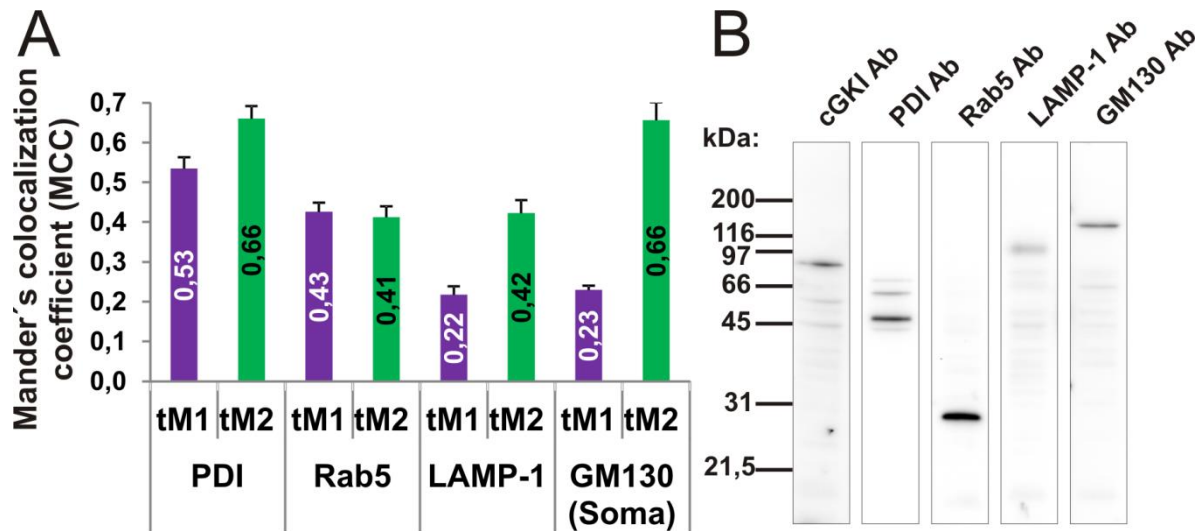

Figure 30 : Colocalization study of cGKI with intracellular membrane markers in DRG GCs (continued). **(A)** Quantification of Mander´s colocalization coefficient for cGKI versus markers (tM1 value) and markers versus cGKI (tM2) above threshold (Manders et al. 1993). Minimum 10 GCs per marker were assessed. MCC values are written within bars. **(B)** Antibodies used for the ICC study were assessed by immunoblotting of E12.5 mDRG PNF lysate (10 µg) in order to demonstrate their specificity. All showed expected band(s) at the correct size with low unspecific signal. Error bars represent SEM.

4.3.3 cGKI ALSO APPEARED TO LOCALIZE CLOSE TO INTRACELLULAR MEMBRANES IN CULTURED F11 CELLS

Interestingly, ICC study of cGKI in cultured F11 cells showed a similar vesicle-like pattern (in magenta, Figure 31A-C). Thereafter, same colocalization study as above was conducted in F11 cells with for example the ER, lysosomal and cis-Golgi markers PDI, LAMP-1 and GM130 (in green, Figure 31A-C). MCCs were measured within each entire cell (ROI were traced around the cell border) and confirmed colocalization to ER, lysosomes and cis-Golgi structures (Figure 31D). Furthermore, cGKI showed colocalization at a different extend to trans-Golgi structures (stained by trans-Golgi network integral membrane protein, TGN38), γ-adaptin-positive structures and Ras-related protein Rab-11 (Rab11)-positive recycling endosomes (Figure 31D) (Eva et al. 2010; Lelouvier et al. 2008). Note that a different set of markers was used in F11 cells compared to the analysis of DRG GCs because some antibodies didn´t appear to work for ICC in the DRG explant system.
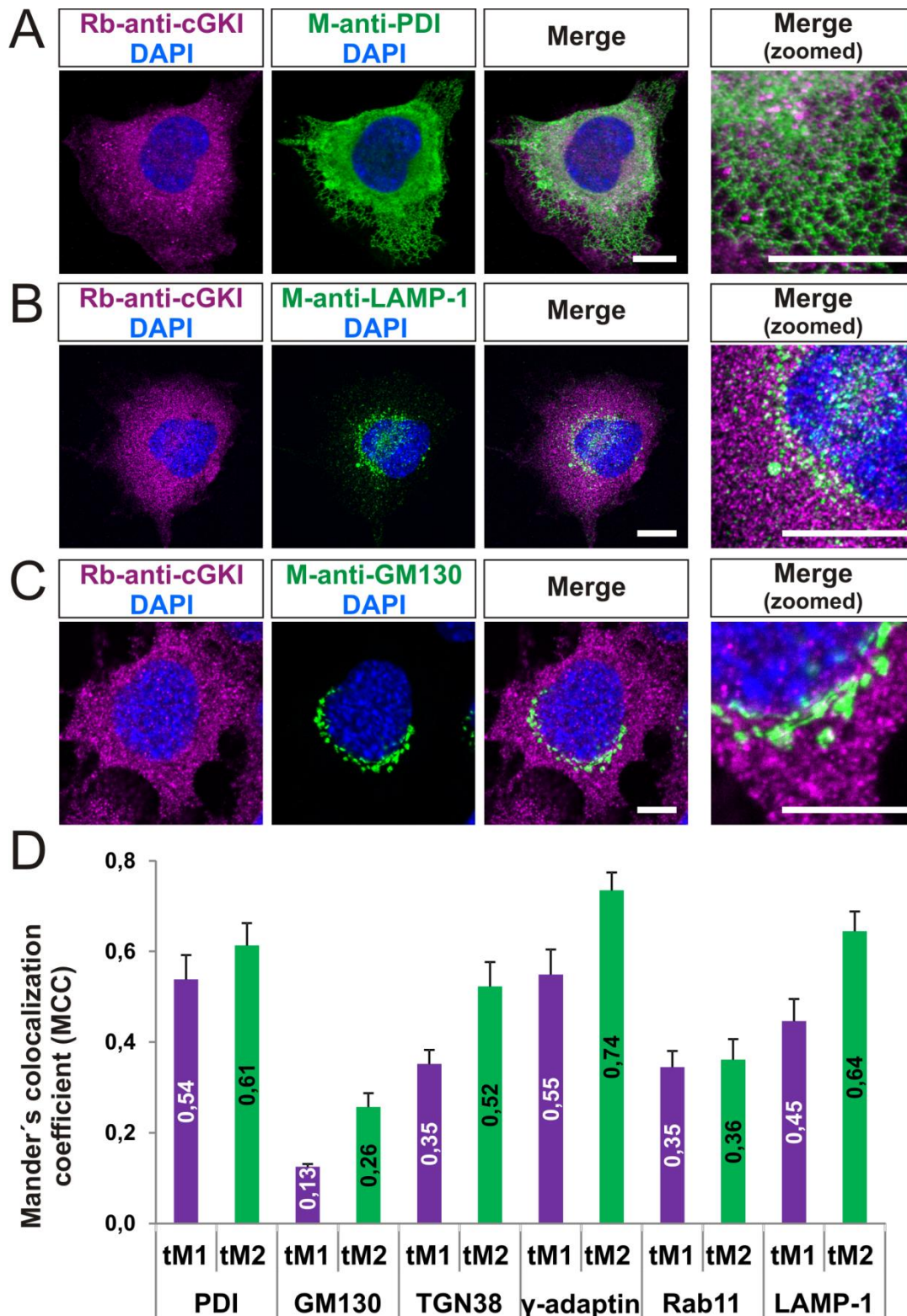
Figure 31: Colocalization study of cGKI with intracellular membrane markers in F11 cells. **(A-C)** Examples of F11 cells co-stained with cGKI (magenta) and either the ER marker PDI **(A)**, the lysosomes marker LAMP-1 **(B)** or the cis-Golgi marker GM130 (all shown in green) **(C)**. Cells were also counterstained with DAPI (blue). **(D)** Quantification of the MCC for cGKI versus markers (tM1 value) and markers versus cGKI (tM2) above threshold (Manders et al. 1993). MCC values are written within bars. Error bars represent SEM. Scale bars: 20 μm.

Taken together, this showed that particularities in the expression pattern and localization of cGKI in the embryonic DRG GC seemed to be conserved in F11 cells

and its compartmentalization close to intracellular membranes might be even broader at a whole-cell level.

4.4 NPR2 LOCALIZED WITHIN LIPID RAFTS IN PC12 CELLS

Almost nothing is known about the subcellular localization of Npr2 at the plasma membrane (PM) in neurons or in other cell types. As cGKI appeared to be compartmentalized in cultured embryonic DRGs and F11 cells, it was of great interest to investigate Npr2 localization pattern at the PM as it is responsible for triggering the cGMP signalling. Unfortunately, available antibodies didn´t allow the ICC-based study of its localization in cultured embryonic DRGs (data not shown). However, biochemical approaches could possibly help studying its partitioning at membranes. Evidences have pointed out the fact that the PM contains cholesterol-rich microdomains forming compartmentalized signalling platform in neuronal and non-neuronal cells (Golub et al. 2004). Partitioning of receptors and other membrane proteins within these so-called lipid rafts might play a role in axon guidance and branching (Guirland et al. 2004; Averaimo et al. 2016; Golub et al. 2004). PC12 cells which are derived from rat adrenal pheochromocytoma were used as they have been reported to express Npr2 at the protein level and it allowed to have a consistent amount of protein for biochemical studies (Greene et al. 1976; Rathinavelu & Isom 1991).

First of all, Npr2 expression was confirmed by immunoblotting of undifferentiated PC12 cell lysates and showed the expected band at around 120 kDa only in the membrane fraction and not in the cytosolic fraction (black arrow, Figure 32A).

Lipid rafts isolation was performed using a detergent-free sucrose density centrifugation (Persaud-Sawin et al. 2009; Ostrom & Liu 2007). Lipid rafts-localized proteins were therefore separated from the others in the so-called "Buoyant" fraction and 10 fractions from the top to the bottom of the centrifuge tube could be immunoblotted separately and compared (Figure 32B). Basically, the lipid rafts fraction had to be confirmed by immunoblot for flotillin-1, a lipid raft marker which appeared to be expressed in PC12 cells (orange arrow, Figure 32A) (Chamberlain et al. 2001). As expected, the fraction number 3 containing the "Buoyant" fraction appeared to contain flotillin-1 and no Rab5 which is known to be absent from lipid rafts (Figure 32C) (Chamberlain et al. 2001). As a known lipid rafts-localized

receptor, trkA was also immunoblotted and appeared in the lipid rafts fraction number 3 in the same way as reported previously in PC12 cells (Figure 32C) (Limpert et al. 2007). Surprisingly, Npr2 seemed to be partly localized within the lipid rafts fraction number 3 (Figure 32C).

These results suggested for the very first time that Npr2 might be compartmentalized to lipid rafts at the PM of PC12 cells. This might therefore suggest a compartmentalization of the Npr2-mediated cGMP signalling.
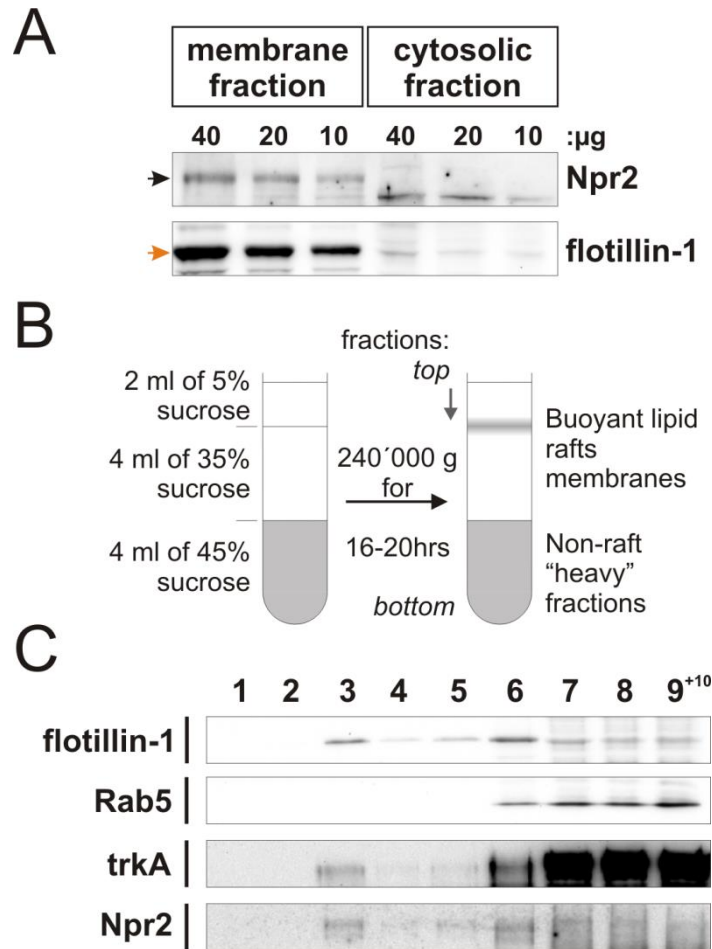
Figure 32 : Study of Npr2 partitioning in lipid rafts (LR) of PC12 cells. **(A)** Confirmation of the Npr2 expression in PC12 cells within the membrane fraction (black arrowhead). **(B)** Cartoon depicting the isolation of LR (Buoyant fraction) by detergent-free sucrose-density centrifugation (Ostrom & Liu 2007). **(C)** Immunoblotting study: ten 1-ml fractions (from top to bottom) of a PC12 cells post-nuclear lysate separated by detergent-free sucrose-density centrifugation. Flotillin-1 was used as a LR marker and Rab5 as a negative marker because it is known to be excluded from it. TrkA was used as a LR-localized receptor positive control. As expected, the third fraction (fraction below the 5% sucrose phase) appeared to be the LR flotillin-1 and trkA-enriched fraction and to be exempt of Rab5 protein. Interestingly, Npr2 also appeared to be partly enriched in the LR fraction number 3. **(B)** was adapted from (Ostrom & Liu 2007).

4.5 PROTEIN PALMITOYLATION IN SENSORY NEURONS

As shown above, cGKI localized at or close to intracellular membrane structures in the C-domain of embryonic DRG GCs in culture. Taken together with the increase in the axonal outgrowth and the GC remodelling effect of the CNP-based stimulation, this suggested that cGKI might regulate protein trafficking from intracellular compartments like vesicles to the PM. This would allow the addition of a bigger amount of proteins and membrane at the PM therefore increasing the area of the GCs and the axonal outgrowth. This process regulation should be fast. Hence, S-palmitoylation was considered as a potential PTM regulated by cGKI as it happens quickly and is reversible (Chamberlain & Shipston 2015). In addition to that, decrease of S-palmitoylation in cultured adult rat DRGs by S-nitrosylation competition or by tunycamicin-mediated inhibition was reported to induce GC collapse and a decrease in GC-mediated neurite extension, respectively (Hess et al. 1993; Patterson & Skene 1994).

4.5.1 PALMITOYLATED PROTEINS SEEMED TO BE ENRICHED IN THE GROWTH CONE OF CULTURED DRGs

Firstly, protein palmitoylation had to be characterized in sensory neurons. The first question that was therefore addressed was whether palmitoylated proteins were present in the embryonic DRG GC. To solve this challenge, a cell culture approach was used. It consisted in a biorthogonal labelling of palmitoylated proteins with a palmitate analogue coupled to an azide and a click chemistry reaction to label them. Hence, N-, O- and S-palmitoylated proteins could be biotinylated and visualized by ICC with streptavidin coupled to a fluorophore (Figure 10) (Gao & Hannoush 2014a; Gao & Hannoush 2014b). This method allowed, for example, to visualize the palmitoylome (in cyan) in cultured F11 cells (Figure 33A). F11 cells were double stained for α-tubulin (in green) so that neurites could be seen (Figure 33A). Interestingly, palmitoylated proteins could be observed in F11 cell GCs (orange arrowheads, Figure 33A and B). Moreover, they seemed to be enriched in the C-domain (white arrow, Figure 33B). Same experiment was then conducted with cultured E12.5 mouse DRGs and the palmitoylome could also be detected at GCs (orange arrowhead, Figure 33C). Similarly, palmitoylated proteins seemed to be

concentrated in the C-domain (white arrow, Figure 33C). Furthermore, double staining with cGKI (in magenta) was performed and showed that palmitoyl-enriched structures partly overlapped with cGKI-enriched structures at the C-domain (Figure 33C).

The omnipresence of palmitoylated proteins in F11 cells and DRG GCs suggested that it might play a major role in axon guidance and branching of those neurons. Moreover, the spatial proximity between palmitoyl-rich structures and cGKI suggested a possible interplay between cGKI-dependent phosphorylation and palmitoylation.
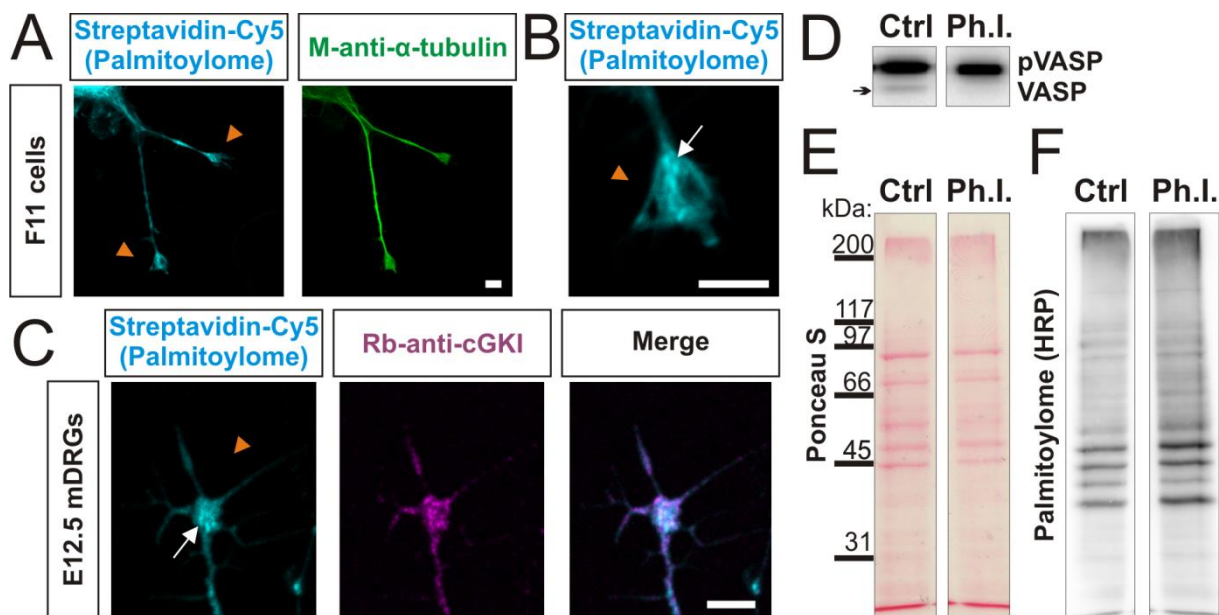

Figure 33 : Biorthogonal labelling of palmitoylated proteins: visualizing the palmitoylome in GCs of cultured F11 cells and mouse embryonic DRGs. **(A)** Palmitoylated proteins were visualized using the click-based approach (shown in cyan) in cultured F11 cells which were also stained for α-tubulin (shown in green). Palmitoylated proteins appeared to be omnipresent at the GCs (orange arrowheads). **(B)** It also appeared to be highly concentrated at the C-domain of the GC (white arrow). **(C)** Similar observations were made in cultured E12.5 mDRGs with a robust presence of the palmitoylome (in cyan) at the GC (orange arrowhead) and the presence of enriched structures at the C-domain (white arrowhead). Interestingly, double staining with cGKI (in magenta) showed that those palmitoyl-enriched structures partly overlapped with cGKI-enriched structures at the C-domain. Scale bars: 5 µm. **(D)** In order to assess the possible interplay between phosphorylation and S-palmitoylation, F11 cell lysates were shortly stimulated with threonine/serine protein phosphatase inhibitors (Ph.I.). Immunoblot analysis of VASP phosphorylation (pVASP) in presence of Ph.I. showed that only the phosphorylated version was detected compared to control in which the non-phosphorylated VASP was still detected (black arrow) indirectly confirming the blockade of phosphatases. **(E)** and **(F)** ABE-based labelling (biotinylation) of palmitoylated proteins was performed on membrane fractions. Samples were separated by SDS-PAGE and transferred onto a nitrocellulose membrane. **(E)** No global change in the protein level was observed by Ponceau S staining compared to control (Ctrl). **(F)** However, visualization of palmitoylomes using streptavidin coupled to HRP showed a global increase in the level of protein S-palmitoylation when phosphatase inhibitors were present.

4.5.2 INTERPLAY BETWEEN SERINE-THREONINE PHOSPHORYLATION AND S-PALMITOYLATION *IN VITRO*

Interplay between phosphorylation and S-palmitoylation of proteins has been shown for some proteins like the calcium- and voltage-gated potassium (BK) channels or the cAMP and cAMP-inhibited cGMP 3',5'-cyclic phosphodiesterase 10A (PDE10A) (Charych et al. 2010; Tian et al. 2008). However, it is still unclear whether phosphorylation plays a more global role in the S-palmitoylation regulation what might be the case knowing the high number of phosphoproteins that are S-palmitoylated (Blanc et al. 2015).

To investigate this in sensory neurons, the F11 cell system was once again used. Cells were harvested and lysed. Lysates were incubated 10 min in 10 µM serine/threonine phosphatases inhibitors caliculin A and okadaic acid. This short incubation was thought to indirectly increase the amount of phosphorylated proteins by blocking phosphatases which dephosphorylate proteins (Shi 2009). The increase of phosphorylation was verified by immunoblotting of VASP like shown previously (Dhayade et al. 2016). In presence of phosphatase inhibitors (Ph.I.), VASP was detected only as phosphorylated (upper band) whereas in the control a certain proportion of VASP was still not phosphorylated (black arrow, Figure 33D). Ponceau S staining also showed that Ph.I. treatment didn´t have an impact on the global protein level (Figure 33E). However, ABE-based labelling of S-palmitoylated proteins showed that indirectly increasing the phosphorylation by adding Ph.I. increased the global S-palmitoylation level (Figure 33F).

In sum, this simple experiment demonstrated *in vitro* that at least serine and threonine phosphorylation might be a global regulator of S-palmitoylation. Serine and threonine kinases like cGKI might therefore phosphorylate substrate proteins what leads to the increase in protein S-palmitoylation.

4.5.3 NPR2-MEDIATED EFFECTS ON CULTURED EMBRYONIC DRG EXPLANTS NEEDED S-PALMITOYLATION TO TAKE PLACE

2-bromopalmitate (2BP) is a large spectrum inhibitor of protein S-palmitoylation (Chamberlain & Shipston 2015). It was reported to inhibit palmitoyltransferases activity (Jennings et al. 2009). Moreover, It has been widely used in studies using cultured non-neuronal and neuronal cells and helped demonstrating the need of S-

palmitoylation in different systems *in vitro* and *in vivo* (Webb et al. 2000; El-Husseini et al. 2002; Mukai et al. 2015a).

Hence, this pharmacological tool was used to block S-palmitoylation in the 3D culture system of E7 chick DRG explants as used before (Figure 17). This time, explants were stimulated or not with 500 nM CNP and two supplementary conditions were tested in which 100 µM 2BP was also added to the culture. Explants were incubated overnight at 37°C, fixed and stained for NCAM. In this system, CNP stimulation still increased the axonal outgrowth compared to control (upper panel, Figure 34A). However, the presence of 2BP seemed to abolish this effect and explants treated with CNP showed similar axon outgrowth like in control supplemented with 2BP only (lower panel, Figure 34A). Quantifications showed that under these conditions, CNP stimulation increased the axonal outgrowth of about 20% ± 4% (10 ng/ml NGF, mean ± SEM, $p<0.001$) and 22% ± 2% (5 ng/ml NGF, mean ± SEM, $p<0.0001$, Figure 34B). As observed, presence of 2BP abolished this effect and no difference was seen between control (2BP) and stimulated samples (2BP CNP, $p>0.05$, Figure 34B). Note that 2BP itself had an inhibiting effect on axonal outgrowth compared to control.
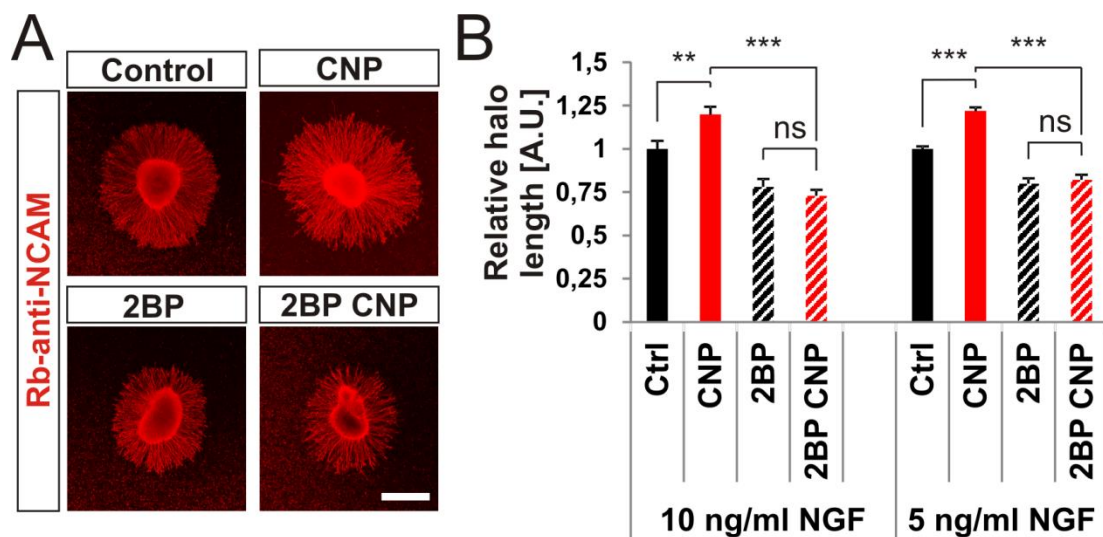
Figure 34 : CNP-mediated effect on axonal outgrowth is abolished by the S-palmitoylation blocker 2BP. **(A)** E7 chick DRG explants were cultured overnight in collagen gel in either the presence of 500 nM CNP, 100 µM 2BP, 500 nM CNP and 100 µM 2BP or its equivalent in buffer (control). Explants were then fixed and stained for NCAM. **(B)** Under these conditions, CNP stimulation increased the axonal outgrowth of about 20% ± 4% (10 ng/ml NGF, mean ± SEM) and 22% ± 2% (5 ng/ml NGF, mean ± SEM). However, blocking S-palmitoylation with 2BP inhibited the CNP-mediated axonal outgrowth increase in both cases. 100 µM 2BP had itself also an inhibiting effect on axonal outgrowth compared to control (-22% ± 4 % in 10 ng/ml NGF and -20% ± 3% in 5 ng/ml NGF, mean ± SEM). Number of explants assessed in 10 ng/ml NGF: 19 (Ctrl), 19 (CNP), 18 (2BP) and 18 (2BP CNP). Number of explants assessed in 5 ng/ml NGF: 13 (Ctrl), 15 (CNP), 16 (2BP) and 16 (2BP CNP). n=3 per NGF concentration. $p<0.0001$ (***), $p<0.001$ (**), $p>0.05$ (ns), unpaired two-tailed t-test. Error bars represent SEM. Scale bar: 500 µm.

Axon halo length was in average about 22% ± 4% (10 ng/ml NGF, mean ± SEM, p<0.05) and 20% ± 3% (5 ng/ml NGF, mean ± SEM, p<0.0001) shorter when S-palmitoylation was blocked compared to control (Figure 34A and B). This showed that at a concentration of 100 µM 2BP had an inhibitory effect on axonal outgrowth which is in line with previous studies where S-palmitoylation was blocked (Hess et al. 1993; Patterson & Skene 1994; Mukai et al. 2015a). Note that two different concentrations of NGF were assessed for this experiment (5 and 10 ng/ml) and the lowest one showed higher significance. Taken together, these results suggested that Npr2-mediated axonal outgrowth needed S-palmitoylation to take place.

In addition, the possible contribution of S-palmitoylation in the Npr2-mediated GC remodelling effect reported above (Figure 18) was also assessed. Again, E7 chick DRG explants were grown overnight on PDL/laminin double-coated substrate and then stimulated 1h with 500 nM CNP in presence or absence of 20 µM 2BP. Under these conditions, CNP stimulation also appeared to increase the average GC area of about 67% ± 4% (mean ± SEM, p<0.0001, Figure 35A and B). However, in presence of 2BP, the average area of CNP-stimulated GCs was decreased to a similar level as in controls (Ctrl and 2BP, p>0.05, Figure 35B). Separating GCs in 3 area populations showed that the CNP-based increase in large GCs (53% ± 4% compared to 11% ± 1% in control, mean ± SEM, Figure 35C) was abolished by blocking S-palmitoylation bringing the percentage down to control levels (Ctrl and 2BP, p>0.05, Figure 35C). Opposite was observed for the small GCs population where presence of CNP decreased the percentage from 58% ± 1% (mean ± SEM) down to 15% ± 3% (mean ± SEM, p=0.006, Figure 35C) whereas 2BP blocked the CNP effect by bringing it up to 59% ± 6% (mean ± SEM, p>0.05, Figure 35C). Note that the medium area GCs percentage was similar in all conditions (around 30%, p>0.05, Figure 35C).

Presence of CNP also decreased the average and maximum filopodia lengths of about 22% ± 2% and 28% ± 2%, respectively (mean ± SEM, p<0.0001, Figure 36A). 2BP blocked this effect and no more difference could be measured between CNP-treated and 2BP control GCs treated with 2BP only (p>0.05, Figure 36A). Note that 2BP alone had a very slight but significant effect on filopodia length. Average and maximum branch lengths were both reduced of about 4% ± 2% (mean ± SEM, p<0.05, Figure 36A). Number of filopodia per growth cone was neither affected by the CNP treatment, nor by the presence of 2BP (p>0.05, Figure 36B).
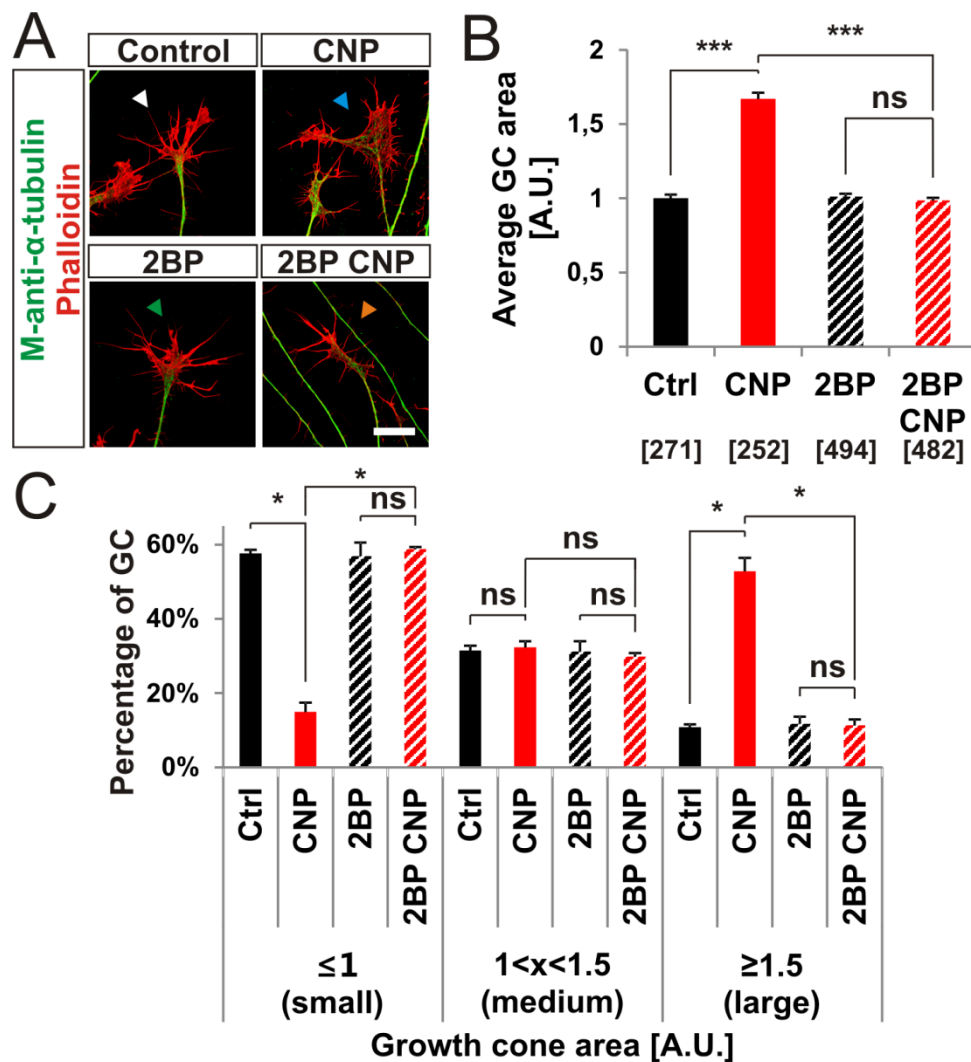
Figure 35 : CNP-mediated GC remodelling is inhibited by the S-palmitoylation blocker 2BP. **(A)** E7 chick DRG explants were cultured overnight on PDL-laminin substrate and stimulated 1-hour with 500 nM CNP or buffer control and in the presence of 20 µM 2BP or not. They were then fixed and stained by ICC for α-tubulin (in green) as well as F-actin (phalloidin, in red) in order to reveal the GCs structure. CNP stimulation increased the GC area as reported above and 2BP seemed itself to not have an influence on the GC morphology. However, it seemed to inhibit the CNP-mediated remodelling. **(B)** CNP stimulation increased the average growth cone area up to 67% ± 4% (mean ± SEM). 2BP abolished this effect by bringing the average GC area at the same level as the control or the 2BP-treated only samples. Number of GCs assessed per condition is shown in-between brackets. n=3. **(C)** GCs could be separated in small, medium and large areas. CNP stimulation induced a severe decrease in the percentage of small GCs down to 15% ± 3% (mean ± SEM) compared to control (58% ± 1%, mean ± SEM). It also drastically increased the percentage of large GCs up to 53% ± 4% (mean ± SEM) compared to control (11% ± 1%, mean ± SEM). Simultaneous presence of 2BP abolished those changes by bringing values to control levels. Note that 2BP alone had no effect on the GC area compared to control. p<0.0001 (***), p<0.05 (*), p>0.05 (ns), unpaired (B) and paired (C) two-tailed t-test. Error bars represent SEM. Scale bar: 20 µm.

These results identified the importance of dynamic S-palmitoylation in the Npr2-mediated GC remodelling of DRG explants in culture.
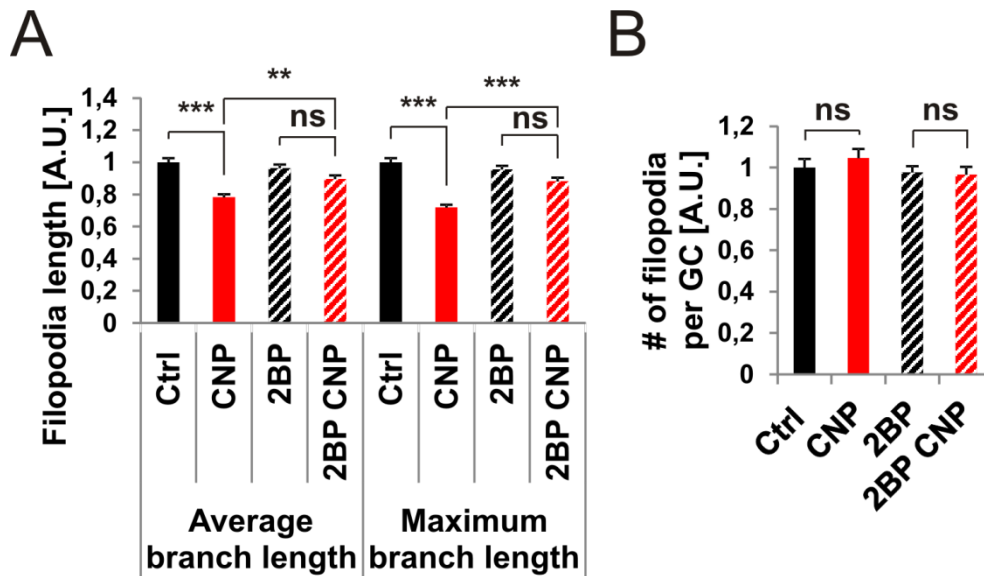
Figure 36 : CNP-mediated GC remodelling is inhibited by the S-palmitoylation blocker 2BP (continued). **(A)** CNP stimulation decreased the average and the maximum branch lengths of filopodia at GCs of about 22% ± 2% and 28% ± 2%, respectively (mean ± SEM). However, in presence of 2BP CNP didn´t induce any changes and both values were similar to controls. Note that 2BP alone had a very slight but significant effect on filopodia length. Average and maximum branch lengths were both reduced of about 4% ± 2% (mean ± SEM). **(B)** Number of filopodia per GC was not changed upon CNP or 2BP stimulation. n=3. p<0.0001 (***), p<0.001 (**), p>0.05 (ns), unpaired two-tailed t-test. Error bars represent SEM.

In order to assess whether S-palmitoylation was needed upstream or downstream of cGKI in the GC remodelling of cultured embryonic DRG explants, the same experiment had to be repeated with a cGMP analogue stimulation so that the signalling cascade could be triggered at the level of cGKI.

E7 chick DRG explants were cultured overnight on PDL-laminin double-coated substrate and were stimulated 1-hour with 50 µM of the cGMP analogue 8-pCPT-cGMP or buffer control and in the presence of 20 µM 2BP or not. They were then fixed and stained by ICC for α-tubulin (shown in green) as well as F-actin (phalloidin, shown in red) revealing the GCs structure. cGMP analogue stimulation seemed to increase the GC area similarly to CNP (orange arrowhead, Figure 37A) and 2BP seemed itself to not have an influence on the GC morphology as GCs looked similar to control ones (white arrowheads, Figure 37A). Indeed, However, it seemed to inhibit the cGMP-mediated remodelling as the area of GCs appeared comparable to controls (white arrowheads, Figure 37A). Indeed, cGMP analogue stimulation increased the average growth cone area up to 69% ± 3% (mean ± SEM, p<0.0001, Figure 37B). 2BP abolished this effect by bringing the average GC area to the same level as the control or the 2BP-treated only samples (p>0.05, Figure 37B). GCs were also separated in small, medium and large areas. cGMP analogue stimulation

induced a severe decrease in the percentage of small GCs down to 12% ± 3% (mean ± SEM) compared to control (57% ± 2%, mean ± SEM, p<0.05, Figure 37C).
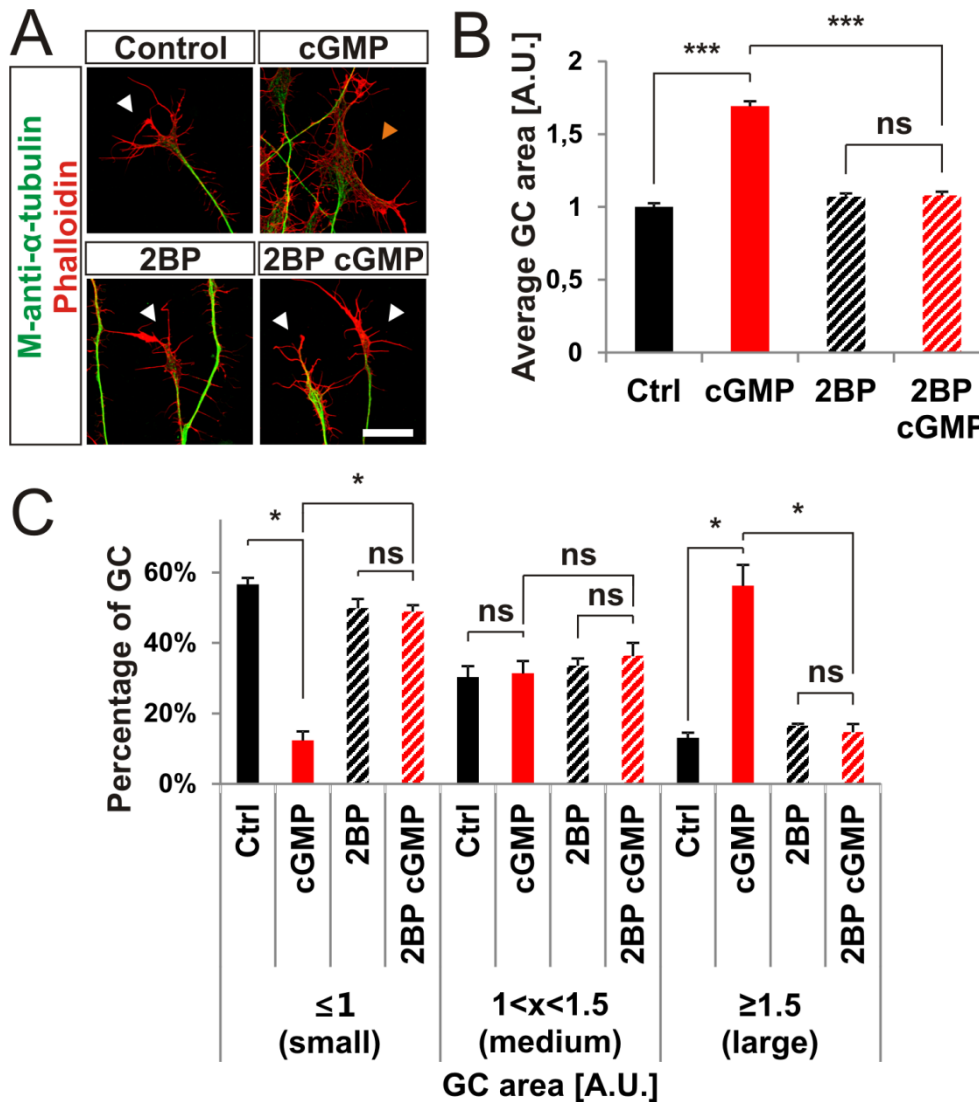

Figure 37 : cGMP-mediated GC remodelling is inhibited by the S-palmitoylation blocker 2BP. **(A)** E7 chick DRG explants were cultured overnight on PDL-laminin substrate and were stimulated 1-hour with 50 μM of the cGMP analogue 8-pCPT-cGMP or buffer control and in the presence of 20 μM 2BP or not. They were then fixed and stained by ICC for α-tubulin (in green) as well as F-actin (phalloidin, in red) in order to reveal the GCs structure. cGMP analogue stimulation increased the GC area similarly to CNP (orange arrowhead) and 2BP seemed itself to not have an influence on the GC morphology as GCs looked similar to control ones (white arrowheads). However, it seemed to inhibit the cGMP-mediated remodelling as the area seemed to be similar to controls. **(B)** cGMP analogue stimulation increased the average growth cone area up to 69% ± 3% (mean ± SEM). 2BP abolished this effect by bringing the average GC area at the same level as the control or the 2BP-treated samples. Number of GCs assessed: 332 (control), 374 (cGMP), 382 (2BP) and 350 (2BP cGMP). n=3. **(C)** GCs could be separated in small, medium and large areas. cGMP analogue stimulation induced a severe decrease in the percentage of small GCs down to 12% ± 3% (mean ± SEM) compared to control (57% ± 2%, mean ± SEM). It also drastically increased the percentage of large GCs up to 56% ± 6% (mean ± SEM) compared to control (13% ± 2%, mean ± SEM). Simultaneous presence of 2BP abolished those changes by bringing all values to control level. Note that 2BP alone had no effect on the average GC area compared to control. p<0.0001 (***), p<0.05 (*), p>0.05 (ns), unpaired (B) and paired (C) two-tailed t-test. Error bars represent SEM. Scale bar: 20 μm.

It also drastically increased the percentage of large GCs up to 56% ± 6% (mean ± SEM, p<0.05) compared to control (13% ± 2%, mean ± SEM, Figure 37C). Simultaneous presence of 2BP abolished those changes by bringing all values to control level (p>0.05, Figure 37C). This indicated that S-palmitoylation is indeed needed downstream of cGKI so that the GC remodelling can take place.

Taken together, blocking S-palmitoylation with 2BP also blocked the Npr2-mediated effects on axonal outgrowth and GC remodelling in cultured embryonic DRGs. Moreover, the contribution of S-palmitoylation in the increase of cultured embryonic DRG GC area appeared to be downstream of cGKI. In light of these results, Npr2-mediated cGMP signalling seemed to need S-palmitoylation to regulate both axonal outgrowth and GC remodelling. This indicated a link between the cGMP signalling cascade and the regulation of S-palmitoylation downstream of cGKI in the embryonic DRG GC.

4.5.4 cGMP SIGNALLING APPEARED TO REGULATE S-PALMITOYLATION IN SENSORY NEURONS *IN VITRO*

To assess whether cGMP signalling regulates S-palmitoylation *in vitro*, the ABE-based approach was initially used to label S-palmitoylated proteins and a streptavidin-based immunoprecipitation was conducted to purify them (Wan et al. 2007). This was performed on membrane fractions from cGMP-stimulated (1 mM 8-pCPTcGMP) and non-stimulated F11 cells and PNFs of CNP-stimulated and non-stimulated E12.5 mouse DRGs (1 µM CNP), respectively. Palmitoylated proteins were then separated by SDS-PAGE and silver stained (Figure 38A and C). Hence, palmitoylomes of stimulated versus non-stimulated cells could be compared by SDS-PAGE-based analysis. cGMP stimulation didn´t appear to have an effect on the overall pattern of S-palmitoylation in F11 cells as no obvious change could be observed (Figure 38A). Similar observation was made in CNP-stimulated embryonic DRGs as no noticeable variation in the overall pattern of S-palmitoylation could be detected (Figure 38C). Immunoblot for Gap43, a well-characterized S-palmitoylated protein, was used as a positive and loading control (Figure 38B and D) (Liu et al. 1993). Note that a control without hydroxylamine treatment (-HA) was used in parallel to assess the specificity of the biotin labelling (Figure 38A and C). Taken together,

the SDS-PAGE-based approach suggested that cGMP signalling might not globally regulate S-palmitoylation in sensory neurons.
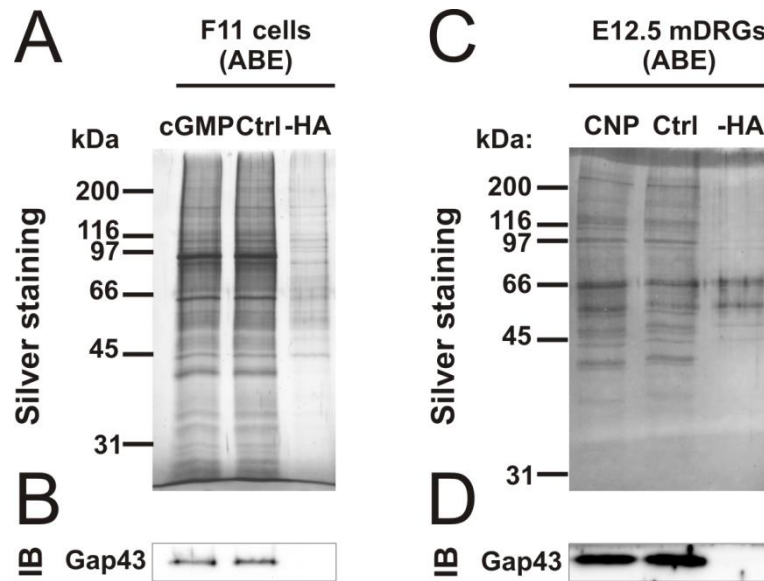
Figure 38 : Neither cGMP, nor CNP seemed to induce a change in the overall pattern of S-palmitoylation of proteins in F11 cells and E12.5 mDRGs SDS-PAGE-based study, respectively. **(A)** and **(C)** Palmitoylated proteins from crude membrane fractions (obtained by ultracentrifugation) of F11 cells (A) and from PNF of E12.5 mDRGs (C) were purified using the ABE-based approach coupled to a streptavidin-based pull-down. Palmitoylomes were separated by SDS-PAGE and silver stained. No apparent change in the overall pattern of protein S-palmitoylation was induced by the cGMP (cGMP analogue 8-pCPT-cGMP) or CNP stimulation. A non-stimulated crude membrane fraction or PNF were used as control in which the hydroxylamine treatment was omitted (-HA). **(B)** and **(D)** Immunoblot (IB) for the known palmitoylated protein Gap43 was used as positive control in both cases showing no change in its palmitoylation and most importantly no signal in the hydroxylamine-free control.

However, the proportion of S-palmitoylated proteins in neurons is known to be really high and detection of a change in the S-palmitoylation using a SDS-PAGE-based approach might not really be appropriate to detect subtle to medium changes (Chamberlain & Shipston 2015). In order to get a more precise picture of the palmitoylome when cGMP signalling is activated, the same approach described above was coupled to a mass spectrometry (MS)-based quantification of proteins. F11 cells lysates from cells stimulated or not with a cGMP analogue were fractionated in cytosol and membrane fractions (cf and mf) and their palmitoylomes were purified by ABE-based labelling and streptavidin-based immunoprecipitation method (Figure 39A). PNF was used in hydroxylamine-free control and immunoblot for Gap43 as a positive and loading control (Figure 39A and B). Samples (membrane and cytosol fractions) were then analyzed by label-free LC-MS (Egelhofer et al. 2013). As a result, palmitoylomes from cGMP-stimulated versus non-stimulated samples could be quantified and compared. When membrane fractions were analyzed (triplicate), it came out that a total of 14 3-hit palmitoylated protein

candidates (known or putative false-positives were discarded) were only detected in the presence of cGMP (Figure 39C). Note that the value 1 was implemented to the control and the log2 of the ratio cGMP-treated versus control cells was then calculated for each protein. Gap43, which was used as a positive control, was detected at a similar value in both stimulated and control samples having therefore a log2 value close to zero (Figure 39C).
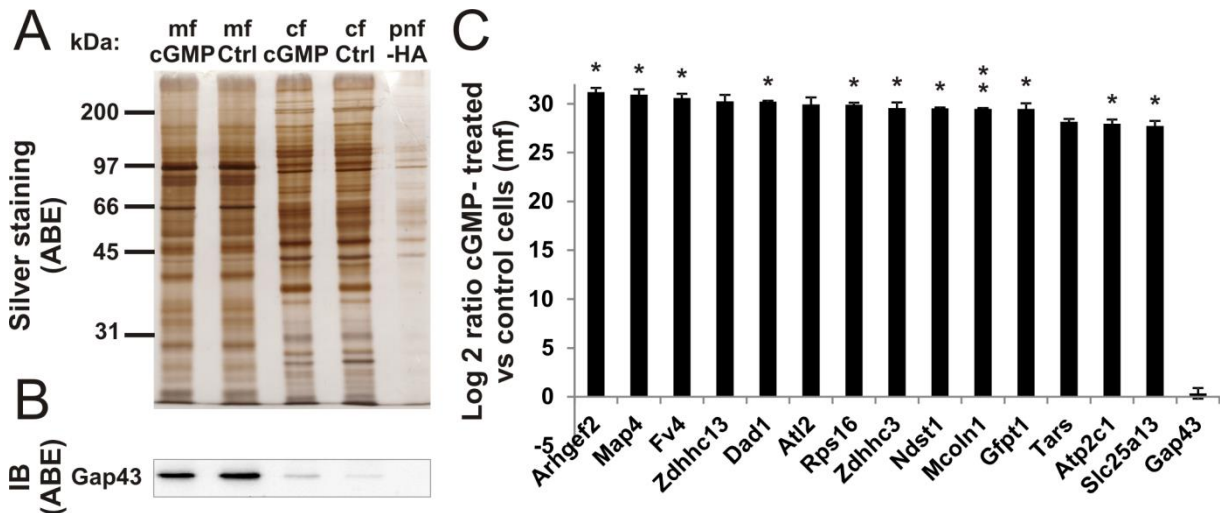
Figure 39 : LC-MS quantification of palmitoylated proteins purified from cGMP-stimulated and control F11 cells. **(A)** Palmitoylated proteins from membrane fractions (mf) and cytosol fractions (cf) of cGMP-stimulated and control F11 cells were purified using the ABE-based labelling and the streptavidin-based pull-down. Samples were separated on a SDS-PAGE and silver stained. A non-stimulated post-nuclear fraction (pnf) was used as control in which the hydroxylamine treatment was omitted (-HA). **(B)** Samples were also immunoblotted for the known palmitoylated protein Gap43. As expected, palmitoylated Gap43 was present in membrane fractions and at a lesser extend in the cytosol ones but not in the hydroxylamine-free pnf control. **(C)** Proteins which were detected only in cGMP-treated membrane fraction in all 3 independent experiments (3-hit) were selected. The value 1 was implemented to the control and the log2 of the ratio was then calculated for each protein. 14 proteins were shown to be only detected (potentially palmitoylated) in the presence of cGMP and they were all within a 27-31 range. As positive control, Gap43 was detected at a value close to 0 indicating no change in its palmitoylation state upon cGMP stimulation corroborating immunoblotting results in **(B)**. Note that known or putative false-positives are not shown. n=3. $p<0.001$ (**), $p<0.05$ (*) or $p>0.05$ (ns), paired two-tailed t-test. Error bars represent standard deviations.

A wide variety of proteins was identified, as the microtubule-associated protein 4 (Map4), the ER-localized GTPase atlastin-2 (Atl2), the lysosomal protein mucolipin-1 (also termed TRPML1, Mcoln1) or the palmitoyltransferases Zdhhc3 and Zdhhc13 (Figure 39C). Interestingly, the majority of them contained a putative cGKI phosphorylation motif and were already reported or purified in other ABE-based or click-based MS studies (Table 1). Using the S-palmitoylation site prediction software CSS palm 3.0 (Ren et al. 2008), most of them were also found to contain one or several putative cysteines that could be palmitoylated (Table 1).

Gene name	Protein name	putative cGKI phosphoryla-tion motif	CSS palm 3.0 (high threshold)	Literature (MS analyses: ABE-based and click-based)
Arhgef2	Rho guanine nucleotide exchange factor 2	RRRS;RKMT	yes	no
Map4	Microtubule-associated protein 4	KKPT;KKVS; KRTS;KRPT; KRMT;KRNT	yes	(Wan et al. 2013; Yang et al. 2009)
Fv4	Retrovirus-related Env polyprotein from Fv-4 locus	KRAT	yes	(Chesarino et al. 2014)
Zdhhc13	Palmitoyltransferase ZDHHC13	no	no	(Li et al. 2012; Wei et al. 2014)
Dad1	Dolichyl-diphosphooligosaccharide--protein glycosyltransferase subunit DAD1	no	no	(Martin & Cravatt 2009)
Atl2	Atlastin-2	RRQT	yes	no
Rps16	40S ribosomal protein S16	RKKT	no	(Forrester et al. 2011; Wilson et al. 2011; Yount et al. 2010)
Zdhhc3	Palmitoyltransferase ZDHHC3	no	yes	(Chesarino et al. 2014)
Ndst1	Bifunctional heparan sulfate N-deacetylase/N-sulfotransferase 1	KRLS	yes	(Li et al. 2012)
Mcoln1	Mucolipin-1	RRAS;RRGS	yes	(Vergarajauregui & Puertollano 2006; Li et al. 2012)
Gfpt1	Glutamine--fructose-6-phosphate aminotransferase [isomerizing] 1	KKGS;RRGS	yes	(Yang et al. 2009)
Tars	Threonine--tRNA ligase, cytoplasmic	KKKS;KKET	yes	no
Atp2c1	Calcium-transporting ATPase type 2C member 1	KRAS	yes	(Kang et al. 2008)
Slc25a13	Calcium-binding mitochondrial carrier protein Aralar2	no	no	(Li et al. 2012)

Table 1 : 3-hit palmitoylated protein candidates which were detected only in the F11 membrane samples stimulated with a cGMP analogue were listed. Putative cGKI phosphorylation motifs were screened as well as putative S-palmitoylated cysteines using the CSS palm 3.0 software set on high threshold (Ren et al. 2008). Candidates were checked whether they were already reported as palmitoylated proteins in previous MS-based analyses using either ABE-based or click-based approaches.

Moreover, 42 2-hit candidates were detected only under cGMP-treatment suggesting the list of 14 3-hit candidates might be underestimated (Supplementary Table 1 and Appendix excel spreadsheet).

Sorting 2 and 3-hit candidates per function emphasized the varied range of proteins that were S-palmitoylated upon cGMP stimulation (Supplementary Table 1 and Figure 40A). Whereas a robust proportion of proteins had a metabolism-related function (26%), proteins involved for example in transcription and translation, signalling, transport and cell adhesion were also detected (Figure 40A). Furthermore, RT-PCR analysis of 3-hit candidates in E12.5 mouse DRGs showed that they were all expressed at the mRNA level when sensory axons bifurcate (Figure 40B). Note that the retrovirus-related Env polyprotein from Fv-4 locus (Fv4) wasn´t investigated as it is a resistance gene to "ecotropic murine leukemia virus" only present in few mouse strains and that its mRNA sequence wasn´t available (Limjoco et al. 1993; Taylor et al. 2001).
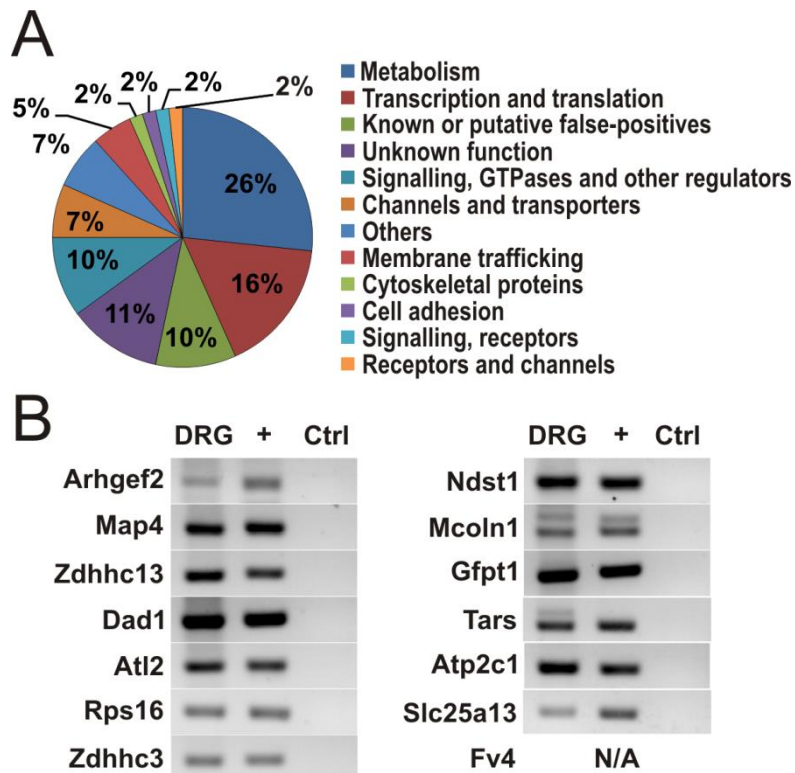
Figure 40 : Analysis of 2 and 3-hit candidates sorted by function and RT-PCR analysis of the mRNA expression of 3-hit candidates in E12.5 mouse DRGs. **(A)** 2 and 3-hit palmitoylated candidate proteins detected only in the cGMP-stimulated F11 membrane fraction (total of 60 proteins) covered a large panel of functions. For example, proteins involved in metabolism (26%), transcription and translation (16%) and signalling (10%) were detected as well as channels and transporters (7%), membrane trafficking-related (5%) and cell adhesion proteins (2%). **(B)** RT-PCR analysis of 3-hit candidates detected in the membrane fraction of F11 cells in E12.5 DRGs (DRG) and in E17 whole mouse embryo cDNA libraries (positive control, +). Note that the third row was loaded with the water control (ctrl). All candidates appeared to be expressed at the mRNA level in mouse embryonic DRGs. Note that Fv4 wasn´t investigated as it is a resistance gene to "ecotropic murine leukemia virus" only present in few mouse strains and that its mRNA sequence wasn´t available (Limjoco et al. 1993; Taylor et al. 2001). Ctrl: water control. N/A, not attributed.

Furthermore, MS analysis of cytosol fractions also allowed to identify 7 3-hit and 75 2-hit proteins that were found to be only palmitoylated upon cGMP stimulation

(Appendix excel spreadsheet). However, these candidates were not further investigated as the cytosol fraction contains far less S-palmitoylated proteins what might lead to a greater amount of putative false-positives.

As hypothesized previously, these results showed that cGMP signalling regulated indeed S-palmitoylation *in vitro* in the DRG-like cell line F11.

4.5.5 ZDHHC13 LOSS OF FUNCTION AND NDST-1 KNOCKOUT SENSORY AXONS BIFURCATED *IN VIVO*

Axonal branching of two palmitoylated candidates identified by MS analysis were investigated at the DREZ of the developing SC by Dil tracing (Schmidt & Rathjen 2011).

First, Zdhhc13 loss of function (LOF) embryos were assessed. Those embryos were lacking the DHHC-containing catalytic domain of the enzyme therefore expressing a Zdhhc13 protein without palmitoyltransferase activity (Saleem et al. 2010). Due to the reduced bone growth phenotype of these mice reminiscent of the Npr2 KO (Chusho et al. 2001; Tamura et al. 2004; Saleem et al. 2010; Song et al. 2014), this enzyme was of particular interest. However, these embryos had a completely normal branching pattern at the DREZ where DRG axons bifurcated like in control (green arrowheads, Figure 41A).
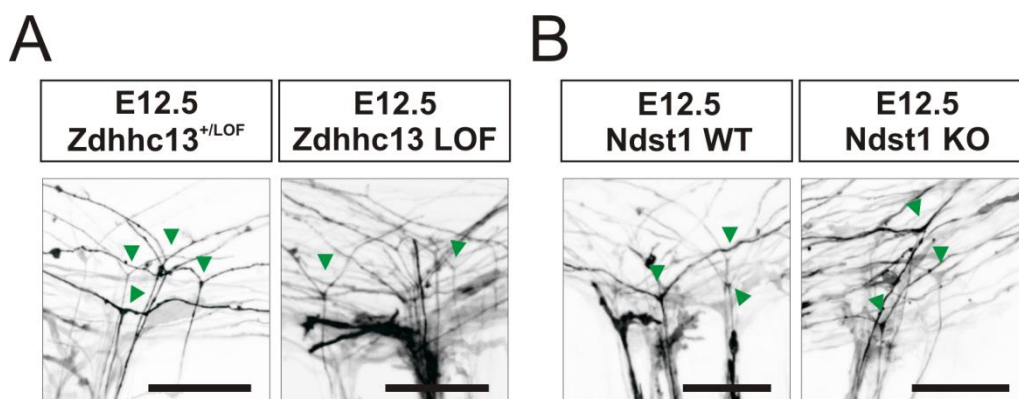
Figure 41 : Study of axonal bifurcation in Zdhhc13 loss of function (LOF) and Ndst1 KO embryos. E12,5 fixed embryo were prepared and DRG axons were traced by Dil tracing. **(A)** and **(B)** In both mutants DRG axons at the DREZ appeared to bifurcate normally like visualized in their respective controls (green arrowheads). Scale bars: 50 µm.

Then, the other candidate to be assessed was the bifunctional heparan sulfate N-deacetylase/N-sulfotransferase 1 (Ndst1). Ndst1 is a Golgi-localized enzyme involved in the "N-sulfation during heparan sulfate and heparin biosynthesis" (Ringvall & Kjelln 2010) . Interestingly, heparan sulfate biosynthesis was reported to be essential in the

Netrin-1-mediated guidance of commissural axons within the SC (Matsumoto et al. 2007). Axonal branching at the DREZ of embryos lacking the Ndst1 protein (Grobe et al. 2005) was also assessed by DiI and no lack of bifurcation could be seen and all axons were bifurcating like in control embryos (green arrowheads, Figure 41B). These results indicated that Zdhhc13 and Ndst1 were both not needed in sensory axon bifurcation at the DREZ *in vivo*.

4.5.6 ZDHHC ENZYMES EXPRESSION IN EMBRYONIC DRGS

As mentioned before, little is known about how S-palmitoylation might be globally regulated. As shown above, phosphorylation might be a key regulator of this PTM (Figure 33F). One possibility would be that it might act directly at the level of palmitoyltransferases, phosphorylating them and therefore activating them, changing their specificity to substrates or even their localization. Recent reports have shown the role of tyrosine phosphorylation in the localization of Zdhhc5 and the activation of Zdhhc3, respectively in neurons (Brigidi et al. 2015; Lievens et al. 2016). Hence, cGKI might regulate S-palmitoylation by directly acting at the Zdhhc enzymes level by phosphorylating them.

Palmitoyl-transferase	Putative cytosolic cGKI phosphorylation motif
Zdhhc1	RRSS[401] (C-terminus)
Zdhhc5	KKVS[704] (C-terminus)
Zdhhc8	KKVS[751] (C-terminus)
Zdhhc23	KKKT[9] (N-terminus)
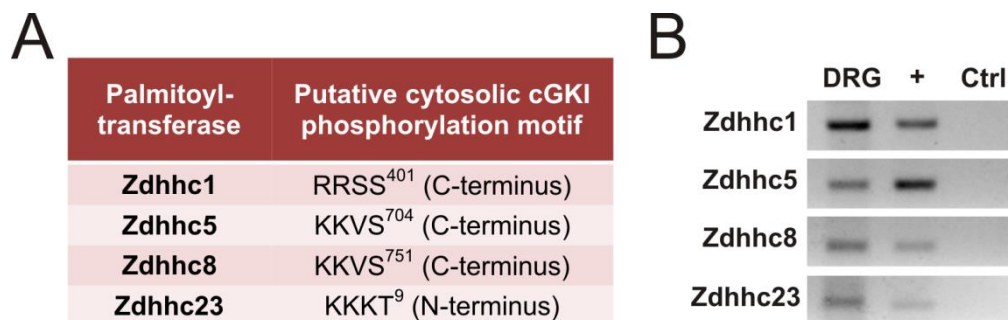
Figure 42 : Palmitoyltransferases containing a putative cGKI phosphorylation motif. **(A)** Mouse Zdhhc1, 5, 8 and 23 were found to have a putative cGKI phosphorylation motif in their cytosolic domains. **(B)** mRNA expression of all 4 enzymes was assessed by RT-PCR of E12.5 mouse DRGs cDNA library (DRG) and all 4 were shown to be expressed. E17 whole mouse embryo cDNA library was used as positive control (+). Ctrl: water control.

The 23 known murine palmitoyltransferases were screened for putative cGKI phosphorylation motifs present in their cytosolic domains. Four were found to contain such a motif, Zdhhc1, 5, and 8 in their C-terminus and Zdhhc23 in its N-terminus (Figure 42A). RT-PCR analysis of their mRNA expression in E12.5 mouse DRGs indicated that all 4 enzymes were expressed at this embryonic stage (Figure 42B).
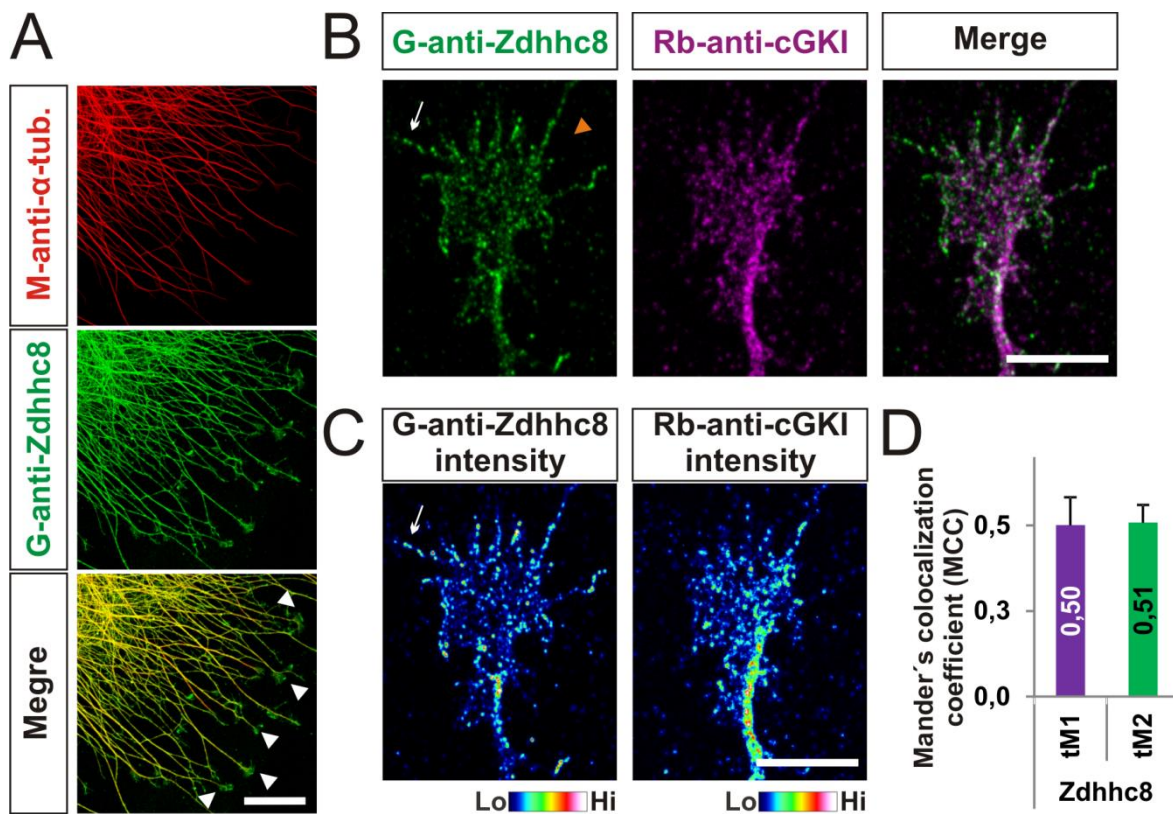
Figure 43 : Zdhhc8 localization in the embryonic DRG GC. **(A)** Zdhhc8 is expressed in cultured E12.5 DRG explants (green). Explants were double-stained for α-tubulin (red) by ICC. **(B)** ICC study of Zdhhc8 expression showed that it was present as a vesicle-like pattern in E12.5 DRG GCs (orange arrowhead). **(B)** and **(C)** Zdhhc8 appeared to be in the P-domain in filopodia (white arrows) and in the C-domain at a lesser extend than cGKI. **(D)** The MCC was calculated and cGKI appeared to colocalize to Zdhhc8 in the DRG GC. tM1: 50% ± 8% and tM2: 51% ± 5% (mean ± SEM). n=10 GCs. Hi, high; Lo, low, α-tub., α-tubulin. Scale bars: **(A)** 100 μm; **(B)** and **(C)** 10 μm.

Zdhhc8 was further investigated in the GC of cultured E12.5 mouse DRGs by ICC. It appeared to be expressed in cultured E12.5 mouse DRG explants (shown in green, Figure 43A). It also clearly localized to GCs (white arrowheads, Figure 43A) where it had a vesicle-like pattern (orange arrowhead, Figure 43B). It seemed to be present in the C-domain rich in cGKI but also in the P-domain within filopodia (white arrows, Figure 43B and C). Colocalization study with cGKI indicated a pretty similar proportion of cGKI-positive structures colocalizing to Zdhhc8-positive structures (tM1=50% ± 8%, mean ± SEM) and vice versa (tM2=51% ± 5%, mean ± SEM, Figure 43D).

These first results on the Zdhhc enzymes expression in embryonic mouse DRGs enlightened the possible link between cGKI and Zdhhc8 in the GC and maybe with other enzymes containing a putative cGKI phosphorylation motif.

4.5.7 ZDHHC5 WAS NOT ESSENTIAL FOR SENSORY AXON BIFURCATION

Overall, although cell biological and biochemical assays demonstrated that cGMP signalling via CNP-Npr2-cGKI regulates S-palmitoylation, my current studies on genetic mouse models so far didn´t give any evidence for its participation in axon bifurcation. However, other Zdhhc enzymes have to be explored using genetic mouse models in order to disturb S-palmitoylation in DRG GCs *in vivo*. Based on its mRNA expression in E12.5 mDRGs and its putative cGKI phosphorylation motif (Figure 42), Zdhhc5 and Zdhhc8 were further considered as possibly playing a role in DRG bifurcation *in vivo*. Zdhhc8 was also reported to play a role in axonal branching *in vivo* (Mukai et al. 2015b). Together with its GC localization in cultured DRGs (Figure 43), this enzyme was speculated to play a role in axonal bifurcation (Mukai et al. 2015b). However, due to breeding problems it couldn´t be assessed on time in this work. Only the close related Zdhhc5 enzyme could be explored.

Hence, KO embryos lacking Zdhhc5 were investigated (Figure 44). Absence of Zdhhc5 in KO embryos was verified by immunoblot of E12.5 head lysates resulting in the absence of a band at around 77 kDa (Figure 44A). However, DiI tracing of E13.5 KO embryos revealed that DRG axons were normally bifurcating at the DREZ (green arrowheads, Figure 44B) as well as forming collaterals like in control WT littermate embryos (red arrowheads, Figure 44B).

Altogether, these results indicated that Zdhhc5 didn´t play a role in sensory axon bifurcation *in vivo*.
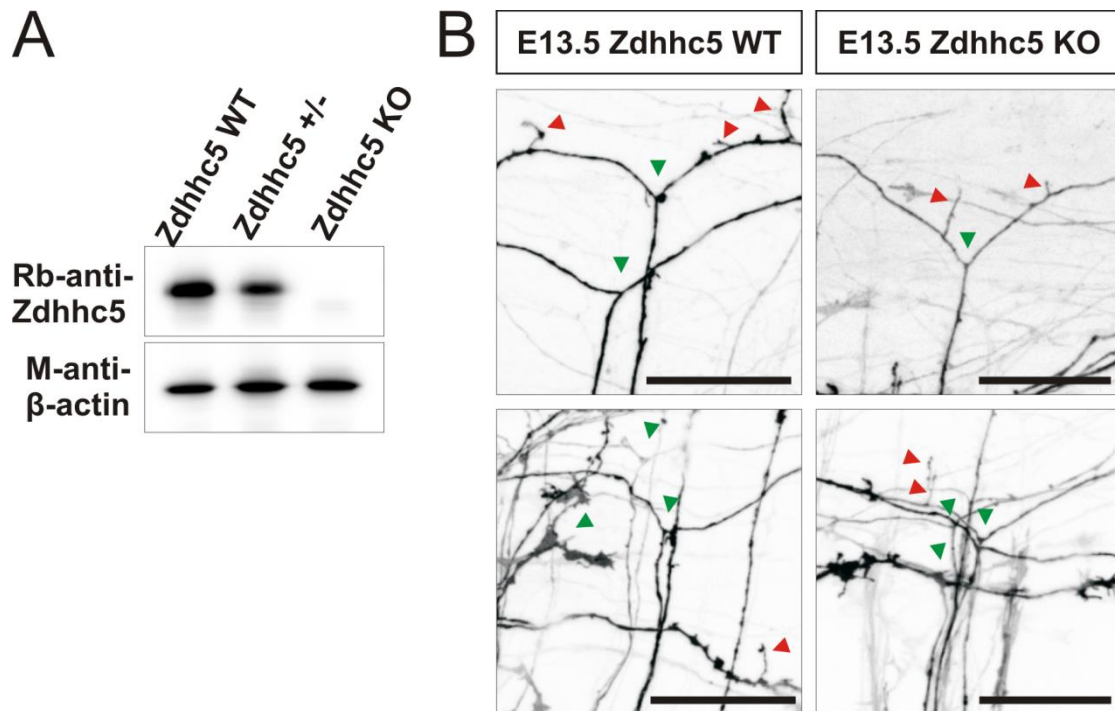
Figure 44 : Deletion of Zdhhc5 didn´t impact the bifurcation of sensory axons at the DREZ. **(A)** E13.5 mouse head lysates were separated by SDS-PAGE and immunoblotted for Zdhhc5 to confirm the absence of the enzyme in KO embryos (band at around 77 kDa). Immunoblot for β-actin was used as a loading control. **(B)** Analysis of E13.5 DRG axons at the DREZ by DiI tracing indicated that in Zdhhc5 KO axons were bifurcating normally (green arrowheads) and forming collaterals (red arrowheads) like in WT littermate embryos. Scale bars: 50 μm.

4.6 SENSORY AXON BIFURCATION WAS NOT DISTURBED IN MICE LACKING HPRT OR SPECFIC CYTOSKELETON PROTEINS

In parallel to the experiments conducted above, several interesting candidate proteins in relation to sensory axon bifurcation were investigated *in vivo* using mutant mice and the DiI tracing method.

4.6.1 HPRT WAS NOT NEEDED UPSTREAM OF GTP IN NPR2-MEDIATED AXON BIFURCATION

Hypoxanthine-guanine phosophoribosyltransferase (Hprt, also termed HGPRT) is an enzyme catalysing the formation of guanosine monophosphate (GMP) from guanine and has been shown to be implicated in the purine nucleotide metabolism (Torres & Puig 2007; Hauryliuk et al. 2015). As Npr2 transforms GTP into cGMP in the process of axonal bifurcation, it was speculated whether Hprt might be needed in embryonic DRGs upstream of GTP in the formation of its mono-phosphorylated version GMP.

DiI labelling of E12.5 Hprt KO mouse DRG axons showed that it was not the case as they were found to bifurcate at the DREZ of the SC (green arrowheads, Figure 45A). Taken together, this suggested that GTP can be produced in an Hprt-independent way in DRG neurons. Most likely, the GMP synthase might be implicated in the production of GMP from xanthosine 5´‑phosphate upstream of GTP or at least, might be enough to compensate the lack of GMP synthesis in Hprt KO embryos (Hauryliuk et al. 2015).

4.6.2 ABSENCE OF CYTOSKELETON PROTEINS LIKE RAC1, COFILIN AND SPASTIN DIDN´T ALTER SENSORY AXON BIFURCATION *IN VIVO*

Evidences demonstrated that specific axon guidance and branching events can regulate the actin and microtubule cytoskeletons to induce a change in growth direction or shape, respectively (Kalil & Dent 2014; Gallo 2011). Hence, several cytoskeleton proteins that were previously reported to play a major role in neurodevelopment were considered in regard to DRG axon bifurcation *in vivo*.

Rac1 (Ras-related C3 botulinum toxin substrate 1) is a plasma membrane-associated small GTPase that was originally shown to be involved in lamellipodia formation in fibroblast (Ridley et al. 1992). It was described to regulate F-actin polymerisation and to form a complex with CLIP170 and the actin binding protein IQGAP1 (Fukata et al. 2002; Lowery & Vactor 2009; Neukirchen & Bradke 2011). Ablation of Rac1 led to defects in axon guidance and branching in the drosophila and strong axon growth as well as axon guidance impairments in the mouse (Ng et al. 2002; Hua et al. 2015). Moreover, its activation at the plasma membrane was shown to be S-palmitoylation-dependent (Navarro-Lerida et al. 2012). Altogether, these particularities led to the investigation of the branching pattern at the DREZ of mouse embryos lacking Rac1 in DRGs *in vivo* using the DiI labelling approach (Chrostek et al. 2006). As revealed in Figure 45B, bifurcation still took place in sensory axons entering the DREZ of the SC when Rac1 was absent in DRGs (cKO using wnt1Cre). This suggested that Rac1 was not needed in this specific branching process.

In addition to Rac1, two other cytoskeleton proteins of interest were investigated: cofilin and spastin. On one hand, cofilin is essential for actin retrograde flow in neurons by regulating the F-actin disassembly in the GC (Flynn et al. 2012; Lowery & Vactor 2009). Moreover, cGMP stimulation of E17 rat cortex primary cells was

reported to increase the phosphorylation state of cofilin suggesting a link between cGMP signalling and cofilin regulation in the GC (Zulauf et al. 2009). On the other hand, spastin is known to be implicated in the microtubule severing needed in the creation of new axon branches at least in cultured neurons what made it an interesting candidate in regard to axon bifurcation (Kalil & Dent 2014). Nevertheless, DiI labelling study of E12.5 cofilin (cKO using wnt1Cre) or spastin mutated DRG axons entering the DREZ didn´t show any lack of bifurcation in absence of these cytoskeleton proteins as they mostly all properly bifurcated (green arrowheads, Figure 45C and D).
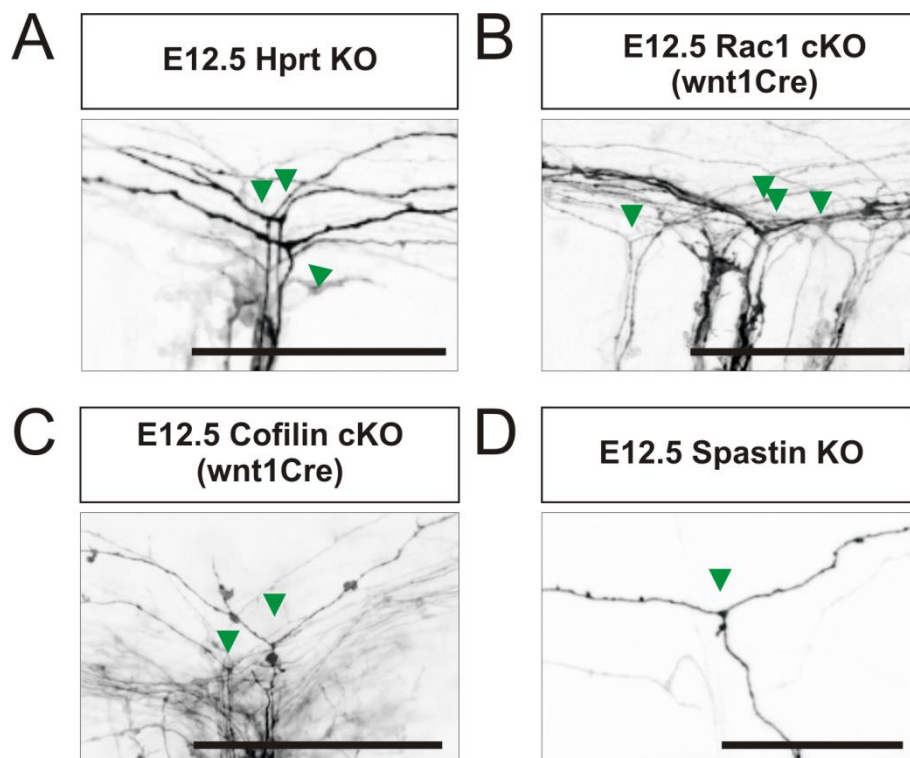
Figure 45 : DiI tracing study of DRG axon branching in different mouse mutants. Examples of DRG axons labelled by DiI that normally bifurcated at the DREZ of the SC (green arrowheads) in E12.5 mutant embryos: **(A)** Hprt KO; **(B)** Rac1 cKO (wnt1Cre); **(C)** cofilin cKO (wnt1Cre); **(D)** spastin KO. Scale bars: 100 µm.

Taken together, these results indicated that, in absence of key cytoskeleton proteins, the bifurcation of DRG axons was still taking place at the DREZ. These didn´t reveal a link between the Npr2-mediated cGMP signalling cascade and the regulation of the actin and microtubule cytoskeletons *in vivo* which is in line with the observations reported above on the localization of cGKI in the DRG GC and its proximity to intracellular membrane structures.

5. RESULTS CHAPTER TWO – FAK-MEDIATED AXON GUIDANCE IN SENSORY NEURONS

5.1 STUDY OF FAK-MEDIATED DRG AXON GUIDANCE

As already shown before (Figure 26D), FAK appeared to play a role in the guidance of sensory projections entering the more anterior part of the spinal cord but wasn´t implicated in sensory axon bifurcation (Figure 26D and E). The lack of FAK led to a misguidance of trkA-positive nociceptive axons as well as peripherin-positive projections at the DREZ of the spinal cord (Figure 26D). In this section, the axon guidance defect observed in FAK mutant embryos was further characterized. Moreover, FAK-mediated guidance of commissural axons was also investigated.

5.1.1 TEMPORAL ANALYSIS OF FAK CONDITIONAL KNOCKOUT DRG AXON MISPROJECTIONS WITHIN THE DORSAL SPINAL CORD

First of all, it was very important to characterize at which embryonic stage FAK might be involved in the guidance of DRG axons entering the SC. To this aim, transverse cervical SC cryosections from E12.5, E13.5 and E14.5 FAK control (FAK$^{fl/fl}$ or FAK$^{fl/wt}$ wnt1Cre$^+$) and cKO (FAK$^{fl/fl}$; wnt1Cre$^+$) were stained by IHC for peripherin (red) and counterstained for DAPI (blue, Figure 46). Peripherin is expressed in embryonic DRG but not in the DSC what allowed the specific visualization of sensory projections in the SC (Zhou et al. 2002). Interestingly, at the earlier stage E12.5 no misguidance of sensory axons stained by peripherin could be observed (Figure 46A). Dorsal funiculi looked dense and fasciculated like in control embryos (blue arrow, Figure 46A). However, starting E13.5 misprojections could be observed with bundles of axons entering prematurely the dorsal horn of the SC (white arrowheads, Figure 46B). In addition to the disorganized DREZ, cells located close to the DREZ were forming an "island" most likely separated from the others by the misguiding sensory axons and localizing within the dorsal funiculus as shown by DAPI staining (white arrow, Figure 46). At the later embryonic stage E14.5 same phenotype persisted with axon bundles invading the dorsal horn of the SC (yellow arrowheads, Figure 46C). Note that the more central part the dorsal funiculus close to the midline looked normal (green

arrowheads, Figure 46C). Furthermore, DSC cells close to the DREZ still looked a bit disorganized but at a much slighter extend than at E13.5 (yellow arrow, Figure 46C). These results showed that FAK is needed in the guidance of a subpopulation of DRG axons entering the SC at least after E12.5.
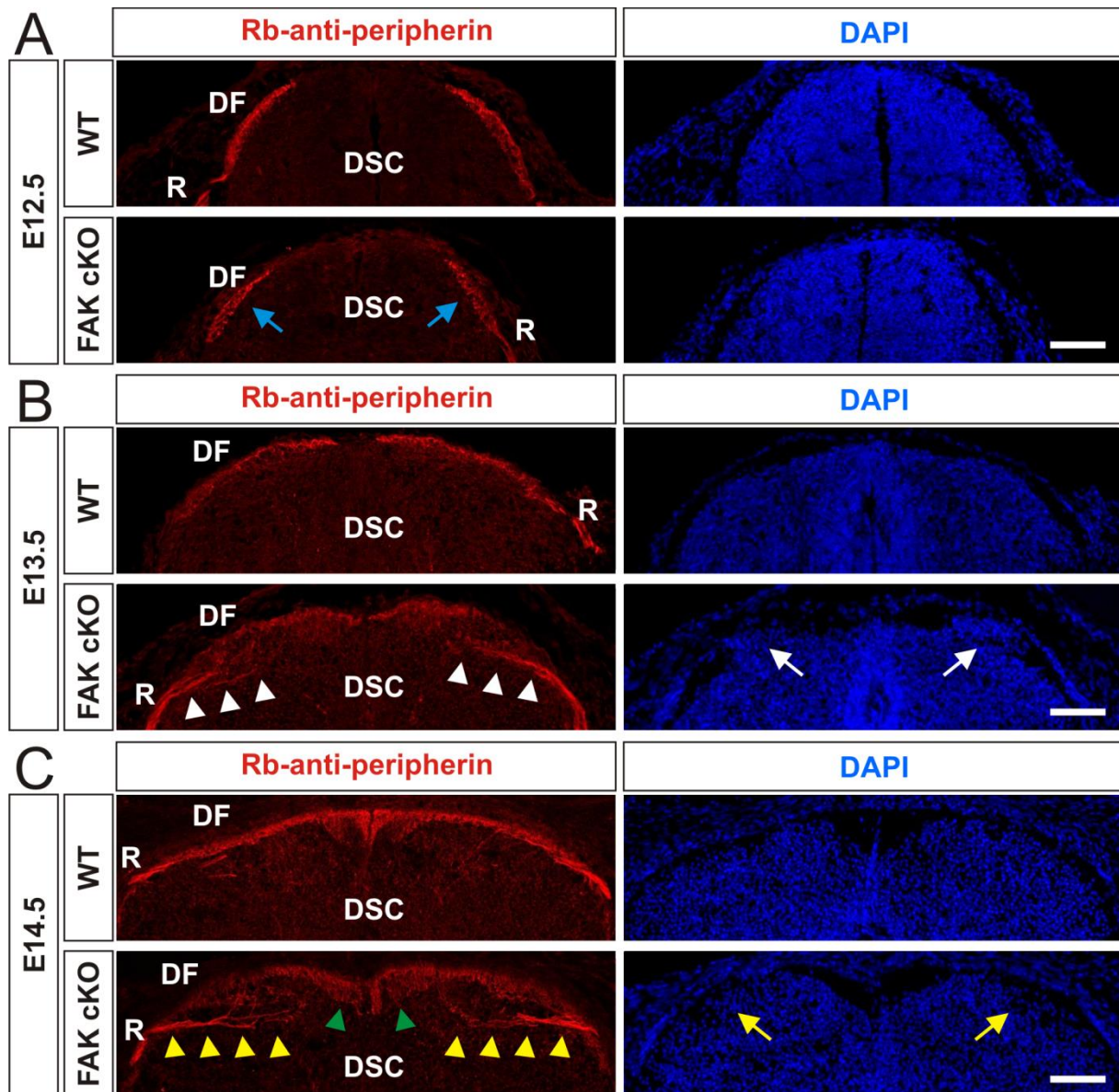
Figure 46 : Effects caused by the loss FAK in DRGs: disturbed axonal guidance at the DREZ. **(A)**, **(B)** and **(C)** Transverse cryosections of fixed SC from FAK mutant embryos were stained for peripherin (red) to visualize sensory axon projections in E12.5 **(A)**, E13.5 **(B)** and E14.5 **(C)** spinal cords. DAPI counterstaining was also performed (blue) to visualize nuclei. **(A)** Sensory projections within the SC looked normal at E12.5 and DRG axons were properly fasciculated within the dorsal funiculi (blue arrows) like in the WT control. **(B)** At E13.5, a subset of FAK cKO sensory axons were shown to invade the deeper layers of the DSC (white arrowheads) forming disorganized dorsal funiculi. DAPI staining also showed an "island" of DSC cells which seemed to be induced by the misprojecting axons (white arrow). **(C)** At the later stage E14.5, misprojecting axons were still seen in FAK cKO (yellow arrowheads) whereas dorsal funiculus parts close to the midline looked quite unaffected (green arrowheads). The DSC structure was still disturbed but at a lesser extend (yellow arrows) compared to WT control. FAK cKO: FAK$^{fl/fl}$; wnt1Cre$^+$. WT: FAK$^{fl/fl}$ in **(A)** and **(B)** or FAK$^{fl/wt}$; wnt1Cre$^+$ in **(C)** . R, dorsal root; DF, dorsal funiculus; DSC, dorsal spinal cord. Scale bars: 100 µm.

5.1.2 CHARACTERIZATION OF FAK CONDITIONAL KNOCKOUT MISGUIDING AXON SUBTYPE

As peripherin is known to be expressed in a common pool of nociceptive and proprioceptive DRG neurons, a more precise IHC analysis was needed in order to identify which subtypes of neurons needed FAK to correctly project in the DSC (Hancock et al. 2011).
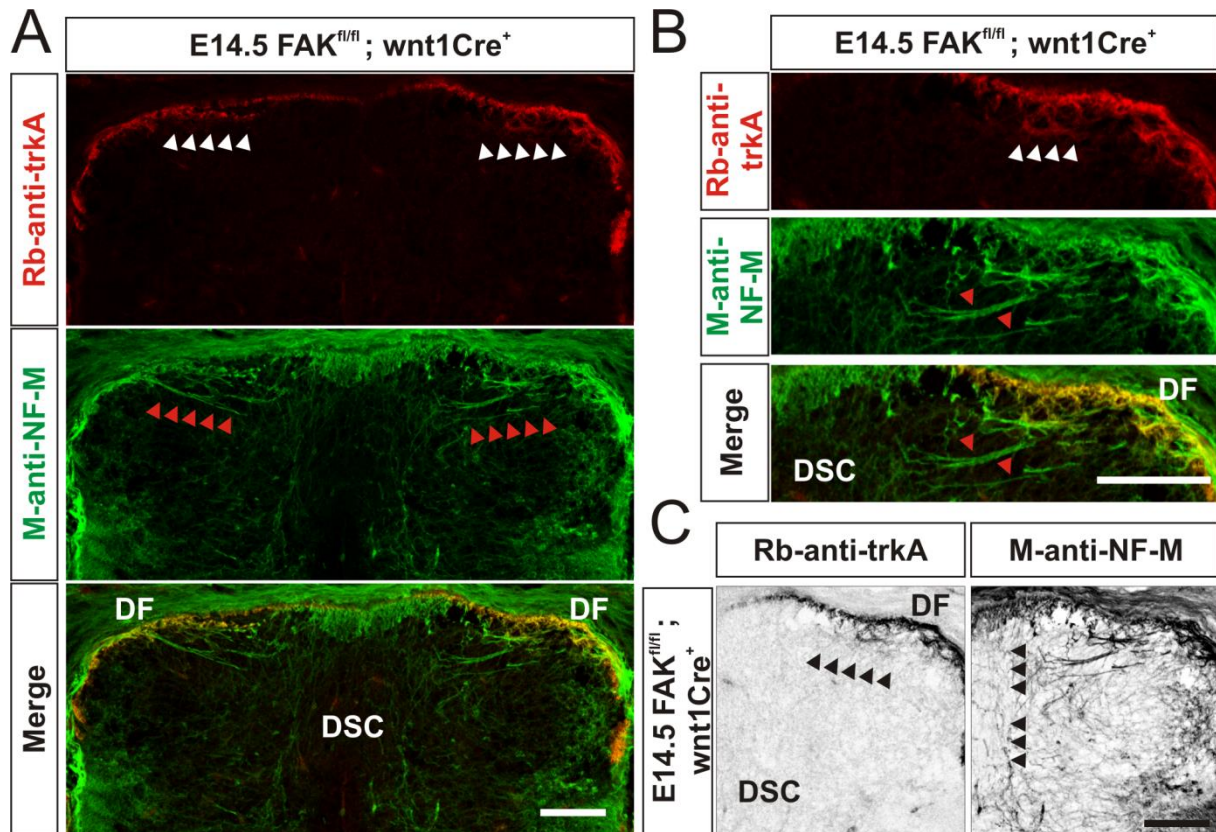
Figure 47 : Subtype characterization of FAK cKO DRG misprojecting axons. **(A)** and **(B)** Visualization of nociceptive and non-nociceptive FAK cKO DRG axons at the DREZ using IHC on SC cross-sections. A subset of trkA-positive nociceptive axon bundles was shown to invade the DSC (white arrowheads) whereas a subset of NF-M-positive but trkA-negative bundles too (red arrowheads). **(C)** Inverted black and white insets from (A) showed that nociceptive and proprioceptive collateral branches appeared to form in FAK cKO (black arrowheads). DF, dorsal funiculus; DSC, dorsal spinal cord. Scale bars: 100 µm.

To this end, E14.5 FAK cKO SC transverse cryosections were double-stained by IHC for trkA and neurofilament-M (NF-M, Figure 47A). TrkA is known to be expressed in nociceptive axons and NF-M is expressed in all differentiated neurons in the developing SC and DRGs (Molliver et al. 1995; Hirokawa et al. 1984). Using both markers it was possible to identify misprojecting trkA-positive axons within the more superficial layers of the DSC (white arrowheads, Figure 47A and B). Moreover, a population of misprojecting axons, which was trkA-negative but NF-M positive, was detected in deeper layers of the DSC (red arrowheads, Figure 47A and B). This

suggested that a subpopulation of nociceptive (trkA-positive) but also putatively proprioceptive and mechanoreceptive DRG axons was wrongly projecting in deeper layer of the DSC in absence of FAK.

5.1.3 FAK DELETION IN NPR2-POSITIVE CELLS ALSO LED TO AN OVERSHOOTING OF DRG AXONS WITHIN THE DORSAL SPINAL CORD

Having characterized the defect in the guidance of a subpopulation of DRG axons entering the SC in the absence of FAK in wnt1-positive cells, it was still not sure whether this phenotype came from the lack of FAK in DRGs or in the DSC. The use of the wnt1Cre driver led to the deletion of FAK in DRGs as previously demonstrated (Figure 26C). However, it also should have led to the knockout of FAK in a population of DSC cells starting embryonic stage E11.5 as previously reported (Figure 48A) (Matsumoto et al. 2007; Kam et al. 2014). Hence, the misguidance phenotype might have come for example from cells localized in the DSC that could not migrate properly ventrally in absence of FAK and therefore attracting prematurely some of the DRG axons to the deeper layers of the DSC as reported for deleted in colorectal cancer protein (DCC) KO embryos (Ding et al. 2005). Moreover, it has been shown that the wnt1Cre mouse line might induce itself some phenotypes in the nervous system (Lewis et al. 2013). However, mice that were investigated always carried the wnt1Cre driver on one allele only and as shown in Figure 46C in control cryosections stained with peripherin no axon guidance defect was seen although the embryo genotype carrying wnt1Cre on one allele (wnt1Cre$^+$; FAK$^{fl/wt}$). This eliminated at least in this context a possible wnt1Cre-dependent phenotype in the DSC or DRGs.

To verify that sensory axons were misguiding because of the lack of FAK in DRGs and not in the DSC, a Npr2-specific tamoxifen-inducible cre mouse line was used to specifically knockout FAK in embryonic DRGs (Npr2$^{CreERT2/+}$, Figure 48B) (Ter-Avetisyan et al. 2014; Schmidt et al. 2013). In addition to that, mice were also crossed with the conditional reporter mouse line R26RtdT so that FAK mutated and WT DRG neurons also expressed the fluorophore RFP for better visualization. Tamoxifen was administrated to a pregnant mouse 11.5 days after vaginal plug-positive control. Embryos were prepared and fixed at E14.5. Visualization of RFP and NF-M-positive sensory axons by IHC on E14.5 transverse SC cryosections showed that in absence of FAK axon bundles were invading the dorsal horn of the SC (white

arrowheads, Figure 48C). Furthermore, the dorsal funiculus appeared to be thicker at the level of the DREZ compared to control embryos (white arrow, Figure 48C). Interestingly, under this treatment nociceptive (blue arrowheads) and proprioceptive (green arrowheads) collaterals could be seen in absence of FAK (Figure 48C). This could also been seen in wnt1Cre-driven FAK cKO where nociceptive (trkA-positive) and proprioceptive collaterals (NF-M-positive long axons) could be visualized (black arrowheads, Figure 47C).

Taken together, these results strongly suggested that FAK mediates the guidance of a subpopulation of sensory axons entering the SC at the DREZ in a cell-autonomous manner.
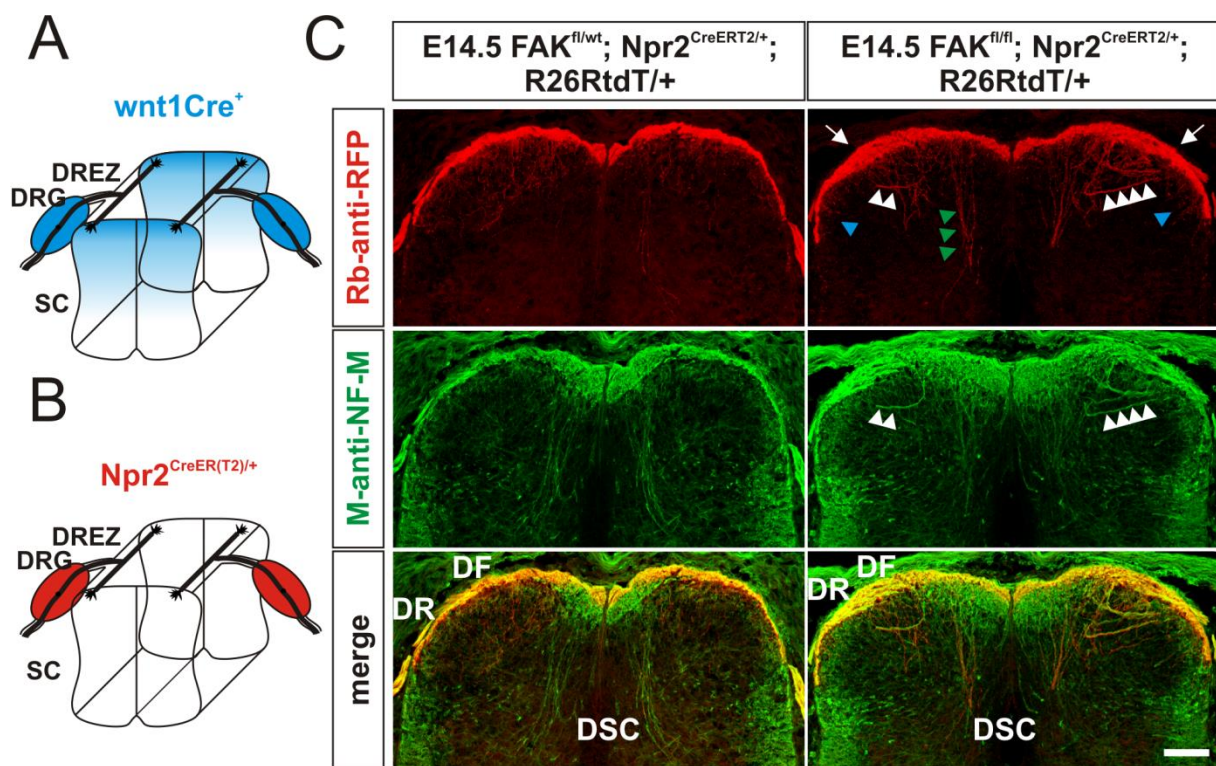
Figure 48 : DRG-specific FAK deletion partly reproduced the wnt1Cre-driven deletion. **(A)** Wnt1Cre-driven cKO allowed to delete FAK in DRGs (around E9.5) but also in the DSC around E9.5-E12.5 (shown in blue) (Echelard et al. 1994; Matsumoto et al. 2007). **(B)** The tamoxifen-inducible Npr2$^{CreER(T2)}$ mouse line allowed to knockout FAK only in DRGs (shown in red) (Ter-Avetisyan et al. 2014). **(C)** The tamoxifen-inducible Npr2$^{CreER(T2)}$ mouse line crossed with FAK floxed and R26RtdT mouse lines allowed to knockout FAK only in DRGs and in the same time to express RFP in the mutated neurons. A subpopulation of mutated axons appeared to invade the DSC (white arrowheads). Dorsal funiculi also looked thicker at the level of the DR (white arrows) compared to control. However, nociceptive (blue arrowheads) and proprioceptive (green arrowheads) collateral bundles seemed to form normally. DREZ, dorsal root entry zone; DRG, dorsal root ganglion; SC, spinal cord; DF, dorsal funiculus; DR, dorsal root; DSC, dorsal spinal cord. Scale bar: 100 μm.

5.2 FAK IS NOT NEEDED IN COMMISSURAL AXON GUIDANCE *IN VIVO*

Previous studies suggested that FAK was involved and essential in netrin-mediated commissural axon guidance toward the floor plate (Liu et al. 2004; Li et al. 2004; Moore et al. 2012). However, these labs used *ex vivo* or cell culture systems and never shown what happened *in vivo* when FAK was missing or inhibited.
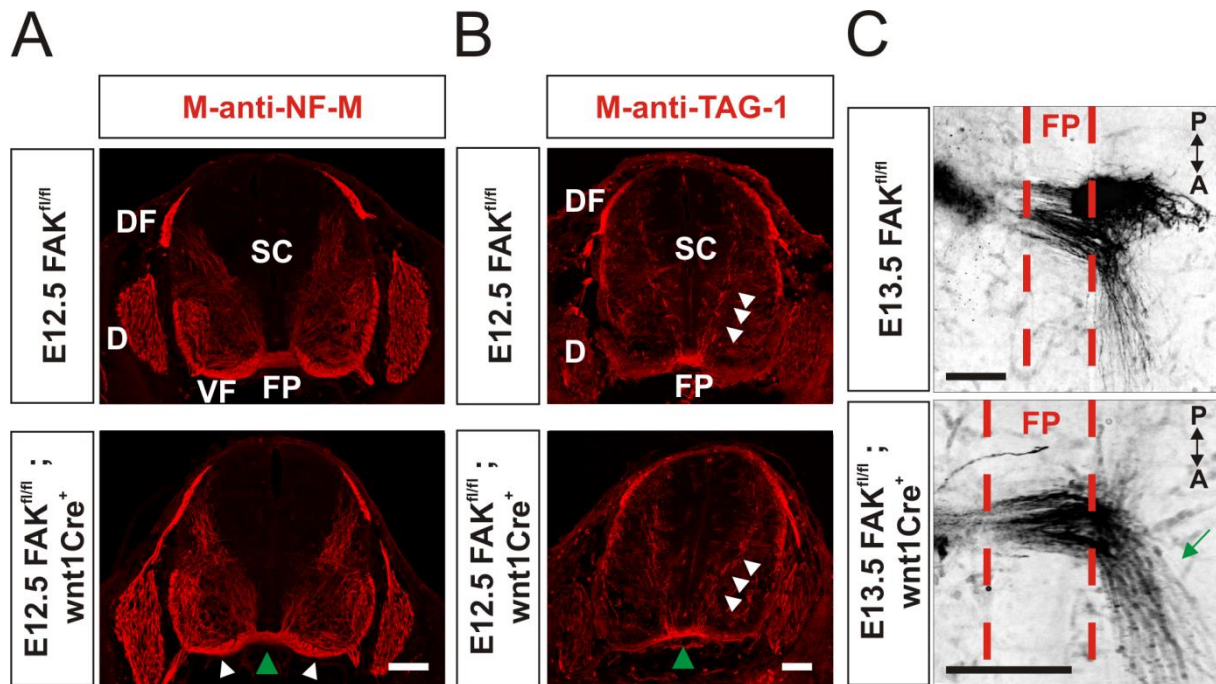
Figure 49 : Commissural axon guidance is normal in FAK mutant embryos. **(A)** Axon pathfinding within the FAK mutant spinal cord visualized by NF-M staining seemed to be normal. Ventral funiculi (white arrowheads) were correctly formed and the floor plate crossed by NF-M-positive axons (green arrowhead). **(B)** TAG-1-positive commissural axons were also correctly projecting toward the floorplate (D-V projection, white arrowheads) and crossing it (green arrowhead) in FAK cKO embryos. **(C)** DiI tracing of FAK cKO commissural axons confirmed that they reached the floor plate, crossed it and turned mostly anteriorly like in the control (green arrow). D, DRG; DF, dorsal funiculus; VF, ventral funiculus; SC, spinal cord; FP, floor plate. Scale bars: 100 µm.

Thus, FAK was knocked out in commissural neurons using the wnt1Cre driver mouse line in order to investigate its importance in the axon guidance of these neurons within the SC (Matsumoto et al. 2007). E12.5 FAK cKO and control transverse cryosections were stained by IHC for NF-M and axonal glycoprotein TAG-1 (TAG-1, Figure 49A and B). NF-M staining pattern showed no difference between FAK cKO and control embryos. Commissural axons seemed to reach the floor plate (FP) and to cross it (green arrowhead, Figure 49A). Moreover, the ventral funiculus appeared to form normally (VF, white arrowheads, Figure 49A). TAG-1 staining revealing pre-crossing commissural axons clearly showed no difference compared to control with axons being sent toward the FP in a normal guidance pattern (white and green

arrowheads, Figure 49B). DiI tracing of these axons at E13.5 confirmed that they were reaching and crossing the FP and subsequently mostly turning anteriorly (green arrowheads, Figure 49C).

Taken together, despite previous reports suggesting the central role of FAK in netrin-mediated commissural axon guidance (Liu et al. 2004; Li et al. 2004; Moore et al. 2012), these results demonstrated that FAK didn´t play a role *in vivo* in this guidance system.

6. DISCUSSION CHAPTER ONE – cGMP SIGNALLING REGULATES S-PAMITOYLATION IN SENSORY NEURONS

During early stages of the mouse embryo development, DRG and CSG primary axons enter the DREZ of the spinal cord and the hindbrain entry zone, respectively, bifurcate and create a T- or Y-shape branching pattern (Schmidt & Rathjen 2010). After a waiting period of about two days, they will send collaterals from their axon shafts that will penetrate deeper layers of the spinal cord or the hindbrain where they will arborize and form synapses (Schmidt & Rathjen 2010). A Npr2-mediated cGMP signalling cascade was shown to trigger the bifurcation of both DRG and CSG axons (Schmidt & Rathjen 2010; Ter-Avetisyan et al. 2014). Each component of the cascade composed of the ligand CNP, the receptor Npr2 and the kinase cGKIα is essential for the bifurcation of these sensory axons (Figure 51A). In the absence of only one of these three components, sensory axons aren´t able to bifurcate anymore. Instead, they form turns reducing therefore the projection complexity of sensory axons to the spinal cord or the hindbrain (Schmidt & Rathjen 2010; Ter-Avetisyan et al. 2014). Nevertheless, signalling events downstream of cGKIα that are involved in sensory axon bifurcation are still unknown. Thus, one of the major open question concerns signalling events that are triggered downstream of the kinase so that growth cone can split and form a correct bifurcation pattern.

6.1 CHARACTERIZATION OF BIOLOGICAL EFFECTS TRIGERRED BY THE NPR2-MEDIATED cGMP SIGNALLING CASCADE IN CULTURED SENSORY NEURONS ARGUES FOR A REMODELLING OF THE PLASMA MEMBRANE TAKING PLACE DOWNSTREM OF cGKI

Previous biochemical and molecular studies aimed to characterize downstream targets of cGKI in sensory axons resulted in the identification of a number of components (Schäffer 2006; Zhao et al. 2009; Stonkute 2010). However, these components could not be confirmed by genetic approaches to be implicated in axon bifurcation.

Due to the failure of biochemical and molecular approaches in discovering relevant target proteins downstream of cGKI in DRG neurons that were needed in axon bifurcation, other approaches had to be considered. Although bifurcation can´t be reproduced in culture by the global or localized addition of CNP to embryonic DRGs, characterization of biological changes after stimulating the Npr2-mediated cGMP signalling pathway allowed to rethink about downstream events that might be essential in DRG axon bifurcation *in vivo.*

F11 cells appeared to be an useful tool to assess cGMP signalling as they express cGKIα and should have a proteome quite similar to embryonic DRGs in term, for example, of cell adhesion proteins and neuronal proteins (Stonkute 2010). Adhesion assays with those cells indicated that changes might happen at the cell surface when cGMP signalling was triggered similarly to the adhesion assay performed with dissociated embryonic mouse DRG neurons on laminin (Figure 14 and Figure 15). The cGMP-mediated increase in the cell adhesion on ECM proteins like laminin, collagen or TN-C or on the IgSF cell adhesion protein contactin-1 indicated that stimulation of cGKIα might lead to downstream events regulating the cell adhesion (Figure 14, Figure 15A, B and C as well as Figure 51B, pathway a). Transposed into the context of the DREZ where DRG axons cross the basement membrane rich in ECM proteins before bifurcating (Figure 50) (Wright et al. 2012; Thorsteinsdóttir et al. 1995), it was logically hypothesized that an increase in cell adhesion might play a role in the GC steering on this pattern leading to the splitting of the GC required for the bifurcation. Integrin signalling (most likely in an inside-out fashion, Figure 23A) was speculated to be activated downstream of cGKI *in vitro* and to play a role *in vivo* (Figure 50, pathway A). However, genetic mouse models in which integrin signalling was inactivated failed to demonstrate this possibility *in vivo* and no robust evidences linking the Npr2-mediated cGMP signalling and the activation of integrin signalling were found *in vitro* (see section 4.2). Therefore, the increase in cell adhesion might be due to other mechanisms. It is conceivable that the translocation of cell adhesion molecules (CAMs) to the cell surface by vesicle trafficking might be enhanced downstream of cGKIα leading to an accumulation of ECM proteins receptors on the side of the basement membrane (Figure 50, pathway B). This would mean a general increase of cell adhesion due to an extra supply of membranes to the GC plasma membrane. For that reason, the study of genetic mouse models lacking single adhesion proteins might not be an adapted approach to confirm that cell adhesion

plays a role in bifurcation *in vivo* as exemplified by the study of IgSF cell adhesion molecule L1CAM KO DRG axons that were found to bifurcate normally at the DREZ (Figure 22). Interestingly, in addition to the general increase in cell adhesion the high cell aggregation observed on both contactin-1 and TN-C substrates in presence of cGMP analogue suggested an increase in the adhesion between cells as well (Figure 15B and D) and transposed to the *in vivo* situation, fasciculation of axons might be enhanced at the DREZ in a cGMP-dependent manner. In line with this hypothesis, a subpopulation of DRG axons was shown to overshoot toward the dorsal horn of the SC in absence of either CNP, Npr2 or cGKI (H Schmidt et al. 2002; Schmidt et al. 2007; Schmidt et al. 2009). A lack of fasciculation might have led to this phenotype similarly to the defasciculation and overshooting phenotype of DRG axons observed when contactin-1 was blocked in the chick embryo SC (Perrin et al. 2001).
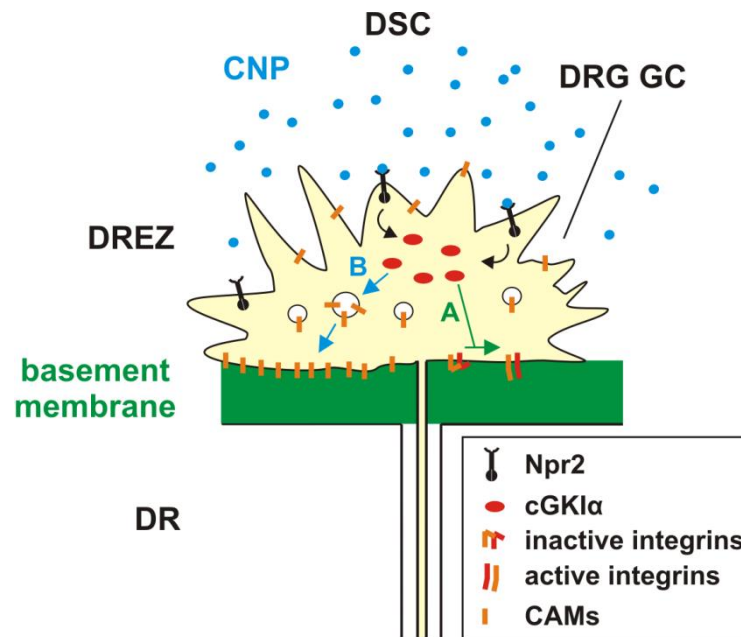
Figure 50 : Hypothetical model of a cGMP-dependent increase in cell adhesion in the DRG GC *in vivo*. DRG GCs entering the DREZ of the developing spinal cord have to cross the basement membrane (in green) which is rich in ECM proteins (Wright et al. 2012; Thorsteinsdóttir et al. 1995). Based on the cGMP-dependent increase in cell adhesion *in vitro* and the pattern of ECM proteins at the DREZ, it was speculated that Npr2-mediated cGMP signalling might regulate either the activation of integrins (**A**, green pathway), or the trafficking of CAMs to the plasma membrane (**B**, blue pathway) localized on the side of the basement membrane. This might therefore induce a growth cone steering and a splitting leading to a bifurcation pattern. DR, dorsal root; DREZ, dorsal entry zone; DSC, dorsal spinal cord; DRG dorsal root ganglion; CAMs, cell adhesion molecules. Adapted from (Calderwood et al. 2013).

Another interesting phenotype that was observed in presence of a cGMP analogue in cultured F11 cells or of CNP in embryonic chick DRG explants as well as dissociated cells is that CNP-Npr2-cGKI signalling appeared to enhance axonal outgrowth (Figure 16 and Figure 17). Interestingly, this effect was already reported and

characterized before in cultured embryonic rat and mouse DRG explants and single cells by the lab of Dr. Le Ma (Zhao & Ma 2009; Zhao et al. 2009; Xia et al. 2013). Moreover, an increase in interstitial branching was also quantified (Zhao & Ma 2009; Zhao et al. 2009). However, the approach used in this thesis was slightly different. Instead of first cultivating DRG neurons with a high concentration of NGF (25 ng/ml) for one day followed by a NGF removal and an extra day of stimulation with either CNP or cGMP versus control conditions (Zhao et al. 2009), neurons were directly stimulated with CNP at the very beginning with a low dose of NGF (10 ng/ml). A high dose of NGF was previously used to induce axon branching in cultured embryonic DRGs (Spillane et al. 2012; Spillane et al. 2013). Thus, in those previous reports, overnight high-dose NGF stimulation might have induced the branching in a NGF-mediated manner prior to the addition of CNP. The effect of CNP on axonal outgrowth might have helped to maintain the pre-existing branching pattern. Therefore, it is most likely that CNP might not induce axonal branching alone in culture as no increase in axonal branching was detected with my approach in presence of a low-dose of NGF. Of course, the stiffness of the collagen gel might also be a preponderant factor in the branching of DRG neurons in culture. Nonetheless, the Npr2-mediated cGMP signalling might trigger mechanisms downstream of cGKI that are involved in axonal outgrowth in sensory neurons (Figure 51B, pathways a and b).

Bifurcation of sensory axons at the DREZ results presumably from a GC splitting ((Schmidt et al. 2007) and Figure 21B) and is thought to take place within minutes (Schmidt & Rathjen 2010; Ponomareva et al. 2014). The GC assay described in section 4.1 had two major advantages: it allowed to characterize the impact of a brief CNP stimulation (1h) on cultured embryonic DRGs and to focus on the most important cellular compartment of the axon in regard to bifurcation which is the GC. This demonstrated that embryonic chick and mouse DRG GCs stimulated with CNP underwent a remodelling to become larger in a CNP-Npr2-cGKI-dependent manner (Figure 18, Figure 19 and Figure 20). Therefore, cGKIα might phosphorylate downstream substrates what leads to this remodelling (Figure 51B, pathway b). It would be also very interesting to study the relationship between CNP-Npr2-cGKI signalling cascade and the exocytosis rate at the plasma membrane of sensory GC in culture in order to assess a possible increase in the membrane supply triggered by this pathway.

The morphogen wnt3 which is expressed by motoneurons in the developing mouse SC was shown to induce axon terminal branching of NT-3 (Neurotrophin-3)-responsive E13.5 mouse embryonic DRG single cells in culture (Krylova et al. 2002). Interestingly, the branching factor wnt3 was also reported in the same study to induce a GC remodelling in cultured sensory neurons leading to an increase in the GC area prior to the branching (Krylova et al. 2002). More recently, membrane expansion preceding the axon arborization triggered by Netrin-1 in cultured E15.5 cortical neurons was shown to be a prerequisite for new branch formation (Winkle et al. 2014). Hence, bifurcation of sensory axons at the DREZ of the developing SC might also need a GC remodelling in order to have a sufficient volume of plasma membrane for the creation of two daughter branches. Interestingly, the enlarged morphology seen in pre-bifurcated sensory GCs at the DREZ might also support this hypothesis (Figure 21).

Taken together, the cell culture approaches used in this work argue for a CNP-Npr2-cGKI-mediated remodelling of the plasma membrane in sensory neurons.

6.2 LOCALIZATION OF cGKI IN THE GROWTH CONE SUGGESTS A REGULATION OF PROTEIN TRAFFICKING FROM INTRACELLULAR MEMBRANES OF THE C-DOMAIN TO THE PLASMA MEMBRANE

The characterization of cGKI localization in the DRG GC led to a more defined picture of what might happen when the kinase gets activated. In fact, the vesicular pattern of cGKI ICC and its colocalization to intracellular membrane markers in F11 cells and cultured embryonic mouse DRGs together suggest a proximity to these membranes (Figure 27, Figure 29, Figure 30 and Figure 31). Moreover, the higher concentration of cGKI within the C-domain of the GC (Figure 27E and G) where organelles arrive from the soma transported along microtubules (Pfenninger 2009) supports the notion of its compartmentalization within the sensory GC allowing the regulation of protein shuttling from intracellular compartments to the plasma membrane. A specific compartmentalization might indeed play a crucial role *in vivo* as recently reported for ephrin-A-dependent cAMP signalling in the pruning of developing retinal axon arbors (Averaimo et al. 2016). Interestingly, the apparent segregation of Npr2 within lipid rafts of PC12 cells might well fit to this idea suggesting a compartmentalized cGMP signal too (Figure 32). The proximity of cGKI

to intracellular membranes also let me rethink on possible downstream events (Figure 51). So far, much of the focus had been directed to the actin and microtubule cytoskeleton proteins. For example, regulation of GSK-3β downstream of cGKI appeared to take place *in vitro* (Zhao et al. 2009). However, this protein and many other cytoskeleton proteins didn´t play a role in DRG bifurcation *in vivo* as revealed by genetic mouse models ((Stonkute 2010) and Figure 45B, C and D) and no strong evidences showed a direct dynamic regulation of microtubules in the embryonic DRG GC in culture (Xia et al. 2013). In addition to that, new approaches allowed to assess membrane exocytosis in axon guidance and branching emphasizing the importance of the membrane supply in response to guidance and branching cues (Pfenninger et al. 2003; Winkle et al. 2016; Winkle et al. 2014; Tojima & Kamiguchi 2015). Together with my results, this would tend to relegate the cytoskeleton to a secondary role acting as a "follower" of the plasma membrane remodelling in the GC.
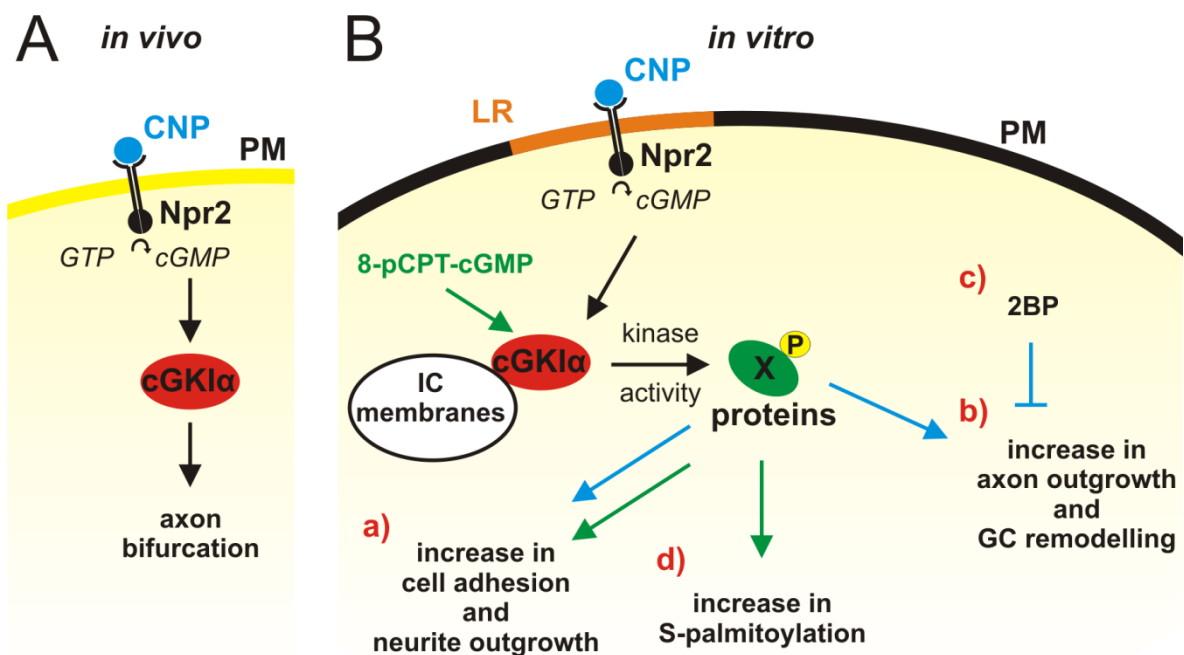
Figure 51 : Models summing up CNP-Npr2-cGKIα signalling cascade *in vivo* and *in vitro.* **(A)** Previous *in vivo* evidences showed that CNP, Npr2 and cGKIα were needed for DRG and CSG axon bifurcation (Schmidt & Rathjen 2010; Ter-Avetisyan et al. 2014). **(B)** Hypothetical model summarizing present *in vitro* results using PC12 cells, F11 cells and embryonic DRGs. In PC12 cells, Npr2 was shown to be localized within lipid rafts (LR, shown in orange at the plasma membrane). cGKIα localization in cultured embryonic DRGs and F11 cells indicated a proximity to intracellular (IC) membranes and mostly in the C-domain of the GC. DRG single cells- and F11 cells-based assays (blue and green pathways, respectively) suggested that a Npr2-mediated or a cGMP analogue stimulation of cGKIα increased the cell adhesion **(a)**. cGMP analogue stimulation also increased the neurite outgrowth of F11 cells **(a)** as well as S-palmitoylation **(d)**. Embryonic DRG-based culture assays (blue pathway) demonstrated that stimulation of CNP-Npr2-cGKIα signalling increased axon outgrowth and induced a GC remodelling **(b)**. Moreover, blocking S-palmitoylation with 2BP abolished those both effects in culture **(c)**. PM, plasma membrane; LR, lipid rafts; IC, intracellular; 2BP, 2-bromopalmitate.

6.3 CELL CULTURE AND BIOCHEMICAL APPROACHES REVEALED AN INTERPLAY BETWEEN THE CNP-NPR2-cGKI PATHWAY AND PROTEIN S-PALMITOYLATION IN SENSORY NEURONS

Although S-palmitoylation plays a central role in the development of the nervous system especially at the level of the synapse (Fukata & Fukata 2010), only few studies reported the impact of the lack of S-palmitoylation in axon development and branching *in vitro* and *in vivo* (Hess et al. 1993; Patterson & Skene 1994; Mukai et al. 2015a). Here the click chemistry approach allowed to highlight the omnipresence of palmitoylated proteins in the C-domain of the GC of cultured F11 cells and embryonic mouse DRG primary cells (Figure 33A, B and C) and its possible importance in sensory neurons development as previously suggested (Hess et al. 1993; Patterson & Skene 1994). Moreover, ABE-based purification of the F11 cell palmitoylome also indicated that the interplay between at least serine/threonine phosphorylation and the global regulation of S-palmitoylation should be considered (Figure 33E and F).

The fact that cGKI appeared to be close to palmitoyl-rich structures in the GC of cultured embryonic mouse DRGs (Figure 33C) and that the CNP-Npr2-cGKI-mediated effect on axonal outgrowth and GC remodelling was completely abolished by blocking S-palmitoylation (Figure 34, Figure 35, Figure 36, Figure 37 and Figure 51B, pathway c) strongly suggest an interplay between the serine/threonine cGKI and the S-palmitoylation in cultured embryonic DRGs. Moreover, ABE-based purification and LC-MS quantification of a cGMP-dependent increase in S-palmitoylation of a specific pool of proteins in F11 cells (Figure 39, Table 1 and Figure 40A) support the idea that S-palmitoylation is regulated downstream of cGKI.

Hence, to find by which mechanism cGKI regulates the S-palmitoylation would be a real breakthrough. From the multitude of phosphorylated substrate proteins (proteins X and Y, Figure 52) the phosphorylation of some of them (proteins X) might lead to their subsequent S-palmitoylation by a change in their affinity to Zdhhc enzymes (palmitoyltransferases), for example (Figure 52, pathway a). Moreover, cGKI might directly regulate Zdhhc enzymes by phosphorylating them therefore increasing their activity or changing their localization and leading to the palmitoylation of a different pool of proteins (proteins Z, Figure 52, pathway b). Interestingly, phosphorylation-mediated regulation of Zdhhc enzymes localization and activity has been recently described in neuronal systems (Brigidi et al. 2015; Lievens et al. 2016). The

localization of Zdhhc8 in the GC of cultured E12.5 mouse DRGs where it colocalizes with cGKI (Figure 43) makes it an interesting candidate. Furthermore, it contains a putative cGKI phosphorylation motif (Figure 42A) and was reported to play a critical role in collateral and terminal branching of cortical axons both *in vitro* and *in vivo* (Mukai et al. 2015a). Besides these both possibilities, S-palmitoylation might also be regulated downstream of cGKI substrates directly or by activation of other signalling pathways (Figure 52, pathway c).
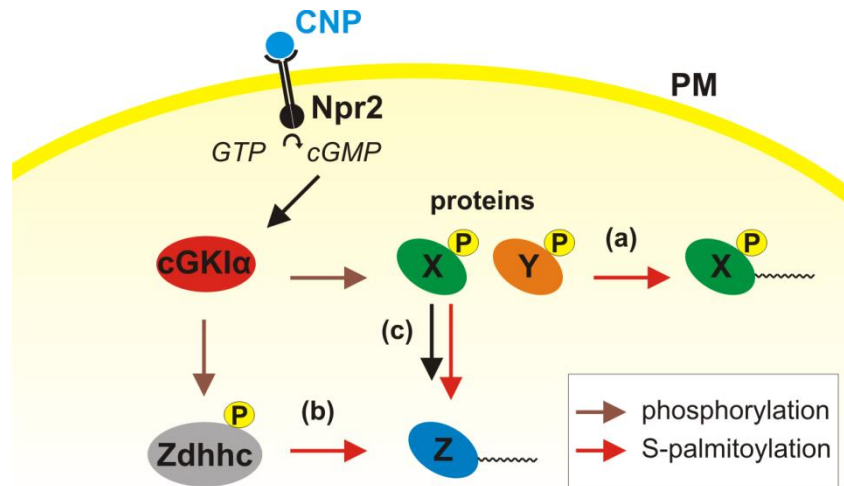
Figure 52 : Hypothetical model depicting possible pathways involved in the regulation of S-palmitoylation downstream of cGKIα. Based on the *in vitro* experiments reported above, S-palmitoylation might be presumably regulated downstream of cGKIα in sensory neurons. Three possible pathways could be therefore implicated in this regulation. **(a)** From the pool of phosphoprotein substrates of cGKIα (proteins X and Y) the phosphorylation of some of them (proteins X) might lead to their subsequent S-palmitoylation. **(b)** However, it might be possible that the kinase directly acts at the Zdhhc enzyme(s) level inducing the S-palmitoylation of specific protein substrates (proteins Z). **(c)** Moreover, S-palmitoylation might be regulated downstream of cGKIα substrate proteins directly or by activation of other signalling cascades. Brown arrows represent phosphorylation steps and red arrows S-palmitoylation steps. PM, plasma membrane.

Altogether, here *in vitro* approaches demonstrated an interplay between the Npr2-mediated cGMP signalling and the S-palmitoylation in sensory neurons involved in the axonal outgrowth and GC remodelling presumably by regulating protein trafficking downstream of cGKI (Figure 51B). Together with the localization of cGKI close to intracellular membrane in cultured DRGs, this shed the light on new aspects that might play a role downstream of the kinase in the creation of a bifurcation pattern (Figure 51A). Unfortunately, *in vivo* evidences of the S-palmitoylation-dependence in sensory axon bifurcation are still lacking. Investigating single palmitoylated protein candidates by the use of genetic mouse models, as reported for Zdhhc13 and Ndst1 (Figure 41), might not be the easiest way as the need of this post-translational modification could be that it involves a synergy of multiple proteins to trigger the GC

splitting *in vivo*. It would make therefore more sense to focus on the palmitoyl-transferases level or even on the fatty acids metabolism level. Intriguingly, a recent study of the drosophila mushroom body axon projections described a regulation of axon bifurcation and guidance by DISCO Interacting Protein 2, a protein that appeared to play a role in acyl-CoA synthesis (Nitta et al. 2017). Thus, more efforts have to be invested upstream of S-palmitoylation in order to be able to inhibit the palmitoylation of proteins that might be needed in sensory axon bifurcation at the DREZ of the developing mouse SC.

7. FUTURE PERSPECTIVES – CHAPTER ONE

- CNP-Npr2-cGKI-mediated GC remodelling strongly suggests an increase in exocytosis of intracellular membranes. Therefore, the use of a fluorescent dye like the Bodipy-ceramide to quantify the proportion of post-Golgi vesicles fused to the plasma membrane in presence of CNP would be very adapted to verify this hypothesis in cultured DRGs (Pfenninger et al. 2003). Moreover, it could be combined with a 2BP-blockade of S-palmitoylation to assess the impact of its loss in a putative CNP-mediated exocytosis.

- The click chemistry-based method to visualize the palmitoylome could be a perfect approach to study any global change in protein palmitoylation in the GC of cultured embryonic DRGs in presence of CNP. This would be in a sense much more accurate than the ABE-based method screening the palmitoylome of whole F11 cells due to the focus that could be given to the GC compartment.

- As shown by the DiI study of WT GC *in vivo* (Figure 21), sensory GCs most likely undergo a splitting before bifurcating. However, it would be more consistent to investigate it for example *ex vivo* using a tamoxifen-Npr2CreERT2 system to induce a sparse expression of a fluorophore in DRG neurons and record the process by using time-lapse microscopy (Ter-Avetisyan et al. 2014). Moreover, it would also give important information on the time scale of the bifurcation and by the same occasion would establish a new approach for assessing the effect of pharmacological blockers on axon bifurcation like 2BP.

- Re-creating DRG axon bifurcation *in vitro* didn´t appear to be possible by the simple addition of CNP. However, combination of CNP with other factors expressed in the developing dorsal horn of the SC, for example, might be needed. Therefore, a screen for supplementary cues might be of interest.

- Further study of genetic mouse models are needed to demonstrate the link between CNP-Npr2-cGKI signalling cascade and S-palmitoylation in embryonic DRG neurons *in vivo* and its potential requirement in axon bifurcation.

- Npr2 localization within PC12 lipid rafts (Figure 32) open new possibilities about how Npr2 might signal. Npr2 by binding to CNP might either be translocated to lipid rafts, forming a signalling platform or even be endocytosed which was already suggested in previous studies (Brackmann et al. 2005; Pandey 2015). Thus, further investigations in PC12 cells and in DRGs should be conducted to shed the light on the significance of this localization.

8. DISCUSSION CHAPTER TWO – FAK-MEDIATED AXON GUIDANCE

8.1 A SUBPOPULATION OF DRG NEURONS NEEDS FAK TO CORRECTLY PROJECT THEIR CENTRAL AXON INTO THE DEVELOPING SPINAL CORD

The correct projection of DRG central axons within the developing mouse or chick SC is mediated by repelling guidance cues such as semaphorins, Slits or netrin-1 (Gu et al. 2003; Ma & Tessier-Lavigne 2007; Masuda et al. 2009). Here the tyrosine kinase FAK was reported not to be involved in DRG axon bifurcation (Figure 26E). However, it was shown to play a role in the guidance of a subpopulation of nociceptive as well as proprioceptive axons entering the DREZ of the developing mouse SC when FAK was conditionally knocked out in wnt1-positive cells (see section 5.1). The fact that in its absence overshooting DRG axon bundles projected toward the DSC from the dorsal roots and that the DREZ was disorganized supports the idea of its role in the guidance of central axons rather than collaterals (Figure 46). Moreover, it appeared to act in DRG axons in a cell-autonomous manner as a subpopulation of DRG-specific KO axons also misguided toward the DSC (Figure 48). This suggests that the tyrosine kinase is positioned downstream of a signalling cascade involved in the guidance of sensory axons. Therefore, one can hypothesize that when FAK is expressed in DRG neurons (WT, Figure 53), growth cones are repelled at the DREZ by so far unknown guidance cues which are expressed in the DSC. Those cues might transduce the repelling signal via specific receptors localized at the DRG GCs plasma membrane what triggers a signalling cascade that should involve FAK at a certain level (WT, Figure 53). In absence of FAK, the guidance cues are still able to bind their specific receptors but the signal can´t be transduced and axons are overshooting within the DSC (FAK cKO, Figure 53). Of course, FAK might also be involved in an integrin-based fasciculation of DRG axons at the DREZ. However, no lack of DRG axon fasciculation was seen in neither embryos lacking the integrin adaptor talin-2 nor integrin ß1 (cKO, wnt1Cre) at the DREZ (Figure 24 and Figure 25). This would suggest that FAK might rather play a role downstream of other signalling cascades.

A number of guidance cues were shown to be important in repelling DRG axons entering the DREZ (Gu et al. 2003; Watanabe et al. 2006; Yaron et al. 2005; Liu et al. 2014; Ma & Tessier-Lavigne 2007). This renders a screen of all possible cues that would need FAK to transduce a repelling signal complicated. However, based on the timing of the overshooting axons appearance which takes place after E12.5 (Figure 46), already two cues does probably not need FAK downstream of their receptors. Semaphorin-3A which binds neuropilin-1 with the association of Plexin A3 and A4 to repel sensory axons at the DREZ (Yaron et al. 2005) as well as Slit1 and Slit2 binding their receptors Robo1 and Robo2 (Ma & Tessier-Lavigne 2007) were reported to play a guidance role earlier in the development and defects in mutant mice were already observable at least at E12.5 and E11.5, respectively. Moreover, semaphorin 5B was described to repel nociceptive axons and not the proprioceptive ones in chick embryos whereas FAK appeared to be important in the guidance of both subtypes (Figure 47) (Liu et al. 2014).
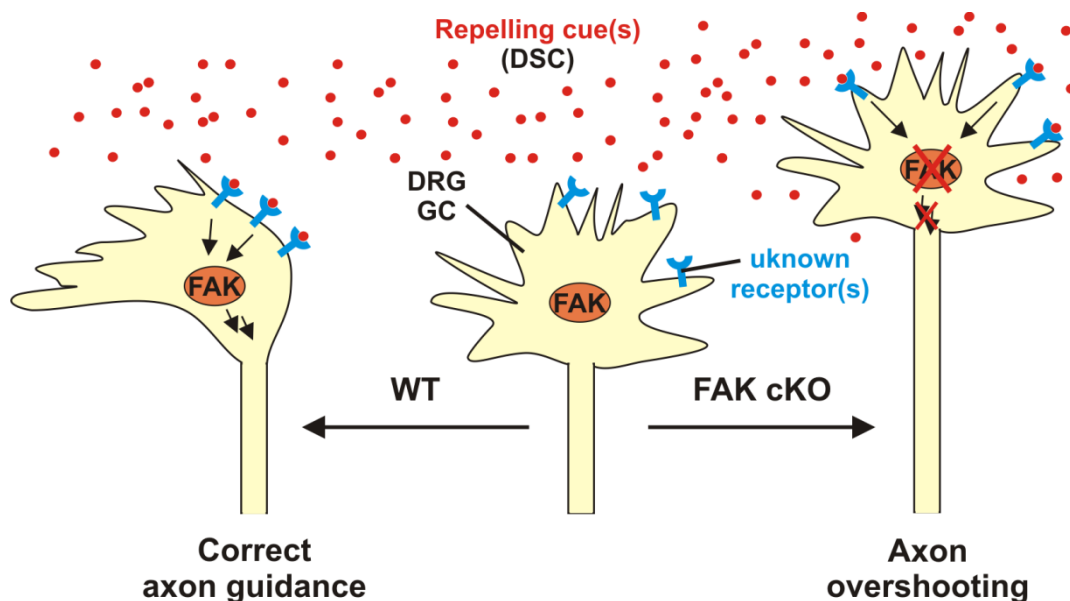
Figure 53 : Hypothetical model of FAK-mediated axon guidance of DRG axons entering the DREZ. In WT DRG GCs, unknown repelling guidance cues can bind their specific receptors what triggers a signalling cascade in which FAK might play a central role. However, in absence of FAK (FAK cKO), the repelling guidance cues might not be able to transduce the signalling cascade leading to an axonal overshooting toward the DSC. DSC, dorsal spinal cord; GC, growth cone; KO, knock-out.

Interestingly, based on the temporal and morphological aspects, loss of FAK led to a phenotype similar to the loss of the guidance cue Netrin-1 (Masuda & Shiga 2005). Netrin-1 expression close to the DREZ was shown to robustly but transiently appear around E12.5 juxtaposed to the DREZ in the mouse embryo in an anterior-posterior gradient (Watanabe et al. 2006; Laumonnerie et al. 2014). Its absence resulted in an

overshooting of a subpopulation of nociceptive and proprioceptive axons within the DSC with a strong phenotype appearing between E12.5 and E13.5 (Watanabe et al. 2006). It was thought to repel DRG axons by binding Unc5c receptor and apparently also other receptors as Unc5c mutant embryos seemed to have a milder phenotype than Netrin-1 KO embryos and that Unc5a is also expressed in DRGs around E12.5 (Watanabe et al. 2006; Masuda et al. 2008; Masuda et al. 2009). Moreover, an island of DSC cells created by the misprojecting axons was also described similar to what observed in absence of FAK (white arrowhead, Figure 46B) (Watanabe et al. 2006). Although the Netrin-1 receptor DCC (deleted in colorectal cancer) is not expressed in embryonic DRGs (Watanabe et al. 2006), FAK-mediated phosphorylation of Unc5c via DCC was shown to be essential *in vitro* suggesting that it could be the case in the DRG guidance at the DREZ but by another mechanism (W. Li et al. 2006). Even more interestingly, the protein DSCAM (Down syndrome cell adhesion molecule), which is expressed in embryonic DRGs (Liu et al. 2009; Barlow et al. 2002), was shown to associate with unc5c and to be needed in the netrin-1-mediated GC collapse of external granule layer neurons of the cerebellum in culture and that FAK was also shown to associate to both proteins as well as to play a central role in this process (Purohit et al. 2012). Further experiments are therefore needed to find out whether FAK plays a role in netrin-1-mediated repulsion of DRG axons at the DREZ and if yes at which level.

8.2 FAK DOES NOT PLAY A ROLE DOWNSTREAM OF NETRIN-1-MEDIATED COMMISSURAL AXON GUIDANCE

Netrin-1-mediated axon guidance is involved in the attraction of commissural axons toward the floor plate of the developing SC (Figure 2B) (Serafini et al. 1996; Lai Wing Sun et al. 2011). This takes place by binding of netrin-1 to DCC receptor transducing an attracting response (Lai Wing Sun et al. 2011). Several studies showed the need of FAK in its response *ex vivo* as well as *in vitro* downstream of DCC using mouse and chick embryos (Liu et al. 2004; Li et al. 2004; Moore et al. 2012). For example, blocking FAK function appeared to block the attraction of commissural axons toward an aggregate of heterologous cells expressing netrin-1 in an *ex vivo* system (Liu et al. 2004). However, its role *in vivo* in the mouse embryo had never been investigated so far. Here, the conditional KO of FAK in commissural neurons using the wnt1Cre

driver indicated that their axons were projecting toward the floor plate normally and crossing it (Figure 49). These results strongly suggest that, at least in the mouse embryo, FAK is not needed in the Netrin-1-mediated commissural axon guidance toward the floor plate *in vivo*. It is conceivable that its function as tyrosine kinase might be compensated in FAK cKO commissural axons, for example, by the proto-oncogene tyrosine-protein kinase Src which was also shown to phosphorylate DCC *in vitro* (Li et al. 2004; Liu et al. 2004; W. Li et al. 2006).

9. FUTURE PERSPECTIVES – CHAPTER TWO

- In order to find out whether FAK is mediating the DRG axon guidance downstream of netrin-1 at the DREZ of the developing mouse SC, cell culture approaches might be used. For example, WT as well as FAK cKO DRG explants or single cells could be cultured in collagen gel as used before (Figure 17) in presence of recombinant netrin-1 to verify if the inhibition of axonal outgrowth would disappear in absence of FAK. Of course, if Netrin-1 didn´t appear to be the guidance cue upstream of FAK in embryonic DRG neurons other known repelling cues as Semaphorin 3A could be screened with this method.

- Once the guidance cue identified, the phosphorylation state, the possible interaction with guidance cue receptors, localization and downstream events of FAK-mediated guidance could be also investigated using biochemical and ICC approaches.

- It would be also of interest to investigate the possible need of FAK in the guidance of CSG axons entering the developing hindbrain.

10. REFERENCE LIST

Abrami, L., Leppla, S.H. & Gisou Van Der Goot, F., 2006. Receptor palmitoylation and ubiquitination regulate anthrax toxin endocytosis. *Journal of Cell Biology*, 172(2), pp.309–320.

Averaimo, S. et al., 2016. A plasma membrane microdomain compartmentalizes ephrin-generated cAMP signals to prune developing retinal axon arbors. *Nature communications*, 7, p.12896.

Avilés, E.C., Wilson, N.H. & Stoeckli, E.T., 2013. Sonic hedgehog and Wnt: antagonists in morphogenesis but collaborators in axon guidance. *Frontiers in Cellular Neuroscience*, 7, p.86.

Barczyk, M., Carracedo, S. & Gullberg, D., 2010. Integrins. *Cell Tissue Res*, 339(1), pp.269–280.

Barlow, G.M. et al., 2002. Mammalian DSCAMs: Roles in the development of the spinal cord, cortex, and cerebellum? *Biochemical and Biophysical Research Communications*, 293(3), pp.881–891.

Bashaw, G.J. & Klein, R., 2010. Signaling from axon guidance receptors. *Cold Spring Harbor perspectives in biology*, 2(5).

Beggs, H.E. et al., 2003. FAK deficiency in cells contributing to the basal lamina results in cortical abnormalities resembling congenital muscular dystrophies. *Neuron*, 40(3), pp.501–514.

van Beuningen, S.F. & Hoogenraad, C.C., 2016. Neuronal polarity: remodeling microtubule organization. *Current Opinion in Neurobiology*, 39, pp.1–7.

Blanc, M. et al., 2015. SwissPalm: Protein Palmitoylation database. *F1000Research*, 4(0), p.261.

Brackmann, M. et al., 2005. Neuronal Ca2+ sensor protein VILIP-1 affects cGMP signalling of guanylyl cyclase B by regulating clathrin-dependent receptor recycling in hippocampal neurons. *Journal of cell science*, 118(Pt 11), pp.2495–505.

Brigidi, G.S. et al., 2015. Activity-regulated trafficking of the palmitoyl-acyl transferase DHHC5. *Nature communications*, 6, p.8200.

Bucci, C. et al., 1992. The small GTPase rab5 functions as a regulatory factor in the early endocytic pathway. *Cell*, 70(5), pp.715–728.

Bullmore, E. & Sporns, O., 2009. Complex brain networks: graph theoretical analysis of structural and functional systems. *Nature Reviews Neuroscience*, 10(3), pp.186–198.

Calderwood, D., Campbell, I.D. & Critchley, D.R., 2013. Talins and kindlins: partners in integrin-mediated adhesion. *Nature reviews. Molecular cell biology*, 14(8), pp.503–17.

Carlsson, S.R. & Fukuda, M., 1989. Structure of human lysosomal membrane glycoprotein 1. Assignment of disulfide bonds and visualization of its domain arrangement. *The Journal of biological chemistry*, 264(34), pp.20526–31.

Chamberlain, L.H., Burgoyne, R.D. & Gould, G.W., 2001. SNARE proteins are highly enriched in lipid rafts in PC12 cells: implications for the spatial control of exocytosis. *Proceedings of the National Academy of Sciences of the United States of America*, 98(10), pp.5619–24.

Chamberlain, L.H. & Shipston, M.J., 2015. The physiology of protein S-acylation. *Physiological reviews*, 95(2), pp.341–76.

Charych, E.I. et al., 2010. Interplay of palmitoylation and phosphorylation in the trafficking and localization of phosphodiesterase 10A: implications for the treatment of schizophrenia. *The Journal of neuroscience : the official journal of the Society for Neuroscience*, 30(27), pp.9027–9037.

Chédotal, A. & Richards, L.J., 2010. Wiring the brain: the biology of neuronal guidance. *Cold Spring Harbor perspectives in biology*, 2(6).

Chesarino, N.M., McMichael, T.M. & Yount, J.S., 2014. Regulation of the trafficking and antiviral activity of IFITM3 by post-translational modifications. *Future Microbiol*, 9, pp.1151–1163.

Chevallet, M., Luche, S. & Rabilloud, T., 2006. Silver staining of proteins in polyacrylamide gels. *Nature protocols*, 1(4), pp.1852–8.

Cho, E. & Park, M., 2016. Palmitoylation in Alzheimer's disease and other neurodegenerative diseases. *Pharmacological Research*, 111, pp.133–151.

Chrostek, A. et al., 2006. Rac1 is crucial for hair follicle integrity but is not essential for maintenance of the epidermis. *Molecular and cellular biology*, 26(18), pp.6957–70.

Chusho, H. et al., 2001. Dwarfism and early death in mice lacking C-type natriuretic peptide. *Proceedings of the National Academy of Sciences*, 98(7), pp.4016–4021.

Cohen, N.R. et al., 1998. Errors in corticospinal axon guidance in mice lacking the neural cell adhesion molecule L1. *Current Biology*, 8(1), pp.26–33.

Conde, C. & Cáceres, A., 2009. Microtubule assembly, organization and dynamics in axons and dendrites. *Nature reviews. Neuroscience*, 10(5), pp.319–332.

Costes, S. V et al., 2004. Automatic and quantitative measurement of protein-protein colocalization in live cells. *Biophysical journal*, 86(6), pp.3993–4003.

Dailey, M.E. & Bridgman, P.C., 1989. Dynamics of the endoplasmic reticulum and other membranous organelles in growth cones of cultured neurons. *The Journal of neuroscience : the official journal of the Society for Neuroscience*, 9(6), pp.1897–1909.

Danielian, P.S. et al., 1998. Modification of gene activity in mouse embryos in utero by a tamoxifen-inducible form of Cre recombinase. *Current biology : CB*, 8(24), pp.1323–6.

Debrand, E. et al., 2012. Mice carrying a complete deletion of the talin2 coding sequence are viable and fertile. *Biochemical and Biophysical Research Communications*, 426(2), pp.190–195.

Dent, E.W., Gupton, S.L. & Gertler, F.B., 2011. The growth cone cytoskeleton in axon outgrowth and guidance. *Cold Spring Harbor perspectives in biology*, 3(3), p.a001800.

Dhayade, S. et al., 2016. Sildenafil Potentiates a cGMP-Dependent Pathway to Promote Melanoma Growth. *Cell reports*, 14(11), pp.2599–2610.

Dietrich, L.E.P. & Ungermann, C., 2004. On the mechanism of protein palmitoylation. *EMBO reports*, 5(11), pp.1053–7.

Ding, Y.Q. et al., 2005. Ventral migration of early-born neurons requires Dcc and is essential for the projections of primary afferents in the spinal cord. *Development*, 132(9), pp.2047–2056.

Dunn, K.W., Kamocka, M.M. & McDonald, J.H., 2011. A practical guide to evaluating colocalization in biological microscopy. *AJP: Cell Physiology*, 300(4), pp.C723–C742.

Echelard, Y., Vassileva, G. & McMahon, a P., 1994. Cis-acting regulatory sequences governing Wnt-1 expression in the developing mouse CNS. *Development (Cambridge, England)*, 120(8), pp.2213–2224.

Egelhofer, V. et al., 2013. Using ProtMAX to create high-mass-accuracy precursor alignments from label-free quantitative mass spectrometry data generated in shotgun proteomics experiments. *Nat Protoc*, 8(3), pp.595–601.

El-Husseini, A.E.D. et al., 2002. Synaptic strength regulated by palmitate cycling on PSD-95. *Cell*, 108(6), pp.849–863.

Engle, E.C., 2010. Human genetic disorders of axon guidance. *Cold Spring Harbor perspectives in biology*, 2(3).

Eva, R. et al., 2010. Rab11 and its effector Rab coupling protein contribute to the trafficking of beta 1 integrins during axon growth in adult dorsal root ganglion neurons and PC12 cells. *The Journal of neuroscience : the official journal of the Society for Neuroscience*, 30(35), pp.11654–69.

Falk, J. et al., 2014. Rab5 and Rab4 regulate axon elongation in the Xenopus visual system. *The Journal of neuroscience : the official journal of the Society for Neuroscience*, 34(2), pp.373–91.

Fan, S.F. et al., 1992. F11 neuroblastoma x DRG neuron hybrid cells express inhibitory mu- and delta-opioid receptors which increase voltage-dependent K+ currents upon activation. *Brain research*, 590(1–2), pp.329–33.

Feng, G. et al., 2000. Imaging neuronal subsets in transgenic mice expressing multiple spectral variants of GFP. *Neuron*, 28(1), pp.41–51.

Flynn, K.C. et al., 2012. ADF/Cofilin-Mediated Actin Retrograde Flow Directs Neurite Formation in the Developing Brain. *Neuron*, 76(6), pp.1091–1107.

Forrester, M.T. et al., 2011. Site-specific analysis of protein S-acylation by resin-assisted capture (Acyl-RAC). *J Lipid Res*, 52, pp.393–398.

Fukata, M. et al., 2004. Identification of PSD-95 palmitoylating enzymes. *Neuron*, 44(6), pp.987–996.

Fukata, M. et al., 2002. Rac1 and Cdc42 Capture Microtubules through IQGAP1 and CLIP-170. *Cell*, 109(7), pp.873–885.

Fukata, Y. & Fukata, M., 2010. Protein palmitoylation in neuronal development and synaptic plasticity. *Nat Rev Neurosci*, 11(3), pp.161–175.

Gallo, G., 2011. The cytoskeletal and signaling mechanisms of axon collateral branching. *Developmental Neurobiology*, 71(3), pp.201–220.

Gao, X. & Hannoush, R.N., 2014a. Method for cellular imaging of palmitoylated proteins with clickable probes and proximity ligation applied to hedgehog, tubulin, and ras. *Journal of the American Chemical Society*, 136(12), pp.4544–4550.

Gao, X. & Hannoush, R.N., 2014b. Single-cell in situ imaging of palmitoylation in fatty-acylated proteins. *Nature protocols*, 9(11), pp.2607–2623.

Gibson, D.A. & Ma, L., 2011. Developmental regulation of axon branching in the vertebrate nervous system. *Development (Cambridge, England)*, 138(2), pp.183–195.

Golub, T., Wacha, S. & Caroni, P., 2004. Spatial and temporal control of signaling through lipid rafts. *Current Opinion in Neurobiology*, 14(5), pp.542–550.

Goossens, T. et al., 2011. The Drosophila L1CAM homolog Neuroglian signals through distinct pathways to control different aspects of mushroom body axon development. *Development (Cambridge, England)*, 138(8), pp.1595–605.

Graus-Porta, D. et al., 2001. Beta1-class integrins regulate the development of laminae and folia in the cerebral and cerebellar cortex. *Neuron*, 31(3), pp.367–379.

Greaves, J. & Chamberlain, L.H., 2011. DHHC palmitoyl transferases: Substrate interactions and (patho)physiology. *Trends in Biochemical Sciences*, 36(5), pp.245–253.

Greene, L.A., Tischlert, A.S. & Kuffler, S.W., 1976. Establishment of a noradrenergic clonal line of rat adrenal pheochromocytoma cells which respond to nerve growth factor (sympathetic neurons/cell culture/catecholamines/differentiation/neurites). *Cell Biology*, 73(7), pp.2424–2428.

Grobe, K. et al., 2005. Cerebral hypoplasia and craniofacial defects in mice lacking heparan sulfate Ndst1 gene function. *Development (Cambridge, England)*, 132(16), pp.3777–3786.

Gu, C. et al., 2003. Neuropilin-1 conveys semaphorin and VEGF signaling during neural and cardiovascular development. *Developmental Cell*, 5(1), pp.45–57.

Guirland, C. et al., 2004. Lipid rafts mediate chemotropic guidance of nerve growth cones. *Neuron*, 42(1), pp.51–62.

V. Hamburger, H.L.H., 1951. A series of normal stages in the development of the chick embryo. *Journal of Morphology*, 88(1), pp.49–92.

Hancock, M.L. et al., 2011. Type III neuregulin 1 regulates pathfinding of sensory axons in the developing spinal cord and periphery. *Development*, 138(22), pp.4887–4898.

Hauryliuk, V. et al., 2015. Recent functional insights into the role of (p)ppGpp in bacterial physiology. *Nature Reviews Microbiology*, 13(5), pp.298–309.

Hayashi-Nishino, M. et al., 2009. A subdomain of the endoplasmic reticulum forms a cradle for autophagosome formation. *Nature Cell Biology*, 11(12), pp.1433–1437.

Helmstaedter, M., Sakmann, B. & Feldmeyer, D., 2009. Neuronal correlates of local, lateral, and translaminar inhibition with reference to cortical columns. *Cerebral Cortex*, 19(4), pp.926–937.

Hérincs, Z. et al., 2005. DCC association with lipid rafts is required for netrin-1-mediated axon guidance. *Journal of Cell Science*, 118(Pt 8), pp.1687–1692.

Hess, D.T. et al., 1993. Neuronal growth cone collapse and inhibition of protein fatty acylation by nitric oxide. *Nature*, 366(6455), pp.562–565.

Hirokawa, N., Glicksman, M.A. & Willard, M.B., 1984. Organization of mammalian neurofilament polypeptides within the neuronal cytoskeleton. *Journal of Cell Biology*, 98(4), pp.1523–1536.

Honig, M.G. & Hume, R.I., 1989. DiI and DiO: versatile fluorescent dyes for neuronal labelling and pathway tracing. *Trends in Neurosciences*, 12(9), pp.333–341.

Hua, Z.L., Emiliani, F.E. & Nathans, J., 2015. Rac1 plays an essential role in axon growth and guidance and in neuronal survival in the central and peripheral nervous systems. *Neural Development*, 10(1), p.21.

Jennings, B.C. et al., 2009. 2-Bromopalmitate and 2-(2-hydroxy-5-nitro-benzylidene)-benzo[b]thiophen-3-one inhibit DHHC-mediated palmitoylation in vitro. *Journal of lipid research*, 50(2), pp.233–42.

Jennings, B.C. & Linder, M.E., 2012. DHHC protein S-acyltransferases use similar ping-pong kinetic mechanisms but display different Acyl-CoA specificities. *Journal of Biological Chemistry*, 287(10), pp.7236–7245.

Kalil, K. & Dent, E.W., 2014. Branch management: mechanisms of axon branching in the developing vertebrate CNS. *Nat Rev Neurosci*, 15(1), pp.7–18.

Kam, M.K.M. et al., 2014. Perturbation of Hoxb5 signaling in vagal and trunk neural crest cells causes apoptosis and neurocristopathies in mice. *Cell death and differentiation*, 21(2), pp.278–89.

Kandel, E.R. et al., 2014. *Principles of Neural Science, Fifth Edition*,

Kang, R. et al., 2008. Neural palmitoyl-proteomics reveals dynamic synaptic palmitoylation. *Nature*, 456(7224), pp.904–9.

Karayiorgou, M. & Gogos, J.A., 2004. The molecular genetics of the 22q11-associated schizophrenia. In *Molecular Brain Research*. pp. 95–104.

Kolodkin, A.L. & Tessier-Lavigne, M., 2011. Mechanisms and Molecules of Neuronal Wiring: A Primer. *Cold Spring Harbor Perspectives in Biology*, 3(6), pp.a001727–a001727.

Krylova, O. et al., 2002. WNT-3, expressed by motoneurons, regulates terminal arborization of neurotrophin-3-responsive spinal sensory neurons. *Neuron*, 35(6), pp.1043–1056.

Kuhn, M., 2016. Molecular Physiology of Membrane Guanylyl Cyclase Receptors. *Physiological Reviews*, 96(2), pp.751–804.

Laemmli, U.K., 1970. Cleavage of Structural Proteins during the Assembly of the Head of Bacteriophage T4. *Nature*, 227(5259), pp.680–685.

Lai, H.C., Seal, R.P. & Johnson, J.E., 2016. Making sense out of spinal cord somatosensory development. *Development (Cambridge, England)*, 143(19), pp.3434–3448.

Lai Wing Sun, K., Correia, J.P. & Kennedy, T.E., 2011. Netrins: versatile extracellular cues with diverse functions. *Development*, 138(11), pp.2153–2169.

Laumonnerie, C. et al., 2014. Netrin 1 and Dcc signalling are required for confinement of central axons within the central nervous system. *Development*, 141(3), pp.594–603.

Lelouvier, B. et al., 2008. Dynamics of somatostatin type 2A receptor cargoes in living hippocampal neurons. *The Journal of neuroscience : the official journal of the Society for Neuroscience*, 28(17), pp.4336–4349.

Lemonidis, K. et al., 2014. The Golgi S-acylation machinery is comprised of zDHHC enzymes with major differences in substrate affinity and S-acylation activity. *Molecular Biology of the Cell*, 25, pp.3870–3883.

Lewis, A.E. et al., 2013. The widely used Wnt1-Cre transgene causes developmental phenotypes by ectopic activation of Wnt signaling. *Developmental Biology*, 379(2), pp.229–234.

Li, W. et al., 2004. Activation of FAK and Src are receptor-proximal events required for netrin signaling. *Nature neuroscience*, 7(11), pp.1213–21.

Li, W. et al., 2006. FAK and Src kinases are required for netrin-induced tyrosine phosphorylation of UNC5. *Journal of cell science*, 119(1), pp.47–55.

Li, Y. et al., 2012. DHHC5 protein palmitoylates flotillin-2 and is rapidly degraded on induction of neuronal differentiation in cultured cells. *Journal of Biological Chemistry*, 287(1), pp.523–530.

Li, Z. et al., 2003. A stimulatory role for cGMP-dependent protein kinase in platelet activation. *Cell*, 112(1), pp.77–86.

Li, Z. et al., 2006. Sequential activation of p38 and ERK pathways by cGMP-dependent protein kinase leading to activation of the platelet integrin α IIbβ3. *Blood*, 107(3), pp.965–972.

Lievens, P.M.-J. et al., 2016. ZDHHC3 Tyrosine Phosphorylation Regulates Neural Cell Adhesion Molecule Palmitoylation. *Molecular and cellular biology*, 36(17), pp.2208–25.

Limjoco, T.I. et al., 1993. Transgenic Fv-4 mice resistant to Friend virus. *Journal of virology*, 67(7), pp.4163–4168.

Limpert, A.S., Karlo, J.C. & Landreth, G.E., 2007. Nerve growth factor stimulates the concentration of TrkA within lipid rafts and extracellular signal-regulated kinase activation through c-Cbl-associated protein. *Molecular and cellular biology*, 27(16), pp.5686–98.

Linder, M.E. & Deschenes, R.J., 2007. Palmitoylation: policing protein stability and traffic. *Nature reviews. Molecular cell biology*, 8(1), pp.74–84.

Lingwood, D. & Simons, K., 2010. Lipid rafts as a membrane-organizing principle. *Science (New York, N.Y.)*, 327(5961), pp.46–50.

Liu, G. et al., 2009. DSCAM functions as a netrin receptor in commissural axon pathfinding. *Proceedings of the National Academy of Sciences of the United States of America*, 106(8), pp.2951–6.

Liu, G. et al., 2004. Netrin requires focal adhesion kinase and Src family kinases for axon outgrowth and attraction. *Nature neuroscience*, 7(11), pp.1222–32.

Liu, R.Q. et al., 2014. Semaphorin 5B is a repellent cue for sensory afferents projecting into the developing spinal cord. *Development (Cambridge, England)*, 141(9), pp.1940–9.

Liu, Y., Fisher, D.A. & Storm, D.R., 1993. Analysis of the palmitoylation and membrane targeting domain of neuromodulin (GAP-43) by site-specific mutagenesis. *Biochemistry*, 32(40), pp.10714–9.

Lohmann, S.M. & Walter, U., 2005. Tracking functions of cGMP-dependent protein kinases (cGK). *Frontiers in bioscience : a journal and virtual library*, 10(1), pp.1313–28.

Longair, M.H., Baker, D. a. & Armstrong, J.D., 2011. Simple neurite tracer: Open source software for reconstruction, visualization and analysis of neuronal processes. *Bioinformatics*, 27(17), pp.2453–2454.

Lowery, L.A. & Vactor, D. Van, 2009. The trip of the tip: understanding the growth cone machinery. *Nature Reviews Molecular Cell Biology*, 10(5), pp.332–343.

Ma, L. & Tessier-Lavigne, M., 2007. Dual branch-promoting and branch-repelling actions of Slit/Robo signaling on peripheral and central branches of developing sensory axons. *J Neurosci*, 27(25), pp.6843–6851.

Madisen, L. et al., 2010. A robust and high-throughput Cre reporting and characterization system for the whole mouse brain. *Nature Neuroscience*, 13(1), pp.133–140.

Manders, E.M.M., Verbeek, F.J. & Ate, J.A., 1993. Measurement of co-localisation of objects in dual-colour confocal images. *Journal of microscopy*, 169(3), pp.375–382.

Martin, B.R. & Cravatt, B.F., 2009. Large-scale profiling of protein palmitoylation in mammalian cells. *Nat Methods*, 6(2), pp.135–138.

Masuda, T. et al., 2008. Netrin-1 acts as a repulsive guidance cue for sensory axonal projections toward the spinal cord. *J Neurosci*, 28(41), pp.10380–10385.

Masuda, T. et al., 2009. Netrin-1 signaling for sensory axons. *Cell adhesion & migration*, 3(2), pp.171–173.

Masuda, T. & Shiga, T., 2005. Chemorepulsion and cell adhesion molecules in patterning initial trajectories of sensory axons. *Neuroscience Research*, 51(4), pp.337–347.

Matsumoto, Y. et al., 2007. Netrin-1/DCC signaling in commissural axon guidance requires cell-autonomous expression of heparan sulfate. *The Journal of neuroscience : the official journal of the Society for Neuroscience*, 27(16), pp.4342–4350.

Mitchell, D.A. et al., 2014. Mutations in the X-linked intellectual disability gene, zDHHC9, alter autopalmitoylation activity by distinct mechanisms. *Journal of Biological Chemistry*, 289(26), pp.18582–18592.

Mitra, S.K., Hanson, D.A. & Schlaepfer, D.D., 2005. Focal adhesion kinase: in command and control of cell motility. *Nat Rev Mol Cell Biol*, 6(1), pp.56–68.

Molliver, D.C. et al., 1995. Presence or absence of TrkA protein distinguishes subsets of small sensory neurons with unique cytochemical characteristics and dorsal horn projections. *Journal of Comparative Neurology*, 361(3), pp.404–416.

Moore, S.W. et al., 2012. Netrin-1 attracts axons through FAK-dependent mechanotransduction. *The Journal of neuroscience : the official journal of the Society for Neuroscience*, 32(34), pp.11574–85.

Mukai, J. et al., 2004. Evidence that the gene encoding ZDHHC8 contributes to the risk of schizophrenia. *Nature Genetics*, 36(7), pp.725–731.

Mukai, J. et al., 2015a. Molecular Substrates of Altered Axonal Growth and Brain Connectivity in a Mouse Model of Schizophrenia. *Neuron*, 86(3), pp.680–696.

Mukai, J. et al., 2015b. Molecular Substrates of Altered Axonal Growth and Brain Connectivity in a Mouse Model of Schizophrenia. *Neuron*, 86(3), pp.680–95.

Myers, J.P., Santiago-Medina, M. & Gomez, T.M., 2011. Regulation of axonal outgrowth and pathfinding by integrin-ECM interactions. *Dev Neurobiol*, 71(11), pp.901–923.

Nakamura, N. et al., 1995. Characterization of a cis-Golgi matrix protein, GM130. *The Journal of Cell Biology*, 131(6).

Navarro-Lerida, I. et al., 2012. A palmitoylation switch mechanism regulates Rac1 function and membrane organization. *EMBO J*, 31(3), pp.534–551.

Navarro-Lérida, I. et al., 2012. A palmitoylation switch mechanism regulates Rac1 function and membrane organization. *The EMBO journal*, 31(3), pp.534–51.

Neukirchen, D. & Bradke, F., 2011. Neuronal polarization and the cytoskeleton. *Seminars in Cell & Developmental Biology*, 22(8), pp.825–833.

Ng, J. et al., 2002. Rac GTPases control axon growth, guidance and branching. *Nature*, 416(6879), pp.442–447.

Nguyen, M.K. et al., 2016. Optogenetic oligomerization of Rab GTPases regulates intracellular membrane trafficking. *Nature Chemical Biology*, 12(April), pp.1–8.

Nitta, Y. et al., 2017. DISCO Interacting Protein 2 regulates axonal bifurcation and guidance of Drosophila mushroom body neurons. *Developmental Biology*, 421(2), pp.233–244.

O'Leary, D.D.M. & Terashima, T., 1988. Cortical axons branch to multiple subcortical targets by interstitial axon budding: Implications for target recognition and "waiting periods." *Neuron*, 1(10), pp.901–910.

Ohno, Y. et al., 2006. Intracellular localization and tissue-specific distribution of human and yeast DHHC cysteine-rich domain-containing proteins. *Biochimica et Biophysica Acta - Molecular and Cell Biology of Lipids*, 1761(4), pp.474–483.

Olive, S. et al., 1995. The F3 neuronal glycosylphosphatidylinositol-linked molecule is localized to glycolipid-enriched membrane subdomains and interacts with L1 and fyn kinase in cerebellum. *Journal of Neurochemistry*, 65(5), pp.2307–2317.

Ostrom, R.S. & Liu, X., 2007. Detergent and detergent-free methods to define lipid rafts and caveolae. *Methods Mol Biol*, 400, pp.459–468.

Pandey, K.N., 2015. Endocytosis and Trafficking of Natriuretic Peptide Receptor-A: Potential Role of Short Sequence Motifs. *Membranes*, 5, pp.253–287.

Pate Skene, J.H. & Virag, I., 1989. Posttranslational membrane attachment and dynamic fatty acylation of a neuronal growth cone protein, GAP-43. *Journal of Cell Biology*, 108(2), pp.613–624.

Patterson, S.I. & Skene, J.H.P., 1994. Novel inhibitory action of tunicamycin homologues suggests a role for dynamic protein fatty acylation in growth cone-mediated neurite extension. *Journal of Cell Biology*, 124(4), pp.521–536.

Perrin, F.E., Rathjen, F.G. & Stoeckli, E.T., 2001. Distinct subpopulations of sensory afferents require F11 or axonin-1 for growth to their target layers within the spinal cord of the chick. *Neuron*, 30(3), pp.707–723.

Persaud-Sawin, D.A., Lightcap, S. & Harry, G.J., 2009. Isolation of rafts from mouse brain tissue by a detergent-free method. *J Lipid Res*, 50(4), pp.759–767.

Pfenninger, K.H., 2009. Plasma membrane expansion: a neuron's Herculean task. *Nature reviews. Neuroscience*, 10(4), pp.251–61.

Pfenninger, K.H. et al., 2003. Regulation of membrane expansion at the nerve growth cone. *Journal of cell science*, 116(Pt 7), pp.1209–1217.

Pinner, A.L. et al., 2015. Decreased protein S-palmitoylation in dorsolateral prefrontal cortex in schizophrenia. *Schizophrenia Research*.

Pollerberg, G.E. et al., 2013. The role of cell adhesion molecules for navigating axons: Density matters. *Mechanisms of Development*, 130(6–8), pp.359–372.

Polleux, F. & Snider, W., 2010. Initiating and growing an axon. *Cold Spring Harbor perspectives in biology*, 2(4).

Ponomareva, O.Y. et al., 2014. Calsyntenin-1 regulates axon branching and endosomal trafficking during sensory neuron development in vivo. *J Neurosci*, 34(28), pp.9235–9248.

Purohit, A.A. et al., 2012. Down syndrome cell adhesion molecule (DSCAM) associates with uncoordinated-5C (UNC5C) in netrin-1-mediated growth cone collapse. *Journal of Biological Chemistry*, 287(32), pp.27126–27138.

Rader, C. et al., 1996. Implications for the domain arrangement of axonin-1 derived from the mapping of its NgCAM binding site. *The EMBO journal*, 15(9), pp.2056–68.

Ramirez, O.A. & Couve, A., 2011. The endoplasmic reticulum and protein trafficking in dendrites and axons. *Trends in Cell Biology*, 21(4), pp.219–227.

Ramón y Cajal, S., 1905. Estructura de los centros nerviosos de las aves. *Madrid*. Available at: https://commons.wikimedia.org/w/index.php?curid=612561 [Accessed January 25, 2017].

Rathinavelu, A. & Isom, G.E., 1991. Differential internalization and processing of atrial-natriuretic-factor B and C receptor in PC12 cells. *Biochemical Journal*, 276(1991), pp.493–497.

Rathjen, F.G. et al., 1987. Membrane glycoproteins involved in neurite fasciculation. *The Journal of cell biology*, 104(2), pp.343–53.

Ren, J. et al., 2008. CSS-Palm 2.0: An updated software for palmitoylation sites prediction. *Protein Engineering, Design and Selection*, 21(11), pp.639–644.

Rico, B. et al., 2004. Control of axonal branching and synapse formation by focal adhesion kinase. *Nat Neurosci*, 7(10), pp.1059–1069.

Ridley, A.J. et al., 1992. The small GTP-binding protein rac regulates growth factor-induced membrane ruffling. *Cell*, 70(3), pp.401–410.

Ringvall, M. & Kjelln, L., 2010. Mice deficient in heparan sulfate n-deacetylase/n-sulfotransferase 1. *Progress in Molecular Biology and Translational Science*, 93(C), pp.35–58.

Roth, A.F. et al., 2006. Global Analysis of Protein Palmitoylation in Yeast. *Cell*, 125(5), pp.1003–1013.

Saiki, R.K. et al., 1988. Primer-directed enzymatic amplification of DNA with a thermostable DNA polymerase. *Science (New York, N.Y.)*, 239(4839), pp.487–491.

Saleem, A.N. et al., 2010. Mice with alopecia, osteoporosis, and systemic amyloidosis due to mutation in Zdhhc13, a gene coding for palmitoyl acyltransferase. *PLoS Genet*, 6(6), p.e1000985.

Sanders, S.S. et al., 2015. Curation of the Mammalian Palmitoylome Indicates a Pivotal Role for Palmitoylation in Diseases and Disorders of the Nervous System and Cancers. *PLoS Computational Biology*, 11(8).

Schäffer, S., 2006. *Investigations about the function of the cGMP-dependent kinase I alpha during the development of the nervous system.* Freie Universtät Berlin.

Schmidt, H. et al., 2009. C-type natriuretic peptide (CNP) is a bifurcation factor for sensory neurons. *Proc Natl Acad Sci U S A*, 106(39), pp.16847–16852.

Schmidt, H. et al., 2002. cGMP-mediated signaling via cGKIalpha is required for the guidance and connectivity of sensory axons. *J Cell Biol*, 159(3), pp.489–498.

Schmidt, H. et al., 2002. cGMP-mediated signaling via cGKIα is required for the guidance and connectivity of sensory axons. *Journal of Cell Biology*, 159(3), pp.489–498.

Schmidt, H. et al., 2007. The receptor guanylyl cyclase Npr2 is essential for sensory axon bifurcation within the spinal cord. *J Cell Biol*, 179(2), pp.331–340.

Schmidt, H. & Rathjen, F.G., 2011. DiI-labeling of DRG neurons to study axonal branching in a whole mount preparation of mouse embryonic spinal cord. *J Vis Exp*, (58).

Schmidt, H. & Rathjen, F.G., 2010. Signalling mechanisms regulating axonal branching in vivo. *Bioessays*, 32(11), pp.977–985.

Schmidt, H., Ter-Avetisyan, G. & Rathjen, F.G., 2013. A genetic strategy for the analysis of individual axon morphologies in cGMP signalling mutant mice. *Methods in Molecular Biology*, 1020, pp.193–204.

Schwander, M. et al., 2004. Beta1 integrins in muscle, but not in motor neurons, are required for skeletal muscle innervation. *J Neurosci*, 24(37), pp.8181–8191.

Senetar, M.A., Moncman, C.L. & McCann, R.O., 2007. Talin2 is induced during striated muscle differentiation and is targeted to stable adhesion complexes in mature muscle. *Cell Motility and the Cytoskeleton*, 64(3), pp.157–173.

Serafini, T. et al., 1996. Netrin-1 is required for commissural axon guidance in the developing vertebrate nervous system. *Cell*, 87(6), pp.1001–1014.

Shattil, S.J., Kim, C. & Ginsberg, M.H., 2010. The final steps of integrin activation: the end game. *Nat Rev Mol Cell Biol*, 11(4), pp.288–300.

Shi, Y., 2009. Serine/Threonine Phosphatases: Mechanism through Structure. *Cell*, 139(3), pp.468–484.

Song, I.W. et al., 2014. Palmitoyl acyltransferase, Zdhhc13, facilitates bone mass acquisition by regulating postnatal epiphyseal development and endochondral ossification: a mouse model. *PLoS One*, 9(3), p.e92194.

Spillane, M. et al., 2013. Mitochondria Coordinate Sites of Axon Branching through Localized Intra-axonal Protein Synthesis. *Cell Rep*, 5(6), pp.1564–1575.

Spillane, M. et al., 2012. Nerve growth factor-induced formation of axonal filopodia and collateral branches involves the intra-axonal synthesis of regulators of the actin-nucleating Arp2/3 complex. *The Journal of neuroscience : the official journal of the Society for Neuroscience*, 32(49), pp.17671–89.

Spruston, N., 2008. Pyramidal neurons: dendritic structure and synaptic integration. *Nature reviews. Neuroscience*, 9(3), pp.206–221.

Stam, C.J., 2014. Modern network science of neurological disorders. *Nature Reviews Neuroscience*, 15(10), pp.683–695.

Stonkute, A., 2010. *cGMP signalling via CNP-Npr2-cGKI, and its role in axonal branching during embryonic development*. Berlin: Freie Universität Berlin.

Sutherland, A.E., Calarco, P.G. & Damsky, C.H., 1993. Developmental regulation of integrin expression at the time of implantation in the mouse embryo. *Development*, 119(4), pp.1175–1186.

Tamura, N. et al., 2004. Critical roles of the guanylyl cyclase B receptor in endochondral ossification and development of female reproductive organs. *Proceedings of the National Academy of Sciences of the United States of America*, 101(49), pp.17300–5.

Taylor, G.M., Gao, Y. & Sanders, D.A., 2001. Fv-4: identification of the defect in Env and the mechanism of resistance to ecotropic murine leukemia virus. *Journal of virology*, 75(22), pp.11244–8.

Ter-Avetisyan, G. et al., 2012. cGMP signaling and branching of sensory axons in the spinal cord. *Future Neurology*, 7(5), pp.639–651.

Ter-Avetisyan, G., Rathjen, F.G. & Schmidt, H., 2014. Bifurcation of axons from cranial sensory neurons is disabled in the absence of Npr2-induced cGMP signaling. *J Neurosci*, 34(3), pp.737–747.

Tessier-Lavigne, M. & Goodman, C.S., 1996. The molecular biology of axon guidance. *Science (New York, N.Y.)*, 274(5290), pp.1123–33.

Thorsteinsdóttir, S. et al., 1995. Expression patterns of laminin receptor splice variants alpha 6A beta 1 and alpha 6B beta 1 suggest different roles in mouse development. *Developmental dynamics : an official publication of the American Association of Anatomists*, 204(3), pp.240–258.

Tian, L. et al., 2008. Palmitoylation gates phosphorylation-dependent regulation of BK potassium channels. *Proceedings of the National Academy of Sciences*, 105(52), pp.21006–21011.

Tian, X. et al., 2015. A Voltage-Gated Calcium Channel Regulates Lysosomal Fusion with Endosomes and Autophagosomes and Is Required for Neuronal Homeostasis. *PLoS Biology*, 13(3).

Tojima, T. et al., 2011. Second messengers and membrane trafficking direct and organize growth cone steering. *Nature reviews. Neuroscience*, 12(4), pp.191–203.

Tojima, T. & Kamiguchi, H., 2015. Exocytic and endocytic membrane trafficking in axon development. *Development, Growth & Differentiation*, 57(4), pp.291–304.

Tom, C.T. & Martin, B.R., 2013. Fat chance! Getting a grip on a slippery modification. *ACS Chem Biol*, 8(1), pp.46–57.

Torres, R.J. & Puig, J.G., 2007. Hypoxanthine-guanine phosophoribosyltransferase (HPRT) deficiency: Lesch-Nyhan syndrome. *Orphanet journal of rare diseases*, 2, p.48.

Ussar, S. et al., 2006. The Kindlins: subcellular localization and expression during murine development. *Exp Cell Res*, 312(16), pp.3142–3151.

Valtcheva, N. et al., 2009. The commonly used cGMP-dependent protein kinase type i (cGKI) inhibitor Rp-8-Br-PET-cGMPS can activate cGKI in vitro and in intact cells. *Journal of Biological Chemistry*, 284(1), pp.556–562.

Vergarajauregui, S. & Puertollano, R., 2006. Two di-leucine motifs regulate trafficking of mucolipin-1 to lysosomes. *Traffic*, 7(3), pp.337–353.

Vitriol, E.A. & Zheng, J.Q., 2012. Growth cone travel in space and time: the cellular ensemble of cytoskeleton, adhesion, and membrane. *Neuron*, 73(6), pp.1068–81.

Wan, J. et al., 2007. Palmitoylated proteins: purification and identification. *Nat Protoc*, 2(7), pp.1573–1584.

Wan, J. et al., 2013. Tracking brain palmitoylation change: Predominance of glial change in a mouse model of Huntington's disease. *Chemistry and Biology*, 20(11), pp.1421–1434.

Wang, L. & Marquardt, T., 2012. Direct live monitoring of heterotypic axon-axon interactions in vitro. *Nature protocols*, 7(2), pp.351–63.

Watanabe, K. et al., 2006. Dorsally derived netrin 1 provides an inhibitory cue and elaborates the "waiting period" for primary sensory axons in the developing spinal cord. *Development*, 133(7), pp.1379–1387.

Webb, Y., Hermida-Matsumoto, L. & Resh, M.D., 2000. Inhibition of protein palmitoylation, raft localization, and T cell signaling by 2-bromopalmitate and polyunsaturated fatty acids. *Journal of Biological Chemistry*, 275(1), pp.261–270.

Wegener, J.W. et al., 2002. cGMP-dependent protein kinase I mediates the negative inotropic effect of cGMP in the murine myocardium. *Circ.Res.*, 90(1524–4571 (Electronic) LA–eng PT–Journal Article PT–Research Support, Non–U.S. Gov't RN–0 (Thionucleotides) RN–31356–94–2 (8–bromocyclic GMP) RN–54364–02–2 (8–((4–chlorophenyl)thio)cyclic–3',5'–GMP) RN–7665–99–8 (Cyclic GMP) RN–EC 2.7.1.37), pp.18–20.

Wei, X., Song, H. & Semenkovich, C.F., 2014. Insulin-regulated protein palmitoylation impacts endothelial cell function. *Arteriosclerosis, Thrombosis, and Vascular Biology*, 34(2), pp.346–354.

Wilson, J.P. et al., 2011. Proteomic analysis of fatty-acylated proteins in mammalian cells with chemical reporters reveals S-acylation of histone H3 variants. *Molecular & cellular proteomics : MCP*, 10(3), p.M110.001198.

Wilson, N.H. & Stoeckli, E.T., 2012. In ovo Electroporation of miRNA-based Plasmids in the Developing Neural Tube and Assessment of Phenotypes by DiI Injection in Open-book Preparations. *Journal of Visualized Experiments*, (68), pp.e4384–e4384.

Winkle, C.C. et al., 2014. A novel Netrin-1–sensitive mechanism promotes local SNARE-mediated exocytosis during axon branching. *The Journal of Cell Biology*, 205(2).

Winkle, C.C., Hanlin, C.C. & Gupton, S.L., 2016. Utilizing Combined Methodologies to Define the Role of Plasma Membrane Delivery During Axon Branching and Neuronal Morphogenesis. *Journal of Visualized Experiments*, (109).

Wright, K.M. et al., 2012. Dystroglycan Organizes Axon Guidance Cue Localization and Axonal Pathfinding. *Neuron*, 76(5), pp.931–944.

Xia, C. et al., 2013. CNP/cGMP signaling regulates axon branching and growth by modulating microtubule polymerization. *Dev Neurobiol*.

Yang, G. et al., 2012. Isoform-specific palmitoylation of JNK regulates axonal development. *Cell Death and Differentiation*, 19(4), pp.553–561.

Yang, W. et al., 2009. Proteome-scale characterization of human s-acylated proteins in lipid raft-enriched and non-raft membranes. *Molecular & cellular proteomics : MCP*, pp.1–53.

Yaron, A. et al., 2005. Differential requirement for Plexin-A3 and -A4 in mediating responses of sensory and sympathetic neurons to distinct class 3 Semaphorins. *Neuron*, 45(4), pp.513–523.

Ye, F., Snider, A.K. & Ginsberg, M.H., 2014. Talin and kindlin: The one-two punch in integrin activation. *Frontiers of Medicine in China*, 8(1), pp.6–16.

Yount, J.S. et al., 2010. Palmitoylome profiling reveals S-palmitoylation-dependent antiviral activity of IFITM3. *Nature chemical biology*, 6(8), pp.610–4.

Zacharias, U., Nörenberg, U. & Rathjen, F.G., 1999. Functional interactions of the immunoglobulin superfamily member F11 are differentially regulated by the extracellular matrix proteins tenascin-R and tenascin-C. *The Journal of biological chemistry*, 274(34), pp.24357–65.

Zhang, B. et al., 2003. Bleeding due to disruption of a cargo-specific ER-to-Golgi transport complex. *Nature Genetics*, 34(2), pp.220–225.

Zhao, Z. et al., 2009. Regulate axon branching by the cyclic GMP pathway via inhibition of glycogen synthase kinase 3 in dorsal root ganglion sensory neurons. *The Journal of neuroscience : the official journal of the Society for Neuroscience*, 29(5), pp.1350–1360.

Zhao, Z. & Ma, L., 2009. Regulation of axonal development by natriuretic peptide hormones. *Proceedings of the National Academy of Sciences of the United States of America*, 106(42), pp.18016–21.

Zhou, L. et al., 2002. Murine peripherin gene sequences direct Cre recombinase expression to peripheral neurons in transgenic mice. *FEBS Letters*, 523(1–3), pp.68–72.

Zou, Y., 2012. Does Planar Cell Polarity Signaling Steer Growth Cones? *Current Topics in Developmental Biology*, 101, pp.141–160.

Zulauf, L. et al., 2009. Cofilin phosphorylation is involved in nitric oxide/cGMP-mediated nociception. *Biochemical and Biophysical Research Communications*, 390(4), pp.1408–1413.

11. CURRICULUM VITAE

Der Lebenslauf ist in der Online-Version aus Gründen des Datenschutzes nicht enthalten.

12. APPENDIX

Detailed MS data spreadsheet of the 2 and 3-hit candidate proteins are enclosed on a CD attached to this thesis (cited as "Appendix excel spreadsheet").

Function	Gene Name	Function	Gene Name
Channels and transporters:		**Cell adhesion:**	
	Atp2c1		Cadm4
	Mcoln1	**Signalling, receptors:**	
	Slc25a13		Clcn3;Clcn4;Clcn5
	Slc30a5	**Signalling, GTPases and other regulators:**	
Cytoskeletal proteins:			**Arhgef2**
	Map4		Aldoa;Aldoart2;Aldoart1
Metabolism:			**Atl2**
	Abcb7		Aatk
	Alg3		Pi4k2a
	Dad1		Pde10a
	Dolpp1	**Receptors and channels:**	
	Edem3		Cacng3
	Ephx1	**Others:**	
	Gfpt1		Tm9sf2
	Glce		**Fv4**
	Gusb		Tmem214
	Mogs		Efr3b
	Ndst1	**Unknown function:**	
	Plod1		Tmem222
	Prdx1		Casd1
	Ptgs1		Zfp493
	Zdhhc13		Ano8
	Zdhhc3		Bzw2
Transcription and translation:			Zfp362;Zfp384;Znf384
	Rps16		C78339
	Eif2s1	**Known or putative false-positives:**	
	Kdm1a		Acta1;Actc1;Actg2;Acta2
	Gcn1l1		Sdhc
	Tars		**Dpysl3**
	Pes1		**Dpysl2**
	Nacad		**Uba1**
	Nsun2		**eno1**
	Srbd1		
	Eif2ak3		
Membrane trafficking:			
	Yipf5		
	Trappc3		
	Tmed10		

Supplementary Table 1 : 2 and 3-hit palmitoylated protein candidates that were only detected by label-free LC-MS in the cGMP-treated F11 cell membrane fraction. The 60 detected proteins were listed by function. 3-hit candidates are written in bold text.